Brain networks in healthy ageing and psychiatric conditions.

Author:
Perry, Alistair

Publication Date:
2017

DOI:
https://doi.org/10.26190/unsworks/20035

Brain networks in healthy ageing and psychiatric conditions

Alistair Giles Perry BSc(Psych); BSc (Hons)

A thesis submitted in fulfilment of the requirements for the degree of Doctor of Philosophy in Psychiatry at the University of New South Wales

SCHOOL OF PSYCHIATRY

FACULTY OF MEDICINE

June 2017

THE UNIVERSITY OF NEW SOUTH WALES
Thesis/Dissertation Sheet

Surname or Family name: Perry

First name: Alistair

Abbreviation for degree: PhD

School: Psychiatry **Faculty**: Medicine

Title: Brain networks in healthy ageing and psychiatric conditions

Conceptualising the human brain upon its large-scale interactions has led to the realisation of integrative neural processes as critical to cerebral functioning. This thesis sought to elucidate the brain patterns of *functional integration* and *segregation* that are associated with the cognitive and behavioural changes in healthy ageing and psychiatric conditions. The network features expressed with age-related cognitive changes are poorly understood within a healthy older population. The brain network disturbances in individuals at high-genetic risk for bipolar disorder (BD) are also unknown.

Study 1 (Chapter 2) leveraged advances in diffusion-tractography to derive the features of structural brain networks in healthy older adults. The integrative features of the core backbone are observed in the connectomes of both young and older adults, reflecting ongoing patterns of efficient brain communication.

Study 2 (Chapter 3) leveraged multivariate analysis to examine in healthy older adults the complex relations between age, functional connectivity, and cognitive performance. A functional sensorimotor subnetwork was identified whose expression is opposed by age against core cognitive processes such as attention and processing speed. Modifiable factors such as increased education are associated with distinct functional networks.

Lastly, study 3 (Chapter 4) investigated the structural networks in patients and also unaffected relatives at high-genetic risk for BD. Relative to matched-controls, alterations to fronto-limbic circuits housing key emotional and cognitive centers were identified within both patient and high-risk groups.

The present works illustrate the expression of large-scale brain network features are associated with phenotypic differences in healthy older adults and psychiatric conditions. Inter-individual differences in the integration of cerebral information processing is strongly implicated here for the respective changes in functioning: Sensorimotor networks supporting lower-order processes are most sensitive to healthy ageing, whilst fronto-limbic disturbances in patient and high-risk groups are consistent with the emotional lability in BD. The integrative features of key-hub regions are also demonstrated throughout these studies as critical to brain communication capacity. This thesis hence contributes as an important body of work in our ability to understand and predict human brain functioning and behaviour.

Originality Statement

I hereby declare that this submission is my own work and to the best of my knowledge it contains no materials previously published or written by another person, or substantial proportions of material which have been accepted for the award of any other degree or diploma at UNSW or any other educational institution, except where due acknowledgement is made in the thesis. Any contribution made to the research by others, with whom I have worked at UNSW or elsewhere, is explicitly acknowledged in the thesis. I also declare that the intellectual content of this thesis is the product of my own work, except to the extent that assistance from others in the project's design and conception or in style, presentation and linguistic expression is acknowledged.

Alistair Perry

24th March 2017

Copyright Statement

Alistair Perry

24th March 2017

Authenticity Statement

I certify that the Library deposit digital copy is a direct equivalent of the final officially approved version of my thesis. No emendation of content has occurred and if there are any minor variations in formatting, they are the result of the conversion to digital format.

Alistair Perry

24th March 2017

Table of Contents

Abbreviations

AAL	Automated anatomical labelling
Aβ	amyloid-beta
ACT	Anatomically Constrained Tractography
AD	Alzheimer's disease
AFD	Apparent Fibre Density
aMCI	amnestic Mild Cognitive Impairment
APOE	Apolipoprotein E
ATP	Adenosine triphosphate
BD	Bipolar disorder
BOLD	Blood-oxygen-level dependent
CC	Clustering coefficient
CCA	Canonical Correlation Analysis
CN	Controls
CPL	Characteristic path length
CR	Cognitive reserve
CSD	Constrained Spherical Deconvolution
CSF	Cerebrospinal fluid
dRL	damped Richardson Lucy
DCM	Dynamic Causal Modelling
DLPFC	Dorsolateral prefrontal cortex
DMN	Default-mode network
DTI	Diffusion Tensor Imaging
DWI	Diffusion-weighted images
dMRI	diffusion Magnetic Resonance Imaging
EPI	Echo Planar Imaging
ICA	Independents Components Analysis
EEG	Electroencephalography
FA	Fractional anisotropy
FD	Framewise displacement
FDG	Fluorodeoxyglucose

FDR	False Discovery Rate
fMRI	functional Magnetic Resonance Imaging
FTD	Frontotemporal Dementia
FOD	Fibre Orientation Distribution
fODF	Fibre Orientation Density Function
FWE	Family-wise error
GEE	Generalized estimating equations
GLM	General Linear Model
GM	Grey matter
HARDI	High Angular Resolution Diffusion Imaging
HR	High-risk
ICA	Independent Components Analysis
IFG	Inferior frontal gyrus
MAS	Memory and Ageing Study
MCI	Mild Cognitive Impairment
MEG	Magnetoencephalography
MD	Mean diffusivity
md-aMCI	multi-domain amnestic Mild Cognitive Impairment
MDE	Major depressive episode
md-nMCI	multi-domain non-amnestic Mild Cognitive Impairment
MMSE	Mini-Mental Status Examination
MNI	Montreal Neurological Institute
MRI	Magnetic Resonance Imaging
NART	National Adult Reading Test
NBS	Network Based Statistic
NFT	Neurofibrillary tangle
nMCI	non-amnestic Mild Cognitive Impairment
ODF	Orientation Density Function
OFC	Orbitofrontal cortex
PET	Positron Emission Topography
PFC	Prefrontal cortex
PiB	Pittsburgh compound B
RCC	Rich club coefficients

rs-fMRI	resting-state functional Magnetic Resonance Imaging
RSN	Resting-state network
SIFT	Spherical-informed filtering tractogram
SMA	Supplementary motor area
STG	Superior temporal gyrus
WM	White matter
VLPFC	Ventrolateral prefrontal cortex
YLD	Years lived with disability
VMPFC	Ventromedial prefrontal cortex

Publications and Presentations

Publications

Perry, A., Wen, W., Kochan, N.A., Sachdev, P.S., Breakspear, M. (2017). The independent influences of age and education on functional brain networks and cognition in healthy older adults. *Human Brain Mapping* 38, 5094-5114

Perry, A., Wen, W., Lord, A., Thalamuthu, A., Roberts, G., Mitchell, P.B., Sachdev, P.S., Breakspear, M. (2015). The organisation of the elderly connectome. *NeuroImage* 114, 414–426.

Roberts, G*., **Perry, A*.,** Lord., A., Frankland, A., Levy, F., Holmes-Preston, E., Lenroot, R., Mitchell, R., Breakspear, M. (2016). Structural dysconnectivity of key emotional and cognitive areas in young people at high genetic risk for bipolar disorder. *Molecular Psychiatry,* DOI: 10.1038/mp.2016.216.

* The authors contributed equally to this work

Roberts, J.A., **Perry, A.**, Lord, A.R., Roberts, G., Mitchell, P.B., Smith, R.E., Calamante, F., Breakspear, M. (2016). The contribution of geometry to the human connectome. *NeuroImage* 124, Part A, 379-393.

Roberts, J.A., **Perry, A.**, Roberts, G., Mitchell, P.B., Breakspear, M. (2017). Consistency-based thresholding of the human connectome. *NeuroImage* 145, Part A, 118-129.

Wirsich, J., **Perry, A.**, Ridley, B., Proix, T., Golos, M., Bénar, C., Ranjeva, J.P., Bartolomei, F., Breakspear, M., Jirsa, V., Guye, M. (2016). Whole-brain analytic measures of network communication reveal increased structure-function correlation in right temporal lobe epilepsy. *NeuroImage: Clinical*, Volume 11, 2016, Pages 707-718

Invited talks

The elderly connectome. The 11th Annual World Congress of the Society for Brain Mapping and Therapeutics, Sydney, Australia, 17-19 March, 2014.

Structural dysconnectivity and network controllability of key cognitive and emotional areas in young people at high genetic risk for bipolar disorder. The 9th Australiasian Workshop on Neuro-Engineering and Computational Neuroscience, Brisbane, Australia, 28th-29th November, 2016.

Poster presentations

Perry, A., Roberts, G., Frankland, A., Levy, F., Holmes-Preston, E., Lenroot, R., Mitchell, R., Breakspear, M. (2016). Structural disturbances of key emotional areas in those at high genetic risk for bipolar disorder. 22nd Annual Meeting of the Organization for Human Brain Mapping, Geneva, Switzerland, 26-30 June, 2016.

Perry, A., Wen, W., Kochan, N.A., Sachdev, P.S., Breakspear, M. (2016). The Weighting of Demographic and Behavioural Factors to the Elderly Functional Connectome**.** 22nd Annual Meeting of the Organization for Human Brain Mapping, Geneva, Switzerland, 26-30 June, 2016.

Perry, A., Wen, W., Kochan, N.A., Sachdev, P.S., Breakspear, M. (2016). Age and education's independent influence on functional brain networks and cognition in healthy older adults**.** Fifth Biennial conference on resting state and brain connectivity, 21-23rd September, 2016

Awards

2016 – Postgraduate Research Scholarship Scheme (Competitive Travel Grants Program). Awarded from the University of New South Wales, Sydney, Australia

Declaration of Contributions to Publications

I made significant contributions to all papers arising out of this thesis in terms of study design, data collection and its management, design of statistical approach, data analysis, and writing of the first and final drafts of manuscripts.

For the publication arising from Chapter 2, I contributed to data collection and management, and undertook sole contribution in terms of the pre-processing of diffusion-weighted images, whole-brain fibre-reconstruction, and network metric computation. I took primary responsibility for study design, statistical analysis, and writing the paper in conjunction with my supervisors, Professor Michael Breakspear and Associate Professor Wei Wen. Professor Perminder Sachdev contributed data, and assisted also with study design and paper preparation. Dr Anbupalam Thalamathu assisted with statistical analysis and writing the paper.

For the publication arising from Chapter 3, I contributed to data collection and management, and undertook sole contribution in terms of the pre-processing of rs-fMRI data and multivariate statistical analysis. I took primary responsibility for study design, data analysis, and writing the paper in conjunction with my supervisor, Professor Michael Breakspear. Associate Professor Wei Wen and Professor Perminder Sachdev contributed data, and assisted also with study design and paper preparation. Dr Nicole Kochan assisted with study design in terms of demographic and cognitive variables employed, and also in paper preparation.

For the publication arising from Chapter 4, I undertook sole contribution in terms of the pre-processing of diffusion-weighted images, whole-brain fibre-reconstruction, and network metric computation. Study design, data analysis, and paper preparation was a collaborative effort between myself, Dr Roberts, and Professor Breakspear. Professor Phil Mitchell contributed data for the study, and also assisted with study design and paper preparation.

Alistair Perry

24th March 2017

Chapter 1: Introduction

1.1 Human brain function

1.1.1 Contemporary views of human brain functioning

Through the 20th century, human behaviour and cognitive processes were predominantly postulated to arise from the functioning of discrete cerebral brain-regions. Under this classical view, localized variability in the composition or functioning of specialized brain centres led to inter-individual differences in psychological processes (Catani, 2005; Fornito et al., 2015). The 21st century, however, spawned rapid advancements in non-invasive human magnetic resonance imaging (MRI) techniques. Spatially embedded (Roberts et al., 2016c) within the brain are complex anatomical wiring patterns that constitute large-scale networks (Hagmann et al., 2007; Sporns, 2013b; Sporns et al., 2005). These discoveries catalysed our knowledge of the intimate association between human brain organisation and behaviour: The large-scale integration of segregated areas within brain networks (Sporns, 2013a, b) give rise to the complex perceptual, cognitive and behavioural features of human existence (Tononi, 2004; Tononi et al., 1994). Even subtle alterations to large-scale brain interactions are thought to underlie the symptomatic expression of neurodegenerative and psychiatric conditions such as Alzheimer's disease (AD) and schizophrenia (Dennis and Thompson, 2014; Fornito and Bullmore, 2015; Fornito et al., 2015; Friston, 1998; Seeley et al., 2009).

1.1.2 Network science

Network science allows the association between distributed brain function and behaviour to be investigated. Network science rests on a branch of mathematics known as graph theory (Euler, 1736). Accordingly, systems are represented as complex networks, defined by their constituent elements (nodes) and interactions (edges). A social network of interactions between facebook friends, for example, is represented by each constituent person (nodes) linked by a relational measure of friendship (edges). Graph-theoretical tools have been applied to the investigation of many real-world systems including (Newman, 2003): food webs (Williams and Martinez, 2000), the neural network of the *Caenorhabditis elegans* (White et al., 1986), mammalian brains (Scannell et al., 1999; Sporns and Zwi, 2004; Stephan et al., 2000), the internet (Faloutsos et al., 1999), electrical and tele-communication grids (Aiello et al., 2000; Albert et al., 2004), and cellular and metabolic networks (Jeong et al., 2000; Kohn, 1999).

1.1.3 Conceptualising the human brain as a complex network

Human brain networks can be represented by structural or functional connectivity (edges) between constituent cerebral areas (nodes) (Fornito et al., 2013; Friston, 1994). *Structural connectivity* denotes the interconnecting white-matter axonal propagations from tracer studies or reconstructed *in vivo* through diffusion MRI (dMRI) and tractography. On the other hand, *functional connectivity* is defined as inter-regional statistical dependences (i.e. correlation coefficients) between remote neurophysiological signals – measured by functional MRI (fMRI), electroencephalography (EEG), or magnetoencephalography (MEG) (Fornito et al., 2013; Sporns, 2013b). *Effective connectivity* is another form of brain connectivity, quantifying the causal influence of one region's neuronal activity upon

another (Friston et al., 2003). Connectivity estimates are combined with spatial knowledge (data-driven or *priori*) of cortical areas to construct a network of brain connectivity patterns. The resultant large-scale network of structural connectivity patterns is defined as the human connectome (Sporns et al., 2005; Stam, 2004).

1.2 Empirical methods: Brain networks

1.2.1 Structural brain networks

1.2.1.1 *Diffusion MRI*

The mapping of axonal trajectories was traditionally performed on non-human brain tissue through in vitro tract-tracing methods. Complex patterns of white-matter organisation were revealed for mammalian species, including the cat (Scannell et al., 1999; Scannell and Young, 1993), primate (Felleman and Van Essen, 1991) and rat cortices (Burns and Young, 2000). Post-mortem studies in human brains were limited to gross reconstructions of large white matter tracts such as the internal capsule (Klingler and Ludwig, 1956). The advent of dMRI allowed, for the first time, the comprehensive reconstruction of human white-matter fibre bundles (Catani, 2005).

dMRI is an MRI acquisition sequence involving the application of spatially-varying gradient pulses, which detect the spin dephasing of protons in water molecules (Bastiani and Roebroeck, 2015; Jones et al., 2013). The intensity of the dMRI signals are reconstructed from the scanner readout (*k*-space) to form diffusion-weighted images (DWI), with diffusion measurements contained within each three-dimensional image grid (i.e. voxel) (Figure 1-1A). Free water diffusion is Gaussian and isotropic, obeying the diffusion equation. Water diffusion in white matter is anisotropic, because water diffusion

is restricted along gradient directions perpendicular to local axonal fibre bundles (Figure 1-1B) (Basser et al., 1994; Chenevert et al., 1990; Le Bihan, 1991)

From the raw dMRI signal, a number of structural properties can be reconstructed for each voxel, which are now briefly reviewed.

1.2.1.2 *Diffusion Tensor Imaging*

Diffusion Tensor Imaging (DTI) (Basser, 1995; Basser et al., 1994; Pierpaoli et al., 1996) is the most frequently employed approach for modelling orientations of the underlying white-matter fibres. Tensor models assume a distribution of unimodal anisotropic diffusion - namely, that fibre-bundles are coherently organised parallel to the principal diffusion axis (i.e. diffusion tensor) (Assaf and Pasternak, 2008; Jones et al., 2013) (Figure 1-1C; middle).

1.2.1.3 *Diffusion Tensor Imaging indices*

The ratio of diffusivities parallel and perpendicular to the principal diffusion axis are also derived to calculate indices of white-matter "microstructural integrity" (Assaf and Pasternak, 2008). Fractional Anisotropy (FA) and Mean Diffusivity (MD) are highly implemented indices in clinical settings: FA yields the ratio of parallel to perpendicular diffusivity within a voxel, whilst MD refers to the average diffusivity (Assaf and Pasternak, 2008; Basser, 1995; Basser et al., 1994).

The extent to which these DTI-indices reflect changes in microstructural "integrity" of white-matter populations are, however, rather controversial (Farquharson et al., 2013; Jones et al., 2013). Consider voxel-populations with multiple underlying fibre-

orientations, as is the case with "crossing" or "kissing" fibre-bundles (Figure 1-1C, bottom panel): DTI-based models erroneously infer isotropic diffusion along less coherently-organised fibre-bundles (Assaf and Pasternak, 2008; Jones et al., 2013), resulting in decreased FA and increased MD values. Given that approximately 90% of white-matter tissue contains crossing-fibre configurations (Jeurissen et al., 2013), the biological interpretability of simple tensor-based models is problematic.

1.2.1.4 *Constrained spherical deconvolution*

Alternative approaches to tensor-based modelling have been developed in order to alleviate the "crossing-fibre" problem (Jones et al., 2013). These models sample within each voxel an orientation density function (ODF) (Descoteaux et al., 2007; Tuch, 2004), or infer a fibre orientation density function (fODF) of the diffusion-signal. The latter procedure typically involves constrained spherical deconvolution (CSD) (Tournier et al., 2007, 2012; Tournier et al., 2008) of the "response function" for diffusion signals. Subsequently obtained with CSD are estimates of fibre orientation distributions (FOD), relating to the relative fibre density along an angular structure. CSD is shown to superiorly sharpen the angular profile of local fibre-orientation estimates (Figure 1-1C; right) (Descoteaux et al., 2009; Farquharson et al., 2013), in comparison to both ODF and tensor-based approaches. Other more complex models of the diffusion signal include *q*-ball imaging (Tuch, 2004) and the damped Richardson Lucy (dRL) algorithm (Dell'acqua et al., 2010).

1.2.1.5 *Tractography*

Estimates of local fibre orientations are sequentially modelled by tractography algorithms to generate streamlines of fibre propagations (Figure 1-1E) (Farquharson et al., 2013; Jbabdi et al., 2015). The development of sophisticated yet user-friendly pipelines has led to an upsurge of research groups employing tractography approaches. For purposes of whole-brain tractography (Figure 1-1F), propagation is repeated at brain tissue voxels to generate comprehensive streamline maps. This procedure is performed until a specific threshold criterion has been met, such as the maximum number of fibres. Streamlines ideally propagate within white-matter tissue, with start/end points situated upon or near the grey/white-matter interface (Smith et al., 2012a).

1.2.1.6 *Choice of tractography algorithm and acquisition sequences*

Our understanding of the spatial and topological features of human brain networks are further influenced by the choice of tractography algorithms. Deterministic algorithms track propagations along the singular peak (Mori et al., 1999; Mori and van Zijl, 2002), with areas containing multiple fibre-orientations pathways either not fully reconstructed (false negatives) or erroneously inferred (false positives) (Figure 1-1E; left) (Jones et al., 2013). Probabilistic tractography (Aganj et al., 2011; Behrens et al., 2003) is typically employed with a more complex diffusion model such as CSD to allow multiple possible propagations through each voxel via the representation of uncertainty of the most likely tract directions via the fODF (Figure 1-1E; right) (Tournier et al., 2010; Tournier et al., 2012). CSD-probabilistic methods are qualitatively shown to reconstruct fibre-bundles more sensitively compared to known anatomy - especially with those of high-angular trajectories (Jeurissen et al., 2011; Tournier et al., 2012). A trade-off for the increased

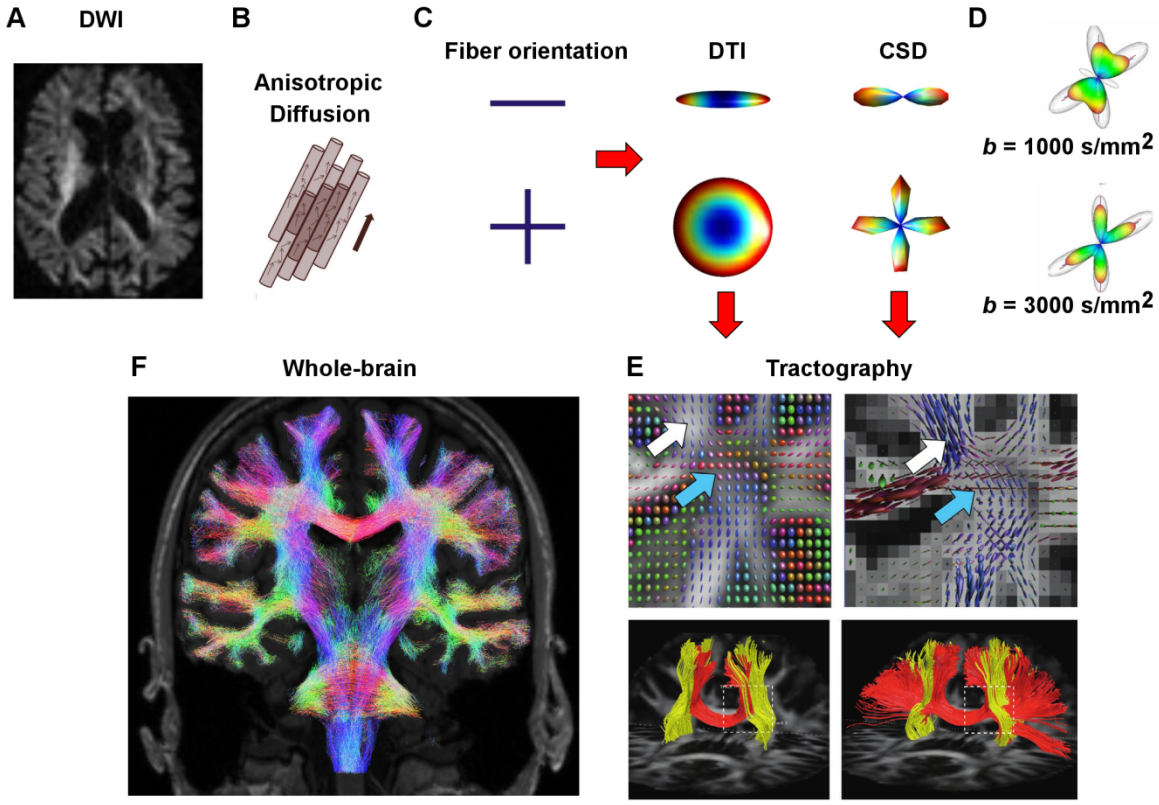

Figure 1-1: *Schematic of the steps involved in fibre reconstruction from dMRI data. A, DWI of an axial slice for a representative elderly subject. B, Diffusivity of water molecules (arrows) showing anisotropy (restricted). C, DTI (middle panel; ellipsoids) and CSD (right; spherical harmonic functions) models for estimates of axonal orientations (left; sticks). DTI resolves the orientation for coherently-organised single-fibre populations (top), whereas it fails for inferring "crossing-fibre" populations (bottom) relative to CSD. D, FODs of CSD approaches at different gradient strengths, with higher b-values (bottom panel) sharpening the angular profile relative to low b-values (top). E, Fibre-orientation estimates (top) and subsequent fibre-tracking (bottom) of CSD (right) and DTI-based (left) approaches for the corona radiata. For populations of "crossing-fibres" (cyan) only CSD separates the individual orientations. F, CSD and probabilistic whole-brain tractography, with streamlines overlayed on the coronal slice of the subject's anatomical T1-weighted scan.*

Adapted from (Bastiani and Roebroeck, 2015; Descoteaux et al., 2009; Maffei et al., 2015)

sensitivity of probabilistic methods is "jittering" tracks which can lead to erroneous false positives (Thomas et al., 2014; Zalesky et al., 2016). The trade-off between the sensitivity of probabilistic methods versus the specificity of deterministic methods is an important issue that remains to be resolved.

High-angular-resolution diffusion-weighted imaging (HARDI) acquisition schemes are essential for reconstructing complex fibre-configurations (Tournier et al., 2011; Tuch et al., 2002). Within HARDI sequences the diffusion weighting (*b*-value; gradient strength and diffusion time) (Le Bihan and Breton, 1985) is typically increased to magnitudes of $b = 2000\text{-}3000$ s/mm^2 (Descoteaux et al., 2009; Tournier et al., 2013). Longer diffusion times result in complete signal loss along the extra-axonal compartment, with increased sensitivity to anisotropic diffusion (i.e. dephasing) within intra-axonal compartments (Bastiani and Roebroeck, 2015; Jones et al., 2013). Whilst the angular resolution of the diffusion profile is sharpened (Descoteaux et al., 2009; Tournier et al., 2013) (Figure 1-2D), the signal-to-noise ratio is however much lower and sequences are more suspectible to noise artifiacts (Andersson and Sotiropoulos, 2016; Pannek et al., 2012a; Zalesky et al., 2016). A large number of diffusion-gradient pulses are also required with HARDI sequences to ensure comprehensive sampling over unique fibre-directions (Jones et al., 2013). Current recommendations for studies aiming to reconstruct complex fibre-configurations are to acquire at least 45 directions over the whole sphere (Tournier et al., 2013). Implementation of HARDI protocols within clinical settings is still relatively rare (Farquharson et al., 2013) due to the time constraints of such sequences and the complexity of the ensuing analyses.

1.2.1.7 *Constructing the human connectome*

The start/termination points of whole-brain streamline maps (Figure 1-2A) are combined with a pre-defined parcellation of the grey matter to identify fibre propagations which connect node pairs. The resultant network of connectivity edges is known as the structural connectome (Figure 1-2C and Figure 1-2D) (Sporns, 2013b; Sporns et al., 2005). These pre-defined parcellation regions should ideally represent clusters of grey-matter voxels within spatially homogenous areas or with a similar functional specialization (i.e. visual vs motor areas) (Fornito et al., 2013; Zalesky et al., 2010b).

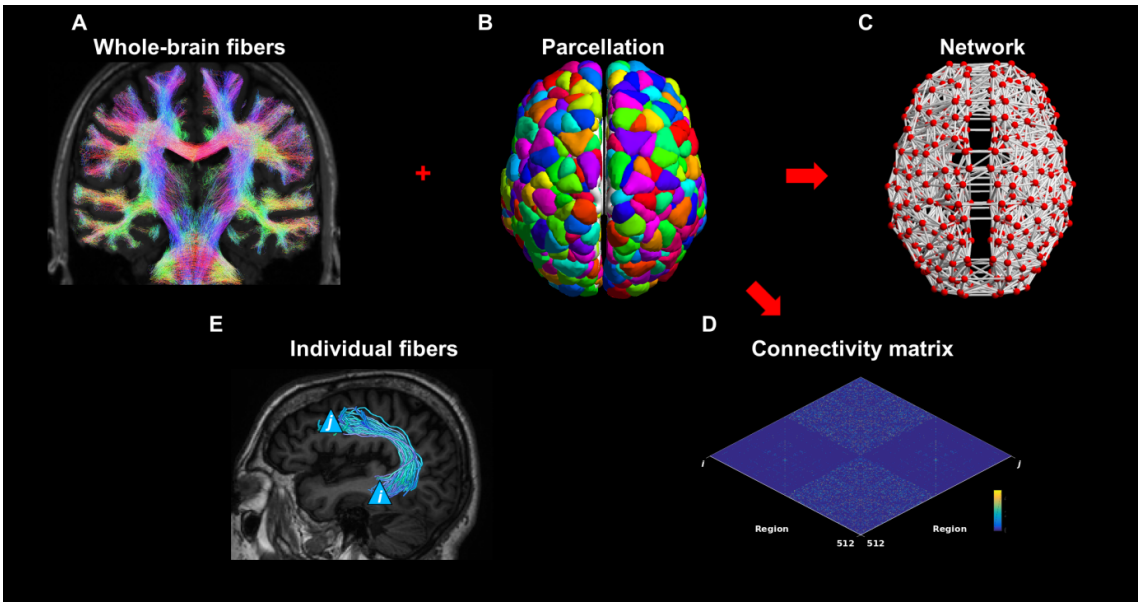

***Figure 1-2**: Construction of structural connectomes. Whole-brain fibres (**A**) are combined with anatomical parcellation regions (**B**). A connection is identified if a streamline starts and terminates within regions i and j respectively, represented upon a network-perspective (**C**; lines linking circles), or as a weighted matrix entry (ith-column and jth-row) within an adjacency graph W (**D**). The top and lower quadrants of W show the high-density of intra-hemispheric connections, whilst the left and right panels indicate relatively very few inter-hemispheric edges (as shown in **C**). E, The fibre propagation between regions i and j denoted by W_{ij}*

The strength of connectivity between node pairs can be weighted by the number of intersecting streamlines, despite the issues inherent with tractography-derived counts (Calamante et al., 2015; Jones et al., 2013). Alternatively, connectomes can be weighted by the mean FA value for voxels along the intersecting fibres. Notwithstanding the controversies regarding DTI-indices, streamline count is correlated to a greater extent with the projection strength of interareal pathways derived by macaque tract-tracing methods (van den Heuvel et al., 2015). Regardless of the approach to reconstructing the diffusion signal, or the choice of tractography scheme, the resultant connectomes are undirected. That is, dMRI cannot distinguish afferent from efferent fibres – a substantial current limitation (Jones et al., 2013).

1.2.2 Functional brain networks

The most commonly employed neuroimaging technique in the construction of whole-brain functional networks is fMRI. Whilst research on connectivity patterns using EEG and MEG is burgeoning, this work here focuses upon fMRI methods.

1.2.2.1 *Functional magnetic resonance imaging*

fMRI sequences measure changes in the contrast of blood oxygen-level dependent (BOLD) signals. BOLD signals are produced by the balance of oxyhaemoglobin and deoxyhaemoglobin in blood vessels (Ogawa, 2012; Ogawa et al., 1990): Local neural activity leads, through pathways poorly understood, to a transient dilation of blood vessels and an influx of oxyhaemoglobin. This changes the ratio of oxy- to- deoxyhemoglobin and resultantly a transient change in the local BOLD contrast (Ogawa, 2012; Ogawa et

al., 1990). Psychological processes leads to the observable accentuation of BOLD signals in specific cerebral areas – hence the BOLD signal is an indirect measure of local evoked neural activation (Belliveau et al., 1991; Ogawa et al., 1992). The temporal co-dependence (i.e. correlation) of activation patterns between spatially-distinct brain-regions defines their functional connectivity (Friston, 1994; Friston et al., 1993; Friston et al., 1994). Patterns of increased functional connectivity (i.e. shared co-activation) between brain-regions may reflect the transfer of neural communication between these areas, or simply the co-activation of those areas driven by other sources.

1.2.2.2 *Resting-state functional magnetic resonance imaging*

Spontaneous brain activity is observed when subjects are resting and not attending to a task (Biswal et al., 1995; Biswal et al., 1997), supporting the notion of ongoing patterns of neural communication during internally directed thought (Fox and Raichle, 2007; van den Heuvel and Hulshoff Pol, 2010). Resting-state fMRI (rs-fMRI) sequences detect the spontaneous fluctuations of BOLD signals: Individuals are typically asked to close their eyes and not think of anything in particular, or rest with their eyes fixating on a cross hair. The influence of cardiac (Chang et al., 2009) and respiratory fluctuations (Birn et al., 2008) remains, however, contentious, as does the meaning of changes in the background global signal and the impact of head motion (Fox and Raichle, 2007; van den Heuvel and Hulshoff Pol, 2010). However, simultaneous electrophysiological recordings have supported the neuronal predominance of rs-fMRI signals (Bianciardi et al., 2009; Shmuel and Leopold, 2008; Shmuel et al., 2002). Post-acquisition pipelines (Cox, 1996; Jenkinson et al., 2012; Yan and Zang, 2010) are designed to remove non-neuronal oscillations from the BOLD signals, such as the sampling of low-frequency spontaneous

fluctuations (0.01-0.1 Hz) (Cordes et al., 2001; Cordes et al., 2000) and the regression of nuisance variables.

As with structural networks, individual grey matter voxels are grouped into predefined parcellation regions. Functional connectivity patterns from task or resting state acquisitions are combined with parcellation templates to construct functional brain networks, which because of the nature of linear correlations, are fully-connected and undirected (Fornito et al., 2013; Sporns, 2013b)

1.2.2.3 *Resting-state networks*

The highly-correlated patterns of intrinsic fluctuations in resting state fMRI data support the relevance of spontaneous BOLD signals. Highly-correlated areas coincide with constellations of brain-regions that share anatomical features and functional specialization (i.e. visual cortices) (Damoiseaux et al., 2006; Fox et al., 2005; Smith et al., 2009). Such spatio-temporal patterns reflect the intrinsic functional organisation of the brain, with highly-correlated areas forming resting-state networks (RSN's). RSN's are typically identified through either the functional correlations of seed-regions of interest, or data decomposition approaches such as Independent Components Analysis (ICA) (Beckmann et al., 2005; McKeown et al., 1998). RSN's highly replicated across the literature include: The heteromodal default-mode network (DMN), sensorimotor, attention-related, primary visual, extra-striate visual, fronto-parietal (bi-lateral) cognitive-control areas, and lastly, auditory networks (Figure 1-3) (Beckmann et al., 2005; Damoiseaux et al., 2006; Smith et al., 2009).

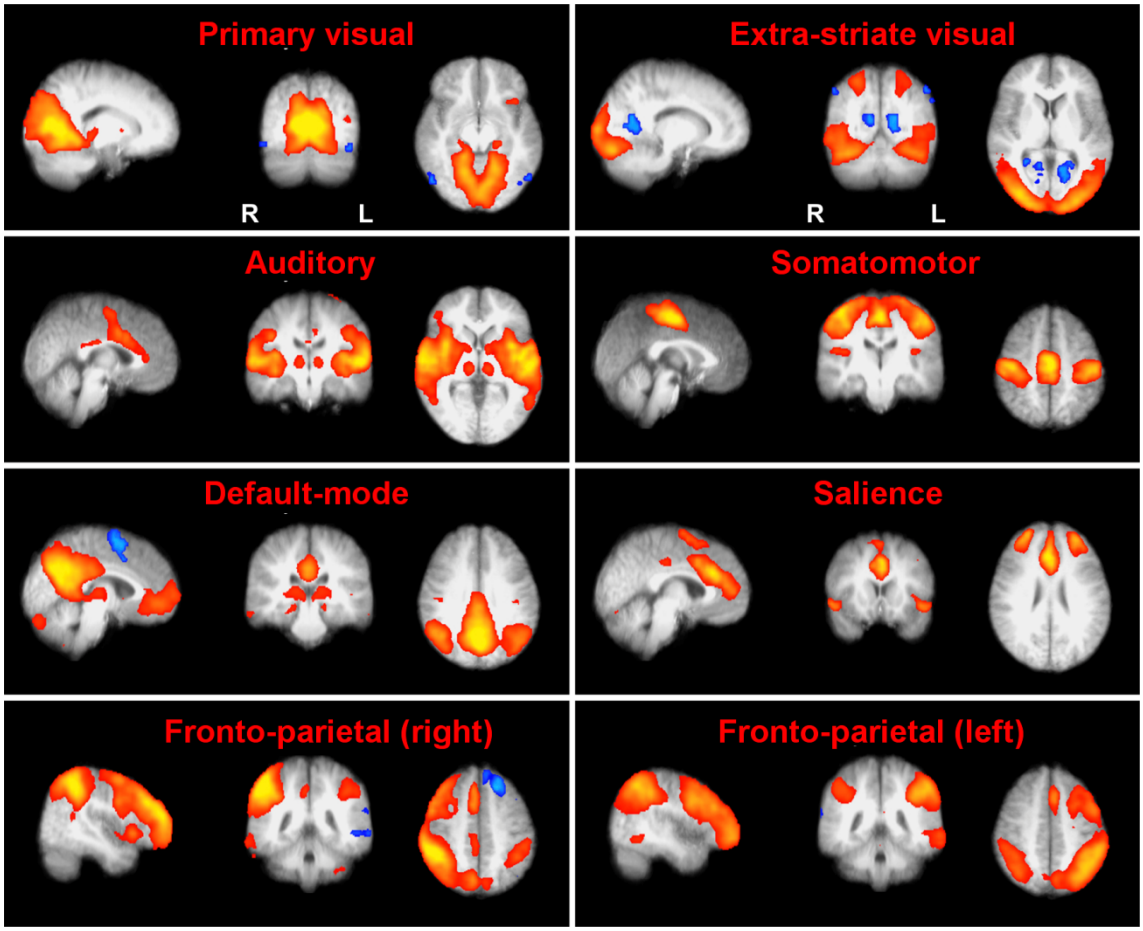

Figure 1-3: *RSN's most commonly identified across rs-fMRI investigations. Z-score maps are overlayed on image, with warmer colours expressing the regions greater contribution to the RSN. Images are presented from sagittal (left column), coronal (middle) and axial (right) perspectives, with the left hand side corresponding to the right-hemisphere.*

Figure adapted from (Beckmann et al., 2005)

1.2.2.4 *Default-mode network*

Brain-regions comprising the DMN include inferior and medial (i.e. posterior cingulate, precuneus) parietal regions, and also medial (i.e. anterior cingulate, medial prefrontal

gyrus) prefrontal cortices (PFC). These regions exhibit higher levels of BOLD signal intensity and functional connectivity in resting state conditions compared to task performance and are have thus been denoted the brain's "default" state (Buckner et al., 2008; Greicius et al., 2003). Traditional fMRI studies reveal DMN activity to attenuate during demanding tasks which require cognitive or executive-control. Decreased functional connectivity is also observed to task-engaged areas such as fronto-parietal centers (Greicius et al., 2003; Lawrence et al., 2003; McKiernan et al., 2003). The integrity and functioning of DMN regions are associated with other higher-order functions such as episodic memory and self-referential processing (Northoff et al., 2006; Raichle, 2015; Seghier, 2013; Utevsky et al., 2014).

1.3 Macroscopic features of human brain networks

1.3.1 Calculation of complex brain network properties

The utilization of graph-theoretical tools in the analysis of structural and functional connectivity patterns affords the quantification of complex brain network properties. Aptly known as graph-metrics (Rubinov and Sporns, 2010), these metrics have revealed complex topological, spatial, and spatio-temporal macroscopic features inherent within functional and structural brain networks (Bullmore and Sporns, 2009; Sporns, 2013b). Graph-metrics define individual elements (nodal-level) of brain-regions embedded within the network, as well as the global architecture of whole-brain interactions (Rubinov and Sporns, 2010). Nodal metrics typically implemented in connectomic investigations include:

1.3.1.1 *Nodal graph metrics*

- *Degree centrality* (Figure 1-4A): Number of binary links that brain region *i* shares with the network. The weighted degree can be calculated by the total sum of all weighed connections for *i*
- *Betweenness centrality*: Fraction of shortest paths between all pairs of brain regions that pass through *i*
- *Clustering coefficient* (Figure 1-4B): The fraction of neighbouring brain areas linked to region *i* that are connected to one another, forming triangles
- *Characteristic path length* (Figure 1-4C): Average shortest path length (minimal number of discrete steps) required to link brain-region *i* in the network
- *Efficiency*: The inverse of the characteristic path length for brain-region *i* in the network

Conventional global graph-metrics employed are typically aggregates of nodal measures over all constituent regions. Their definitions are redundant and hence not listed here.

1.3.2 Small-world characteristics of brain networks

Networks demonstrate a "small-world" topology if their interactions preserve the cliquey/high-clustering of lattice-like graphs, but also display the long-range connections characteristic of random networks (Figure 1-5A) (Watts and Strogatz, 1998). As with many other real-world networks, both structural and functional brain networks exhibit small-worldness (Bassett and Bullmore, 2006; Sporns, 2013b; Sporns and Zwi, 2004).

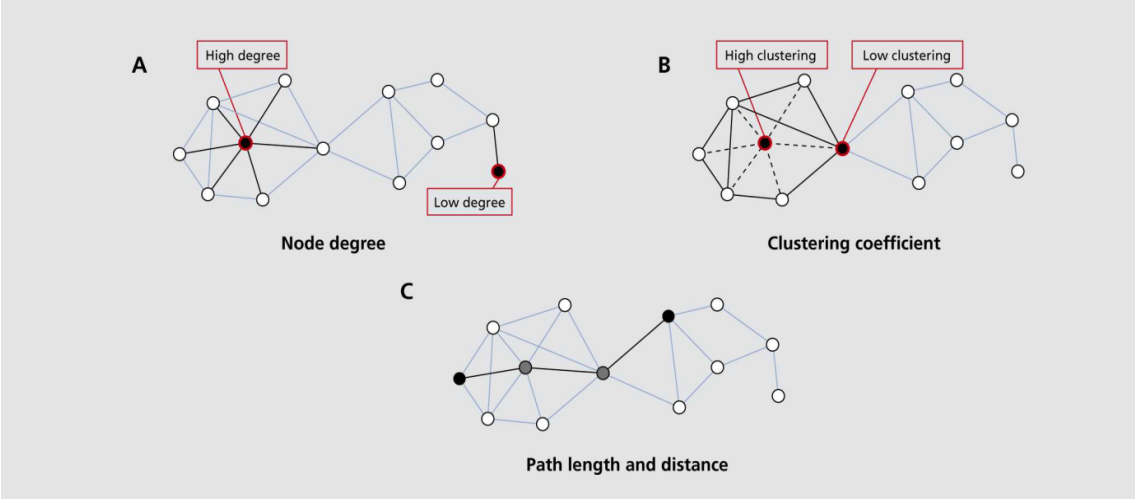

Figure 1-4: Representation of key graph-metrics employed in brain network investigations. A graph is represented by its constituent edges (lines) linking nodes (circles). A, Degree centrality corresponding to the number of links (bold) attached to each node, shown for highly-connected (left; degree of five) and sparsely-connected nodes (right; degree of one). B, Clustering coefficient, relating the extent each nodes' topological neighbours are also linked. Connections of highly-clustered regions (left) form multiple triangles (dashed) with other regions. C, Shortest number of paths required to link two nodes to each other, shown as three steps along the bold line.
Adapted from (Sporns, 2013b)

These observed features reflect the underlying structural organisation, which shapes the opposing requirements for *functional integration* and *functional segregation* in the brain (Friston et al., 1996a; Friston et al., 1995; Sporns, 2013a).

1.3.3 Functional segregation

As with lattice-like graphs, the connections of brain networks are highly-clustered or cliquey - as reflected through the *global clustering coefficient* (average nodal clustering coefficient) (Figure 1-5A; left panel). These cliques speak to the brain's modular

organisation (Meunier et al., 2010; Sporns and Betzel, 2016): Regions densely-connected amongst themselves form clusters of communities which share a common functional specialisation or spatial neighbourhood (e.g. visual cortices) (Honey et al., 2007; Rubinov and Sporns, 2010) (Figure 1-5D). Sparser connections connect with other communities, indicating their *functional segregation* within the brain network (Figure 1-5B; left). The *functional segregation* of specialised brain-regions hence confers the rapid and efficient spread of information processing for task-demands (Bullmore and Sporns, 2012; Sporns, 2013b).

1.3.4 Functional integration

Like random graphs, brain networks also exhibit many short paths (i.e. *low characteristic path length*) that link brain regions (Figure 1-5A; right) (Bassett and Bullmore, 2006). These short-communication paths ensue a high *global efficiency* (inverse of the characteristic path length over the whole-network) of brain networks, indicating a high capacity for information transfer (Rubinov and Sporns, 2010). The presence of a few long-range connections ensures the *functional integration* of *segregated*/specialized areas (Figure 1-5B; right) (Sporns, 2013a), which supports complex perceptual and cognitive processes (Friston et al., 1995; Tononi, 2004).

The macroscopic features of "small-world" brain networks flesh out the opposing requirements for *functional integration* and *segregation* in the human brain. This delicate balance may optimise brain function critical for human cognition and behaviour (Figure 1-5C) (Bullmore and Sporns, 2012; Sporns, 2013a). Within psychopathological states, for example, increased *functional segregation* may reflect isolated neural processing and

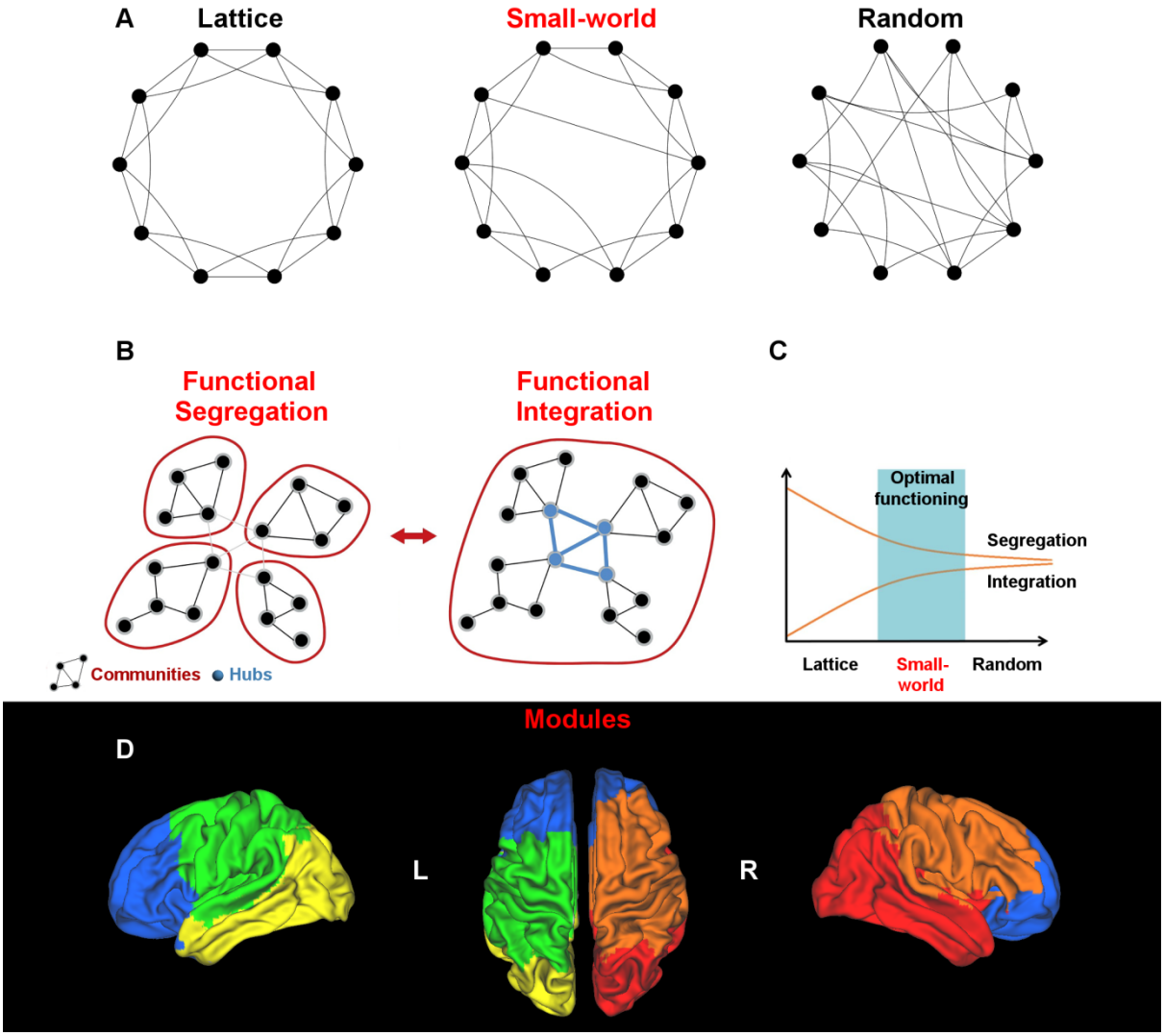

Figure 1-5: *Modular, small-word features of brain networks. A, Representations of connections (lines) between nodes (black circles) of different graphs, showing small-world networks (middle panel) preserve the high-clustering of lattice-like graphs (left), whilst also short communication paths of random networks (right). B, Graph illustrations of functional segregation (left) and functional integration (right) in brain networks. Connections clusters in communities (left; red borders) reflective of segregation, but are integrated to other communities by efficient short-paths. C, Optimum brain state (shading) achieved by balancing segregation and integration. D, Communities (different colours) identified by community-detection algorithms on human structural networks.*

Adapted from (Aerts et al., 2016; Perry et al., 2015; Sporns, 2013a)

the "dysconnectivity" of spatially-distributed areas (Catani, 2005). On the other hand, highly-integrated random networks could lead to overly rigid and inflexible neuronal processes (Fornito and Bullmore, 2015; Fornito et al., 2015).

1.3.5 Relation between structural and functional brain networks

The anatomical landscape has been demonstrated to shape the brain's functional interactions: Within healthy adults, strong structural connectivity is predictive of greater functional connectivity patterns (Hagmann et al., 2008b; Honey et al., 2009; Skudlarski et al., 2008), while weaker functional connections occurs over long-range distances (Goñi et al., 2014; Hermundstad et al., 2013). The topology of structural path interactions also predicts functional connectivity: The presence of local detours along clustered-cliques of brain-regions are associated with increased functional connectivity (Goñi et al., 2014). This boosting resonates with the enhanced functional connectivity within densely-connected and segregated communities (Betzel et al., 2013; Hagmann et al., 2010; van den Heuvel and Sporns, 2013a). However, structural-functional relations are not one-to-one, as strong and variable functional connections are observed over indirect structural linkages (Honey et al., 2009; Mišić et al., 2016). The non-overlapping patterns nonetheless support the proposal that the relatively stable structural architecture shapes variable and diverse functional connectivity patterns (Honey et al., 2010; Mišić et al., 2016).

1.3.6 Neural brain dynamics

Throughout this work, functional connectivity estimates predominately refer to "static" inter-regional correlations averaged over the entire rs-fMRI scan (Zalesky et al., 2014). Focusing upon "windows" of shorter time-courses has uncovered the rich spatiotemporal dynamics of RSN's (Chang and Glover, 2010; de Pasquale et al., 2015; Deco and Jirsa, 2012; Smith et al., 2012b; Zalesky et al., 2014): At rest, brain regions temporally decouple from their core respective subsystems and synchronise with other regions. These dynamic brain patterns are attributed to the system exploring a broad diversity of functional repertoires (Deco et al., 2013; Ghosh et al., 2008; Honey et al., 2007).

Structural connectomic data can be integrated into computational models that simulate local neuronal (i.e. network nodes) activity along axonal pathways (i.e. edges). In brief, dynamic brain fluctuations are revealed within critical operating points at the brink of transition to ordered brain states (Deco and Jirsa, 2012; Deco et al., 2013). The integrative features of highly-connected structural "hub-regions" have been shown to be critical for synchronization and flexibility of such simulated neural patterns (Alstott et al., 2009; Gollo et al., 2015; Senden et al., 2014; Senden et al., 2012; Váša et al., 2015). These findings reinforce the importance of the anatomical scaffold to large-scale dynamic neuronal interactions.

1.3.7 Hub-regions

The degree-distribution (i.e. number of links) of structural brain-regions shows a non-Gaussian shape (Gong et al., 2009a; Hagmann et al., 2007; Zalesky et al., 2010b). These distributions (Barabási and Albert, 1999) reveal the presence of "hubs" that are more

highly-connected than other regions (van den Heuvel and Sporns, 2013b). Structural hub-regions particularly overlap with DMN regions, orbitofrontal, and lateral prefrontal areas (Figure 1-6; left) (Gong et al., 2009a; Hagmann et al., 2008b; van den Heuvel and Sporns, 2013b). Structural hubs also exhibit a high-degree of spatial overlap with hub areas identified from functional connectivity patterns (Figure 1-6; right) (Buckner et al., 2009; Power et al., 2013). Spatially-similar areas also exhibit other definitions of a region's structural "hubness", such as *betweenness centrality*, *nodal efficiency*, and *participation index* (i.e. extent of inter-modular links) (Gong et al., 2009a; Hagmann et al., 2008b; van den Heuvel and Sporns, 2013b). This reveals that these hub-regions are not only highly-connected, but are also critical sources for *functional integration* within the human brain.

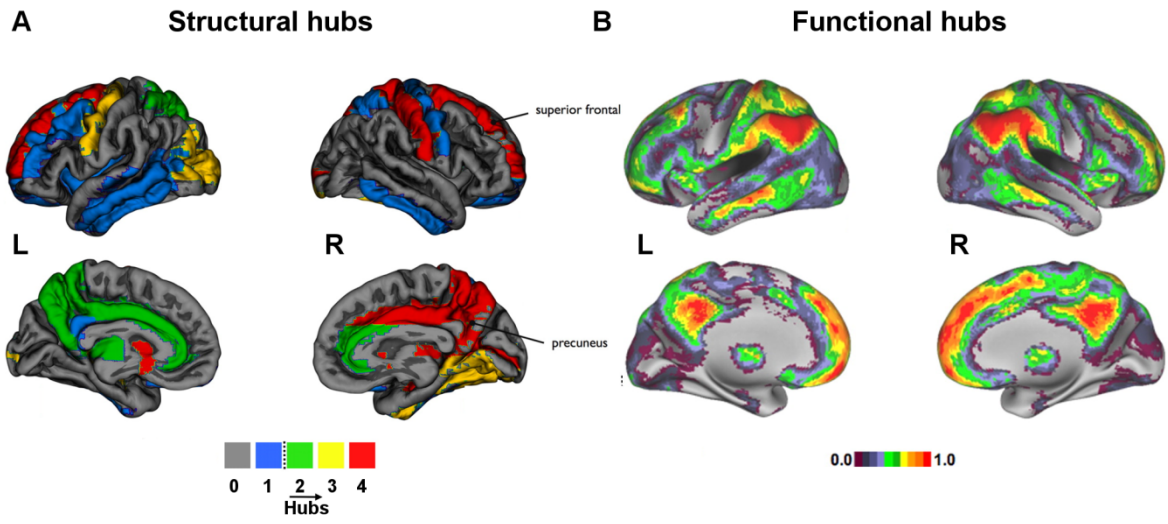

Figure 1-6: *Hub-regions across structural and functional human brain networks. A, Structural hub-regions identified by high-ranking accumulated scores over multiple nodal metrics of "hubness", with warmer colours indicating increased hub-structure (hubs shown from green to red). B) Intrinsic functional connectivity strength maps derived from rs-fMRI data, with warmer colours indicating increased connectivity of hub-regions.*

Adapted from (Buckner et al., 2009; van den Heuvel et al., 2010)

1.4 Features of hub-regions within structural and functional brain networks

1.4.1 The connections between hub-regions form a rich-club

The wiring amongst hub-regions appears to be densely-connected, forming a core anatomical backbone known as the "rich-club" (van den Heuvel and Sporns, 2011) (Figure 1-7A; left). This term denotes the preferential wiring between "rich-club" regions, which are more highly-connected than expected by their degree alone. Rich-club organisation is assessed by the rich club coefficient (ϕ), derived from the relative ratio of connectivity within brain-regions of degree-values > k (Figure 1-7B). The robustness of rich-club organisation as a general principle finds support through its presence in a number of non-human nervous systems, including the nematode worm (Towlson et al., 2013), and also the macaque, cat and mouse brains (Buckner et al., 2009; de Reus and van den Heuvel, 2013; Fulcher and Fornito, 2016; Harriger et al., 2012; van den Heuvel et al., 2015).

1.4.2 Rich-club connections are pivotal for global brain communication

Identification and classification of rich-club regions allows connections of the structural connectome to be segregated into different types: Rich-club (linking rich-club regions), feeder (rich member to non-rich region), and local (non-rich to non-rich) connections (Figure 1-7A) (van den Heuvel et al., 2012). Relative to the other connection classes, rich-club connections display greater streamline density, higher-levels of microstructural organisation (i.e. FA, MD), myelination (i.e. magnetization transfer ratio), and longer physical fibre-lengths (Collin et al., 2014b; van den Heuvel et al., 2012; van den Heuvel

and Sporns, 2013a). Global brain communication appears to take advantage of these architectural features of rich-club connections: Models suggest that network traffic is disproportionately routed along the rich-club for the shortest communication path between one region and another (van den Heuvel et al., 2012) - and also for connections bridging segregated functional communities (de Reus et al., 2014; de Reus and van den Heuvel, 2013; van den Heuvel and Sporns, 2013a). Brain communication paths are also observed to follow ordered sequences of specific connection types, known as "path motifs". The most over-representative motifs are those between lower-degree regions, for which traverse and exit through the rich-club (de Reus and van den Heuvel, 2013; van den Heuvel et al., 2012).

Global workspace theories postulate that a specific functional subsystem does not underlie a particular cognitive function (Dehaene et al., 1998; Dehaene and Naccache, 2001). These theories instead propose that a core system characterised by complex interactions between the segregated subsystems gives rise to perceptual and cognitive brain states. This core system resonates with the wiring patterns of the rich-club, for which neural signalling appears to take advantage of its efficient, short communication paths (van den Heuvel et al., 2012). The projections of rich-club connections allow the integration of multiple functional sources, and may thus reflect a neural substrate of this "global workspace" (van den Heuvel and Sporns, 2013a).

1.4.3 Dynamic properties of hub-regions

As reviewed above, temporally resolved rs-fMRI data reveals the presence of dynamic (nonstationary) connectivity patterns (Calhoun et al., 2014). Such patterns have also been

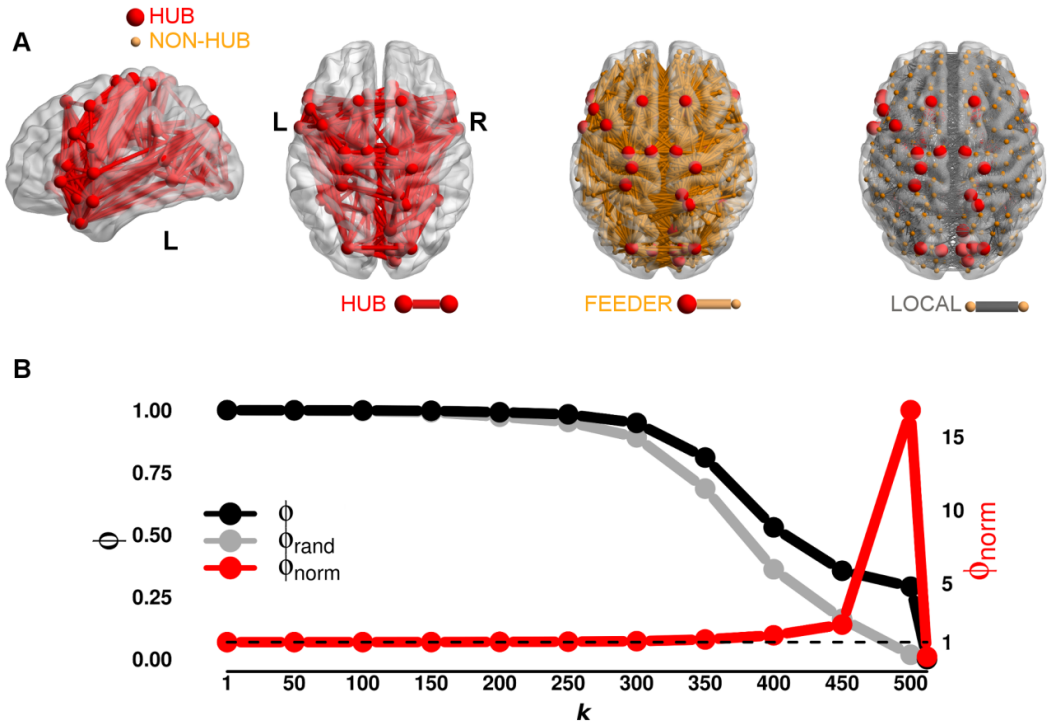

***Figure 1-7**: Identification of hub-regions and rich-club architecture in structural brain networks. A, Brain regions are identified either as hubs (red circles) or non-hubs (orange), on virtue of their highly-connected structure (i.e. degree). Hub-identification allows structural connections to be classified as either hub-connections (red lines; linking hub-to-hub); feeder (orange; hub-to-non-hub) or local links (grey; linking non-hubs). B, Rich-club coefficients across k-levels (i.e. degree-levels) for empirical (ϕ; black), degree-preserving randomised networks (ϕ_{rand}; grey), and the ratio of ϕ over ϕ_{rand}, yielding ϕ_{norm} (red). Rich-club architecture is present if rich-club connectivity within ϕ exceeds ϕ_{rand}, reflected by ϕ_{norm} values (right y-axis) greater than 1 (dashed).*

reported in MEG data (de Pasquale et al., 2015). The links fluctuating most frequently appear to be long-range inter-modular connections - particularly for projections of DMN and fronto-parietal hub-areas (Zalesky et al., 2014). Interestingly, these fluctuations are also characterised by changes in the spatiotemporal structure of connectivity patterns: Intermittent periods of topological efficiency are observed, with the links of such hub-regions more pronounced in brain states of high-efficiency (de Pasquale et al., 2015;

Zalesky et al., 2014). The dynamic behaviour of hub-connections during resting-state supports task-based findings of their capacity to flexibly reorganise under increasing cognitive demand (Bassett et al., 2011; Cocchi et al., 2013; Zalesky et al., 2014). It is thus apparent that under both resting and task-conditions, the dynamic behaviour of hub-regions allows the efficient integration of information from multiple functional sources.

1.4.4 Wiring and metabolic cost of rich-club connections

Brain networks are thought to minimise wiring costs, whilst maximising computationally advantageous features (Bullmore and Sporns, 2012). For example, the "small-worldness" (i.e. short-range connections) within brain networks is indicative of the drive to minimise the costs of spatial embedding (Roberts et al., 2016c). The metabolic cost of the human brain, which is strikingly disproportionate to the total body weight (Karbowski, 2007), is primarily expended on the maintenance of neural signalling (Attwell and Laughlin, 2001). Genetic co-expression of rich-club connections is interestingly strongest for genes regulating the oxidative synthesis and metabolism of adenosine triphosphate utilization (ATP) (Fulcher and Fornito, 2016). This specific genetic coupling of rich-club connections, along with their considerable flow of network traffic, implicates their greater metabolic demand during neural signalling (Bullmore and Sporns, 2012; Fulcher and Fornito, 2016). Relative to non-hub areas, hub-regions also exhibit greater levels of aerobic glycolysis (Collin et al., 2014b), glucose metabolism (Tomasi et al., 2013) and regional blood flow (Liang et al., 2013). However, the increased metabolic and wiring costs incurred by rich-club architecture may be offset by their efficient-routing patterns and densely-myelineated axons (Bullmore and Sporns, 2012; Collin et al., 2014b).

1.5 Summary of graph-theoretical applications to human brain networks

Connectomic approaches have identified unique features of large-scale neural architecture, which is thought to be critical for shaping neural dynamics. The early potential of graph-theoretical applications was realised with the seminal discoveries of "small-world" features: These features reflect the opposing requirements for *integration* and *segregation* of cognitive information processing. Investigations have not yet had the opportunity to utilize recent developments in dMRI acquisition and streamline reconstruction methodology. The fledging promise of connectomic approaches was further fostered by the discovery of the anatomical core backbone – wiring patterns which are critical for integrated, efficient global brain communication. The functional repertoire of the rich-club translates beyond "static" network features, with the capacity of hub-connections to dynamically transition between functionally-specialized areas. Changes to these brain network features may reflect changes to the delicate balance of functional integration and segregation. The subsequent changes to brain functioning are theorised to underlie age-related cognitive changes and psychiatric conditions, which I now review.

1.6 Connectomic applications to normal ageing

1.6.1 Cognitive changes associated with normal ageing

Gradual changes in cognitive ability characterise normal human experience for individuals as they progress through their lifetime. Cognitive ageing is considered distinct from the declines associated with the neurodegenerative aspects of Alzheimer's Disease (AD), or its prodromal stage, "Mild Cognitive Impairment" (MCI) (Deary et al., 2009).

Changes in cognitive performance occur across a swathe of neuropsychological tests, which comprise domains such as episodic memory, working memory, reasoning, visuospatial ability, and processing speed (Deary et al., 2009; Hedden and Gabrieli, 2004; Park and Reuter-Lorenz, 2009). All these domains reflect "fluid-based" mental abilities dependant on an individual's cognitive processing ability. Interestingly, from early adulthood, age-related reductions appear to be similar across these domains (Deary et al., 2009). In contrast, cognitive functions accrued (i.e. "crystallized") over the lifespan - such as verbal abilities and semantic knowledge – are relatively preserved until later life (Park and Reuter-Lorenz, 2009).

The sensitivity of "fluid-based" domains have led to postulations of ageing as being characterized by changes to cognitive functions which require large-scale neural processing (Grady, 2012; Park and Reuter-Lorenz, 2009). Processing speed, one of the functions most sensitive to changes with age (Hoogendam et al., 2014; Schaie, 1996), also appears to account for varying performance across the other fluid domains (Baltes and Lindenberger, 1997; Finkel et al., 2007). In turn, it has been further postulated that an individual's slowing is a general cognitive factor that underlies ageing changes (Salthouse, 1996; Salthouse, 2000). However, marked inter-individual differences exist in the trajectory of age-related changes - this complexity is exacerbated by the contribution of general medical, genetic, vascular, physiological, dietary and lifestyle factors (Deary et al., 2009). Elucidating macroscopic brain features that are tightly coupled with ageing is imperative to identify potential treatments which can modify these cognitive changes. Even "healthy" cognitive changes impact on the performance of everyday activities and occupational duties (Fisher et al., 2014; Salthouse, 2012). Identification of brain-behaviour patterns associated with normal ageing are also

important to disentangle their trajectories from the deleterious declines inherent within AD and MCI.

1.6.2 Mild cognitive impairment and Alzheimer's disease

The most common form of dementia, AD, is a debilitating neurodegenerative disorder characterised by progressive declines in episodic memory (Ballard et al., 2011). It is estimated that approximately 5% of individuals aged 60 or above suffer from dementia. The years lived with disability (YLD) from AD exceed medical conditions such as cancer and cardiovascular disease (World Health Organization, 2003). In the later stages of AD, the more advanced impairments in domains such as memory, executive functioning, language, and visuospatial ability lead to a loss of overall functioning (Salmon and Bondi, 2009; Weintraub et al., 2012). AD patients also experience a host of neuropsychiatric disturbances such as apathy, depression, anxiety, agitation, and psychosis (Mega et al., 1996; Porsteinsson and Antonsdottir, 2015). The forgetting of faces or names is also distressing to caregivers. As the risk for late-onset AD progressively increases with age (Blennow et al., 2006; Plassman et al., 2007), the ageing global population represents an impending international health epidemic and is thus an utmost research priority: The prevalence of AD within the United States alone is expected to more than double by 2030 (Federal Interagency Forum on Aging Related Statistics, 2004). Although there being no clear pathogenic marker for the development of AD, some individuals are more genetically susceptible than others (Ballard et al., 2011). Apolipoprotein E (*APOE*) 4 allele carriers (Genin et al., 2011; Mahley et al., 2006) are estimated to have an odds ratio of 14.9 for disease-onset (Farrer et al., 1997; Mahley et al., 2006).

It has been proposed that the pathophysiological cascade of AD is triggered by the accumulation of amyloid-beta(Aβ) plaques (Jack et al., 2013; Jack et al., 2010). However, the precise pathogenic mechanisms are unclear. It remains disputed whether abnormal tau aggregation - causing neurofibrillary tangles (NFTs) - mediates the causal link between plaque accumulation and AD pathogenesis (Jack et al., 2010). Nonetheless, the clinical deterioration that characterises AD is widely assumed to be triggered by either of these pathological insults which lead to atrophy, the death of surrounding neurons, and synaptic dysfunction (Hardy and Selkoe, 2002; Jack et al., 2010). Although physicians currently lack an objective *in vivo* MRI tool to accurately detect AD neuropathology, MRI biomarkers are commonly utilized to assist in the diagnosis of the disease (Ballard et al., 2011). Traditional biomarkers of neuropathological Aβ accumulation include reduced cerebrospinal-fluid (CSF) amyloid-beta ($A\beta_{42}$) levels (Sunderland et al., 2003), and the binding of amyloid-based radiotracers with Positron Emission Topography (PET)-MRI (Duara et al., 1986). Binding patterns that are indicative of neuropathological accumulation of amyloid include the increased uptake of Pittsburgh Compound-B (PIB) (Klunk et al., 2004). Corresponding decreases in fluorodeoxyglucose 18F (FDG) reflect corresponding decreases in neuronal activity (Friedland et al., 1983). The atrophy of medial temporal structures such as the hippocampus and entorhinal cortex is a highly consistent MRI biomarker of AD (Scheltens et al., 1992). It's accuracy in classifying patients, however, has not reached that required for a diagnostic tool.

Cognitive dysfunction in older individuals that do not meet the threshold required for the clinical diagnosis of dementia is defined as Mild Cognitive Impairment (MCI) (Petersen et al., 2001; Petersen et al., 2009). Individuals with MCI have an increased rate of conversion to Alzheimer's (Fischer et al., 2007; Ward et al., 2012), and are hence

assumed to be experiencing a transitory, pre-clinical stage. Indeed, many of those with MCI demonstrate attenuated AD biomarkers (Belleville et al., 2014). However, the appropriateness of this "transitory" construct is questionable, as not all MCI individuals will later develop AD (Petersen et al., 2009). The variability in progression outcomes can be attributed to the large heterogeneity of MCI cohort. Conversion rates are even lower for general-population samples than those derived from clinical settings such as memory clinics (Ritchie et al., 2001). Furthermore, the operationalization of MCI is also disputed, as the cut-off criteria for MCI is influenced by normative psychological data, and the choice of clinical outcomes which define impairment (Bondi et al., 2014; Petersen et al., 2009). Attempts to reduce the heterogeneity within MCI cohorts centre upon classifying individuals into the following subtypes (Petersen et al., 2001; Petersen et al., 2009): amnestic MCI (aMCI) individuals with deficits in a memory-related domain; non-amnestic MCI (nMCI) characterised by complaints in a single non-memory domain; and multiple-domain MCI (i.e. md-aMCI or md-nMCI). Traditional MRI biomarkers are currently not sufficient on their own to accurately predict MCI classification or converters (Gomar et al., 2011; Shaffer et al., 2013; Trzepacz et al., 2014).

1.6.3 Traditional neuroimaging investigations of age-related changes

1.6.3.1 *Grey matter changes with normal ageing*

The neurobiological correlates of age-related changes in healthy elders have traditionally focussed on morphological changes derived from T1-weighted MRI (Rodrigue and Kennedy, 2011). Macroscopic reductions in regional GM size are typically greatest within prefrontal cortices, followed by parietal association areas, and subcortical structures (Dennis and Cabeza, 2008; Park and Reuter-Lorenz, 2009; Raz et al., 2005).

Decreased episodic memory and executive functioning with normal ageing have been associated with the macroscopic volumetric changes in hippocampal and prefrontal cortices, respectively. The regional specificity of other cognitive domains is less clear. Reductions in the thickness of cortical folds have also been revealed with age in similar areas (Hedden and Gabrieli, 2004; Peters et al., 2011). However, the specificity of regional age-related changes for both morphological measures is generally mixed or contradictory (Rodrigue and Kennedy, 2011).

1.6.3.2 *White matter changes with normal ageing*

Consistent with so called "dysconnection theories" of psychiatric neurological disorders (Catani, 2005), age-related cognitive changes have been proposed to emerge from a loss of integrity of WM fibre-bundles which support cognitive processes (Bennett and Madden, 2014; O'Sullivan et al., 2001). Patterns of decreased FA and increased MD are well-documented with normal ageing. Changes to these DTI-derived indices of "microstructural integrity" are assumed to reflect the demyelineation and axonal loss observed in post-mortem tissues (Peters, 2002; Tang et al., 1997). DTI-based correlates of normal ageing are typically measured within skeletonised populations of WM voxels and also reconstructed fibre-bundles. Processing speed and executive functioning observe the strongest associations across the cognitive domains for correlates of age-related WM changes (Bennett and Madden, 2014; Brickman et al., 2012; Salami et al., 2012; Ystad et al., 2011). However, the spatial specificity of WM areas/tracts that are most sensitive to the influence of age is still unclear. Whilst age-related changes are traditionally conceptualized to be more pronounced within anterior WM areas (Cabeza and Dennis, 2012; Sullivan and Pfefferbaum, 2003), the involvement of later-myelinating regions are

also implicated (Bartzokis, 2004; Brickman et al., 2012). Given WM patterns and age are both intricately linked to inter-individual cognitive differences, establishing causal relations remains a challenge. Partial support is although provided for WM changes to mediate the link between normal ageing and cognitive performance (Borghesani et al., 2013; Salami et al., 2012; Samanez-Larkin et al., 2012).

1.6.3.3 *Changes to large-scale communication patterns with age*

Traditionally, age-related variability in cognitive performance has been largely attributed to changes in particular anatomical pathways or structures (Andrews-Hanna et al., 2007). Univariate approaches however neglect the highly-complex patterns of neural interactions, and hence may only partially capture the complexity of normal ageing. Changes to large-scale neural communication across the lifespan were reported to account for age-related reductions in cognitive performance in a seminal investigation (Andrews-Hanna et al., 2007). Here, decreases in the measures of structural connectivity (decreased FA) and resting-state functional connectivity within the DMN were identified to be closely associated with age. Furthermore, changes to both connectivity patterns were associated with decreased performance across a range of cogntive domains (Andrews-Hanna et al., 2007). Age-related changes in large-scale communication is not surprising, given that the cognitive functions most sensitive to age are the fluid-based domains which require integrated, coordinated patterns of neural interactions. Age-related cognitive changes could thus be caused by changes in the balance of *functional integration* and *segregation* in structural and functional brain networks. Following this train of thought, multivariate connectomic approaches provide a more comprehensive tool to potentially understand the processes underlying normal ageing.

1.7 Structural connectomic investigations of healthy ageing

1.7.1 Structural connectomic changes with age

Only a few investigations of structural network changes with ageing have been conducted. Of those, the complexity of spatial and topological properties assessed are also limited. A relatively large study revealed a decreased efficiency of brain networks of healthy older adults (including MCI individuals) with increasing age (Wen et al., 2011). Global architectural changes with age suggest a decreased capacity for integrative brain communication, supported by a positive association between network efficiency and fluid-based performance (Wen et al., 2011). However, these structural brain networks were constructed and weighted from DTI-based approaches, limiting their interpretability. Lifespan studies have generally observed a decreased density of connections with age (Bennett and Madden, 2014; Gong et al., 2009b; Otte et al., 2015). Consistent observations of age-related changes in efficiency and other global architectural features (i.e. increased path length) further support a decreased integrative capacity of older brain networks underlying reductions in cognitive performance (Baggio et al., 2015; Otte et al., 2015; Zhao et al., 2015).

1.8 Functional network investigations of healthy ageing

1.8.1 Connectivity within large-scale systems

Investigations of functional resting-state connectivity patterns have predominately used RSN's identified through seed-based methods, or ICA. Functional connectivity has been consistently reported to decline with age within large-scale networks, independent of grey-matter changes. These changes to within-network functional connectivity patterns

appear to be partially associated with decreased cognitive functioning (Andrews-Hanna et al., 2007; Archer et al., 2015; Chan et al., 2014; Fjell et al., 2015; Geerligs et al., 2015; Onoda et al., 2012). Reductions are primarily observed within the DMN and other higher-order subsystems such as the fronto-parietal and salience networks (Betzel et al., 2014; Geerligs et al., 2015). These observations have been largely identified through univariate calculations of average or total functional connectivity strength. However, connectomic brain regions can be assigned to their respective functional affiliations. Consequentially, decreases in within-network connectivity have been revealed to be intricately associated with changes to the functional architecture: Less efficient local networks (Geerligs et al., 2015) and decreased modularity (Cao et al., 2014).

1.8.2 Connectivity between large-scale systems

Functional connectivity between large-scale networks increases with age (Betzel et al., 2014; Chan et al., 2014; Geerligs et al., 2015; Grady et al., 2016). Interestingly, these opposing patterns (within versus between) point to decreases in within-network functional integration as well as increases for between-network integrations. Given brain-regions within functional subsystems are linked by similar roles (Sporns, 2013a; van den Heuvel and Sporns, 2013a), increased between-network connectivity patterns with healthy ageing speaks to a reduction in functional specialisation/segregation (Chan et al., 2014). The decreased modularity of functional networks with age is a corollary of this decreased segregation/specialization (Betzel et al., 2014; Cao et al., 2014; Geerligs et al., 2015). Increased functional segregation is indeed associated with greater memory (age-regressed) domain performance (Chan et al., 2014), highlighting the functional relevance

of the delicate balance between integration and segregation. However, this effect was not seen for any other cognitive domain.

1.8.3 Whole-brain functional network changes with healthy ageing

Examination of changes to whole-brain functional connectivity patterns with healthy ageing are also relatively scarce. Lifespan (Cao et al., 2014; Tomasi and Volkow, 2012a) and between-group investigations (Achard and Bullmore, 2007) have revealed decreases in network efficiency and long-range connectivity with age. These macroscopic changes are indicative of decreased functional integration with ageing, which at first glance contradicts the increases in integration observed for between-network communication. Opposing patterns of increased/decreased integration with age could however implicate distinct actions of age-related changes on different sets of connections/subnetworks. Although lifespan studies allow a comprehensive representation of the influence of age and the possibility of non-linear changes (Cao et al., 2014), these study designs introduce a host of methodological considerations: The population size of the older participants included is typically relatively small, and investigations require strict controls to ensure that ageing effects are not confounded by demographic and medical conditions.

Macroscopic functional network changes have also been replicated over narrower age spans (Marques et al., 2015; Sala-Llonch et al., 2014). Within an older cognitively-normal population (mean age, 65 years; *SD*, 11.8), decreases in edge-wise functional connectivity with age were reported for sets of edges that were particularly long-range projections (Sala-Llonch et al., 2014). The spatial specificity of the edges that were implicated is, however, unclear. The co-expression of macroscopic network features and age-related

cognitive changes has received little empirical attention. The aforementioned investigation only observed that the relations between increasing age and verbal memory changes were mediated by the clustering coefficients of frontal and sub-cortical areas (Sala-Llonch et al., 2014). Furthermore, other cognitive domains were not investigated. Interestingly, similar investigations of cognitively-normal older adults (Marques et al., 2016; Marques et al., 2015) revealed a strong effect of increased educational attainment (years) on functional connectivity patterns. Modelling the influence of education has revealed that inter-individual variability in cognitive functioning can be accounted for factors other than age (Stern, 2002, 2012). However, the influence of education and other protective factors on the association between age-related cognitive changes and connectivity remains to be elucidated.

1.9 Systematic investigation of hub-regions in normal ageing and Alzheimer's

1.9.1 Age-related changes to hub-regions and connections

The integral value of hub-regions and their connections to human brain functioning strongly suggests that this neural substrate may also be implicated in age-related cognitive changes. As noted in healthy adults, neural signalling appears to take advantage of this anatomical backbone's higher-capacity for network communication. The decreased integration of long-range connections observed with age implicates changes to the routing of communication along rich-club paths. Indeed, changes to the structural (Gong et al., 2009b) and functional (Cao et al., 2014) topology of hub-regions have been identified to co-vary age. Interestingly, although changes appear to predominantly impact on the

topological structure of core DMN areas, the spatial distribution of hub-regions has also been demonstrated to be largely consistent across the lifespan (Betzel et al., 2014; Cao et al., 2014)

The sensitivity of hub-connections to healthy ageing is reflected by the inverted-U trajectory of functional rich-club organisation with age (peaking at around 40 years) (Cao et al., 2014). The efficiency of the functional connectivity patterns of the anatomical hub connections (both hub and feeder classes) has also been identified to be susceptible to age (Betzel et al., 2014). Only one study (Baggio et al., 2015) has systematically investigated age-related changes to structural rich-club organisation - revealing no influence of age. However, this study used a relatively modest population size which spanned a large age-range (i.e. n = 30; 39-79 years): More highly powered studies are clearly needed.

1.9.2 Hub-regions in Alzheimer's Disease

A "dysconnectivity syndrome" has been proposed to underlie the disturbances of AD (Delbeuck et al., 2003; Seeley et al., 2009). Structural brain connections provide theoretical accounts of disease progression with an attractive substrate for the "transneuronal spread" of pathological AD agents (i.e. Aβ) (Jones et al., 2016; Raj et al., 2012; Zhou et al., 2012). The vulnerability of large-scale subsystems in AD is widely evident, as disrupted neural communication, particularly within the DMN, is a hallmark feature of patients (Damoiseaux, 2012; Greicius et al., 2004; Seeley et al., 2009; Toga and Thompson, 2014). The centrality of anatomical hub-regions could potentially render themselves, and the interactions they support, more susceptible to pathogenic spreading (Fornito et al., 2015). Indeed, Aβ deposition sites in AD are found to overlap with hub-

regions derived by functional connectivity patterns, particularly for areas coinciding with the DMN (Buckner et al., 2009). Across AD and other psychiatric disorders, the disproportionate metabolic requirements of hub-regions have been increasingly posited to increase their vulnerability to pathogenic stressors (Buckner et al., 2009; Crossley et al., 2014; Zhou et al., 2012). PET imaging findings are supportive of such "hub-opathy" in AD, because patients display hypometabolism patterns for areas overlapping with Aβ deposition sites (Edison et al., 2007; Förster et al., 2012; Oh et al., 2016). Lastly, a large meta-analysis (Crossley et al., 2014) of 392 studies involving 26 disorders revealed that grey-matter lesions in brain disorders are more likely to occur in regions identified as hubs in healthy adult connectomes: Distinct from other disorders, temporal lobe hubs have a higher lesion probability in AD (Crossley et al., 2014).

Graph-theoretical investigations have revealed the functional architecture of brain networks in AD patients and MCI individual's express disruptions in the balance of functional integration and segregation (Dennis and Thompson, 2014). More recent applications have revealed that the decreased large-scale integration (i.e. reduced efficiency) in AD networks is associated with disturbances in long-distance projections (Dai et al., 2014; Lui et al., 2015). Moreover, disrupted long-distance projections selectively disturb the connectivity patterns of hub-regions in patients (Liu et al., 2014) - particularly for anterior-posterior DMN connections. It is highly suggestive to think that the fragmentation of global brain communication in patients is driven by disturbances to hub-regions/connections, thus supporting "hubopathy" models of AD. The connectivity patterns of hub-regions have also been identified as useful biomarkers for disease progression, and for classifying patients from controls (Dai et al., 2014; Lui et al., 2015).

The strength of this hubopathy view requires further validation. For example, a recent structural connectomic investigation (Daianu et al., 2015) of AD reported disruptions in mainly peripheral brain-regions. The sensitivity of detecting disturbances may be limited by methodological issues: This investigation employed dMRI acquisition and reconstruction methods, which are not optimal for resolving crossing and kissing fibre bundles. Furthermore, networks were constructed using a coarse parcellation template, which excludes subcortical interactions. Increasing the size of parcellation regions can result in the reduced spatial specificity of fibres which project to and from these cortical brain areas (Zalesky et al., 2010b).

1.10 Connectomics of psychiatric disorders

1.10.1 Contemporary mental health issues

The plight of individuals suffering mental health issues is increasingly being brought to attention within our society. The lifetime incidence of a psychiatric disorder in developed nations is approximately 25% (W. H. O. World Mental Health Survey Consortium, 2004; Wittchen and Jacobi, 2004). Psychiatric disorders are characterised by disturbances in behaviour, cognition, and mood - severe enough to impact on everyday functioning (American Psychiatric Association, 2013). The repercussions impact substantially on quality of life across the lifespan. Many psychiatric disorders are associated with abnormal perceptual and cognitive processes. Connectomic approaches provide a suitable theoretical and methodological framework for understanding the brain network alterations which may underpin these deviations from healthy human cognition and behaviour (Fornito and Bullmore, 2015; Fornito et al., 2015).

1.10.2 Bipolar Disorder

Individuals with bipolar disorder (BD) experience severe fluctuations in mood and energy levels. These fluctuations range from the highs of manic episodes - characterized by elevated (but often irritable) moods and grandiosity – interspersed with low states of depressed mood and negative thinking (American Psychiatric Association, 2013; Saunders and Goodwin, 2010). Estimates of the population rates of BD are as high as 8.3% (Akiskal et al., 2000), although the disorder encompasses a heterogenous group of phenotypical subtypes. Diagnoses of BD are classified into BD I or II subtypes: BD I is characterised by clear-cut manic episodes with psychosis (delusions, thought disorder and hallucinations) and are often severe enough to require hospitalization. Individuals diagnosed with BD II largely experience depressive episodes, inter-mixed with hypomanic states (Akiskal and Pinto, 1999; Piver et al., 2002; Saunders and Goodwin, 2010). Because hypomanic episodes are not as severe as manic states in BD I, BD II is under-diagnosed in both population and clinical samples (Akiskal et al., 2000) Given that suicide rates in affected individuals are higher than those with any other axis I psychiatric disorder, the accurate diagnosis and effective treatment of BD is imperative (Balázs et al., 2006; Chen and Dilsaver). Furthermore, individuals within hypomania and mania stages are poor at judging the remittance of episodes, leading to poor adherence to pharmacological and behavioural interventions. Impairments in BD are not restricted only to affective domains: Cognitive deficits also occur in executive (Altshuler et al., 2004; Green et al., 2007; Pavuluri et al., 2006), psychomotor (Bora et al., 2009; Malhi et al., 2007) and verbal-based abilities (Bearden et al., 2006; Martínez-Arán et al., 2005; van Gorp et al., 1999).

The peak age for illness-onset of BD is between 15 to 20 years (Goodwin and Consensus Group of the British Association for Psychopharmacology, 2009; Perlis et al., 2004; Weissman et al., 1988). The accurate diagnosis of BD is complicated by its episodic course. The occurence of a major depressive (MDD) episode typically precedes the clinical-threshold for manic symptoms (Angst et al., 2011; Chengappa et al., 2003). The clinical presentations of depressive episodes may also mask the hypomanic features of individuals, in turn leading to a misdiagnosis from the physician. The accurate diagnosis has implications for treatment options which stabilise the mood fluctuations, as their efficacy is influenced by the time of treatment initiation and phenotypic characteristics (Goodwin and Consensus Group of the British Association for Psychopharmacology, 2009): Mood stabilisers such as lithium and atypical antipsychotics are effective in manic individuals (Geddes et al., 2004; Goodwin and Consensus Group of the British Association for Psychopharmacology, 2009; Saunders and Goodwin, 2010), whilst atypical antipsychotics such as quetiapine are more efficacious for treating bipolar depression (De Fruyt et al., 2012). Lithium, however, is more effective for long-term stabilization (Geddes et al., 2004). Despite the depressive stages of the disorder, the evidence for the effectiveness of antidepressants on their own is inconsistent (Sidor and MacQueen, 2012) - particularly for alleviating manic symptoms. Consequently, a combination of lithium, antipsychotics and antidepressant agents are often administered at various stages of the disorder (Geddes and Miklowitz, 2013).

1.10.3 Neurobiological correlates of bipolar disorder

The issues besetting the diagnosis of BD reinforce the need for an accurate classification of patients, and also to identify those at future risk for the disorder. It has been proposed that bipolar is underlined by disruptions to a constellation of key frontal, limbic and striatal brain regions (Frangou, 2014; Phillips and Swartz, 2014; Strakowski et al., 2012). The role of these areas for emotional, interoceptive and cognitive functions has been well established: Disturbances to the circuity between such areas hence speaks to the dysregulation of emotional and cognitive control that is characteristic of BD patients. Upon the presentation of cognitive and emotional stimuli, patients at various illness stages display abnormal activation and connectivity between fronto-limbic areas (Chase and Phillips, 2016; Phillips et al., 2008). Two putative pathophysiological brain circuits have emerged in the literature, for which both involve the dysfunctional modulation of emotional reactivity in the amygdala and other limbic structures (Phillips et al., 2008; Phillips and Swartz, 2014): The first implicates ventrolateral prefrontal cortices (VLPFC) in their modulation of external emotional cues, whilst the latter involves involuntary regulation attributed to ventromedial prefrontal (VMPFC) areas such as the orbitofrontal cortex (OFC) and anterior cingulate. BD symptomatology has also been attributed to heightened reward sensitivity, reflected by the abnormal circuitry between ventral striatal and PFC areas (Phillips and Swartz, 2014)

Our current knowledge of the structural underpinnings of abnormal brain functioning in BD is guided by DTI-based studies. DTI-derived alterations are typically localised to fronto-limbic white-matter skeletons/fibre-bundles (Phillips and Swartz, 2014). Reductions of FA in anterior portions of the corpus callosum is a commonly replicated finding, with consistent support for abnormalities in other major fibre-bundles

such as the anterior cingulum, uncinate fasciculus, and the superior longitudinal fasciculus (Chaddock et al., 2009; Haller et al., 2011; Roberts et al., 2016b; Wang et al., 2008). However, the direction of findings and anatomical specificity of disturbances are largely inconsistent (Nortje et al., 2013; Phillips and Swartz, 2014).

1.10.4 Structural connectomic investigations of bipolar disorder

A large structural connectomic investigation of 216 BD I patients (Collin et al., 2015) found reduced connectivity strength for inter-hemispheric connectivity in patients – mirroring the FA reductions observed within the corpus callosum. Inter-hemispheric degradation was associated with the reduced capacity for information processing (i.e. decreased network efficiency). Decreased inter-hemispheric communication was replicated in a much smaller connectomic study (Leow et al., 2013). This investigation also identified disturbances localised to fronto-limbic areas, as reflected through nodal-level metrics: The brain networks of patients exhibited longer characteristic path lengths in regions such as orbitofrontal, hippocampal, and cingulate structures. Alterations to the integrative capacity of these key emotional and cognitive control areas speaks to structural underpinnings of the unstable mood regulation in patients. The mean age of patients (around 40 years) in both investigations is however much older than the typical age of illness onset (Loranger and Levine, 1978). In turn, both studies are limited in their capacity to determine whether the connectomic disturbances represent aetiological biomarkers of the disorder, or reflect illness burden.

1.10.5 Functional graph-theoretical investigations of bipolar disorder

Relatively few whole-brain investigations of resting-state functional connectivity patterns have been conducted into BD. The functional networks of patients - constructed from the synchrony of EEG signals (Kim et al., 2013) - reveal macroscopic features indicative of both increased segregation and integration. The latter may be attributable to the increased randomization of connectivity patterns in BD. Decreased synchronization was also identified for signals emanating from a subnetwork involving fronto-central regions. EEG recordings however lack the spatial specificity possible with rs-fMRI acquisitions. A large rs-fMRI investigation revealed reduced functional connectivity patterns in a combined group of schizophrenic and BD patients with psychosis (Baker et al., 2014): Connections within fronto-parietal association networks were preferentially implicated.

1.10.6 Rich-club degradation in schizophrenia and bipolar

Schizophrenia is one of the most extensively investigated psychiatric disorders. "Dysconnectivity" models (Fornito et al., 2012b; Friston, 1998; Stephan et al., 2009) have long proposed that abnormal functional integration underpins the cognitive and behavioural disturbances of patients: hallucinations, delusions, apathy, and cognitive disorganization. Cross-disorder comparisons of the neurobiological correlates of BD and schizophrenia is useful given syndromal features such as psychosis are shared across the disorders (Keshavan et al., 2011). A substantial overlap has also been demonstrated for genetic susceptibility of the two disorders (Cardno and Owen, 2014; Lichtenstein et al., 2009).

Schizophrenia has emerged as a candidate for hubopathy models of psychiatric disorders. Disturbances to executive and association areas within patients impact upon hubs within frontal and temporal cortices (Crossley et al., 2014; Rubinov and Bullmore, 2013; van den Heuvel et al., 2010). Selective disruptions to these core cognitive areas speaks to the disorganised behavioural patterns that are characteristic of the disorder. Structural connectomic investigations have consistently revealed widespread degradations to pathways between hub-regions - rich-club connections - in schizophrenia (Collin et al., 2014a; Klauser et al., 2016; van den Heuvel et al., 2013). Rich-club degradations are associated with compromised network architectures (Collin et al., 2014a; van den Heuvel et al., 2013), strongly suggesting disruptions to the neural substrate to underpin global brain dysfunctioning in patients. Furthermore, rich-club degradations correlate with less variability in functional connectivity patterns (van den Heuvel et al., 2013), and clinical ratings such as increased illness duration and poor global functioning (Collin et al., 2014a). Interestingly, the only systematic investigation of rich-club architecture in BD revealed the relative preservation of the anatomical backbone in patients (Collin et al., 2015). The discrepancy between schizophrenic and BD suggests rich-club disruptions are not ubiquitous, but perhaps specific to the syndromal features of the disorder (Crossley et al., 2014).

1.11 High-risk populations of psychiatric disorders

1.11.1 Individuals at high-genetic risk for bipolar disorder

Unaffected relatives of individuals diagnosed with heritable psychiatric illnesses are at high risk of developing the disorder. These individuals are largely free from the burden

associated with illness onset, including medication use. Neurobiological disturbances in unaffected relatives can thus potentially shed light on disorder endophenotypes, and serve as biomarkers for predicting illness-onset (Weissman et al., 1986)**.** Bipolar disorder is a prime candidate for studies of unaffected relatives, with heritably estimates shown to be between 59 and 85% (McGuffin et al., 2003; Purcell et al., 2009). First-degree relatives have a ~7-14-fold increased risk of diagnosis of the disorder (Mortensen et al., 2003; Purcell et al., 2009). First-degree relatives demonstrate subclinical disturbances in mood and anxiety, and also higher rates of major depressive disorder (DelBello and Geller, 2001; Perich et al., 2015).

The developmental period prior to the peak age of BD onset is characterised by profound behavioural changes and critical brain maturation. Aberrations to these maturational processes have been postulated to lead to cognitive and emotional disturbances (Baker et al., 2015; Casey et al., 2010; Paus et al., 2008). In turn, first-degree relatives at this critical age can be conceptualised as individuals at "high-risk" for developing BD (Goodwin and Jamison, 2007; Loranger and Levine, 1978). A longitudinal investigation of healthy 15-19 year olds over a two-year period revealed disproportionate developments in hub-hub structural connectivity with age (Baker et al., 2015): Increases in structural connectivity in this study were predominately concentrated upon projections between subcortical, parietal and frontal regions - which house core cognitive control and emotional centres (Alvarez and Emory, 2006; Cole and Schneider, 2007; Liakakis et al., 2011).

1.11.2 Connectomic investigations of unaffected relatives of bipolar patients

There has been little research in this area that has used connectomics. The only existing structural connectomic investigation of unaffected first-degree relatives using tractography reported no significant differences to either healthy controls or BD I patients (Forde et al., 2015). However, this study was based on a relatively small sample size, thus lacking power. In addition, the field strength of the scanner (i.e. 1.5T MRI) may have not allowed sufficiently accurate structural connectomes to sensitively capture group differences. In addition, the mean age of the unaffected relatives was 42 years – after the peak age of onset - meaning that the population group may represent biologically resilient relatives.

1.11.3 Other neurobiological correlates of high-risk subjects

Studies of DTI-derived indices of white matter connectivity (FA, etc.) in high-risk individuals have revealed changes along fronto-limbic tracts, where disturbances are shared also with patients (Frazier et al., 2007; Roberts et al., 2016b; Sprooten et al., 2013; Sprooten et al., 2011). Shared disruptions in functional connectivity patterns have also been identified in unaffected siblings in RSN's containing frontal, striatal, and subcortical regions (Khadka et al., 2013; Lui et al., 2015; Meda et al., 2012). Within both modalities, disruptions have been variously identified as either shared across unaffected relatives and patient probands, or unique to one group. This renders interpretations of the genetic vulnerability of first-degree relatives difficult.

The inferior frontal gyrus (IFG) has emerged as a potential endophenotypical candidate underlying BD. In healthy adults, the normal functioning of the IFG is imperative for the integration of cognitive and emotional input (Cai et al., 2014; Liakakis et al., 2011). Abnormal functional activation of the IFG has been reported in both unaffected relatives (Brotman et al., 2014; Roberts et al., 2013) and BD patients (Foland-Ross et al., 2012; Hafeman et al., 2014; Hajek et al., 2013a) in tasks assessing inhibition and emotional processing. Through Dynamic Causal Modelling (DCM), the observed hypoactivation of the IFG (Roberts et al., 2013) has been modelled within its broader network of regions responsible for emotion perception (i.e. anterior cingulate) and cognitive control (i.e. DLPFC) (Breakspear et al., 2015a): Alterations to large-scale effective connectivity in this study were unique to a young cohort at high-risk for BD, suggestive of their increased vulnerability for illness-onset throughout critical maturational stages.

1.11.4 Individuals at high-risk for schizophrenia

Schizophrenia is another psychiatric disorder with a strong genetic involvement (Harrison and Weinberger, 2005; O'donovan et al., 2008). Structural connectomic investigations of unaffected siblings of patients have revealed that this familial risk is associated with a compromise to the structural rich-club (Collin et al., 2014a): Compared with healthy controls, disturbances in rich-club density are more pronounced in patients and intermediate in unaffected siblings. An association between rich-club degradation and symptom severity in patients suggests the neurodevelopmental vulnerability of the core anatomical backbone is associated with disease-progression, as well as illness risk.

1.12 Summary of connectomic approaches to normal ageing and psychiatric disorders

In sum, widespread empirical evidence suggests inter-individual differences in cognition and behaviour are underscored by changes in the capacity of large-scale brain network communication. Connectomic approaches afford a complementary approach to investigate these changes, relative to traditional univariate brain measures. Indeed, alterations in the delicate balance of functional integration and segregation of cortical information processing are apparent in both healthy ageing and psychiatric conditions - providing strong ground to propose that the expression of macroscopic network features reflects inter-individual phenotypical differences across these populations. Furthermore, high-cost hub-regions (and their connections) - critical for large-scale network communication - appear to be selectively implicated in behavioural and cognitive changes. Disruptions to hub-regions may not be ubiquitous, as fronto-limbic alterations in BD reverberate with the emotional lability that is characteristic of patients.

Investigations of both ageing and BD patient cohorts have not yet benefited from the recent advances in dMRI acquisition and fibre-reconstruction, or the complex analysis of connectomic data. The investigations also typically use small to modest sample sizes, lacking sufficient power. Systematic investigation of the expression of connectomic features related to inter-individual differences in cognitive performance are clearly lacking within a healthy older population. Structural network disturbances in young adults at high-risk for BD also remain to be elucidated. Addressing these issues holds potential to identify biomarkers that are involved in pathophysiological mechanisms of illness-onset.

Chapter 2: The Organisation of the Elderly Connectome

2.1 Abstract

Investigations of the human connectome have elucidated core features of adult structural networks, particularly the crucial role of hub-regions. However, little is known regarding network organisation of the healthy elderly connectome, a crucial prelude to the systematic study of neurodegenerative disorders. Here, whole-brain probabilistic tractography was performed on high-angular diffusion-weighted images acquired from 114 healthy elderly subjects (age 76-94 years; 64 females). Structural networks were reconstructed between 512 cortical and subcortical brain regions. We sought to investigate the architectural features of hub-regions, as well as left-right asymmetries, and sexual dimorphisms. We observed that the topology of hub-regions is consistent with a young adult population, and previously published adult connectomic data. More importantly, the architectural features of hub connections reflect their ongoing vital role in network communication. We also found substantial sexual dimorphisms, with females exhibiting stronger inter-hemispheric connections between cingulate and prefrontal cortices. Lastly, we demonstrate intriguing left-lateralized subnetworks consistent with the neural circuitry specialised for language and executive functions, while rightward subnetworks were dominant in visual and visuospatial streams. These findings provide insights into healthy brain ageing and provide a benchmark for the study of neurodegenerative disorders such as AD and Frontotemporal Dementia (FTD).

2.2 Introduction

The human brain is a large-scale complex network known as the human "connectome" (Sporns et al., 2005). The application of graph theoretical analysis to human neuroimaging data has uncovered topological features of the connectome that mirror other complex systems (Fornito et al., 2013; Sporns, 2013b). These network features include "small-worldness" (Achard et al., 2006; Sporns and Zwi, 2004; Stephan et al., 2000), highly-connected "hubs" (Hagmann et al., 2008b; van den Heuvel and Sporns, 2011, 2013b), and a modular structure (Hagmann et al., 2008b; Meunier et al., 2009). Knowledge of the connectome has accelerated through recent advances in diffusion-weighted imaging, including optimal acquisition parameters (Sotiropoulos et al., 2013; Tournier et al., 2013), improved reconstruction algorithms (Behrens et al., 2003; Tournier et al., 2010), and diffusion models (Aganj et al., 2011; Behrens et al., 2007; Jbabdi et al., 2012; Tournier et al., 2008).

A crucial architectural feature of the adult human connectome is the presence of highly-connected regions ("hubs"), that are also densely connected with each other (van den Heuvel and Sporns, 2013b). These regions form what is known as a "rich-club", and occur in cortical regions such as the precuneus, cingulum (anterior and posterior), insula, superior frontal and parietal areas, temporal regions, and also subcortical structures (van den Heuvel and Sporns, 2011, 2013b). Rich-club connections in human (Collin et al., 2014b; van den Heuvel et al., 2012) , macaque (Harriger et al., 2012) and cat cortices (de Reus and van den Heuvel, 2013) have high topological efficiency, longer anatomical fibres, increased inter-modular connectivity and route a large proportion of network traffic. The structural rich-club may thus act as a central backbone that integrates communication between segregated brain regions (van den Heuvel and Sporns, 2013b).

This is exemplified by the disproportionate reduction in network "communicability" and/or "efficiency" when hub-regions or their connections are artificially lesioned (Crossley et al., 2013; de Reus et al., 2014; van den Heuvel and Sporns, 2011) .

These hub-regions overlap with transmodal areas known to be pivotal within-and-between core neurocognitive systems such as the cognitive control, default mode, and salience network (Crossley et al., 2013; Dwyer et al., 2014; Sepulcre et al., 2012; Spreng et al., 2013; Tomasi and Volkow, 2011; Uddin et al., 2011; van den Heuvel and Sporns, 2013a). Interestingly, alterations in functional connectivity of these large-scale systems in elderly populations have been associated with changes in working memory, processing speed and executive functions (Campbell et al., 2012; Damoiseaux et al., 2008; He et al., 2014; Lim et al., 2014; Wang et al., 2010). These disruptions are thus suggestive of topological changes occuring to hub connections with ageing. Hub-regions are also metabolically costly, evident through their increased metabolic expenditure and wiring cost (Collin et al., 2014b; Liang et al., 2013; van den Heuvel et al., 2012). This increased energy expenditure of hub-regions further highlights their potential for age-related changes, as their high metabolic cost has been shown to potentially render such regions more vulnerable to pathological processes in neurodegenerative disorders (Crossley et al., 2014; Liang et al., 2013; Tomasi et al., 2013). Indeed, hub-regions have shown to be more likely susceptible to normal ageing processes such as amyloid deposition (Buckner et al., 2009; Toga and Thompson, 2014).

During cognitively demanding tasks, older adults increase their recruitment of contralateral brain regions, suggesting compensatory mechanisms (Cabeza et al., 2002; Davis et al., 2012; Park and Reuter-Lorenz, 2009). Left-hemisphere networks are well known to be dominant in language tasks, whilst the right-hemisphere is associated with

visuospatial abilities (Geschwind and Galaburda, 1985; Herve et al., 2013; Toga and Thompson, 2003). Although connectomic investigations (Caeyenberghs and Leemans, 2014; Nielsen et al., 2013; Tomasi and Volkow, 2012b) have examinated lateralized organisation at the nodal-level, no study has specifically investigated lateralization of the elderly connectome.

Sexual dimorphism has also been an active area of research for the last few decades, with increasing interest from connectomic investigations (Dennis et al., 2013; Duarte-Carvajalino et al., 2012; Gong et al., 2009b; Ryman et al., 2014). Across the lifespan, males have been shown to demonstrate greater performance in visuospatial tasks, whilst females excel on verbal tasks (Gur et al., 2012; Hoogendam et al., 2014; Kimura, 2004). Preferential wiring for inter-hemispheric structural connections was recently observed in female adolescents, whilst localised intra-hemispheric connectivity characterises cortical networks in young men (Ingalhalikar et al., 2014). Whether such topological differences persist into late adulthood is not known.

Hitherto, the structural connectomes of healthy elderly populations have been investigated through lifespan longitudinal studies (Betzel et al., 2014; Caeyenberghs and Leemans, 2014; Gong et al., 2009b). Whilst these incorporate sufficiently large numbers of subjects across the life span, the number of elderly subjects is invariably modest. The organisation of healthy older connectomes hence remains relatively unknown and has not benefitted from recent advances in the acquisition and analysis of structural connectomes. The present study addresses this gap by characterising network topology in elderly structural connectomes generated from high-angular resolution fibre bundles. For comparative purposes, structural networks of a young adult population (17-30 years old) are also investigated.

2.3 Methods

2.3.1 Participants

142 cognitively healthy elderly individuals were drawn from the Sydney Memory and Ageing Study (MAS) (Tsang et al., 2013). The longitudinal study involves community-dwelling older adults aged 76-94 years, randomly recruited from the electoral roll. Participants in the present study were cognitively healthy, defined as performance on all neuropsychological test measures were within 1.5 standard deviations of normative published mean values (Tsang et al., 2013). Individuals not meeting these criteria, or who were reported to exhibit a decline in daily living activities by an informant, were excluded if they met international consensus criteria for MCI (Winblad et al., 2004), decided by a clinical case panel chaired by neuropsychiatrists, psychogeriatricians, and psychologists (Sachdev et al., 2010). Other exclusion criteria included dementia, mental retardation, schizophrenia, bipolar disorder, multiple sclerosis, motor neuron disease, active malignancy, or inadequate comprehension of English to complete a basic assessment.

2.3.2 dMRI acquisition

dMRI data were acquired from all subjects on a Philips 3T Achieva Quasar Dual MRI scanner (Philips Medical System, Best, The Netherlands), using a single-shot echo-planar imaging (EPI) sequence (TR = 13586 ms, TE = 79 ms). For each diffusion scan, 61 gradient directions (b = 2400 s/mm²) and a non-diffusion-weighted acquisition (b = 0 s/mm²) were acquired over a 96mm² image matrix (FOV 240 mm x 240 mm²); with a slice thickness of 2.5 mm and no gap, yielding 2.5 mm isotropic voxels.

2.3.3 Diffusion image pre-processing

The diffusion MRI scan of each participant was visualised within FSLView (Smith et al., 2004b). Participants were excluded from the study if their scan revealed the presence of artefact due to motion effects. Twenty-two participants were excluded due to diffusion artefact, along with six others whose networks were not completely connected. We thus analysed the structural connectomes from 50 males and 64 females (Table 2-1).

Table 2-1. *Demographic information of elderly subjects*

Gender (M/F)	Male (n = 50)	Female (n = 64)
	Mean ± *SD*	Mean ± *SD*
Age (years)	83.35 ± 4.74	82.61 ± 4.02
Education (years)*	13.37 ± 3.87	11.57 ± 2.91

* $p < .01$ (t-test)

To correct for head motion, the gradient direction matrix was rotated using a customised in-house algorithm (Leemans and Jones, 2009; Raffelt et al., 2012b). Next, to reduce spatial intensity inhomogenities, bias corrections was performed on the b0 image and subsequently applied to all DWI (Sled et al., 1998a). Lastly, a Higher Order Model Outlier Rejection model (Pannek et al., 2012b) identified voxels with residual outliers in signals of the DWI.

2.3.4 Whole-brain fibre tracking

We employed the probabilistic streamline algorithm (iFOD2) (Tournier et al., 2010) to generate high-resolution whole-brain fibre tracks until 5 million in number were reached. The orientation of fibre distributions (FOD) were estimated within MRtrix software (Tournier et al., 2012), by performing constrained spherical deconvolution (CSD, *lmax* = 8) of the diffusion signal (Tournier et al., 2008). Using the default parameters for images of such acquisition (step size = 1.25 mm, minimum length = 12.5 mm, max length = 250 mm, FA termination = 0.1, max angle = 45º), iFOD2 tracked the most probable fibre propagations by sampling a probability density function of the FOD at points along each candidate path. iFOD2 has been shown to improve the accuracy of reconstructing high-angular fibre bundles (Tournier et al., 2012) and prevent biases caused by overshoot (Tournier et al., 2010).

2.3.5 Construction of whole-brain structural networks

The standard AAL template (Tzourio-Mazoyer et al., 2002a) was subdivided into 512 cortical and sub-cortical parcellation regions of approximately uniform size (Zalesky et al., 2010b). The AAL parcellation is widely used in structural network investigations (Caeyenberghs and Leemans, 2014; Gong et al., 2009b; Lo et al., 2010; Shu et al., 2012; Shu et al., 2011), but does not include information on the GM-WM boundary for each parcel. We note that the echo-planar readout in diffusion acquisition induces geometric distortions within the diffusion image (Holland et al., 2010b). Thus, the spatial alignment of anatomical information (i.e. GM-WM boundary) from the T1 image and the diffusion-weighted image are not particularly accurate (Smith et al., 2012a), precluding an explicit check of the GM-WM boundary for each parcel. However, following our dense seeding

(see below), all parcels in the group connectome had substantial connections. It is hence highly unlikely that any of the parcellated regions do not include a GM-WM boundary, being hence "hidden" from the WM.

Parcellations within subject-space were achieved by employing affine linear registrations within FSL (Smith et al., 2004b). First, the parcellated template was co-registered to the Montreal Neurological Institute (MNI) T1 2mm brain template. The MNI template was then co-registered to the subject's FA image. The parcellation template (in MNI space) was subsequently transformed into subject-space by applying the transformation matrix generated from registering the MNI template to the FA image.

Within a weighted graph G_w, a weighted connection w_{ij} (if $w_{ij} \geq 3$) represents the number of streamlines from region i terminating within a 2mm radius of j. w_{ij} were adjusted by the mean fibre length between i and j (Hagmann et al., 2008b), as fibre densities are known to be over-estimated in longer fibre bundles (Smith et al., 2013b). These weighted networks were rendered sparse by thresholding to preserve the same connection density across subjects. All analyses reported here are on connectomes at 7.5% sparsity, whilst other sparsities (5% and 10%) are reported within supplementary materials. We note that there do not exist reliable benchmarks for human tractography using a parcellation comparable to the present one. Density in anatomical studies from primates and rodents varies greatly according to the anatomical parcelleation and tracing method. The sparsity levels included in the present study are thus guided by prior practise. It is common practice for rs-fMRI, and to a lesser extent structural networks, to implement a variety of threshold levels around 10% (Sporns, 2013b). However, by selecting a multiple of thresholds, we ensure the topological distribution of the elderly connectome we report is not biased by the density of the networks (van Wijk et al., 2010). Binary

networks were constructed from these sparse weighted networks, by setting all connections to one. Average connectomes of the current population were also generated. Summary of the steps involved in structural brain network reconstruction is illustrated in Figure 2-1. All network and surface visualisations were generated using BrainNet Viewer (Xia et al., 2013) and CARET (Van Essen et al., 2001) software packages respectively.

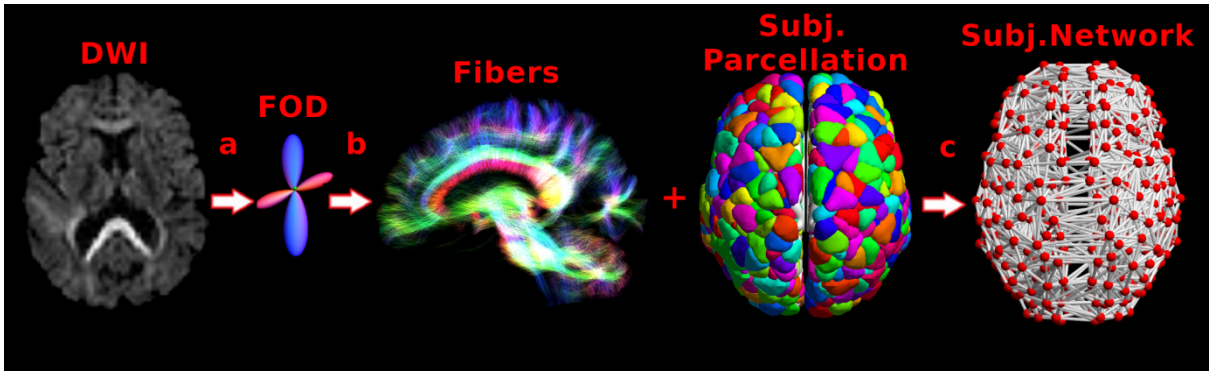

Figure 2-1: *Steps involved in connectome construction for a representative elderly subject. A, FODs were estimated by performing constrained spherical deconvolution of the diffusion signal within single-fibre voxels of the DWI. B, High-angular whole-brain fibre tracks were constructed from probabilistic sampling of the FOD. C, Networks representing structural connectivity information generated from the whole-brain fibre tracks were constructed. A connection (white lines) between region i and j (red dots) of the parcellation (in subject space) was said to be present if a track from i terminated within a 2mm radius of j.*

2.3.6 Graph theoretical characterisation

2.3.6.1 *Nodal-level measures*

All nodal-level network measures employed were computed using the Brain Connectivity Toolbox, and have been described elsewhere (Rubinov and Sporns, 2010). Formal definitions are given in Appendix 1.

2.3.6.2 *Community structure*

A community detection algorithm (Blondel et al., 2008) was employed. The most optimal division of modularity (Q) was calculated and a fine-tune tuning algorithm was subsequently employed (Sun et al., 2009). The partition with the highest modularity was retained.

2.3.7 Hub nodes and connection classes

2.3.7.1 *Identification of hub-regions.*

Network hubs may be defined according to various network criteria. Here, hub-regions were identified according to aggregate ranking across multiple metrics (Betzel et al., 2014). First, for each subject, each node's "hubness" was calculated from its composite average ranking across degree, betweenness and subgraph centrality scores. The top 15% composite scores (N = 76) were used to identify hub-regions within each subject, whist the top 15% most consistent hubs across subjects were defined as hub-regions across the group.

2.3.8 Connection classes

Partitioning nodes into hubs and non-hubs allowed connections to be classified into three types: (1) hub connections, linking hub nodes; (2) feeder connections, linking non-hub nodes to hub nodes; (3) local connections, linking non-hub nodes (van den Heuvel et al., 2012).

2.3.9 Architectural features of connection classes

2.3.9.1 *Network density and cost*

The network cost for each connection was defined as its density (number of streamlines) times its physical length. The network cost for each connection class was calculated as the average cost of its connections. Cost/density ratios for each connection class were calculated as the network cost percentage, divided by its density percentage (van den Heuvel et al., 2012).

2.3.9.2 *Network Traffic*

The amount of network traffic along each connection class was based upon the percentage of its connections routing the shortest path between any region *i* and *j*. Here, the shortest path(s) was defined by the minimum number of paths (steps) to reach *j* from *i*, instead of the topological distance (van den Heuvel et al., 2012).

2.3.10 Network Communicability

The communicability metric measures the "ease of communication" between *i* and *j*, and is defined by all possible walks of *k* length (steps) between these regions (de Reus et al., 2014; Estrada and Hatano, 2008). Although being a generalisation of shortest path "efficiency" information, the communicability measure does advantageously take into account multiple and longer paths between such regions (de Reus and van den Heuvel, 2014), thus potentially capturing the "parallel processing" nature of brain networks (Alexander and Crutcher, 1990) and thus may be more sensitive to age-related changes impacting upon large number of communication paths. Walks of longer *k* lengths

between *i* and *j* have lower contributions to the communicability function than shorter ones, and is defined formally as:

$$C_{ij} = \sum_{k=0}^{k=10} \frac{(G^k)_{ij}}{k!} = (e^G)_{ij}, \quad (1.1)$$

where G denotes the connectivity matrix, satisfying $G_{ij} = 1$ if region i and j are connected, and $G_{ij} = 0$ if not. Because a large number of walks can be yielded from large k walk lengths between *i* and *j*, C_{ij} was computed until walks of length $k = 10$. C_{ij} was averaged across all nodal pairs to calculate the overall network communicability within the entire network (de Reus et al., 2014).

2.3.11 Rich-club organisation

A modified algorithm (Samu et al., 2014) to calculate the weighted richness of hub connections within each subject was implemented. Formal definition of this algorithm, and the examination of the significance of rich-club architecture within these hub connections are detailed in Appendix 1.2.1 and 1.2.3.

2.3.12 Computational attack of hub nodes and their connections

To examine the criticality of hub nodes and their connections to global network communicability, lesions were simulated by randomly removing connections (binary-wise) from each connection class. Because the distribution of connections is by definition unequal across classes (van den Heuvel et al., 2012), the same number of connections were removed across each class for each subject. This action was performed in 25%

increments (up until 75%) and average results over 1000 randomly simulated lesions at each increment level were calculated. The change in global network communicability after random edges from each connection class were lesioned, was expressed as a percentage of the intact network's communicability.

2.3.13 Statistical Analysis

2.3.13.1 *Architectural features of hub-regions and their connections*

Non-parametric permutation testing was used to assess statistical significance of class differences in connnection metrics (de Reus and van den Heuvel, 2013). First, the difference between the two classes for each subject were computed for a given metric. Second, for each permutation (N = 5000), the metric values were randomly assigned to two random groups and their group difference was computed, resulting in a null distribution of differences. The proportion of the null-distribution values that exceeded the observed original difference was computed and assigned a p-value (one-tailed).

2.3.14 Lateralization and sex differences

2.3.14.1 *Network-Based Statistic*

A general linear model (GLM) was employed to identify differences in weighted edge-wise connectivity. We identified subnetworks that differed significantly between the groups on each effect using the Network-Based Statistic (NBS) software package, which achieves control over family-wise error (Zalesky et al., 2010a). The NBS is based on the principles underpinning traditional cluster-based thresholding of statistical parametric maps and hence proceeds to identify subnetworks of topologically connected

suprathreshold connections. Networks were permuted 5000 times to obtain the empirical null distribution of the largest network component. A family-wise error (FWE) corrected *p*-value for the network component was estimated by the proportion of permutations for which a network of equal or greater size was identified.

To identify significantly lateralized subnetworks, a repeated measures GLM was employed. For each subject, left intra-hemispheric weighted networks were treated as one condition, whilst right intra-hemispheric networks were treated as the other. For between-group analyses of sexual dimorphisms, age and education level were treated as covariates. Conservative *t*-test thresholds were employed to yield strong, suprathreshold lateralizations in connectivity ($t = 5.5$, corresponding to an uncorrected $p < 0.0001$), and also sexual dimorphisms ($t = 3.5$, $p = 0.0003$).

2.4 Results

2.4.1 Identification of hub-regions and rich-club architecture

Brain regions identified as hubs, by virtue of having consistently high composite scores across subjects are illustrated in Figure 2-2. These hubs (for index of surface colours see Figure 2-2C) are distributed bilaterally in subcortical structures (Figure 2-2B), and cortical (Figure 2-2A) regions including the insula, anterior cingulate, precentral gyrus, precuneus, superior frontal, supplementary motor area (SMA), temporal poles, occipital areas, and also the left IFG. Connections (red lines) between hub-regions are visualised (average connectome) on a circular graphical representation (Irimia et al., 2012; Krzywinski et al., 2009), arranged to their AAL region (Figure 2-2C). This allows straightforward identification of intra-and-inter-hemispheric connections that exist

between hub-regions. The outermost circular bar represents the hub parcellation region (and surface colour), whilst the middle and innermost bars indicate their average composite score (light red to very dark red), and consistency across subjects respectively (light blue to very dark blue). Sub-cortical structures and cortical regions including the anterior cingulate, insula, left precentral gyrus, left temporal pole, and left IFG have the highest composite scores and greatest consistency across subjects. Weighted rich-club architecture is found to be present ($\Phi[norm]>1$) and significant for these hub connections (Figure 2-2e) in all subjects (mean $p = < 0.0001$). These hub-regions are consistently top ranked for the nodal metrics used to calculate their composite score (Figure A2-1), and are also consistently identified as hubs across different sparsity levels (Figure A2-2).

2.4.2 Architectural features of hub nodes and their connections

Connections with each each subject were classified as either hub (left panel), feeder (middle), or local (right) connections (Figure 2-3A, visualised here on the average connectome). Local connections accounted predominantly for the cost (left column) and streamline density (right column) across the network, followed by feeders, whilst hub connections comprised only a small percentage (Figure 2-3B). Non-parametric permutation testing of the cost/density ratios revealed that hub connections are more costly than predicted by their density alone, in comparison to both feeder and local connections ($p < 0.0001$) (Figure 2-3B, middle text column). Cost/density ratios of feeders were also significantly greater than the ratio of local connections ($p < 0.0001$). These patterns of findings were also identified for analyses of mean fibre lengths across connection classes (Figure 2-3B, $p < 0.0001$). Feeder connections significantly route the majority of traffic for the shortest communication path (i.e 40% of shortest paths must

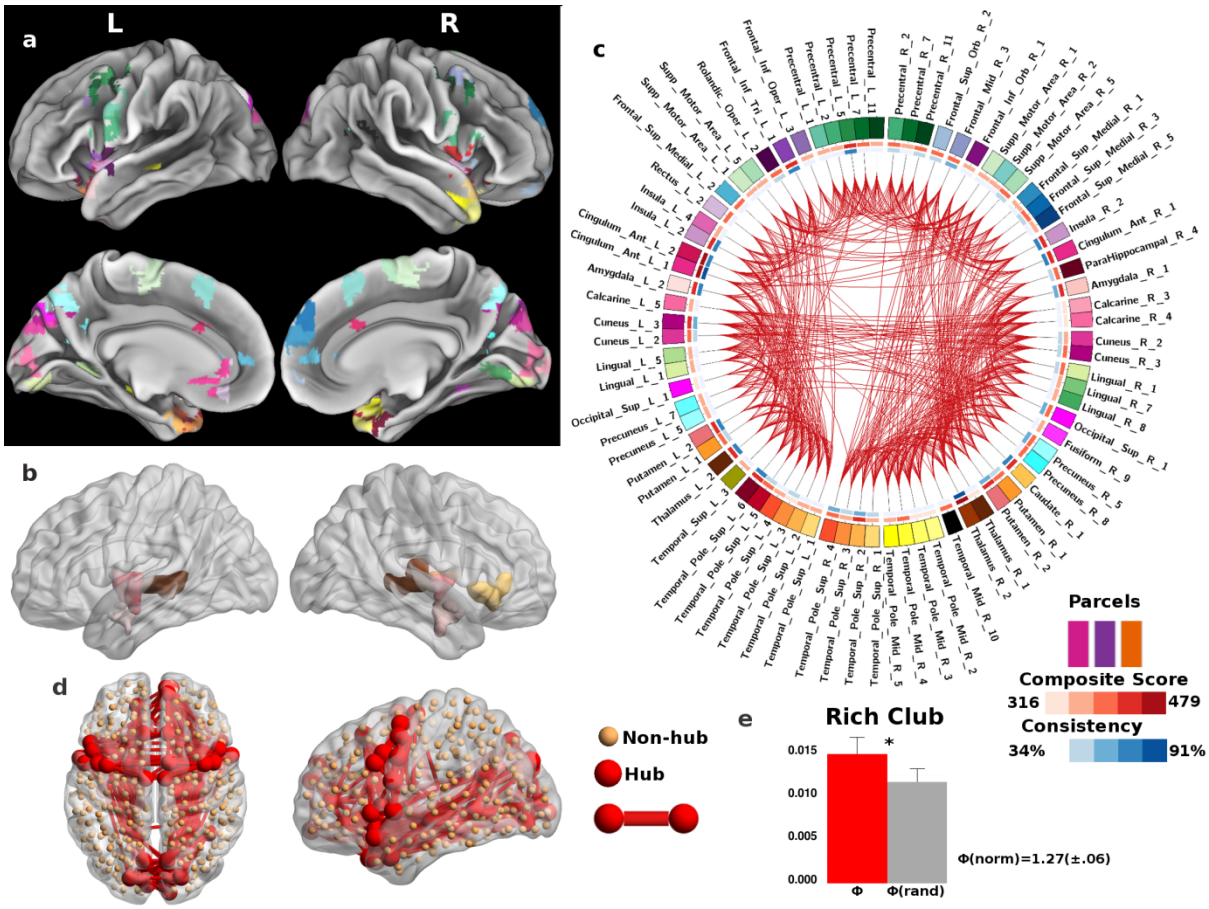

Figure 2-2: *Identification of hub brain-regions and rich-club architecture within the elderly connectome. Surface and volumetric representation of cortical (A) and sub-cortical (B) hub-regions respectively. Refer to* ***C*** *for the parcellation regions the surface colours index. C, Circular representation of hub-regions and connections among each other (red lines), with regions arranged according to their respective AAL region and hemispheric location (right-hemispheric on the right axis, left on the left). The outermost circular bar represents the hub parcellation region and their index colour (represented in* ***A*** *and* ***B****), whilst the middle and innermost bars indicate their average composite score (light red to very dark red) and consistency across subjects respectively (light blue to very dark blue). D****,*** *Network perspective of connections (red lines) among hub-regions (red dots). E, For these connections, the mean across subjects for the weighted rich-club coefficient Φ(h) (red column) , average random rich-club coefficient Φ(rand) (grey column), and normalised rich-club coefficient Φ(norm).*

route through at least one hub) between regions ($p < 0.0001$, Figure 2-3D, right column). Hub connections route a significantly greater percentage of traffic than local connections ($p < 0.0001$). These analyses are consistent at other sparsity levels (Figure A2-3).

2.4.3 Computational attack of hub connections

To examine the role of hub connections to global network, simulated lesioning was performed on each connection class (Figure 2-3E). The mean percentage change in global network communicability when lesioning hub connections were significantly greater than lesioning the same number of feeder connections ($p < 0.0001$) except at the 75% increment level. Lesioning local connections had the least impact on communicability ($p < 0.0001$) at all increment levels.

2.4.4 Comparison to a young adult population

To aid the topological comparison of elderly and adult connectomic data, the structural networks were also examined from a subset of the young adult control population within study 3 (Chapter 4; cf 4.3.1). Here, the young population comprised of seventy-eight individuals (43 females) between the ages of 18 and 30 (mean age, 23.48 years). Although both groups were acquired on the same MRI scanner, dMRI data were acquired differently in the young controls (Appendix 4.2.1), leading to also subtle differences in the pre-processing and fibre reconstruction parameters relative to elderly subjects (Appendix 4.2.1. and 4.2.2). To avoid age and gender interactions, will limit the comparison to female subjects only in both cohorts.

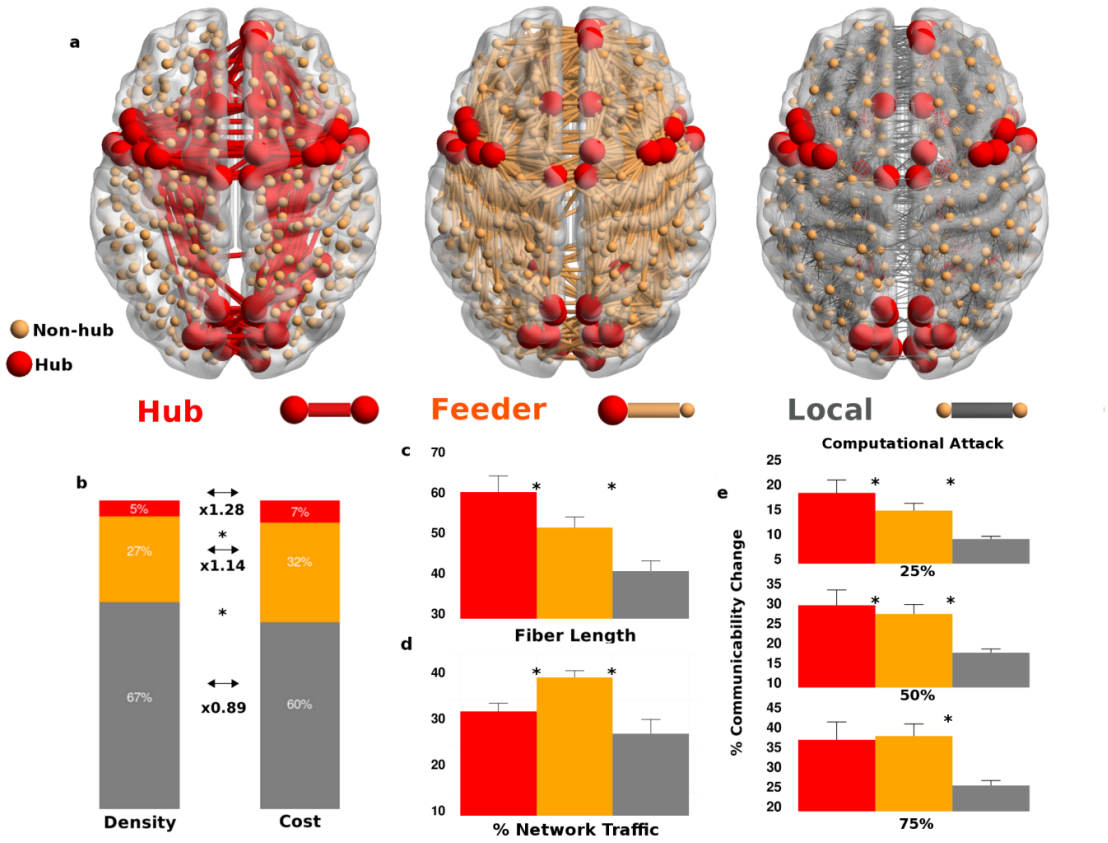

Figure 2-3: *Architectural features of the different connection classes. A, Hub connections (left panel) linking (red lines) hub (red dots) regions, feeder connections (middle, orange lines) linking hub to non-hub (orange dots), or local (right, grey lines) connections linking non-hub regions. B, Mean contributions of each connection class to density (number of streamlines) (left column) and cost to the network (right). The middle text column represents the mean cost/density ratios for each connection class. C, Mean fibre length (mm) for each connection class. D, The mean percentage of network traffic each connection class routes for the shortest path route. E, Mean percentage change in network communicability after removing specified number of edges from connection class, at 25% (top), 50% (middle), and 75% (bottom) increments.*

* $p < .0001$, permutation testing ($N = 5000$)

The comparison of connection classes and their architectural features across the young and old cohorts is illustrated in Figure 2-4. Visual inspection of the topological

distribution of connection class across the young (Figure 2-4A) and elderly (Figure 2-4B) cohorts is dominated by the overall consistent, with only relatively minor qualitative differences evident. In the young cohort, hub connections appear slightly more dispersed, while they also show increased inter-hemispheric connectivity (especially posteriorly) for feeder and local classes (for sagittal perspectives, see Figure A2-4). The architectural features between connection classes in the younger cohort are generally similar to those of the elderly cohort (both male and female), presented in section 2.4.2 (cf Figure 2-3, bottom panel). However, several notable differences between the two cohorts are apparent: The mean fibre lengths across the young female cohort (Figure 2-5D) are markedly longer than the corresponding connection classes in the elderly female cohort (Figure 2-5G). The proportion of network traffic routed through hub and feeder connections is slightly larger in young females (Figure 2-5E), whilst traffic routing through local connections is less in the younger relative to the elderly females (Figure 2-5H).

A direct visual comparison of the distribution of hubs regions in each of these age cohorts is provided in Figure A2-4A. Considerable consistency in the distribution hub-regions across the elderly and young adult populations: 72% of hubs identified in elderly females are also hubs in young females. The figure also shows subtle differences between the two cohorts: A cluster of hub nodes unique to the elderly appear within the right temporal pole, left mid-frontal, and prefrontal cortices. Conversely, a cluster of hub regions unique to the younger cohort are found in superior frontal, precentral, and ventral striatal areas.

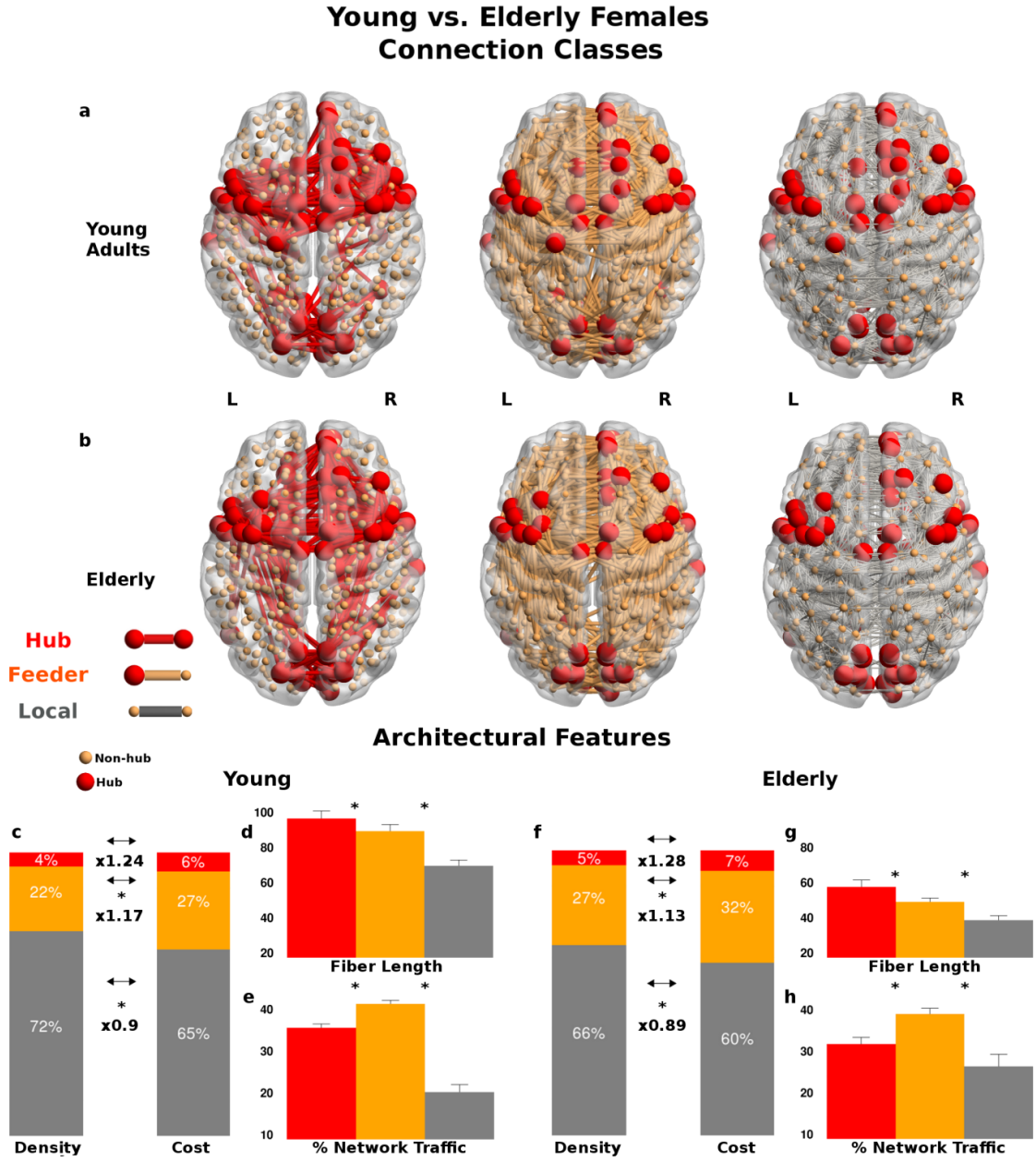

Figure 2-4: *Comparison of connection class architectural features across young adult and elderly females.* ***A*** *and* ***B****, Superior perspective of connections classified as either those of hub (left panel), feeder (middle), or local (right) connections in the young (top) and elderly connectomes (bottom).* ***C*** *and* ***F****, Mean contributions of each connection class to density (number of streamlines) (left column) and cost to the network (right) in young and elderly females, respectively. The middle text column represents the mean cost/density ratios for each connection class.* ***E*** *and* ***G****, Mean fibre length (mm) for each connection class in young and elderly females, respectively.* ***E*** *and* ***B****, The mean*

percentage of network traffic each connection class routes for the shortest path route within young and elderly females, respectively.

* $p < .0001$, permutation testing ($N = 5000$)

2.4.5 Community structure and intra/inter-modular connectivity

The average elderly connectome (at 7.5% sparsity) partitioned optimally into five distinct modules ($Q = 0.67$, Figure 2-5). The five modules are: left precuneus-occipital-temporal (yellow), left parietal-frontal (green), right frontal-prefrontal (orange), right precuneus-occipital-temporal (red) and a bilateral prefrontal network (blue). Six and five modules were obtained at 5% and 10% sparsity respectively. A force-vector algorithm that acts to cluster densely, mutually connected nodes (Jacomy et al., 2014), yields a network perspective of the connectome (Figure 2-5C). This reveals the intriguing topological organisation of inter-and-within-module connectivity. The clear division of both hemispheres (division running at an angle), demonstrates the dominance of inter-module intra-hemispheric connectivity. Notably, the integration of the inter-hemispheric community structure is almost entirely achieved through the bilateral prefrontal cortex. In addition, hub-regions (bigger circles) are predominately located along the boundaries of modules, and also embedded within their community affiliation, revealing their intra-and-inter-module connectivity. The mean *Pi* (inter-module connectivity) and mean *Z* scores (intra-module connectivity) for hub-nodes were significantly greater than non-hub nodes ($p < 0.0001$, Figure 2-5D).

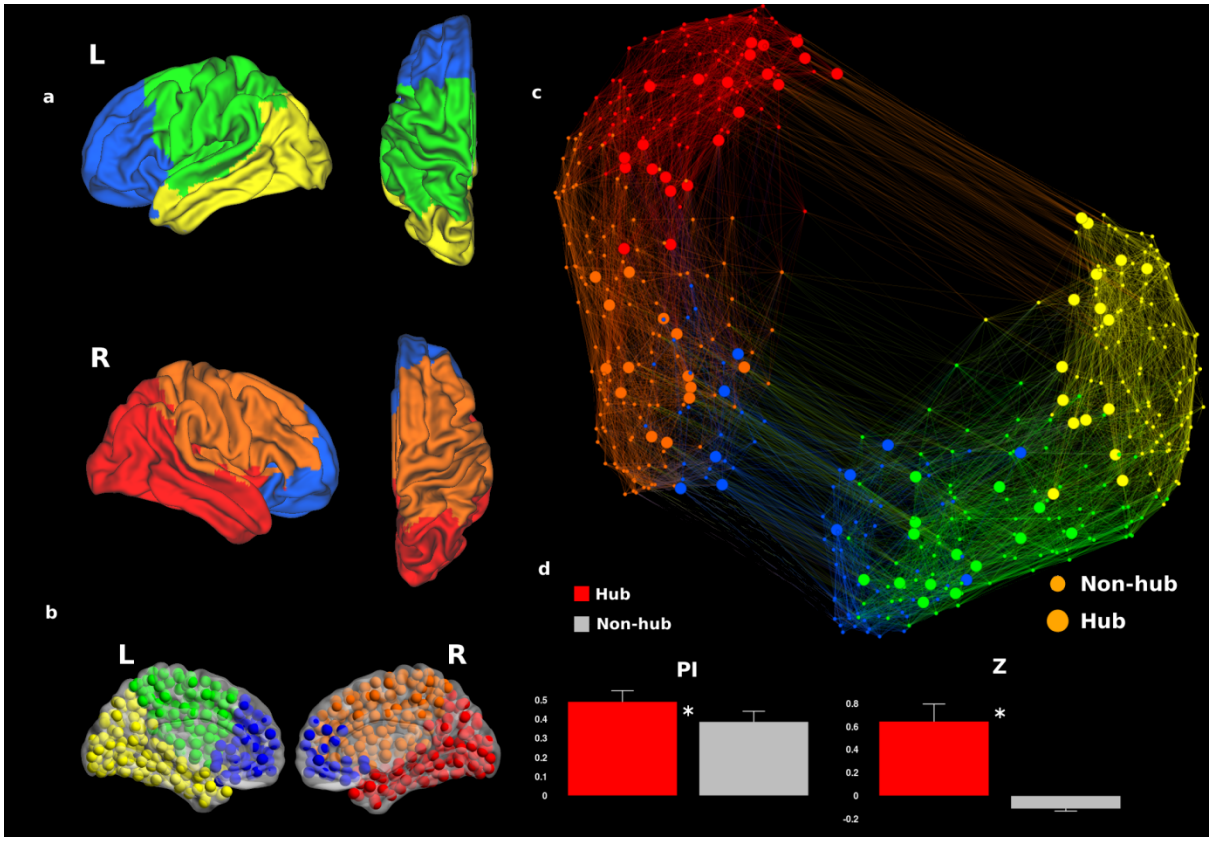

Figure 2-5*: Community structure and intra-and-inter-module connectivity in the elderly connectome. Surface (**A**), and nodal representation (**B**) of community structure in the group average connectome, showing the formation of five distinct modules (indexed by different colours). C, Network perspective of the elderly average connectome through employing a force-vector algorithm, designed to cluster nodes (circles) by virtue of being densely mutually connected. D, Mean PI (inter-module participation, left panel) and Z-scores (intra-module participation, right panel) for hub and non-hub regions.*

* $p < .0001$, permutation testing ($N = 5000$)

2.4.6 Lateralization

Application of the NBS identified significant lateralization of weighted connectivity in two distinct left lateralized clusters ($t = 5.5$, $p < 0.001$, FWE-corrected) and three right-lateralized clusters ($t = 5.5$, $p < 0.0001$, FWE-corrected):

2.4.6.1 *Left-lateralized subnetworks*

Tracking of the fibre bundles corresponding to the first left-lateralized subnetwork reveals a large tract that is consistent with the cingulum and interior fronto-occipital bundles, connecting occipital, precuneus, thalamic, and cingulate structures to orbitofrontal areas (Figure 2-6A). The second subnetwork involves three distinct components; the first (Figure 2-6B) consistent with the frontal aslant, connecting the SMA to the inferior frontal operculum; the second (Figure 2-6C) consistent with the direct arcuate fasiculus, wiring superior temporal and inferior frontal regions; and the third (Figure 2-6D) connecting temporal (superior and middle) areas to angular and supramarginal regions.

2.4.6.2 *Right-lateralized subnetworks.*

The first right-lateralised subnetwork invokes two distinct components; one consistent with superior longitudinal circuits spanning from superior temporal regions to the insula and ventral striatum, whilst the second component involving loops between precuneus and occipital regions (Figure 2-6E). The second subnetwork is consistent with superior longitudinal circuits connecting inferior parietal areas to the insula (Figure 2-6F). The last subnetwork is consistent with the circuits of optic radiations connecting the thalamus to medial temporal and occipital areas, but also includes connections between temporal (middle and medial) and occipital structures (Figure 2-6G).

Each cluster identified above was also significantly lateralized ($p < 0.0001$, *t*-test, $N = 5000$ *perms*) - within only right-handed subjects ($n = 109$) - in concordance with the NBS findings.

2.4.7 Sexual dimorphisms.

We also identified gender-associated subnetworks (Figure 2-7, $t = 3.5$, $p < 0.05$, FWE-corrected). Three distinct subnetworks were more strongly expressed in females, all involving increased inter-hemispheric connectivity: The first (Figure 2-7, top row, $p = 0.015$, FWE-corrected) includes connection between middle cingulate structures, and also between the left middle cingulate and right SMA. The second (Figure 2-7A, middle, $p < 0.0001$, FWE-corrected) includes connections spanning bilateral anterior cingulate structures, and also anterior cingulate and superior frontal structures. The third (right, $p = 0.015$, FWE-corrected) encompasses connections from the left IFG to the right middle and superior frontal regions. The strongest gender-related differences in males (Figure 2-7, red) encompassed two similar subnetwork of connections; The first ($p = 0.004$, FWE-corrected) encompassed connections within the left-hemisphere, spanning from subcortical (thalamus, putamen) and anterior cingulate structures to prefrontal (orbitofrontal, rectus, and superior medial) cortex. The second ($p = 0.047$, FWE-corrected), within the right hemisphere, connected the ventral striatum to orbitofrontal cortex, with further connections to frontal superior medial regions.

2.5 Discussion

We sought to elucidate key features of the healthy elderly connectome, leveraging recent advances in the acquisition and analysis of brain networks. We found the topology and architectural features of hub-regions to be consistent with connectomic data from a young

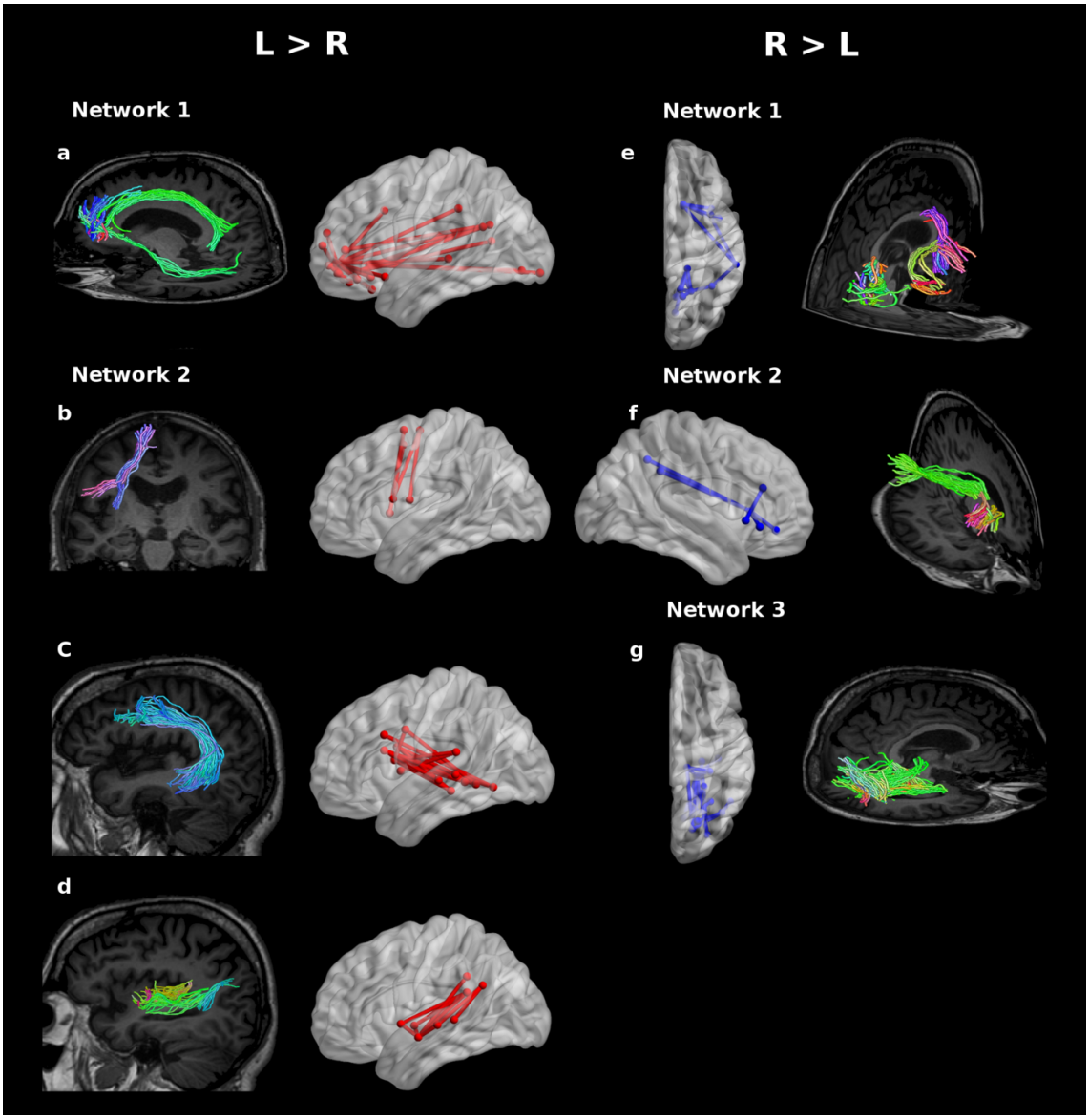

*Figure 2-6: Subnetwork clusters identified by the NBS to demonstrate lateralized connectivity. The figure shows two significant ($p < .05$, FWE-corrected) network left-lateralized (left panel, **A**, **B**, **C**, and **D**) clusters, and three right-lateralized (right panel, e, f, and g) network clusters.*

healthy adult cohort, and also with prior research in young adults (van den Heuvel and Sporns, 2011, 2013b) . We also report the presence of strongly lateralized subnetworks, and focal sexual dimorphisms in network organisation within the elderly connectome.

2.5.1 Hubs in the elderly connectome

Hub-regions identified in the elderly connectome are highly consistent with the topology we identified in the structural networks of a young adult population, although subtle differences do occur. Hub-regions identified here have also predominately been revealed as structural hubs - according to various definitions - in other investigations of healthy adults (Collin et al., 2014b; van den Heuvel et al., 2012; van den Heuvel et al., 2010; van den Heuvel and Sporns, 2011). In our data, superior parietal and posterior cingulate regions were not identified as hubs in either the young or eldery connectomes, in contrast with most previous investigations. Hub-regions in the elderly connectome with the largest composite scores, and also showing the highest consistency across subjects, include subcortical structures (i.e. thalamus, striatum, and the amygdalae), and cortical regions such as the anterior cingulate, insula, and precentral gyrus. The majority of these regions have been shown to be the most highly connected (both weighted and binary-wise) in other studies of adult structural networks (Collin et al., 2014b; van den Heuvel and Sporns, 2011), where their nodal properties rank highly across multiple measures (Betzel et al., 2014; Crossley et al., 2014; van den Heuvel et al., 2010; van den Heuvel and Sporns, 2011). Notably, these are core regions that have been proposed to form the adult "rich club": Densely connected hubs, with enriched inter-hub connectivity suggesting an integral role in large-scale network communication (van den Heuvel and Sporns, 2011, 2013b). Here we also we reveal that the topology of core hub-regions follow a consistent distribution across the healthy lifespan.

Many of the specific architectural features of hub connections are also consistent with young adults (Collin et al., 2014b; Crossley et al., 2014; van den Heuvel et al., 2012).

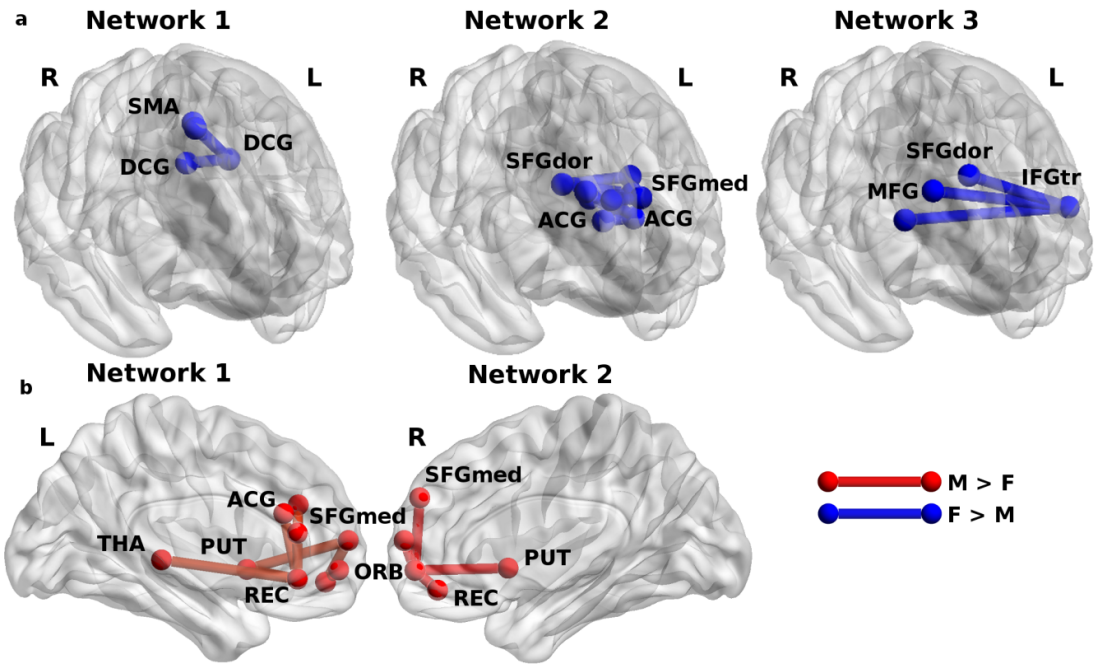

Figure 2-7*: Focal gender differences in subnetwork connectivity identified by the NBS. A, Blue lines represent the significant ($p < .05$, FWE-corrected) subnetworks of anatomical connections between nodes (blue dots) where the NBS identified the strongest connectivity greater in females, relative to males. B, Red lines and dots indicates the localised connectivity of subnetworks strongest in males.*

SMA, Supplementary Motor Area; DCG; Middle Cingulate, SFGdor, Superior Frontal; SFGmed, medial Superior Frontal; ACG, Anterior Cingulate Gyrus; MFG, Middle Frontal; IFGtri, Inferior Frontal Triangularis ; THA, Thalamus; PUT, Putamen; REC, Rectus; ORB, Orbitofrontal.

Hub connections (including feeders) were found to exhibit longer projection distances and increased cost-to-density ratios (more costly than predicted by their density alone), underlining their likely high-cost to brain networks. Hub connections were also found to exhibit weighted rich-club architecture, route a greater proportion of network traffic (relative to their density), and possess stronger inter-and-intra-modular connectivity. Most notably, virtual lesioning of hub connections were found to result in a disproportionate reduction in global network communicability, in comparison to the

removal of feeder (except at the last increment level) and local connections. These high-cost features of hub connections in the elderly appear to be offset by their functional advantages in integrating brain regions of distributed large-scale systems. Given these features are found within our younger cohort, and also previously published adult connectomic data (Collin et al., 2014b; van den Heuvel et al., 2012), these findings thus suggests the critical role of hub connections to large-scale network communication is ongoing across the lifespan.

The critical role of hub-regions and their connections to large-scale brain network dynamics is generating wider empirical attention. Hub-regions overlap with multiple large-scale functional networks (Braga et al., 2013; Crossley et al., 2013; Sepulcre et al., 2012; Spreng et al., 2013; Tomasi and Volkow, 2011; van den Heuvel and Sporns, 2013a; Yeo et al., 2014), and their connections have been shown to be involved in a disproportionately greater amount of integration of these networks (van den Heuvel and Sporns, 2013a). Furthermore, hub-regions are predominately those regions important to the integration of dynamic large-scale networks during various cognitive states (Dwyer et al., 2014; Elton and Gao, 2014; Fornito et al., 2012a; Sripada et al., 2014), and overlap with areas implicated for their higher-order roles within-and-between such systems (Grahn et al., 2008; Lindquist et al., 2012; Menon and Uddin, 2010; Shackman et al., 2011; van den Brink et al., 2014). Interestingly, the brain regions typically reported to display these characteristics in large-scale systems are transmodal subcortical (i.e. thalamus, caudate nucleus) and limbic (i.e. insula, anterior cingulate) areas also identified to be most representative of hubs in the elderly connectome (the precuneus was a notable exception in our data). In turn, this provides further plausibility regarding the stability

across normal ageing of not only the topology of core architectural brain features, but also their pivotal roles in large-scale network communication.

Despite these similarities across the age cohorts, we did observe some possible age-related changes to hub-regions (and their connections). Notably, the mean fibre length of connections to hub-regions (both hub and feeder connections) in elderly females were found to be 40mm shorter than young females. We also observed an increase in the routing of simulated traffic in the elderly connectome through local connections and a corresponding decrease of hub-to-hub routing. These findings can be interpreted within the hallmarks of normal ageing. First, previous investigations of functional connectomic lifespan changes reported that long-distance connections are disproportionally affected in normal ageing (Cao et al., 2014; Tomasi and Volkow, 2012a; Wang et al., 2012). Second, cognitive domains (i.e. working memory, executive functions, processing speed) that consistently decline with healthy ageing rely on the integration and coordination of distributed large-scale systems, where long-distance connections are pivotal (Crossley et al., 2013; Dwyer et al., 2014; Lim et al., 2014; Park and Reuter-Lorenz, 2009; van den Heuvel and Sporns, 2013a). Finally, the fragility of healthy adult brain networks to simulated (computational) attack of hub connections has been posited to reflect pathogenic processes (i.e. amyloid deposition) in normal ageing and underlying neurodegenerative disorders such as AD, where the high metabolic activity of such regions has shown to render them more susceptible (Buckner et al., 2009; Crossley et al., 2014; Toga and Thompson, 2014; Tomasi et al., 2013). The present findings, taken together with the literature regarding normal ageing, suggest while the core architectural features of hub connections remain pivotal in the elderly, their capacity for large-scale communication is reduced.

Several methodological challenges do limit the implications for direct age-related analysis. First, for direct statistical contrasts to be performed, the diffusion acquisition parameters should be identical between the two populations; otherwise the distribution of connectivity, regardless of age effects, will be non-uniform (Tournier et al., 2013; Vaessen et al., 2010; Zalesky et al., 2010b). Changes in the *b*-value, for example will impact upon the diffusion signal to noise ratio – changes that will likely propagate through the diffusion pipeline leading to systematic differences (such as the distribution of inferred fibre lengths). Data from the young adult population employed here were chosen on the merits that the diffusion images were acquired on exactly the same MRI scanner. We do not, however, perform direct contrasts, but limit our comparison to a quantitative visualization. Second, differences in head motion, brain volume, white matter volume, brain anatomy and challenges in the appropriate matching of education and general medical issues are other substantial challenges that require substantial future work before direct comparisons between young and elderly connectomes can be confidentially made.

2.5.2 Lateralization effects

The first left-lateralized subnetwork cluster we identified in the elderly is consistent with the cingulum bundle and inferior fronto-occipital fibres, connecting occipital, precuneus, thalamic and cingulate structures to orbitofrontal regions. This is consistent with the left-lateralized FA values commonly found within anterior portions of adult cingulum bundles (Takao et al., 2013). This lateralization is notable given segments of the cingulum bundle, and orbitofrontal structures, are thought to be essential for executive functions including decision-making and emotional processing (Grabenhorst and Rolls, 2011; Heilbronner and Haber, 2014; Schoenbaum et al., 2009; Shackman et al., 2011).

The first bundle of the second left-lateralized subnetwork interconnects parietal (angular and Geschwind's area) regions with temporal (middle and superior) areas, and the second is consistent with arcuate fasciculus circuits connecting Wernicke's to Broca's area. These are perisylvian circuits specialised for language (Catani et al., 2005; Price, 2012). The other bundle is consistent with the frontal aslant connecting the SMA to the inferior frontal operculum, which has been reported to be leftward lateralized in adults (Catani et al., 2012; Vergani et al., 2014). The SMA and rolandic areas are activated during the movements essential for speech production (Bouchard et al., 2013; Brown et al., 2009; Price, 2012), thereby suggesting this subnetwork is specialised for sensorimotor integration. Nevertheless, these strong leftward lateralizations are surprising given decreased functional specialisation of both prefrontal and language networks is typically reported with age (Antonenko et al., 2013; Bergerbest et al., 2009; Cabeza et al., 2002; Davis et al., 2012).

We also identified three rightward lateralizations. The third of these is associated with visual circuits, consistent with the optic radiation wiring the thalamus to both occipital and medial temporal regions (Bassi et al., 2008; Bürgel et al., 1999; Thiebaut de Schotten et al., 2011b). The two other right-lateralized subnetworks are both consistent with superior longitudinal fasiculus bundles spanning from supramarginal and superior temporal regions to the insula and ventral striatum. These bundles are found to be right-lateralized in adults (Thiebaut de Schotten et al., 2011a; Thiebaut de Schotten et al., 2011b), but of more significance is that the degree of lateralization in these circuits has recently been associated with increased speed for visuospatial processing for targets in the left hemifield (Thiebaut de Schotten et al., 2011a). These findings suggest these

lateralized subnetworks remain specialised for visual and visuospatial processes in the elderly.

2.5.3 Sexual dimorphisms

We not only replicate findings of increased inter-hemispheric connectivity within female youths (Ingalhalikar et al., 2014), but show it is localised to subnetworks of circuits wiring cingulate structures (middle and anterior), as well as prefrontal cortices (lateral and middle). This observation builds upon prior evidence of distinct sexual dismorphisms within these anatomical areas, such as increased grey matter volume in the prefrontal cortices of females (Feis et al., 2013; Luders and Toga, 2010), as well as greater FA values within the corpus callosum (Kanaan et al., 2012; Phillips et al., 2013; Schmithorst et al., 2008). Nevertheless, focal identification of these subnetworks is of interest, given that language and executive functions are associated with the same circuits (Gasquoine, 2013; Koechlin et al., 1999; Price, 2012), and females across all age groups demonstrate greater performance in cognitive tasks assessing these functions (Gur et al., 1999; Hoogendam et al., 2014; Kimura, 2004). Furthermore, increased FA of the corpus callosum has been associated with increased behavioural performance and inter-hemispheric functional connectivity during language-based tasks (Antonenko et al., 2013; Davis et al., 2012). Thus, it is possible the increased connectivity of these subnetworks in females facilitates superior performance in verbal-based abilities.

We also find stronger connectivity in males in subnetworks connecting ventral striatal, anterior cingulate and prefrontal regions (orbitofrontal and superior medial). The subnetworks encompass circuits that have been attributed to decision-making and regulatory functions (Basten et al., 2010; Grabenhorst and Rolls, 2011; Winecoff et al.,

2013; Zald and Andreotti, 2010). Interestingly, males generally demonstrate more efficient behavioural regulation, and also differential functional activation in these areas for tasks involving emotion processing and decision-making (Lighthall et al., 2012; Ross and Monnot, 2011; van den Bos et al., 2013; Whittle et al., 2011). This pattern of stronger wiring found in males is thus consistent with the observed gender differences in tasks associated with these circuits.

2.5.4 Conclusion

In sum, our study is the first systematic investigation of network organisation in the elderly connectome. Notwithstanding the methodological caveats highlighted above, we provide preliminary evidence that the topology and architectural features of hub-regions are preserved into the healthy elderly. Moreover, our findings provide a benchmark for future longitudinal and clinical investigations, arguing that elucidating the topology and cost of hub regions may be key to connectomic changes. In particular the architectural features shown here provide a benchmark for further connectomic investigations to dissociate healthy ageing from neurodegenerative disorders.

Chapter 3: The independent influences of age and education on functional brain networks and cognition in healthy older adults

3.1 Abstract

Healthy ageing is accompanied by a constellation of characteristic changes in cognitive processes associated with alterations in functional brain networks. The relationships between brain networks and cognition during ageing are moderated by the influence of cognitive reserve factors in a complex and incompletely understood manner. Here, we leverage multivariate analyses to elucidate the dependence of latent patterns (or modes) of resting state functional connectivity on demographic and cognitive measures in 101 cognitively-normal elders. We identified three modes of co-variation capturing interdependences between phenotypic measures and functional brain networks. The first significant mode (p=0.00043) captures the opposing influence of age and core cognitive processes such as attention and processing speed on functional connectivity patterns. The bilateral functional subnetwork expressed by this mode links lower-order sensorimotor and visual regions through key areas such as the parietal operculum and posterior insula. The second mode (p=0.012) links a strong and independent association between educational attainment and connectivity patterns, whilst the third (p=0.041) captures weak brain-behaviour relations. The opposing pull of age on attention and processing speed within the first mode suggests the parietal operculum and posterior insula are crucial to age-related changes in sensorimotor functioning. The connectivity of this network is influenced predominantly by intrinsic factors such as age. The influence of

extrinsic factors such as education split into a second, independent mode which confers reserve benefits by acting upon between-network interactions tied to key hub-regions.

3.2 Introduction

Normal ageing is associated with progressive changes in cognitive function which impact upon on functioning and inter-personal relations (Stuck et al., 1999; Willis et al., 2006). Fluid-based cognitive functions are particularly sensitive to change with specific, age-related underlying neurobiological processes that are incompletely understood (Grady, 2012; Park and Reuter-Lorenz, 2009). It is crucial to disambiguate these normal age-related changes from the neurobiological pathology of neurodegenerative disorders such as AD (Dennis and Thompson, 2014). Traditionally, the more rapid progression of atrophy (indexed by volumetric size and thickness) in prefrontal, hippocampal, and parietal cortices is thought to underpin progressive age-related cognitive changes (Dennis and Cabeza, 2008; Park and Reuter-Lorenz, 2009; Raz et al., 2005). However, investigations that have reported macroscopic changes associated with age-related declines are rather inconsistent or contradictory (Rodrigue and Kennedy, 2011).

Alterations in univariate measures of brain structure such as local cortical thickness, only partially capture the neurobiological processes underpinning age-related cognitive changes. Conceptualisation of human brain function as being shaped by interactions (connections) between its constituent elements (brain regions) has underpinned seminal observations that healthy brain networks are topologically organised in a highly complex, and interconnected manner (Bassett and Bullmore, 2006; Bullmore and Sporns, 2012; Sporns, 2013b). Such networks delicately balance functional

integration and segregation of spatially-distinct brain-regions, giving rise to cognitive and perceptual states (Friston et al., 1995; Sporns et al., 2000; Tononi et al., 1994). Networks can be constituted by structural connections, such as inferred from dMRI tractography (Hagmann et al. 2008), or functional connections measured by temporal correlations of spontaneous fluctuations in BOLD signals between brain regions (Biswal et al., 1995; Fornito et al., 2013; Fox and Raichle, 2007).

The sensitivity of fluid-based cognitive functions to normal ageing, which require integrated and coordinated neural communication, suggests age-related changes may be attributable to the corresponding changes in large-scale communication (Andrews-Hanna et al., 2007). Evidence for this proposal is supported by reduced functional connectivity within specialised resting-state networks such as the DMN, whilst inter-network connectivity is conversely found to increase (Andrews-Hanna et al., 2007; Betzel et al., 2014; Chan et al., 2014; Geerligs et al., 2015; Tsvetanov et al., 2016). Such changes appear partially associated with poorer cognitive performance (Andrews-Hanna et al., 2007; Chan et al., 2014; Fjell et al., 2015; Onoda et al., 2012; Salami et al., 2014) although the complete picture of whole-brain network activity and age-related changes in cognition across multiple domains is lacking.

Measures of intra/inter-network communication in this field have typically been derived from pair-wise estimates of connectivity between representative seed-regions, or aggregated across regions of respective networks. Graph-theoretical techniques afford characterisation of multivariate complex interactions within functional brain networks (Fornito et al., 2013; Sporns, 2013b). Applications of graph-theoretical techniques to the study of ageing have reported alterations in the connectivity of specific subnetworks, and decreases in connectivity pronounced over long-range distances (Cao et al., 2014;

Marques et al., 2015; Sala-Llonch et al., 2014; Tomasi and Volkow, 2012a). Disruptions to long-range communication are proposed to reflect decreased integration and increased segregation of functional brain networks with age, further substantiated by widely observed changes in global network topology (Bullmore and Sporns, 2012; Cao et al., 2014; Sala-Llonch et al., 2014). Hitherto, only few investigations of functional networks in healthy elderly populations have been undertaken (Marques et al., 2015; Sala-Llonch et al., 2014), which is surprising given that the trajectories of cognitive decline are not uniform across the lifespan (Deary et al., 2009; Schaie, 1996).

The relationship between age-related cognitive changes and functional brain networks is moderated by cognitive reserve (CR) in a manner that remains poorly understood. Higher levels of educational attainment, intelligence, occupational status and particular lifestyle factors confer protection against the effects of ageing on cognition as well as the onset of Alzheimer's symptomatology (Stern, 2012; Valenzuela and Sachdev, 2006). Such factors - postulated to contribute to an individual's CR (Stern, 2002) - are associated with a relative preservation of brain structure and more efficient neural activity during cognitive demands (Bartrés-Faz and Arenaza-Urquijo, 2011). Increased educational attainment is also associated with increased connectivity in distributed cortical networks (Marques et al., 2016; Marques et al., 2015). However, it remains to be elucidated whether CR confers greater resilience upon cognitive networks sensitive to age-related decline, or rather indirectly via non-task specific networks (Bartrés-Faz and Arenaza-Urquijo, 2011; Stern, 2009; Stern et al., 2008).

Multivariate analyses allow a broad picture of brain-behaviour relationships. Using canonical correlation analysis (CCA) Smith et al. (2015) studied the inter-relationships between 158 phenotypic measures and whole-brain functional connectivity

patterns in a large cohort of healthy younger adults (Van Essen et al., 2013). Intriguingly, the covariation between the full suite of phenotypic markers and functional connectivity loaded onto a single positive-negative axis. Positive personal traits (e.g. life satisfaction, education years, and fluid intelligence) shared strong co-variations with connectivity patterns. Conversely, characteristically negative traits (e.g. substance use, rule-breaking behaviour) load negatively onto these brain-behaviour associations. A recent CCA-based investigation of brain networks in ageing revealed specific co-variation of intra-and-inter-network connectivity with particular cognitive domain scores (Tsvetanov et al., 2016). However, the relative influence of both age and CR proxies within these co-variation patterns was not examined.

Here we use CCA to examine inter-relations amongst age, cognitive performance, and CR in relation to patterns of functional connectivity in 101 cognitively-normal elders. In particular, we ask whether the single axis of associations between behavioural indicators of cognition and functional brain networks seen in young adults (Smith et al., 2015b), persists under the influence of ageing. Cognitive domains loading against age are potentially most susceptible to decline. We ask whether proxies for CR exert their influence upon the same networks associated with age, or rather onto independent brain-behaviour modes.

3.3 Methods

3.3.1 Participants

Cognitively normal individuals were drawn from a longitudinal, population-based study (the Sydney Memory and Ageing Study (Sachdev et al., 2010)). At the baseline of this

longitudinal study, community-dwelling participants initially between 70-90 years of age were randomly recruited from the electoral roll. Imaging and phenotypic data for the present study were acquired during the fourth wave of this study (approximately 6 years following study baseline). Subjects were classified as cognitively normal at the current wave if their performance on neuropsychological test measures was less than 1.5 *SD*s below normative values (Tsang et al., 2013). Exclusion criteria at study entry included a Mini-Mental Statement Examination (MMSE) (Folstein et al., 1975) adjusted (Anderson et al., 2007) score below 24, a diagnosis of dementia, developmental disability, a history of schizophrenia, bipolar disorder, multiple sclerosis or motor neuron disease, active malignancy, or inadequate comprehension of English to complete a basic assessment. 135 participants met inclusion criteria. The study was approved by the Ethics Committee of the University of New South Wales and participants gave written, informed consent.

3.3.2 Neuropsychological measures

A comprehensive neuropsychological battery was administered by trained graduate psychologists to cover five cognitive domains of attention/processing speed, memory, language, visuospatial ability, and executive function (Kochan et al., 2010; Sachdev et al., 2010). Each domain consists of a composite of individual tests (Table 3-1). Memory was further subdivided into verbal memory after exclusion of a visual retention test. The individual test scores for each subject were transformed into quasi *Z*-scores based upon the mean and standard deviation of tests scores for a healthy, reference group (n=723) phenotyped at study baseline. Domain scores were calculated as the average of the quasi *Z*-scores of tests comprising each domain. If necessary, the signs of the *z*-scores were reversed so that higher scores reflect better performance.

The National Adult Reading Test (NART) (Nelson and Willison, 1991) was administered to a subset of the current population at study baseline. The NART IQ estimates premorbid intelligence levels (Bright et al., 2002).

Table 3-1. *Neuropsychological tests to measure cognitive domain scores*

Cognitive Domain	Neuropsychological Test
Attention/Processing Speed	• Digit Symbol-Coding (Wechsler, 1997a) • Trail Making Test (TMT) A (Strauss et al., 2006)

Memory	• Logical Memory Story A delayed recall (Wechsler, 1997b)
	• Rey Auditory Verbal Learning Test (RAVLT) (Strauss et al., 2006):
	  o RAVLT total learning; sum of trials 1-5
	  o RAVLT short-term delayed recall; trial 6
	  o RAVLT long-term delayed recall; trial 7
	• Benton Visual Retention Test recognition (Benton et al., 1996)

Verbal Memory	• As above, but not including the Benton Visual Retention Test.
Language	• Boston Naming Test – 30 items (Kaplan, 2001) • Semantic Fluency (Animals) (Strauss et al., 2006)
Visuospatial Ability	• Block Design (Wechsler, 1981)
Executive Function	• Controlled Oral Word Association Test (Strauss et al., 2006) • TMT B (Strauss et al., 2006)

3.3.3 Acquisition and pre-processing of MRI data

Eyes-closed rs-fMRI data consisting of 208 time-points were acquired with a T2* weighted echo-planar imaging sequence (TE = 30 ms, TR = 2000 ms, 1.87 x 1.87 x 4.50 mm^3 voxels) on a Philips 3T Achieva Quasar Dual MRI scanner. Structural T1-weighted MRI were also acquired (TR = 6.39 ms, TE = 2.9 ms, $1mm^3$ isotropic voxels). FSLView

was used to visualise every MRI scan for artifact inspection. Subjects were removed if severe signal dropout (particularly around orbitofrontal areas) or spatial distortions were present. Data from 111 participants thus entered the study.

Steps in pre-processing were performed using the Data Processing Assistant for Resting-State fMRI (DPARSF, v3.2 advanced edition) software package (Yan and Zang, 2010), which calls functions from SPM8 (http://www.fil.ion.ucl.ac.uk/spm/). Basic pre-processing steps included slice-timing, realignment to mean functional image, co-registration of the structural image, linear detrending, and nuisance regression of head motion (24 paramters) (Friston et al., 1996b) and WM/CSF signals (Ashburner and Friston, 2005). Native functional images were transformed into an average population-based T1 template and then MNI space (3mm^3 voxels). rs-fMRI images were smoothed (6mm) and temporal band-pass filtering applied (0.01–0.08 Hz). Global signal regression was not performed. Full description of the steps involved for the acquisition and pre-processing of rs-fMRI data are provided in Appendix 3 (A3.1 and 3.2).

Data from one-hundred and one subjects were included in the main analysis (Table 3-2, left-column). Of the initial subject population (n = 135), fifteen were removed due to severe signal loss (thirteen within rs-fMRI scans), ten had incomplete cognitive information, whilst nine failed adequate co-registration between their T1-weighted and mean functional image. No significant differences for demographic (Table 3-1) or cognitive (Table A4-1) information (p<0.05, t-test) were found to the subset of subjects (n = 91; Table 3-2, right column) receiving a NART IQ assessment at study baseline**.**

Table 3-2. *Basic demographic and cognitive information of subjects.*

Cohort	**All subjects (*n* = 101)**	**With baseline IQ (*n* = 91)**
NESB (*n*)	10	1
M/F (*n*)	44/57	39/52
	Mean (+- *SD*)	Mean (+- *SD*)
Age (years)	82.65 (3.81)	82.45 (3.73)
Education (years)	12.71 (3.64)	12.51 (3.55)
MMSE	29.45 (0.90)	29.40 (0.93)
NART IQ	N/A	109.98 (9.41)

NESB, Non-English speaking background

3.3.4 Construction and normalization of functional brain networks

Full description of the steps involved for the construction and normalization of functional brain networks are provided in Appendix 3 (3.3 and 3.4). In brief, the Pearson's correlation coefficient of the mean BOLD signals between all pairs of 512 uniformly-sized regions (Zalesky et al., 2010b) was calculated to construct the functional connectivity matrix *M*. Fisher's transformation was applied to *M*, and subsequent upper-triangle values were concatenated across all subjects, forming matrix N_1.

3.3.5 Normalization and demeaning of connectivity matrices

The connectivity matrices N_1 were normalized and demeaned according to the procedure of (Smith et al., 2015b) (also available online at http://fsl.fmrib.ox.ac.uk/analysis/HCP-

CCA/hcp_cca.m), resulting in the matrix N_2 for subsequent analyses. The mean frame-wise displacement (FD) (Power et al., 2012) was calculated to also remove potential confounding effects of head motion in N_2 to form N_3. There was no significant effect of age on subject motion (FD) ($p > 0.39$, $r = -0.09$)

3.3.6 CCA

Eight subject measures were chosen for inclusion in the CCA: Age, education years, and the domain scores for attention and processing speed, language, executive function, visuo-spatial ability, memory, and verbal memory. NART IQ scores were only included in an auxiliary analysis as only a subset of subjects were administered this test at wave 1.

Principal Components Analysis was implemented via the FSLNets toolbox (Smith et al., 2014) within MATLAB to reduce the dimensionality of N_3 to eight eigenvectors (corresponding to the number of non-imaging measures employed). CCA was then applied to these reduced data yielding eight modes which constitute weighted linear combinations of orthogonalized subject measures and functional connectivity eigenvectors: Each mode represents canonical correlations which correspond to the maximum residual covariation between the two variate sets in decreasing rank order. Each CCA mode m is represented by the vectors U_m and V_m, representing the individual subject weights for subject measures and connectivity matrices respectively:

- U_m is the extent to which each subject is (positively or negatively) correlated to population variation in subject measures within mode m
- V_m is the extent to which each subject is correlated to population variation in brain connectivity within mode m

The correlation of U_m and V_m yields r_m, the strength of the population co-variation in mode m shared between brain connectivity and subject measures.

3.3.7 Association of connectivity edges and nodal regions within each mode

We next assessed which connectivity edges are most strongly associated with population variations in connectivity captured within mode m. First, to obtain the relative weight (and directional signs) of each edges association with the connectivity within mode m, we correlated V_m with the original connectivity estimates in N_3, resulting in a vector A_{Fm}. The connectivity edges identified most strongly associated with either positive or negative co-variations between U_m and V_m, were chosen as the top 250 (representing 0.0019% of all network edges) strongest connections with positive and negative signs within A_{Fm} respectively.

3.3.8 Statistical analyses

To determine the significance of interdependence between the variates sets within each mode m, Wilk's Lambda (λ) was first calculated and transformed into Rao's Approximation F-statistic (Rao, 1952). Shared variances captured between the respective variate sets of mode m were determined as significant if $p<0.05$, thus rejecting the null hypothesis ($H0$) that subject measures and functional components are independent of each other within mode m.

3.4 Results

Multivariate analysis were employed to capture the latent relations between age and cognitive changes with respect to resting-state connectivity in 101 cognitively-normal elders. We further investigated the mitigating influence of cognitive reserve factors such as education years amongst these age-related associations with connectivity. In the full sample, we first assessed the complex relationships between age, gender, education and six cognitive domains: verbal memory, memory, visuospatial function, executive function, language and attention/processing speed. Performance across these cognitive domains is highly correlated (Figure 3-1); Performance positively correlates with years of education, and generally negatively with age, particularly for attention/processing speed (p<0.001). As expected, memory and verbal memory (being largely redundant) correlate very strongly. Verbal memory (p<0.001) and visuospatial function (p<0.05) are significantly correlated with female sex (Figure 3-1). In a subsample of the main cohort, we also examined relations with IQ (Figure A4-1).

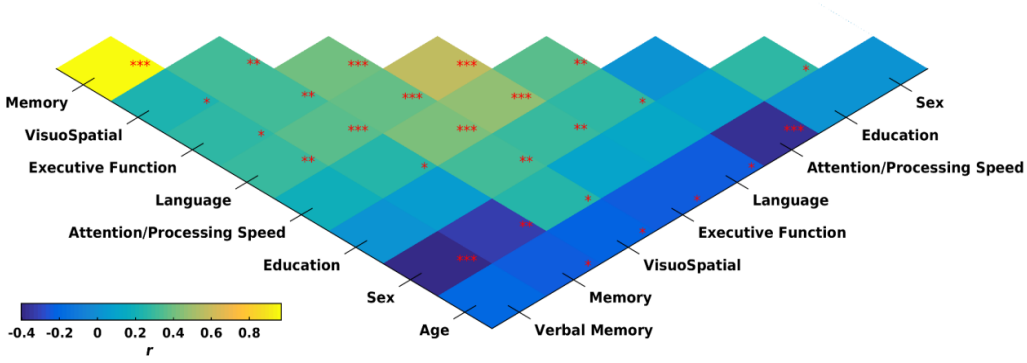

Figure 3-1: *Strength and direction of relations between cognitive and demographic measures*

** p<0.05, ** p<0.01, *** p<0.001; FDR-corrected*

We next used CCA to examine the primary modes that relate these (correlated) demographic and cognitive variables to patterns of resting state fMRI data. CCA identified three significant canonical modes (p<0.05) of interdependence between these non-imaging measures and functional connectivity (Table 3-3).

Table 3-3. *Significant CCA modes in the main-analysis*

CCA Mode	**One**	**Two**	**Three**
df_1	64	49	36
df_2	496.76	441.03	384.80
F	1.77	1.55	1.48
λ	0.30	0.45	0.57
r^2	0.32	0.21	0.20
RI	0.072	0.030	0.023
p	0.00043	0.012	0.041

RI, redundancy index

Each CCA mode consists of a set of weights that reflect the loading of the cognitive and demographic variables onto the corresponding resting state patterns (Figure 3-2). The first mode (p<0.00043) is characterised by a split between all cognitive domains (particularly memory, attention and processing speed) which load along a positive axis, and age which loads strongly and negatively (Figure 3-2A, left panel). Language and education have close to zero loading within this mode. The opposing pull of attention and processing speed versus age can be seen by plotting the subject specific measure weights versus the corresponding connectivity weights, coloured according to age (Figure 3-2D) or attention processing speed (Figure 3-2E). Younger subjects (Figure 3-2D, blue circles)

cluster in the top right corner of the panel, indicating how they weigh positively with the corresponding connectivity-behaviour relations. Likewise, fast and attentive performers (Figure 3-2E, green to dark red) also load positively on the first CCA mode. These plots show that faster, attentive, younger performers weight positively, whereas poorer performers, whom are also older, contribute to negative associations within this mode.

In contrast, the second mode (p<0.012) is characterised by an independent positive association of education years with connectivity (Figure 3-2B, 3-2F). Although executive function loads moderately on this mode, all other variables load very weakly (in both directions). While age and memory load negatively, their contributions are weak.

There also exists a weakly significant third mode (p<0.041). This mode splits cognitive measures into moderately positive visuospatial and memory weights versus weakly negative attention and processing speed (Figure 3-2C). Age and education weight close to zero.

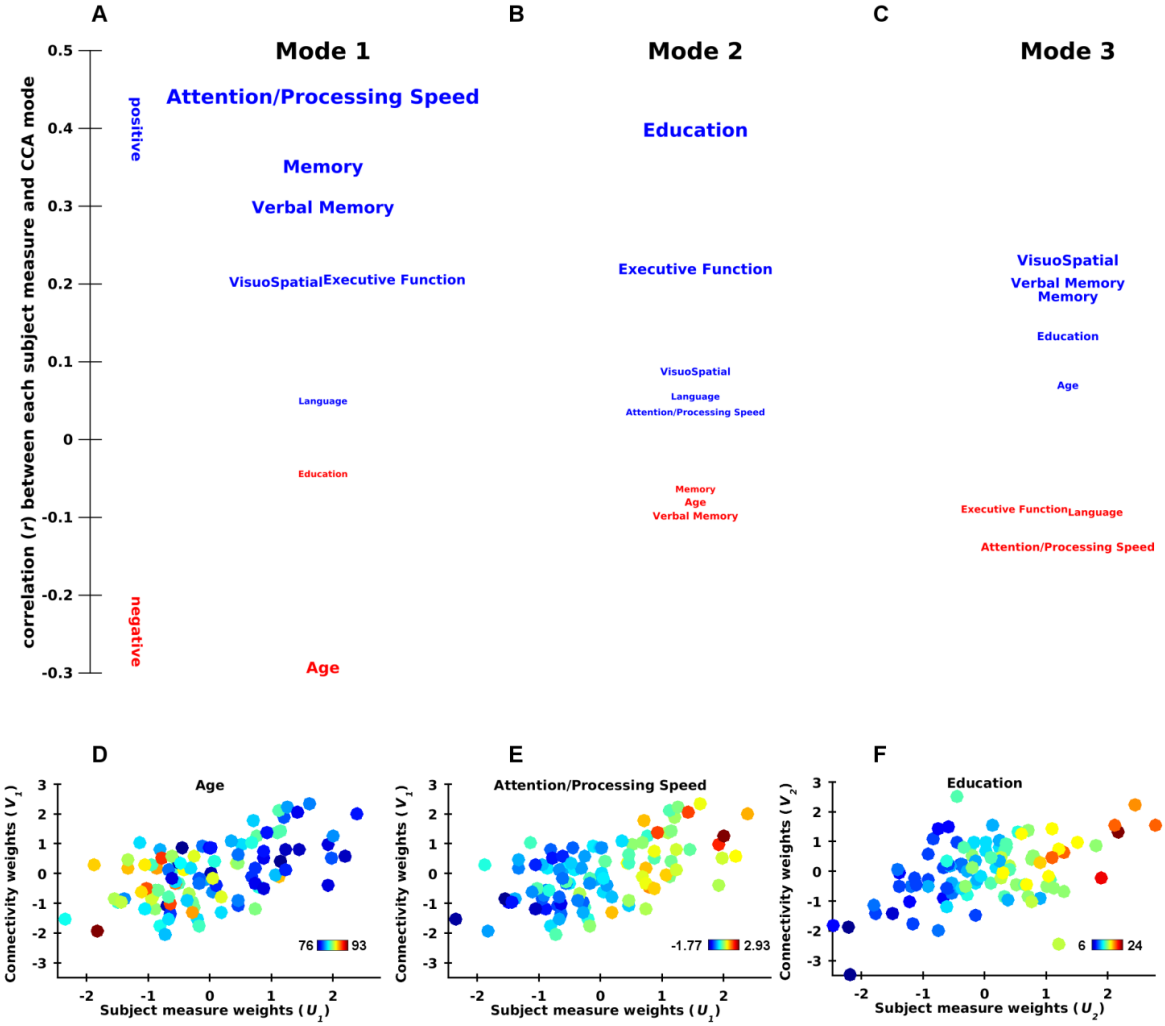

Figure 3-2: *Associations between cognitive and demographic measures captured by the significant CCA modes. A-C, Correlation between subject measures and functional connectivity variation (V_m), with the strength and direction of the relations indicated by vertical position and font size. D-F, Scatter plots showing for each subject (data points) their weighting towards non-imaging measures (U_m, x-axis) and functional connectivity patterns (V_m, y-axis), captured for the first (D-E) and second modes (F). Colour is scaled according to subjects age (D), Attention/Processing Speed performance (E), and education level (F).*

Each of these three CCA modes also load onto patterns of functional brain connectivity. To study these, we calculated the 250 edges most strongly associated with each mode in both the positive and negative directions. The functional connectivity edges most strongly expressed by positive associations in the first mode (mean $r = 0.64$, $SD = 0.02$) primarily involve bi-lateral connections between occipital, temporal (inferior and medial portions), superior parietal, and pre/post central gyral regions (Figure 3-3A). Functional connections between occipital areas and pre/post-central regions within the right hemisphere are also evident. To disentangle the functional basis of this network of strongly associated connections, we assigned regions in our parcellation to broader functional network clusters; default-mode, cognitive-control, somatomotor, dorsal attention, salience ventral attention, visual, and limbic networks (Yeo et al., 2011). Hence, revealing that positive edges in the first mode are predominately clustered between visual, somatomotor, and to a lesser extent, dorsal attention networks. Of note is the convergence of connections upon bi-lateral parietal operculum/posterior insular areas. This topological distribution motivates visualisation of the network using a force-vector algorithm (Jacomy et al., 2014) which spatially co-localises nodal brain regions (circles) that are mutually and densely interconnected (Figure 3-3B);. “Hub” nodes (top 5% highly-connected regions within the network; larger circles) representing rolandic and insular areas are centrally positioned and exhibit a high clustering of strong connections to other regions. Cortical regions that organise around these hubs derive from multiple functional networks.

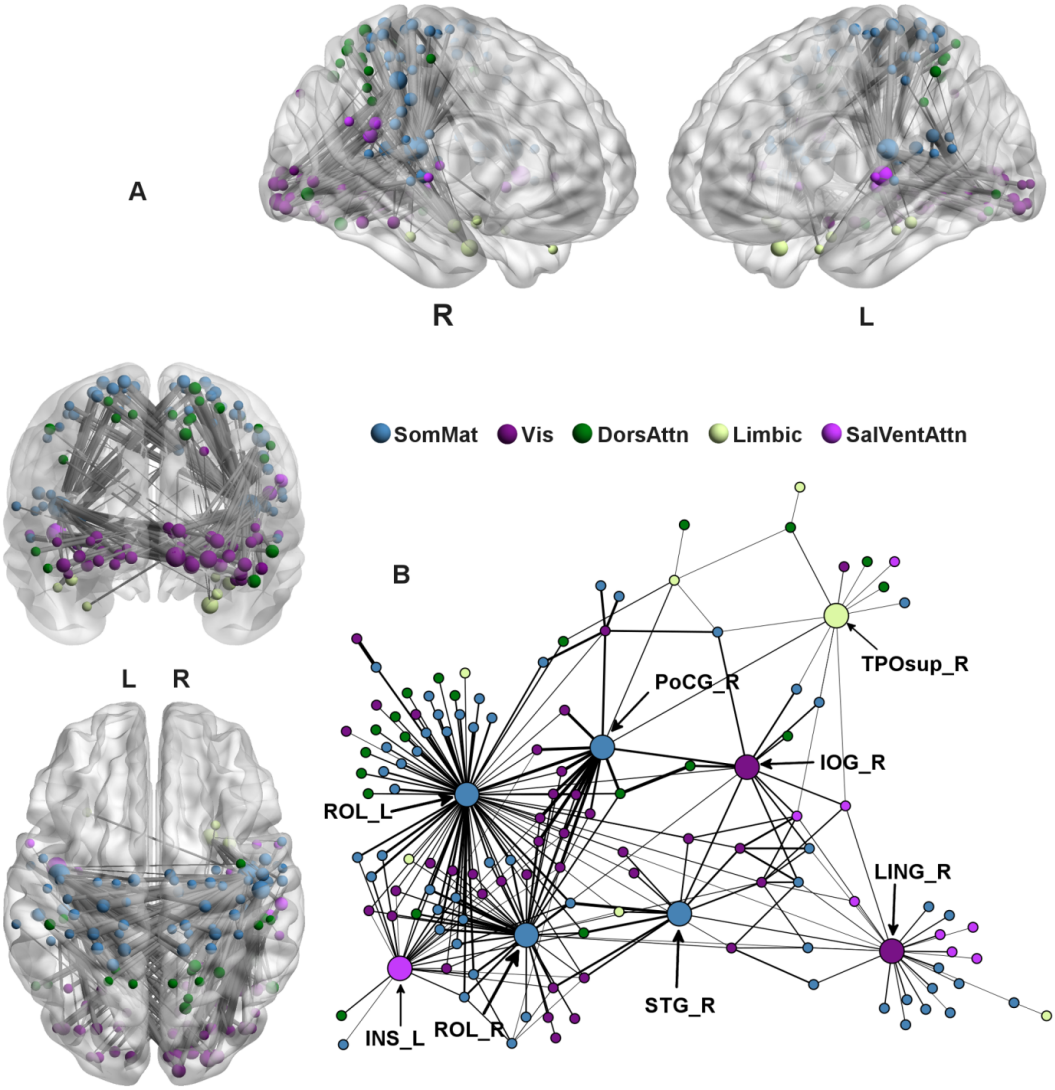

***Figure 3-3**: Connectivity edges most positively expressed by the first CCA mode. A, Connectivity edges exhibiting strongest positive associations with functional connectivity patterns (V_1). Line width indexes strength of correlation. Circle size is scaled to the number of connections each region shares within the network, whilst coloured to functional network affiliation (Yeo et al., 2011). The brain meshes are presented from axial (bottom left panel), posterior (middle left), and customised perspectives of the left (top left; elevation = 0, azimuth = -120) and right-hemisphere (top right; azimuth = -240). B, Force-vector perspective, clustering regions (circles) both mutually and densely interconnected (lines weighted by the mean functional correlation across N_1). Larger circles indicate the most top 5% highly-connected regions within the network.*

INS, Insula; IOG, Inferior Occipital Gyrus; PoCG, Post-central Gyrus, ROL, Rolandic Operculum; STG, Superior Temporal Gyrus; TPOsup, Superior Temporal Pole; L, Left-hemisphere; R, Right-hemisphere

We then identified the functional connectivity edges most negatively expressed by the first mode (mean = -0.27, *SD* = 0.03). These connections form two distinct clusters: The first cluster inter-connects pre-motor, pre/post central gyri and superior medial frontal areas (SMA, pre-SMA, superior frontal gyri) (Figure 3-4A). A second cluster involves inter-hemispheric connections between inferior parietal areas, and additional connections between these areas and left superior parietal regions (Figure 3-4B). On a coarser scale these edges connect default-mode and cognitive control networks areas to regions affiliated with all other networks except for limbic areas, particularly default-mode connectivity with both the somatomotor and dorsal attention networks.

The edges most strongly expressed within the second mode are quite distinct from the networks identified within the first mode, mirroring the divergent loading of phenotypic measures onto these two modes. The edges exhibiting the strongest positive associations (*mean* = 0.73, *SD* = 0.01) with the second mode stretch between visual cortices and dorsolateral prefrontal areas, whilst connections from superior parietal (dorsal attention) and pre/post-central gyri (somatomotor) converge at both dorsolateral and ventrolateral regions, lying within default and control networks (Figure 3-5A). Assigning regions to their respective functional networks shows that edges from the default and control networks inter-connect preferentially with visual, somatomotor, and dorsal attention networks (Figure 3-5B).

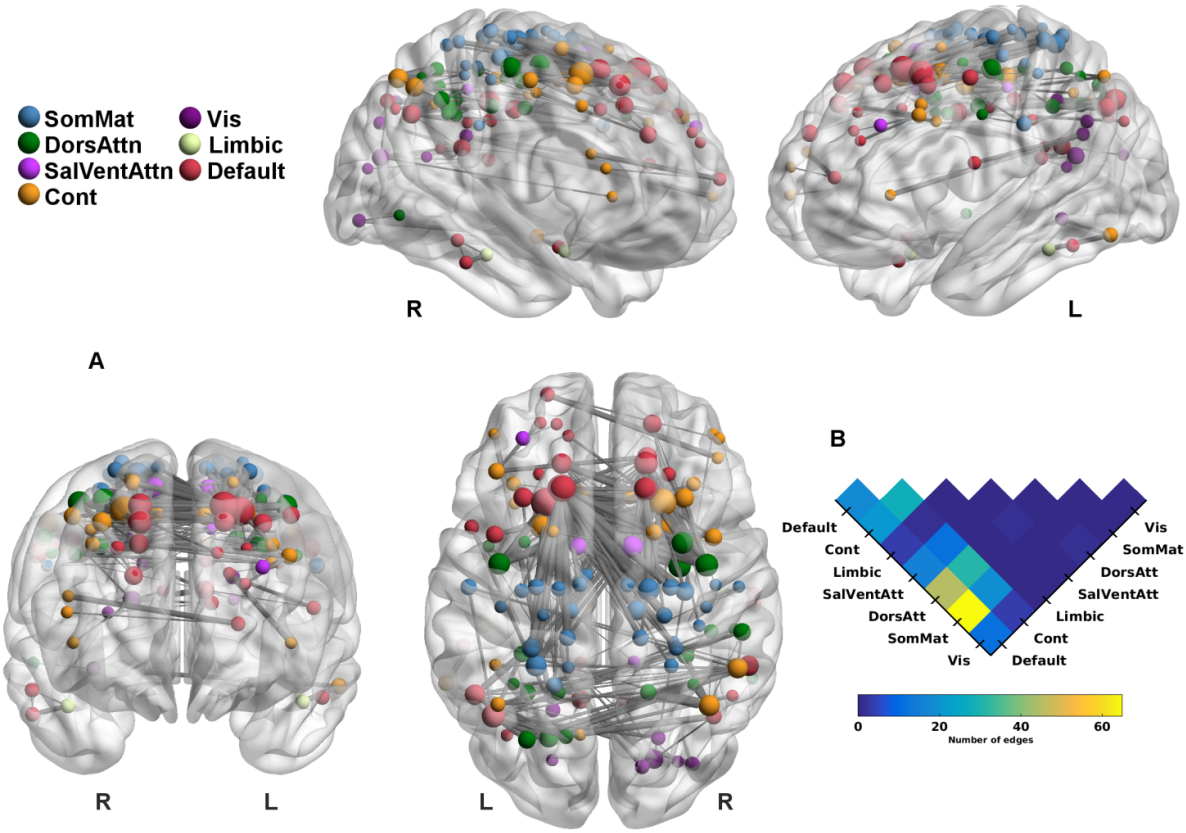

Figure 3-4: *Connectivity edges most negatively expressed by the first CCA mode. A, Connectivity edges exhibiting strongest negative associations with functional connectivity patterns (V_1) captured by the first mode. Line width indexes strength of correlation. Circle size is scaled to the number of connections each region shares within the network, whilst coloured to their functional network specialisation. The brain meshes are presented from axial (bottom-middle), posterior (bottom-left), and angular perspectives of the left (top-middle) and right-hemisphere (top-right). B, Coarse perspective of connectivity distributions across the functional networks, with warmer colours indicating greater number of connections.*

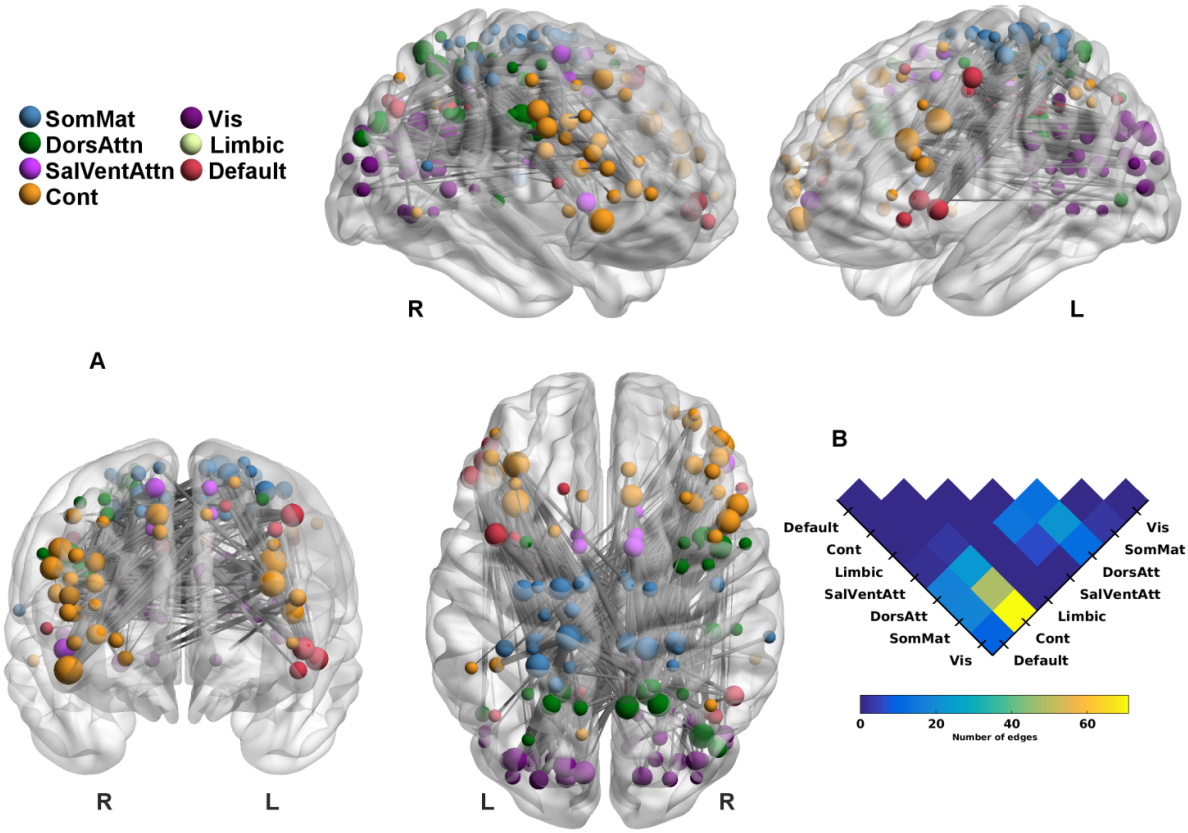

Figure 3-5: *Connectivity edges most positively expressed by the second CCA mode. A, Connectivity edges exhibiting strongest positive associations with functional connectivity patterns (V_2), hence representing connections expressed by the increased education level of elders. Line width indexes strength of correlation. Circle size is scaled to the number of connections each region shares within the network, whilst coloured to their functional network specialisation. The brain meshes are presented from axial (bottom middle panel), posterior (bottom left), and angular perspectives of the left (top right) and right-hemisphere (top-left). B, Coarse perspective of connectivity distributions across the functional networks, with warmer colours indicating greater number of connections.*

The edges exhibiting the strongest positive associations (*mean* = 0.64, *SD* = 0.02) with the third mode also comprise distinct networks to the prior two modes. Functional connections predominately cluster around ventrolateral and orbitofrontal divisions of left prefrontal nodes encompassing default-mode, cognitive control, and limbic areas (Figure

A4-2A). Edges stretch between these areas and bi-lateral frontomedial regions (anterior cingulate and superior portions), the left cingulate (middle and posterior portions), and left inferior parietal lobe. Assigning these networks to functional subdivisions of the brain shows they are predominately distributed within-and-between default-mode and control network areas, with additional connections between all other networks (except for visual) (Figure A4-2B).

3.4.1 Additional analyses: The influence of sex, verbal memory and intelligence

Given the strong correlations between sex and cognitive performance across specific domains (Figure 3-1), we undertook an additional CCA with sex (males coded as 1) included (hence with nine functional components). Two significant CCA modes were identified ($p<0.05$, Table A4-2), showing subtle differences to the principle modes explored above (Figure A4-3). In the first mode (Figure A4-3A), cognitive domains are again spread along the positive axis, with (male) sex loading most strongly on the negative axis followed by age and education years. The strong independent association of education with connectivity remains in the second mode (Figure A4-3B), whilst gender and the cognitive domains demonstrate weak to moderate associations.

The construct of memory in the main analysis includes verbal memory and is hence partly redundant (and thus strongly correlated) when verbal memory is also coded separately. However, two significant CCA modes (Table A3-3) were also identified with the removal of verbal memory scores with almost identical loading distributions to those in the main analysis (Figure A4-4).

To check the dependence of our findings on the number of regions within the parcellation scheme, the analysis was performed identically with a coarser brain template of 256 uniformly-sized regions (Zalesky et al., 2010b). The positive-negative split of cognitive domains and age remains present within the first modes albeit slightly less significant (Table A4-5, Figure A4-5A). The second mode is again characterised by a strong independent association with connectivity, although it no longer exceeds statistical significance (p=0.054; Figure A4-5B).

Education and intelligence are highly-correlated (Figure A4-1), and both considered central to cognitive reserve (Stern, 2009). The positive co-variation between greater education years and increased connectivity captured by the second mode in the main analyses thus raises an interesting question regarding the contribution of intelligence. We thus performed CCA (with nine functional components) using the full cohort of subjects whom received NART IQ assessment at study baseline (n=91). This analysis yielded two significant modes (p<0.05; Table A4-5). The modes capture latent relations that are similar to the main analysis, although interesting differences between education and intelligence emerge (Figure 3-6). Within the first mode, NART IQ loads positively and of similar magnitude to memory and visuospatial ability. Although NART IQ scores also bear a moderate positive association with connectivity captured by the second mode, the strength of this loading is weaker than education. Thus NART IQ splits across mode, with a component in opposition to age and a component loading independently with education.

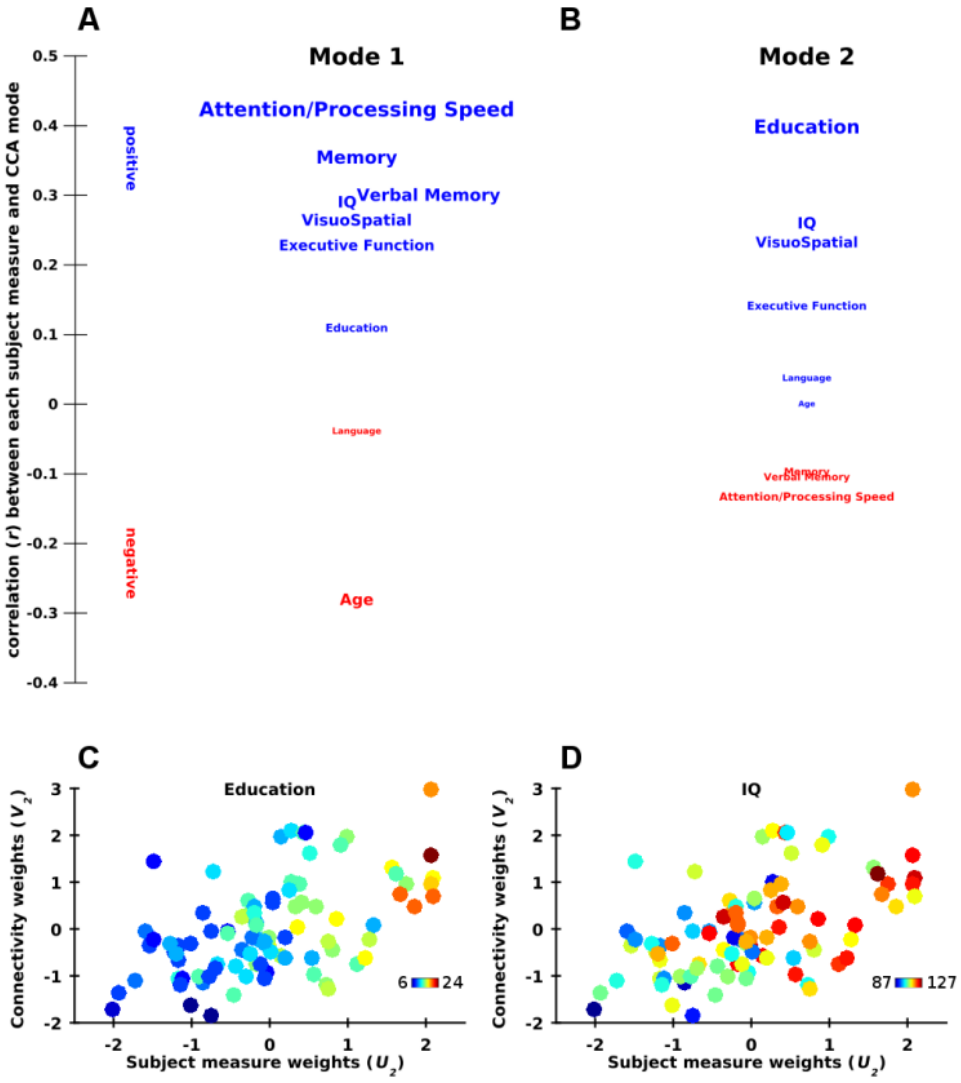

Figure 3-6: *Associations between behavioural and demographic measures captured by the CCA modes significant with including intelligence scores. A-B, Correlation between subject measures and functional connectivity variation (V_m), with the strength and direction of the relations indicated by vertical position and font size. C-D, Scatter plots showing for each subject (data points) their weighting towards non-imaging measures (U_m, x-axis) and functional connectivity patterns (V_2, y-axis), captured for the second modes. Colour is scaled according to participants education level (C) and NART IQ scores (D).*

The strong influence of education when also including IQ in the CCA model suggest the functional connectivity patterns captured here may be distinct from the main analysis. The edges exhibiting the strongest positive associations (*mean* = 0.74, *SD* = 0.015) are distributed throughout the cortex (Figure 3-7). Several key features are evident: Connections converge (larger circles) upon parietal default-mode areas including right -and medial (precuneus) portions, as well as superior (dorsal attention), and paracentral areas (somatomotor). Edges connect these areas to default-mode and dorso- and ventrolateral- prefrontal areas as well as lateral pre- and postcentral- gyri. Only a small proportion of function connections (24/250 edges = 9.6%) also occur within the corresponding mode of the main analysis (Figure A4-7). Visualising this network with an edge bundling connectogram which acts to cluster hierarchical relationships shows that edges predominately cluster between default-mode (red circles) and control-network (orange) areas to all other networks except for limbic regions (Figure 3-7B). Notably, the edges cluster around key default-mode and control-network regions (larger circles).

3.5 Discussion

We used a multivariate approach to elucidate the complex relationships between demographic factors, cognitive performance and functional brain networks in cognitively-normal elders. Whereas a single mode links cognitive and behavioural traits to functional connectivity patterns within healthy adults (Smith et al., 2015b), we identified three modes capturing significant interdependencies between phenotypic measures and connectivity. The first mode opposes cognitive performance and age on

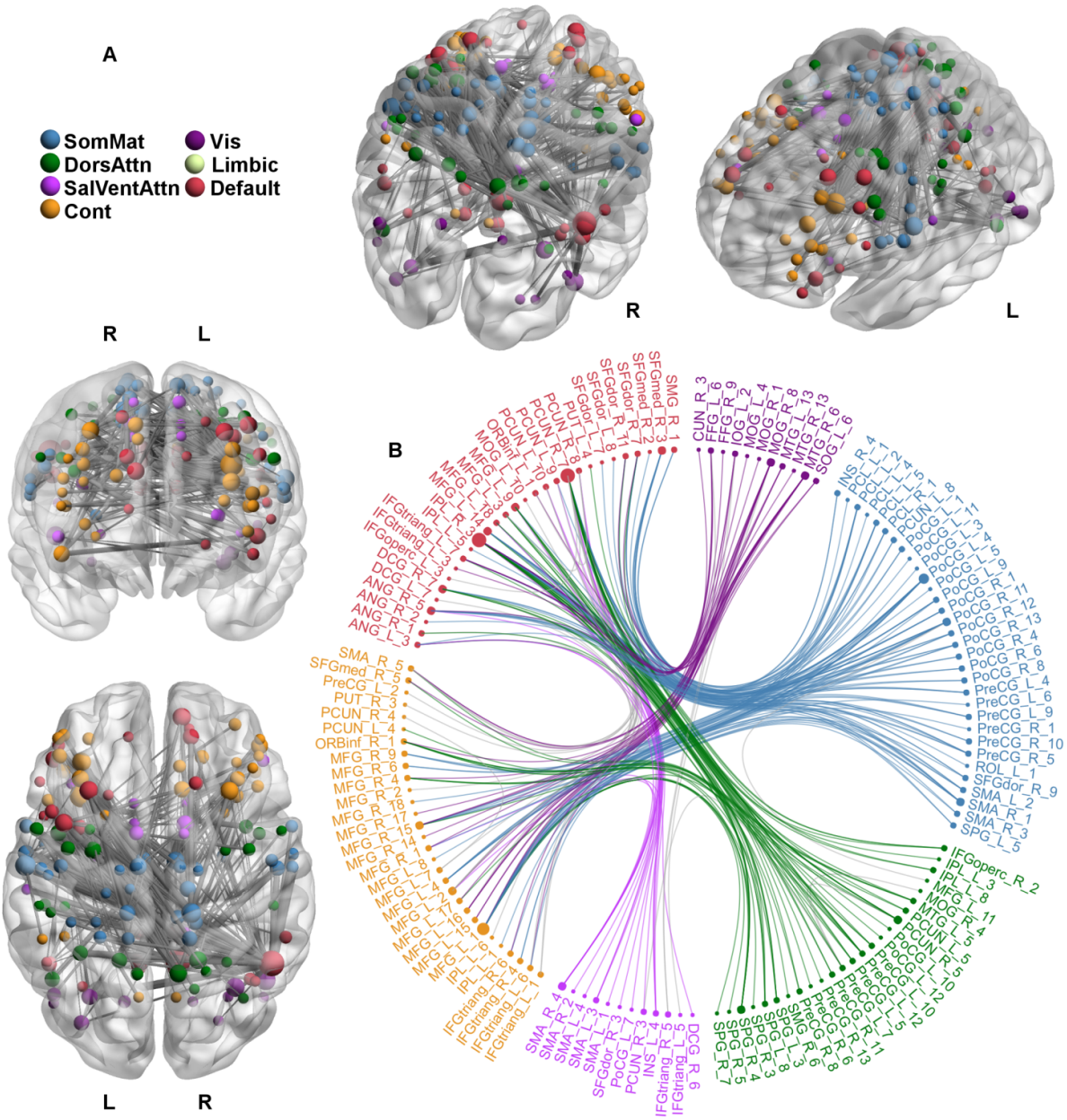

Figure 3-7: *Connectivity edges most positively expressed by the second CCA mode including intelligence scores. A, Connectivity edges exhibiting strongest positive associations with functional connectivity patterns (V_2), hence representing connections expressed by increased education level of elders. Line width indexes strength of correlation. The brain meshes are presented from axial (bottom-left panel), posterior (middle-left), and customised superior (top-middle) and lateral (top-right) perspectives. B, Edge-bundling connectogram which clusters the hierachial relationships between these set of connections. Positions of regions are according to their network affiliation.*

Edges are coloured by their respective affiliation if they link to either default-mode or control-network regions. All other possible interactions are coloured grey. For both (A) and (B), circle size is scaled to the number of connections each region shares within the network, whilst coloured to their functional network specialisation.

connectivity patterns. The second mode distinctly accounts for an independent and positive association of education with connectivity, whilst the third mode captures only weak relations. Age thus appears to exert an influence on brain-behaviour relations by splitting the single mode expressed in younger adults into three separate modes, with age and CR loading orthogonally.

All cognitive domains in the first mode load along a positive axes, mirroring positive traits within healthy adults (Smith et al., 2015b). Age, on the other hand, is positioned on the negative pole. This mode thus captures opposing associations between cognitive performance and age to connectivity. Greater attention and processing speed most strongly oppose age-related changes, suggesting functional connectivity changes are strongest for circuits supporting such functions. Indeed, cognitive function in these domains robustly predicts normal ageing (Park and Reuter-Lorenz, 2009) and cognitive decline in other tasks (Baltes and Lindenberger, 1997; Finkel et al., 2007; Salthouse, 1996). The functional connections most positively expressed within this mode are between visual and somatosensory cortices, with additional involvement of parietal association areas. These regions are distinctly linked by bi-lateral insular (posterior) and operculum (parietal) areas - areas not only associated with sensorimotor tasks (Cauda et al., 2012; Chang et al., 2012; Roski et al., 2013), but also integration of these systems (Sepulcre, 2014; Sepulcre et al., 2012). Age-related changes observed here builds upon reductions in resting-state connectivity with age within senorimotor systems (Betzel et

al., 2014; Chan et al., 2014; Geerligs et al., 2015), as well as for the parietal operculum itself (Cao et al., 2014; Tomasi and Volkow, 2012a).

There conversely exists a network of functional connections negatively expressed by this mode involving links between pre-motor, pre- and- post-central gyri and superior medial frontal areas - regions involved for planning and performing motor output (Gollo et al., 2015; Nachev et al., 2008; Tremblay and Gracco, 2010). Whereas deficits in motor performance occur with age (Ketcham and Stelmach, 2001; Seidler et al., 2010), increased functional (bilateral) activations are reported during motor tasks for these areas in older subjects (Heuninckx et al., 2008; Kleerekooper et al., 2016; Seidler et al., 2010). Increased activations are attributed as compensation of decline in neural integrity (Cabeza et al., 2002), and/or the decreased functional specialisation of brain regions (Seidler et al., 2010). Although relative decreases in connectivity for better (and younger) performers may reflect correlates of the aforementioned postulations, the association of connection edges here are much weaker than those observed with positive expressions.

Of interest, education loads only weakly on the networks expressed by the age-related changes in cognitive performance (i.e mode one). This is in apparent contradiction to the mitigation of age-related cognitive-decline observed for CR proxies (Stern, 2002). In our data, education instead loads upon a second mode, whose functional connections are distinct from the first mode. Connections occur between visual, salience, superior parietal, and somatomotor regions, converging upon the lateral prefrontal areas - circuitry (especially fronto-parietal links) consistently implicated in cognitive control (Cocchi et al., 2013; Koechlin et al., 2003; Spreng et al., 2010). Executive function partially loads onto this mode, revealing increased education may provide partial neuroprotection.

IQ and education both represent typical proxies of CR, and are highly-correlated (Stern, 2012). However, in our auxiliary CCA, we observed that IQ loads with other cognitive domains in opposition to age on the first mode, while education remains independently captured by the second mode. The relatively higher association of intelligence towards the first mode suggests age-related changes are influenced by intrinsic rather than extrinsic/modifiable factors such as education level. Nonetheless, functional connections within the second mode are predominately between key default-mode (inferior and medial parietal) and control-network transmodal hub-areas (middle frontal), to all other networks. There is strong evidence that higher-order cognitive functions are subserved by these transmodal areas (Cole and Schneider, 2007; Raichle, 2015; Seghier, 2013; Utevsky et al., 2014). The predominance of between-network interactions is salient given the dynamic integration of functional subsystems are critical upon task-demands (Bassett et al., 2011; Braun et al., 2015; Cocchi et al., 2013). A third mode linked relatively weak positive associations between connectivity patterns to memory and visuo-spatial abilities. Although only weakly significant, the third mode may capture cognitive correlates relatively independent of subject's age and education.

Including participants' sex with the CCA model revealed a similar latent structure of phenotypic inter-relations to the first mode of the original analysis. Sex (males) loaded negatively, hence with age and in opposition to memory performance. Males demonstrate poorer performance on verbal-based memory tasks (Gur et al., 2012; Hoogendam et al., 2014; Kimura, 2004): Our data reveals the functional connectivity patterns associated with these sexual dimorphisms.

The relatively large cohort and the multivariate nature of CCA bring new insights into the relationship between age, cognition and functional brain networks. However, these

findings should be interpreted in light of a number of limitations. The cross-sectional and association-based nature of the study design precludes causal inferences. A formal analysis of the influence of age would mandate a longitudinal within-subjects design. Furthermore, the influence of education on CR via functional connectivity patterns also requires further validation.

3.6 Conclusion

In sum, the present study expands upon a recent multivariate analysis of behaviour and functional brain networks in young adults (Smith et al., 2015b) through extension into cognitively-normal elders. Under the influence of age, we find brain-behaviour relations spilt into more than one mode, with age and education loading onto separate modes of functional connectivity. Age-related changes are most strongly exerted upon sensorimotor networks subserving core cognitive processes such as attention and processing speed. We identify that extrinsic factors such as higher education obtainment may confer its influence on cognitive reserve independent of age-related effects, but rather upon critical between-network interactions. The influence of age and education upon normal ageing reported here provides an important benchmark for the study of Alzheimer's. Whereas effects of education and sex are often controlled for within ageing investigations, the present multivariate approach further highlights the rich and complex phenotypic inter-influence on functional connectivity patterns.

Chapter 4: Structural dysconnectivity of key cognitive and emotional hubs in young people at high genetic risk for bipolar disorder

4.1 Abstract

Emerging evidence suggests that psychiatric disorders are associated with disturbances in structural brain networks. Little is known, however, about brain networks in those at high risk of BD, with such disturbances carrying substantial predictive and etiological value. Whole-brain tractography was performed on diffusion-weighted images acquired from 84 unaffected high-risk individuals with at least one first-degree relative with bipolar disorder (HR), 38 young patients with BD and 96 matched controls with no family history of mental illness (CN). We studied structural connectivity differences between these groups, with a focus on highly connected hubs and networks involving emotional centres. HR participants showed lower structural connectivity in two lateralised sub-networks centred upon bilateral inferior frontal gyri and left insular cortex, as well as increased connectivity in a right lateralised limbic sub-network compared to CN subjects. BD was associated with weaker connectivity in a small right-sided sub-network involving connections between fronto-temporal and temporal areas. Although these sub-networks preferentially involved structural hubs, the integrity of the highly connected structural backbone was preserved in both groups. Weaker structural brain networks involving key emotional centres occur in young people at genetic risk of BD and those with established BD. In contrast to other psychiatric disorders such as schizophrenia, the structural core of the brain remains intact despite the local involvement of network hubs. These results add

to our understanding of the neurobiological correlates of BD and provide predictions for outcomes in young people at high genetic risk for bipolar disorder.

4.2 Introduction

Large-scale brain networks arise from white matter tracts that link cortical regions and subcortical structures, following topologically complex (Sporns, 2013b; Sporns et al., 2005), geometrically constrained principles (Roberts et al., 2016c). Disturbances to these networks have been observed in a variety of neurological and psychiatric disorders, including schizophrenia (Zalesky et al., 2011), depression (Bai et al., 2012), attention-deficit hyperactivity disorder (Cao et al., 2013), mild cognitive impairment (Bai et al., 2012), and epilepsy (Widjaja et al., 2015). Even subtle perturbations to brain networks can cause disturbances in cognitive and emotional processes (Stephan et al., 2006), particularly if they target highly connected hubs in executive, emotional and association regions (Collin et al., 2014a; van den Heuvel et al., 2010).

BD is a disabling psychiatric disorder characterised by episodic disturbances in emotion and cognition. Studies have inferred reduced WM integrity in BD from alterations to DTI-derived indices, such as FA (Heng et al., 2010; Nortje et al., 2013; Vederine et al., 2011; Xekardaki et al., 2011). Although findings are somewhat inconsistent, there is a trend towards DTI-derived alterations in BD patients compared to controls in circuits linking prefrontal, striatal and limbic regions. Such findings suggest a link between the emotional and cognitive phenotype of BD and dysfunction in the networks supporting these functions.

Unaffected first-degree relatives of patients with BD have an odds ratio of ~7-14 of developing BD (Mortensen et al., 2003). Given the strong heritability of WM morphology (Chiang et al., 2012), studying individuals at familial risk of developing BD may help identify neurobiological factors that pre-empt the development of BD as well as factors associated with resilience. This objective is particularly pertinent in young first-degree relatives whom have not yet passed the peak age of illness onset (Arat et al., 2015). Studying unaffected relatives also mitigates the influence of illness-related confounds such as psychotropic medication (Whalley et al., 2011). A number of studies have revealed evidence of WM alterations in unaffected first-degree relatives although the spatial distribution and extent of these impairments remains uncertain (Emsell et al., 2014; Frazier et al., 2007; Linke et al., 2013; Mahon et al., 2013; Matsuo et al., 2012; Roybal et al., 2015; Sprooten et al., 2013; Sprooten et al., 2011; Versace et al., 2010).

Whilst DTI-derived indices have shed light on disturbances in specific WM pathways, such methods are insensitive to complex interactions among multiple brain regions. Developments in the acquisition of DWI and fibre-bundle reconstruction have allowed structural brain networks to be mapped with increased precision. The application of graph theoretical techniques to these networks has shown that healthy brain networks demonstrate 'small-world' features (indicative of balanced integration and segregation), minimising total fibre length (Bassett and Bullmore, 2006; Sporns, 2013b). Such organisational properties appear to be compromised in many disorders, exemplified by the burgeoning connectomic research elucidating network aberrations in schizophrenia (Bassett et al., 2008; Fornito et al., 2012b). Disturbances appear to involve highly-connected hub-regions (Crossley et al., 2014), particularly those hub-regions with dense wiring amongst themselves, known as the 'rich club' (van den Heuvel and Sporns, 2011).

Intriguingly, this core architectural feature may also be compromised in unaffected relatives of schizophrenia patients (Collin et al., 2014a).

Whist prior connectomic studies of BD show impairments in connectivity across the callosum and amongst limbic regions (Collin et al., 2015; Leow et al., 2013), the rich club backbone may be preserved (Collin et al., 2015). A recent study of unaffected relatives of BD patients did not reveal any structural network differences in either patients, or controls (Forde et al., 2015). However, this study had a modest sample size (n=58), and the mean age of unaffected relatives was 42 years, suggesting that many would have already passed the typical onset age of BD illness (<30 years) (Goodwin and Jamison, 2007) and may represent a resilient group of high-risk individuals. Alterations of topographical network organisation in unaffected first-degree relatives of patients with BD who have not passed the peak age of onset remains to be elucidated.

We leveraged recent advances in tractography and complex network analyses to investigate whole-brain structural networks in a large young sample of young unaffected 'high risk' (HR) first-degree relatives of patients with BD, patients with BD, and control subjects (CN). Crucially, our study cohort is relatively young (<30years), encompassing the peak age of illness onset. We studied specific sub-network differences in connectivity, as well as the topological properties of the highly connected 'rich club', and the global network architecture of the brain. We hypothesised that structural connectome disturbances in key regions involved in emotional regulation would be an early marker of vulnerability to BD.

4.3 Methods

4.3.1 Participants

218 richly phenotyped participants aged 12-30 years comprised three age- and gender-matched groups: 1) 84 participants at 'high-risk' (HR) for BD, 2) 96 controls (CN) without a family history of mental illness, and 3) 38 BD participants. Sample ascertainment and separate clinical assessments for younger (12-21) and older (22-30) age categories are provided in an epidemiological study of the population cohorts (Perich et al., 2015), and also within Appendix 5.1. We pooled data across both age cohorts unless there was a specific correlation between a brain network measure and an age-specific clinical variable in either group. Summary demographic and clinical data are presented in Table 4-1 and Appendix 5 (5.6 and Table A5-1).

Table 4-1*: Demographic information for control, high-risk, and Bipolar patient groups*

Demographic data	**CN (*n*=96)**	**HR (*n*=84)**	**BD (*n*=38)**	**Difference Statistic**	***p***
Females*, n (%)*	53 (55.2)	45 (53.6)	23 (60.5)	$\chi^2 = 0.52$	.77
Males*, n (%)*	43 (44.8)	39 (46.4)	15 (39.5)	$\chi^2 = 0.52$	.77
Intelligence Quotient*, mean (SD)*	117.7 (10.3)	116.3 (10.7)	117.3 (12.0)	$F = 0.36$	.69
Age*, mean (SD)*	22.6 (3.8)	22.4 (4.7)	23.9 (3.4)	$F = 2.08$	.13

CN, Controls; HR; High-risk; BD, Bipolar Disorder

4.3.2 Diffusion MRI acquisition, pre-processing, and whole-brain tractography

DWI data were acquired using a 3T Philips Achieva X MRI scanner. Full description of the acquisition parameters are provided in Appendix 5.2.1. The pre-processing of DWI

data, and subsequent whole-brain streamline generation is almost identical to the steps involved in Chapter 2 (*cf* 2.3.3 and 2.3.4). In brief, pre-processing steps included motion correction, rotation of the gradient matrix, and bias correction (Appendix 5.2.1). CSD was then employed in conjunction with probabilistic tractography (iFOD2 algorithm) (Tournier et al., 2010) to generate 5 million high-resolution whole-brain streamlines, representing the most probable propagations of fibre tracts between brain regions.

4.3.3 Construction of structural networks

The steps involved in the construction of whole-brain structural networks derived from these data are similar to those applied within Chapter 2 (*cf* 2.3.5). For full description of the steps involved in connectome construction see Appendix 5.2.3. In brief, the standard AAL template (Tzourio-Mazoyer et al., 2002a) was subdivided into 512 cortical and sub-cortical parcellation regions of approximately uniform size (Zalesky et al., 2010b). Subject-specific parcellations were combined with the individual's whole brain tractography to generate weighted structural networks where each network edge corresponds to the total number of streamlines that intersect pairs of region, adjusted by the physical fibre length between those regions (Hagmann et al., 2008b). All main analyses reported here are on structural networks thresholded with a connection density of 10%; brain network investigations typically employ threshold levels centring around this value (Sporns, 2013b). We also checked the robustness of our main results at sparsity levels of 7.5% and 12.5%.

4.3.4 Network-based statistics

We tested for group differences in sub-networks of these structural connectomes. To achieve this, we used a GLM in conjunction with the NBS (Zalesky et al., 2010a), a permutation-based method to control for FWE over the large number of connectome edges tested (*cf 2.3.12.3*). An omnibus *F*-test (F=6.0, corresponding to an uncorrected p=0.003) was first conducted to test for the influence of group on sub-networks of connections, based upon their topological extent. Two-sample one-tailed *t*-tests were then calculated to test for differences in sub-network connectivity between specific pairs of groups. A conservative test threshold of t=3.3 (p=0.002) was chosen in order to yield strong, supra-threshold differences (Zalesky et al., 2012). A liberal height threshold of t=3 (p =0.003, uncorrected) is the default optimization within the statistical tool, which identifies relatively larger and more distributed subnetworks of connections.

4.3.5 Complex network analyses

4.3.5.1 *Hub nodes and connection classes*

Each brain region's "hubness" was defined by virtue of its (binary) nodal degree; that is the total number of edges connected to each region. The top 15% degree-ranking scores were used to identify hub-regions within each individual. The top 15% most consistent hubs across the CN group were then defined as hub-regions (Figure 4-1A). This cut-off threshold centers upon values typically employed in brain network research (Perry et al., 2015). Classification of regions as either hubs (red) or non-hubs (grey) allowed network connections in each individual to be categorised into three connection classes: 1. hub connections (red), linking hub nodes; 2. feeder connections (orange), linking hubs to non-hub nodes; and 3. local connections (grey), linking non-hub nodes.

4.3.5.2 *Rich club organisation*

High degree hubs connect to other highly connected hubs more often than to peripheral nodes of low degree simply by virtue of their high degree. A *rich club* is said to exist when the connections among high degree hubs are enriched above what would be predicted by their degree alone (van den Heuvel and Sporns, 2011). This organisation can be summarized by the *rich club coefficient* (RCC; Appendix 1.2.2). We calculated the RCC of the individual structural connectomes across a range of degrees (*k*-levels). Significance testing of group differences in RCCs was assessed across all node degrees encompassing hub nodes using a false discovery rate (FDR) correction (Benjamini and Hochberg, 1995).

4.3.5.3 *Network segregation and integration*

We calculated two traditional graph-theoretical measures of global network topology: a measure of integration (*characteristic path length*, CPL), and a measure of segregation (*clustering coefficient*, CC) (Appendix 1.3) (Rubinov and Sporns, 2010).

4.3.5.4 *Nodal strength*

For each region, we also calculated the nodal strength, namely the number of weighted connections that region shares with the network (Appendix 1.1).

4.3.6 Statistical Analyses

Generalized estimating equations (GEE) (Liang and Zeger, 1986) were used to accommodate within-family correlations when assessing effects of diagnostic category,

age-group interactions, and when investigating if group effects were influenced by depressive mood state (Appendix 5.3.1 and 5.3.2). Corrections for multiple testing of the effects of diagnostic category were carried out with FDR correction (Benjamini and Hochberg, 1995). *Post hoc* comparisons were carried out using Sidak's adjustment for multiple comparisons.

4.4 Results

4.4.1 Hub-regions and connection classes

The structural connectomes of the young CN cohort exhibit a core-periphery hierarchy, consistent with that previously documented in healthy mid-life and elderly adults (Perry et al., 2015; van den Heuvel and Sporns, 2011, 2013b) (Figure 4-1A). Densely connected hub regions form a bilateral structural core, including bilateral cortical regions located within dorsolateral and ventrolateral prefrontal cortices, anterior and middle cingulate, superior parietal and frontal, temporal poles, fronto-temporal, medial temporal, paracentral and precuneus areas, and subcortical structures (Table A5-2). The topological distribution of hub-to-hub connections consist of long-range tracts, with mid-length feeder and short local connections (Figure 4-1B). There were no significant group differences in the relative proportion of hub, feeder and local edges between our three groups (Wald χ^2 >1.1, p>0.20) (Wald χ^2 >2.9, p>0.23), nor in the relative proportion of weighted streamlines across these classes (Wald χ^2 >1.4, p>0.50, Figure 4-1C)

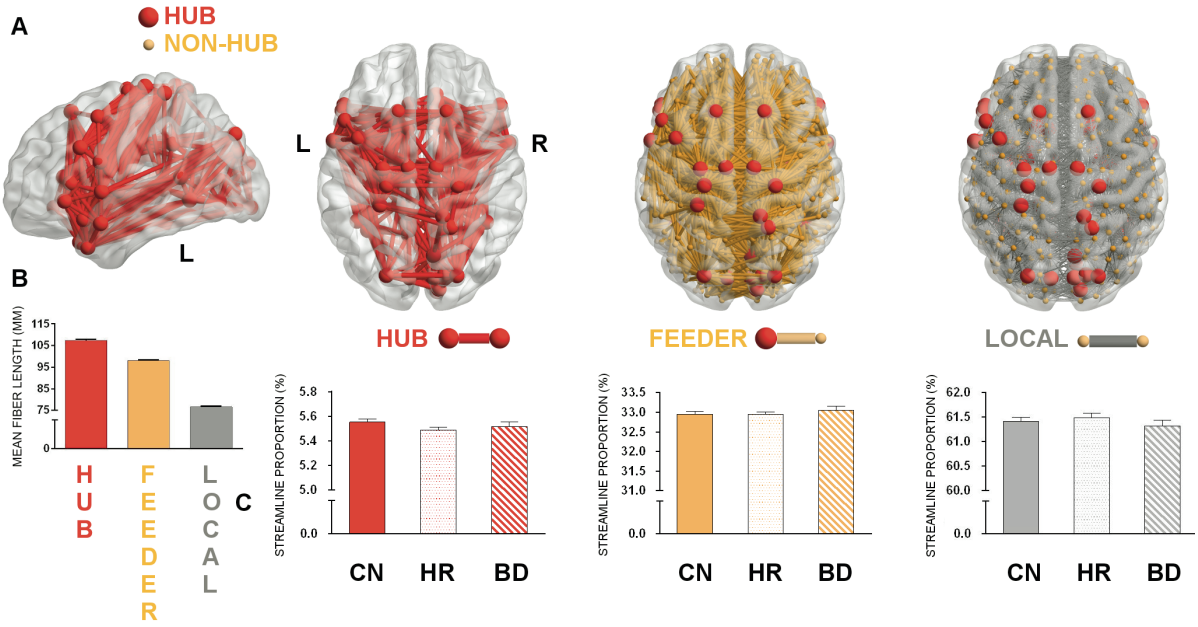

***Figure 1**: Hub-regions and connection classes across the population groups. A , Distribution of brain-regions into hubs and non-hubs, with connections grouped into classes (hub, feeder, or local). B, Mean fibre length of each connection class across controls. C, Density of connections: Left to right shows hub, feeder and local connections.*

CN, Controls; HR, High-risk; BD, Bipolar Disorder; L, left; R, right.

4.4.2 Sub-network connectivity differences: Network Based Statistics

We applied NBS to study between group sub-network differences. Application of an omnibus *F*-test revealed a strong and significant effect of group (F=6.0, $p_{corrected}$=0.018). Post-hoc *t*-tests revealed significant effects for CON>HR, HR>CON and CON>BD contrasts. The HR group show decreased connectivity in two lateralized structural networks compared to the CN group, both containing structural hubs. A left-lateralized network centres upon the left IFG and insular cortex, with connections between superior frontal and postcentral areas ($p_{corrected}$=0.01, hedge's g=0.86, Figure 4-2A). A right-lateralized network largely encompasses connections from middle and superior frontal gyri to IFG and superior temporal poles ($p_{corrected}$=0.005, hedge's g=0.96, Figure 4-2B).

Notably, 5 of the 10 nodes comprising the left sub-network are hubs (pars triangularis of the IFG, postcentral gyrus, insula and superior frontal gyrus), which is unlikely to occur by chance (p=0.009, n=5000 perms). Of the edges comprising this subnetwork, 33% are hub-to-hub and 44% are feeder (hub to local) connections, compared to much smaller proportions (5% and 32% respectively) in the whole brain network (Figure A5-1). The right sub-network includes 3 structural hubs (par orbitalis of the IFG, superior temporal pole, caudate). Although there are no hub-to-hub edges comprising this subnetwork, there are twice as many feeder edges (63%) compared to the whole brain (32%).

A right-temporal network was more *strongly* connected in HR compared to CN participants ($p_{corrected}$<0.02, hedge's g=0.87, Figure 4-2C), with connections connecting the hippocampus (a hub-region) with middle and superior temporal gyri. One small right-lateralized network showed weaker connectivity in BD compared to CN participants ($p_{corrected}$=0.027, hedge's g=0.93, Figure 4-2D). Notably all edges connected a single hub region (the rolandic operculum) with neighbouring fronto-temporal areas.

Sub-networks derived from a more liberal test threshold (t=3.0) are provided in Figure A5-2. For the CN>HR comparisons, this liberal threshold yields larger, but still lateralised sub-networks which remain centred upon IFG/insular regions of the corresponding hemispheres. These network differences are also expressed at sparsity levels of 7.5% and 12.5% (Figure A5-3). No significant group effects were found for any of the other group contrasts (CN<BD, HR>BD, and HR<BD).

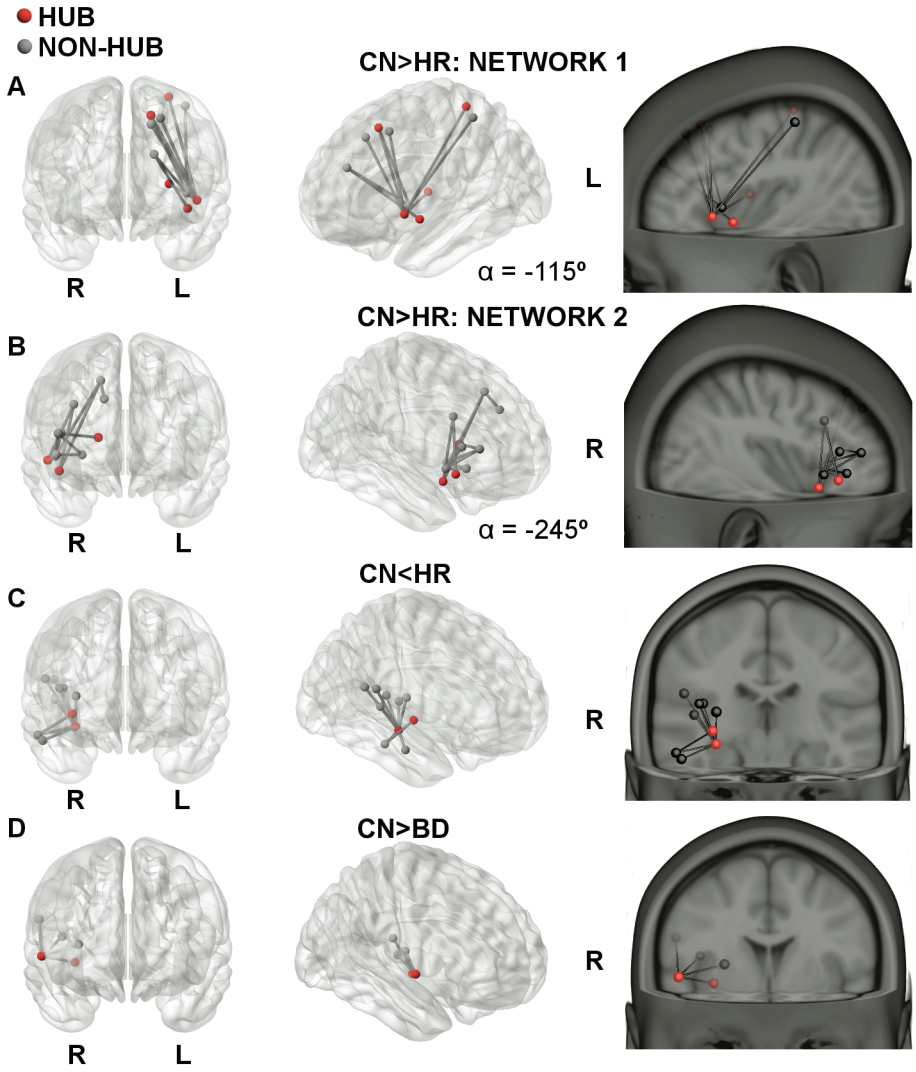

Figure 4-2: Significant sub-networks of connections for group contrasts identified by the NBS. Connections (lines) between nodes (circles) exhibiting significant ($p<0.05$, FWE-corrected; $t=3.3$) post-hoc group differences in streamline count. A and B, CN>HR; C, CN<HR; D, CN>BD. Perspectives are from angular (middle panel), saggital (top right only), and coronal views.

CN, Controls; HR, High-risk; BD, Bipolar Disorder; L, left; R, right; α, azimuth.

The distribution of node degree in our data is heavy-tailed, showing an approximately log-normal distribution (Figure A5-4). The classification of the top-15% of connected nodes as hubs centers upon thresholds previously employed in brain network research (Perry et al., 2015; van den Heuvel and Sporns, 2011, 2013b). In our data, this

threshold is one standard deviation above the mean, thus capturing the heavy right hand tail (Figure A5-4A). We also identified hubs at more conservative (12.5%) and liberal (17.5%) cut-off points (Figure A5-5). These supplementary analyses show that the relatively high proportion of hubs within the networks is robust to the exact choice of hub threshold.

4.4.3 Topological Network Analyses

4.4.3.1 *Rich club organisation*

These NBS results suggest preferential involvement of hub nodes in group effects. To study whether these effects on hub nodes extend to involve hub-to-hub (rich) connections, we studied the rich club coefficients (RCC). Data from all three groups show a highly enriched hub-to-hub (rich club) connectivity across a broad range of node degree (Figure 4-3A). However, there were no statistically significant differences ($p_{corrected}$>0.59) in the RCC between our three cohorts.

4.4.3.2 *Nodal Strength*

While the enrichment of the structural core is preserved, there remains the possibility that the localized connectivity of hubs differs between our three cohorts. This was tested by analyzing the strength of all nodes (Figure 4-3B, Table 4-2). Decreased strength of the HR group compared to the CN group occurred in the left parahippocampus and right IFG (left panel). Decreased nodal strength for the BD compared to both HR and CN groups was evident in the right precentral gyrus and left insula (middle). Decreased node strength for both HR and BD groups compared to CN was observed in the left SFG, left hippocampus and left middle occipital gyrus (right). While these effects occur in cortical

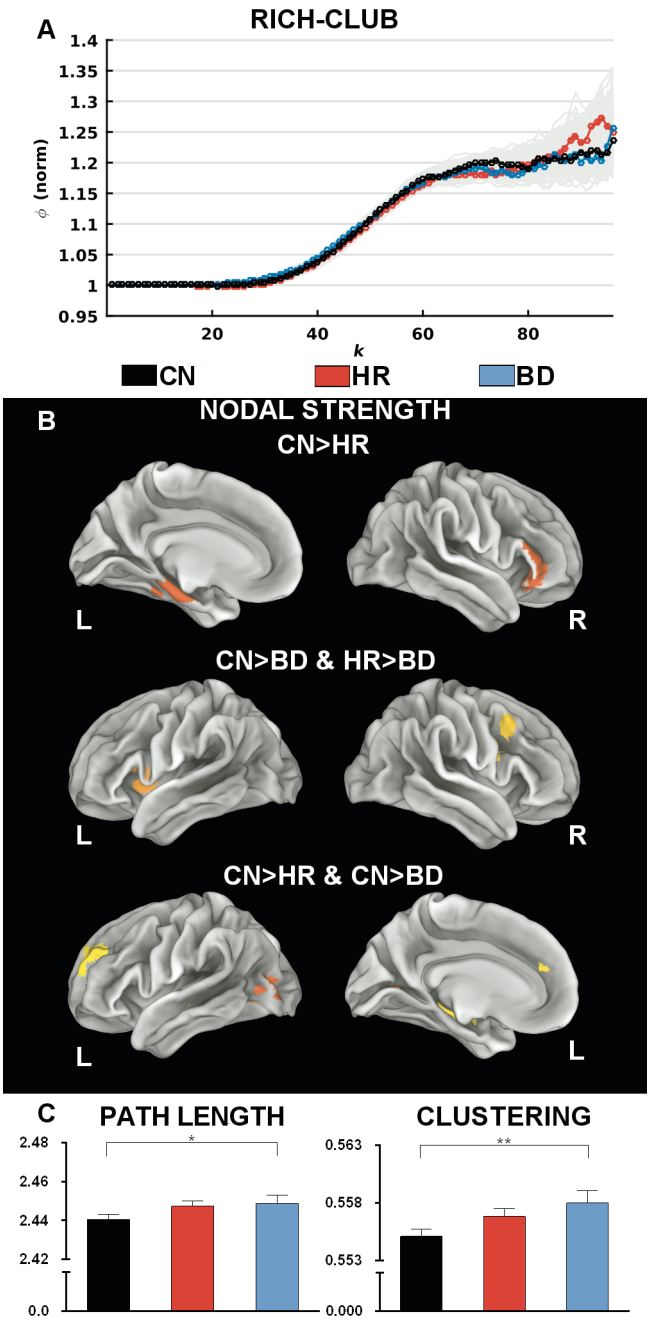

***Figure 4-3**: Group contrasts of nodal, global, and rich-club graph metrics. A, Mean normalized rich-club coefficients across different k-levels for the population groups. Grey lines depict group uncertainty, obtained through permutation of group labels. B, Regions exhibiting significant group ($p<0.05$, FDR-corrected) differences in nodal strength. C, Mean global graph metric values across population groups.*

CN, Controls; HR, High-risk; BD, Bipolar disorder; L, left; R, right; *, $p<0.05$; **, $p<0.01$.

regions that contain hub nodes such as the IFG, insula and hippocampus, it is noteworthy that none of these eight nodes are themselves hubs.

4.4.3.3 *Integration and segregation*

A significant main effect of group was detected for both the CC ($p_{corrected}$=0.016) and CPL ($p_{corrected}$=041), with a significantly higher CC ($p_{corrected}$=0.008, hedges g=0.446) and longer CPL ($p_{corrected}$=.049, hedges g=0.313) in BD subjects compared to the CN group (Figure 4-3C). Corresponding values in the HR group were intermediate to the BD and CN groups.

***Table 4-2**: Significant group differences in nodal strength*

Region	**Node**	***p*[1]**	**Post-hoc contrasts**					
			CNvsHR	*g*	**CNvsBD**	*g*	**HRvsBD**	*g*
Left Superior Frontal Gyrus	211	0.015	↑ CN***	0.55	↑ CN**	0.66	-	-
Left Hippocampus	83	0.015	↑ CN**	0.48	↑ CN**	0.70	-	-
Right Precentral Gyrus	511	0.017	-	-	↑ CN***	0.66	↑ HR*	0.40
Left Insula	197	0.026	-	-	↑ CN***	0.63	↑ HR*	0.49
Left Middle Occipital	202	0.039	↑ CN*	0.38	↑ CN***	0.74	-	-
Left Parahippocampal Gyrus	198	0.039	↑ CN***	0.52	-	-	-	-
Right Inferior Frontal Gyrus / Pars Triangularis	504	0.039	↑ CN***	0.54	-	-	-	-

CN, Controls; HR, High-risk; BD, Bipolar Disorder
[1] FDR-corrected
*** $p < 0.001$; ** $p < 0.01$; * $p < 0.05$

4.4.3.4 *Auxiliary analyses*

Current mood state was not significantly associated with total strength of NBS identified networks (p>0.07), or graph metrics (p>0.16), suggesting that these disturbances are not driven by mood but reflect an underlying trait disturbance. For nodal strengths, the precuneus demonstrated an effect of mood (p<0.001).

Given that a major depressive episode (MDE) often precedes the onset of mania in those who will later develop BD (Perich et al., 2015), the occurrence of a MDE in subjects at genetic risk for BD may represent a developmental stage of BD. We therefore undertook additional analyses to address this issue. We first subdivided our HR group into those with at least one lifetime depressive episode (n=22) or an anxiety disorder (n=15). For the HR>CN sub-network (Figure 4-2C), HR participants with a lifetime anxiety disorder show less connectivity compared to those without (p=0.037). No sub-group differences were evident for the remaining three NBS identified networks (p>0.12), nor for the graph metrics (p>0.60). We also removed subjects with a prior MDE from within the HR group and re-analyzed the between group effects. Highly significant group differences (p<0.001) in structural connectivity remained for all NBS contrasts involving the HR cohort.

Within the BD group, current use of lithium, mood stabilisers or antidepressants were not associated with CPL (p>0.32) or CC (p>0.34). Current antipsychotic use was significantly associated with lower CC (p=0.024). Measures of illness severity in the BD group (age of onset and total number of mood episodes) were not significantly associated with any connectivity measures.

Five of the 84 HR participants (6%) had a single relative within the BD group. We removed these 5 individuals from each group (10 in total) and repeated the corresponding analyses. As per the original contrasts, there were no significant

differences in global graph metrics or NBS subnetworks (p>0.27) between the HR and BD groups. The greater nodal strength in HR compared to BD subjects in the left insula (i.e. Figure 4-3B, middle panel) remained significant when removing these subjects (p=0.007), although the effect in the right precentral gyrus drops below statistical threshold (p=0.054).

4.5 Discussion

In sum, our young HR cohort show weaker structural connections than the CN group in two lateralised sub-networks centering upon fronto-temporal hubs, and stronger connectivity in a right lateralised prefrontal network. The young BD group show reduced connection strengths in a single left fronto-temporal sub-network. While key structural hubs such as the IFG and insula are repeatedly involved in these sub-networks, the inter-connected structural "rich club" backbone does not differ between groups. The perturbed sub-networks thus involve key emotional and cognitive circuitry, but "hang off" a preserved structural core. Lack of substantial correlations with key clinical indices suggest that these effects represent a trait marker of increased risk for BD and not an effect of mood state or medications.

The two lateralized networks that showed decreased connectivity in the HR group centre upon bilateral prefrontal gyri, inferior frontal gyri, and the left insular cortex. These regions recapitulate those reported to have reduced WM volume and density, and reductions in FA in prior studies of unaffected relatives of BD patients (Chaddock et al., 2009; Kieseppä et al., 2003; McIntosh et al., 2005; Sprooten et al., 2013; Sprooten et al., 2011; Tzourio-Mazoyer et al., 2002a) in addition to those with established BD (Adler et al., 2006; Beyer et al., 2005; Bruno et al., 2008; Chaddock et al., 2009; Coffman et al.,

1990; Haznedar et al., 2005; Kafantaris et al., 2009; Nugent et al., 2006). The specific involvement of the IFG adds to a converging body of evidence from structural and functional studies of BD (Breakspear et al., 2015a; Brotman et al., 2014; Chen et al., 2011; Hajek et al., 2013b; Papmeyer et al., 2015; Roberts et al., 2013). Likewise, the involvement of the insula adds to a growing number of reports of structural and functional differences in HR cohorts (Kempton et al., 2009; Matsuo et al., 2012; Sepede et al., 2012; Thermenos et al., 2010). Both the IFG and anterior insula are key areas for emotional, interoceptive and cognitive regulation (Goldin et al., 2008; Menon and Uddin, 2010; Sprengelmeyer et al., 1998). We extend prior research by suggesting that, rather than being focal abnormalities in HR individuals, these changes occur in distributed structural networks that integrate interoception and emotional regulation with executive function and cognitive control.

The stronger structural connections in the HR cohort centre upon the right hippocampus (a hub-region) and connect neighboring insular and STG areas. Again, these regions recapitulate those previously identified as having both altered FA (Mahon et al., 2013; Roybal et al., 2015) and decreased radial diffusivity (Versace et al., 2010) in high-risk individuals. The presence of this sub-network of stronger connections could be a compensatory response to the weaker sub-networks elsewhere in this our HR cohort, preserving adaptive emotional regulation. Alternatively, increased integration amongst this sub-network could confer risk in its own right, as cognitive function is thought to arise from a delicate balance of integration and segregation in structural networks (Sporns, 2013b): The hippocampus is associated with memory and regulatory function during emotional processing (Richardson et al., 2004) whilst the STG is involved in social cognition processes such as facial emotion recognition (Neves et al., 2015). Therefore,

strengthened connections between the hippocampus, other temporal regions and the insula could contribute to hypervigilance to emotional stimuli and social cues. Disambiguating these possibilities – and recalling that only a subset of our HR subjects will convert to BD – is to be the subject of future prospective study of this cohort.

Several observations pertain to the effects in our young BD group. We observed a small right-sided sub-network of weaker connections between a rolandic opercular hub-region and neighbouring fronto-temporal areas (insula, Heschl's gryus). This sub-network is distinct to, and *not* an extension of the network of right sided regions in the HR group. In addition, there were also subtle changes in measures of network integration and segregation specific to the BD group, although here the HR group showed an intermediate ("dose-dependent" response). We observed both shared and unique differences in node strength between groups. Hence, there are findings that are distinct to each of the HR and BD groups as well as effects where the HR group falls between the CN and BD group. The former (group-specific) changes may speak to the influence of mood stabilising medication and/or compensatory responses to mood episodes in the BD group, as well as the heterogeneous nature of the HR group. Disambiguating these will again be the focus of future work as we follow this cohort longitudinally.

4.6 Conclusion

To optimize the sensitivity of our constructed connectomes, we employed state-of-the-art probabilistic tractography. In contrast, the majority of existing high-risk studies of BD have used voxel-based or track based spatial statistics derived from deterministic algorithms, challenging direct comparison between the present results and previous

findings. A key finding relative to the present study is a decrease in the enrichment of hub-to-hub connections in schizophrenia patients (van den Heuvel et al., 2013) and their unaffected relatives (Collin et al., 2014a): Despite involvement of key emotional and cognitive structural hubs in weakened sub-networks, we find preserved integrity of the rich club structure in young people with BD and our HR cohort, mirroring a recent finding in older BD patients (Forde et al., 2015). Although schizophrenia and BD show a substantial genetic overlap (Moskvina et al., 2009), this difference mirrors the relative preservation of cognitive function in BD (McCormack et al., 2015), and may be a key neurobiological difference between the disorders. Testing such a hypothesis will require large, multi-disorder studies of psychotic and affective phenotypes.

Chapter 5: Discussion

Throughout this thesis, I sought to investigate the expression of structural and functional brain networks across young adult and elderly population cohorts. Neuroimaging data were treated through connectomic approaches, conceptualizing the human brain upon its complex structural and functional interactions. The spatial, topological, and spatiotemporal macroscopic features of these large-scale networks in relation to their ability to understand and predict human brain functioning were investigated through three studies. More specifically, I identified macroscopic features within elderly brain networks indicative of normal ageing and age-related cognitive changes. Furthermore, I also identified disruptions to large-scale structural networks in patients with BD and those at high-genetic risk for the disorder. I discuss the present findings here in light of the key features of human brain organisation - patterns of *functional integration and segregation*. Changes to the balance between these key features are reflective of inter-individual differences in cerebral processing capacity that drive phenotypic and genotypic expression. The core of this discussion is devoted to the implications of the reduced integrative capacity of hub-regions and their connections. Finally, I raise consideration of the limitations inherent within this work, which provide a catalyst for preliminary analyses and further neuroimaging studies of elderly and younger adult psychiatric populations.

In Chapter 2, I provided a systematic description of the structural connectomic features characteristic of healthy older adults. In reference to young adult connectomic data, I found the continued presence of the high-cost features of hub-regions and their connections within the “elderly connectome” - reflective of their ongoing role in global

brain communication. Interestingly, the capacity of these hub-connections for functional integration appears to be reduced in the elderly, which I postulate to be characteristic of age-related cognitive changes.

The functional brain networks of a subset of these elderly participants were examined in chapter 3. I leveraged multivariate analysis to investigate the expression of functional connectivity patterns with respect to cognitive changes that occur with ageing in healthy elders. Here, a diffuse functional sensorimotor subnetwork was identified whose expression opposes age against core cognitive processes such as attention and processing speed. I further revealed the functional connectivity within this subnetwork to be relatively resilient to modifiable factors such as increased education years.

In chapter 4 I shifted focus to large-scale structural disruptions which underlie BD and unaffected relatives at high-genetic risk for the disorder. Within the high-risk population, I identified trait disturbances in circuits supporting emotional and cognitive control. These disturbances are suggestive of the neurodevelopmental vulnerability of such high-risk individuals, which potentially pre-empts the development of emotional instabilities. The structural backbone was also otherwise found to remain relatively intact in both patient and high-risk groups, which provides an interesting comparison to other psychiatric conditions.

5.1 Functional integration and segregation in the elderly connectome

Early connectomic investigations were heralded for their seminal discoveries of the modular, “small-world” organisation of structural wiring patterns in humans and other

species (Hagmann et al., 2008b; Hagmann et al., 2007; Sporns et al., 2000; Sporns and Zwi, 2004). Chapter 2 identified features expressive of the continued presence of *functional integration* and *segregation* within the "elderly connectome". Within healthy older adults, a modular organization (i.e. *segregation*) is observed - and more importantly - the existence of highly-connected hub-regions. The dense-wiring (i.e. hub-connections) among these hub-regions form the core anatomical backbone known as the "rich-club" (van den Heuvel and Sporns, 2011). Consistent with adult connectomic data, the rich-club in older adults exhibit architectural features indicative of its high-capacity for *functional integration*: increased inter-modular links, greater projection lengths of fibres, and disproportionate routing of network traffic (Collin et al., 2014b; van den Heuvel et al., 2012; van den Heuvel and Sporns, 2011; van den Heuvel and Sporns, 2013a; van den Heuvel and Sporns, 2013b). Presumably, the high-volumetric-and-metabolic costs ensued by the wiring patterns of hub-regions (Bullmore and Sporns, 2012) are offset by the substrate's ongoing role for network communication in the elderly brain.

5.2 Changes to the integrative capacity of hub-connections in normal ageing

The continual role of the rich-club for global brain communication in healthy older adults is interesting in light of the cognitive changes associated with normal ageing and AD. Age-related cognitive changes are foremost observed for fluid-based functions which require integrated and coordinated neural processes (Park and Reuter-Lorenz, 2009). The critical role of rich-club wiring for facilitating dynamic patterns of neural fluctuations (Gollo et al., 2015; Senden et al., 2014; Senden et al., 2016; van den Heuvel and Sporns, 2013b) suggests that the integrative capacity of hub-regions may be influenced by age.

The continued existence of hub-connections within healthy older adults is indicative of their role of maintaining functioning, relative to the marked deteriorations in AD. However, chapter 2 does reveal macroscopic features that reflect the reduced integrative capacity of hub-connections and subsequent cognitive changes in later-life: Subtle decreases in the projection length and routing of network traffic of hub-connections are demonstrated in older participants. These findings suggest that, despite the preservation of their overall topological structure, reductions in the integrative capacity of hub-connections occur. This postulation is in agreement with the sparse ageing literature in this area: Whilst the spatial location of hub-regions are relatively consistent across the lifespan, there are reductions in the enrichment of the functional (Cao et al., 2014) and structural rich-club (Betzel et al., 2014; Zhao et al., 2015).

5.3 Neurobiological correlates of age-related cognitive changes

In Chapter 3, I identified the expression of a more specific functional subnetwork linking lower-order visual and somatomotor areas to oppose increasing age against greater attention and processing speed. Multivariate analysis revealed younger, better cognitive performers weighed towards increased expression of this subnetwork. In contrast, the patterns of older, poorer performers are reflected by relative decreases in this subnetwork. Whilst these functional links don't necessarily overlap with the structural rich-club as shown in Chapter 2, these findings nonetheless reinforce that macroscopic brain network features are tied to age-related cognitive changes. External factors, such as increased education, can potentially modify age-related changes (Stern, 2002). Interestingly, these factors had a weak effect on this age-related subnetwork. Increased education instead

conferred enhanced functional connectivity patterns between higher- and lower- level cognitive networks. This is salient, given that between-network interrelations depend critically upon task-states (Bassett et al., 2011; Braun et al., 2015; Cocchi et al., 2013).

The neurobiological correlates of age-related changes are most commonly conceptualized as degenerative processes that underlie cognitive decline. An alternative framework, however, embodies the adaptive effects with normal ageing that endow the maintenance of cognitive functioning (Moran et al., 2014). Cognitive functions can be maintained within healthy individuals in later life, as exemplified by tasks assessing accrued knowledge (Deary et al., 2009; Park and Reuter-Lorenz, 2009). A large lifespan study which employed DCM for MEG data, indeed revealed the synaptic connectivity strengths of older brains are attenuated to the short-term sensory learning of auditory stimuli (Moran et al., 2014). This finding suggests that older individuals demonstrate less-complex connectivity patterns that are optimized over the lifespan for robustly encoding multiple sensory inputs (Moran et al., 2014). The increases in between-network functional connectivity observed in healthy older adults during resting and task-states further reflects complex functional reconfigurations with age (Betzel et al., 2014; Chan et al., 2014; Geerligs et al., 2015). Within chapter 2, the relative increase in older subjects for network routing along less-complex wiring patterns (i.e. local connections) could indicate adaptive reconfigurations. The connectivity patterns associated with increased education years - as identified in chapter 3 – is also potentially reflective of factors which can confer adaptive reorganizations. By narrowly conceptualizing ageing as a degenerative process, prior investigations may neglect the complex influences of age and other factors on brain connectivity patterns.

5.4 Large-scale networks are compromised in young adults with mental illness

The macroscopic features identified in the elderly connectome are altered within both BD patients and unaffected relatives. Alterations to structural connectivity patterns reflects the "disconnection" of neural processing, which potentially underpins clinical phenomena (Fornito and Bullmore, 2015; Fornito et al., 2015; Friston, 1998). The dysregulation of emotional and cognitive control within patients suggests a dysconnectivity in networks which support such functions (Phillips and Swartz, 2014; Strakowski et al., 2012). Indeed, in Chapter 4, structural disturbances of fronto-limbic circuits was revealed in patients - and also in high-risk individuals. The few prior connectomic investigations have consistently revealed inter-hemispheric degradations in patients (Collin et al., 2015; Leow et al., 2013). Disturbances in high-risk individuals studied in my thesis occur within large-scale networks largely involving anterior insula and IFG areas, which bridge key emotional, cognitive, and somatosensory areas. These alterations recapitulate deviations in brain function that can arise from the disruption of communication between specialized areas (Fornito et al., 2015). These disturbances are unique to high-risk individuals, which is perhaps reflective of their vulnerability at critical developmental periods - further suggesting the clinical utility of connectomic approaches in predicting later illness-onset. Features indicative of widespread alterations (i.e. reduced global efficiency) to network communication are apparent only within patients - and hence perhaps represent markers of illness-expression.

Emerging frameworks of emotional experience and psychopathology have repositioned brain (dys)functioning in light of its interactions with internal body systems (Seth and Friston, 2016; Stephan et al., 2016). These interactions are postulated to occur

through a process known as interception: Physiological changes are sensed from "within", such as those from autonomic and visceral afferent, which yield changes particularly in the limbic cortices (Craig, 2003; Critchley et al., 2004). Following Bayesian ideas, contemporary *active interoceptive inference* models have postulated these hierarchical representations to be encoded as prediction signals (i.e. probability distributions) in agranular cortices (Barrett et al., 2016; Seth and Friston, 2016): Descending predictions of bodily states are compared to the ascending sensory input from lower-order regions - with the difference between the two derived as the *prediction error* (Friston, 2008; Friston and Kiebel, 2009). The signal encoded in this prediction error *actively* updates the higher-order representations. Prediction errors serve allostatic needs by engaging visceromotor responses that are central to our affective content and feelings, such as heart palpitations and blushing (Barrett et al., 2016; Seth and Friston, 2016). Emotional experience can hence be considered a circular process, where interoceptive signals inform and update these prior beliefs.

It is notable that the agranular cortices postulated to embed interoceptive predictions are fronto-limbic areas (Barrett et al., 2016; Gu et al., 2013; Seth and Friston, 2016). The regulation of cognitive and emotional processes are well-supported by these areas, exemplified by regions such as the anterior cingulate, anterior insula, IFG, and orbitofrontal cortex (Bechara et al., 2000; Craig, 2009; Liakakis et al., 2011; MacDonald et al., 2000). The dysregulation of mood and energy levels within BD naturally implicates the "hub-opathies" of fronto-limbic areas involved in interoceptive processes. The disturbed subnetworks identified for high-risk participants in Chapter 4 is not only suggestive of interoceptive disturbances, but also of patterns of broader network dysfunction involving lower ends of the cortical hierarchy. The symptomatic expression

of mania/hypomania in BD could first be attributable to fronto-limbic dysfunction that leads to abnormal world representations. For example, features of the external milieu are perceived in BD patients as increasingly salient and/or threatening (Green et al., 2007; Jones et al., 2005). A system breakdown may also relate to the inability to update these abnormal internal models (O'Donnell et al., 2017) - based upon the predictive errors which propagate from (extero- and intero-) sensory cortices. These proposed models of abnormal *interoceptive inference* in patients accommodate the larger-scale patterns of network dysfunction observed in BD (Breakspear et al., 2015a; Collin et al., 2015). Furthermore, they encompass the considerable inter-individual heterogeneity in the clinical and neurobiological presentation of BD.

5.5 The connectivity patterns of hub-regions are implicated in cognitive and behavioural changes

A central theme emerging across the three main studies of this thesis relates the integrative capacity of hub-regions to phenotypic and genotypic differences. Whilst changes in the communication capacity of the anatomical backbone is reflected within older adults in Chapter 2, Chapter 3 also implicates their functional connectivity patterns as important to the integrative capacity of sensorimotor, default-mode and control-network hub-areas. Chapter 4 extends these findings by highlighting the disruption to hub-regions as potentially pre-empting the development of affective instabilities. With hindsight, the selective involvement of hub-regions within these studies is perhaps not surprising, given their topological structure within the human connectome supports their heteromodal functions, and also their putative role in critical (unstable) brain dynamics (Senden et al., 2014; van den Heuvel and Sporns, 2013b). The selective disturbances of

hub-regions across a variety of psychiatric conditions have catalysed postulations regarding their increased vulnerability to pathological processes (Crossley et al., 2014): First, the embedded topological structure of connections may increase their propensity for axonal transport of disease-causing agents in certain neurodegenerative disorders such as AD (Fornito et al., 2015). Second, the increased metabolic rates of hub-regions increase their vulnerability to pathogenic metabolic processes (Crossley et al., 2014; Fulcher and Fornito, 2016). The pathogenic mitochrondial processes implicated in BD hence resonates with the disruptions to hub-regions within high-risk individuals (Clay et al., 2011; Stork and Renshaw, 2005).

5.6 Benchmarks for neurodegenerative and other psychiatric disorders

The systematic investigation of healthy older adults through Chapters 2 and 3 contributes an important benchmark to understand the deviations from healthy ageing. The fragmented network breakdown in AD patients (Dennis and Thompson, 2014) has also raised the possibility of sensitive disruptions to the long-range hub-connections. Changes in the integrative capacity of hub-regions may be differ in their spatial properties in AD compared to healthy ageing. The findings of Chapter 3 implicate age-related cognitive changes to occur foremost in lower-order sensorimotor hub-regions. Previous work suggests that disturbances to default-mode and temporal-hubs are characteristic of AD patients. On the other hand, the advanced volumetric decline in cortical size (Douaud et al., 2014) and thickness (Fjell et al., 2012) has been revealed within AD patients in areas that are also sensitive to normal ageing changes. Regardless, the influence of education on core DMN and fronto-parietal hubs in Chapter 3 is also an interesting reference point:

CR proxies are associated with decreased volumetric size in AD patient groups (Bartrés-Faz and Arenaza-Urquijo, 2011). Although few studies exist, increased functional connectivity patterns observed for patients with high CR may reflect compensatory processes (Bosch et al., 2010; Bozzali et al., 2015; Solé-Padullés et al., 2009).

The delineation of structural disturbances in BD patients and high-risk individuals is also an important reference to schizophrenia patients. Features shared across the two disorders include clinical features such as psychosis (Keshavan et al., 2011), genetic susceptibility (Potash and Bienvenu, 2009), and brain abnormalities associated with the genetic risk (Baker et al., 2014; Caseras et al., 2015). Schizophrenia has emerged as an archetypical disorder with structural rich-club degradation (van den Heuvel et al., 2013): Disturbances are further associated with illness severity (Collin et al., 2014a), and also found in those at high-risk for psychosis (Collin et al., 2014b; Schmidt et al., 2016). The widespread disturbances across frontal, parietal, and temporal hub-regions associated with schizophrenia (Crossley et al., 2014; Klauser et al., 2016) may reflect the increased severity in impairments relative to BD (Vöhringer et al., 2013). Discrete disturbances to cognitive and emotional hub regions in BD and at-risk populations is hence more intimately related to the unstable mood swings characteristic of this disorder. Conceptualization of hub-degradation as disorder-general is perhaps an overgeneralization (Crossley et al., 2014). To further disentangle the potentially unique neurodevelopmental disturbances in BD and schizophrenia, studies of structural connectivity disturbances in the unaffected relatives of both proband groups are required.

5.7 Limitations and future directions

5.7.1 Selective biases of hub-regions

As reviewed above, considerable evidence has implicated the selective involvement of hub-regions and their connections for inter-individual differences in cognition and behaviour. However, the topological features of hub-regions may bias their identification in brain-behaviour correlates. Behavioural observations may become apparent only after changes to the integrative capacity of embedded hub-regions has a cascading influence upon broader network interrelations (Crossley et al., 2014): The cascade of grey-or-white-matter changes with normal ageing or psychiatric-onset could initially impact non-hub regions or local connections. AD provides a mechanistic neurodegenerative example. The global loss of functioning in AD patients may be evident only in clinical settings once neurotoxins have spread to the longer axonal projections of hub-regions (Fornito et al., 2015; Zhou et al., 2012). The combination of multiple MRI modalities and the use of a longitudinal study design are required to delineate the initial events that lead to cognitive and behavioural changes versus downstream events that may lead to later symptoms.

It is worth noting that disturbances to hub-regions and their connections observed in Chapter 4 are present even in the relatives unaffected by BD. As noted, rich-club degradation is evident in the unaffected relatives of schizophrenia probands (Collin et al., 2014a). Together, these findings in high-risk populations are highly suggestive that symptomatic presentation is not merely due to the selective disturbances of hub-regions. Furthermore, the "control" group matched to the high-risk population within Chapter 4 also have had psychiatric episodes, including anxiety and depression. Group differences were robust to the removal of high-risk participants with any affective disturbances.

5.7.2 Integrating structural and functional connectivity

It remains to be elucidated the extent to which changes to the underlying architecture in both young and elderly populations shape functional connectivity patterns. In each chapter, the brain network features that were investigated were those constructed from either structural or functional connectivity alone. Although structure is a robust predictor of function in the human brain, the relation is not one-to-one, as differential dynamic interactions are shown to emerge across the scaffolding (Deco et al., 2013). The limitation of employing one MRI modality is apparent when interpreting changes to inter-regional communication which is routed through the backbone (Chapter 2): Changes to the integrative capacity of hub-connections could plausibly influence subsequent decreases in long-range functional connectivity. Interestingly, as noted, ageing is associated with increases in functional connectivity patterns over long-range communication paths (i.e. binary paths) (Betzel et al., 2014). While long-range paths are assumed to implicate the wiring of hub-regions, that study did not demarcate the different connection classes. Future studies of normal ageing would also benefit from employing high-temporal resolution fMRI data which captures the brain spontaneous fluctuations over time (Zalesky et al., 2014). The decreased integrative capacity of hub-regions could perhaps drive decreases in the functional repertoire of neural fluctuations (Deco et al., 2013; Senden et al., 2014; Senden et al., 2016). Increases in functional connectivity patterns over long-range paths with age have been proposed to be reflective of less-variability in brain dynamics (Betzel et al., 2014).

Investigation of structural-functional relations in psychiatric populations provides another layer to advance our understanding of pathophysiological mechanisms behind such disorders. It is unknown whether trait disturbances to emotional and cognitive control networks in high-risk populations are also associated with alterations to functional connectivity patterns. Changes to the "normal" relation between structural and functional connectivity patterns in patients are commonly perceived as alterations to brain dynamics (Wang et al., 2015): Both increases (van den Heuvel et al., 2013) and decreases (Cocchi et al., 2014) in the strength of structural-functional coupling has been revealed in schizophrenia connectomes. The relations between structural and functional connectivity patterns are typically assessed over sets of identical connectomic connections/subnetworks. However, this approach neglects the spatially-distinct functional configurations that are shaped from the underlying architecture (Mišić et al., 2016). Structural disturbances to the functionally diverse fronto-limbic areas in individuals at high-risk for BD may influence broader patterns of brain dysfunction.

5.7.3 Controllability of structural networks

The application of concepts from network control theory have afforded recent exploration of how structural wiring patterns can drive temporal brain states. Those brain states which require a substantial energy expenditure to reach are proposed to be analogous to modes of cognitively-demanding function. *Controllability* quantifies this energetic input required to traverse the brain system. Replicating a previous study (Gu et al., 2015), analyses of our data shows that highly-connected hub-areas (weighted connectivity) exhibit high *average controllability* (Figure 5-1A; Top-right corner) for steering the network into states with little energy required. On the other hand, weakly-connected areas

have high *modal controllability* (B; Top-left) for systems requiring substantial energy expenditure. Preliminary controllability analysis was conducted for the regions exhibiting significant nodal strength differences between control and high-risk populations in Chapter 4 (i.e. Figure 4.3). Here, the control group display significantly greater *modal controllability* for both the left parahippocampal ($p_{corrected}$=0.01; C) and left superior frontal gyrus ($p_{corrected}$=0.009; D), whilst the R inferior frontal gyrus approaches significance ($p_{corrected}$=0.06). The decreased modal controllability in high-risk individuals suggests that disturbances to fronto-limbic areas culminates in substantially more energy required to reach cognitive or emotional states. Although future analyses are clearly warranted, no other investigations have thus far revealed patterns of altered network controllability in psychiatric populations.

5.7.4 Limitations of cross-sectional designs

The investigations in this thesis were all undertaken within cross-sectional settings. Coincidentally, the young and elderly cohorts were investigated at respective critical periods of brain maturation and neural decline. Given that the longitudinal status of participants that convert to threshold BD is currently unknown, cross-sectional studies of high-risk populations (Chapter 4) are problematic: It remains to be elucidated whether the structural disturbances (relative to controls) are predictive of future progression, or rather features that ensure resilience. Longitudinal follow-up is warranted in this elderly cohort to determine if connectivity changes are also predictive of further reductions in processing speed. Future longitudinal investigations would further benefit efforts to disentangle the protective effect of education years on neurocognitive networks. Interestingly, preliminary analysis reveals that the relative change in attention and processing speed

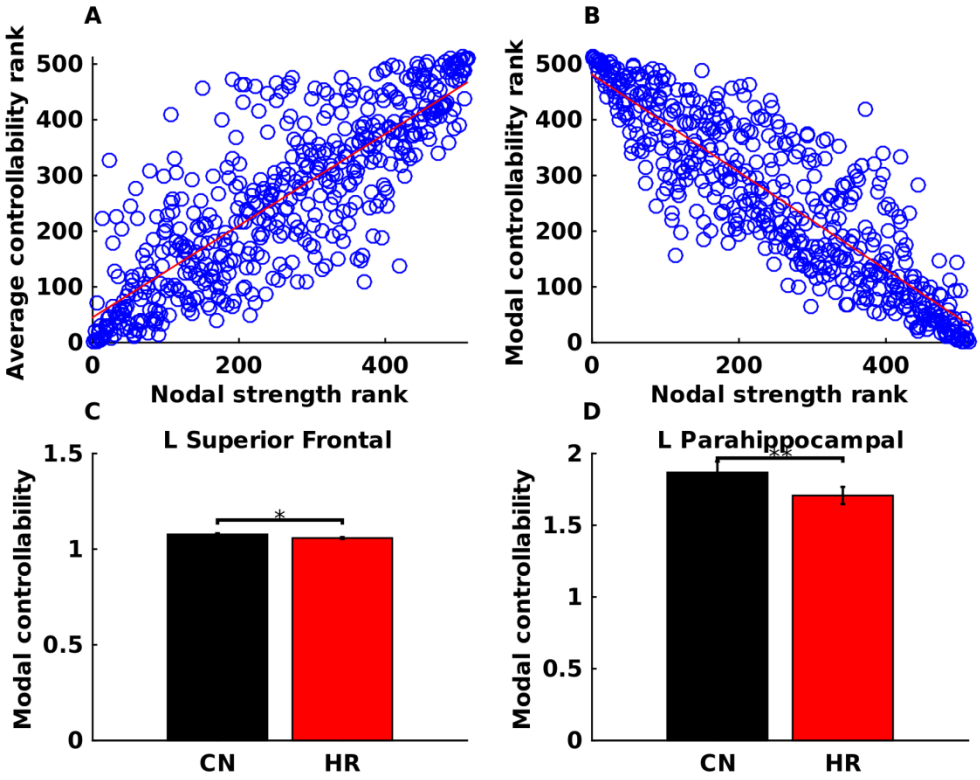

Figure 5-1: *Controllability of structural networks in control and high-group groups. A, Scatter plot of average controllability as a function of nodal strength for each node (blue circles), showing a highly-correlated positive association (red line). B, Modal controllability as a function of nodal strength, showing an inverse relationship. Mean modal controllability for (**A**) Left superior frontal and (**B**) Left parohippocampal brain-regions across control (black bars) and high-risk groups (red).*

* $p<0.05$; **$p<0.01$

performance over time is significantly associated (r=0.37,p=0.0001) with age-related functional connectivity patterns captured by the first CCA mode (i.e. V_1): Individuals who experience greater reductions in performance from study baseline, are those with negative contributions towards functional connectivity variations in the present wave (~6 years after study baseline). However, functional connectivity estimates were not measured at baseline – hence it is unclear if connectivity changes mirror cognitive reductions over time.

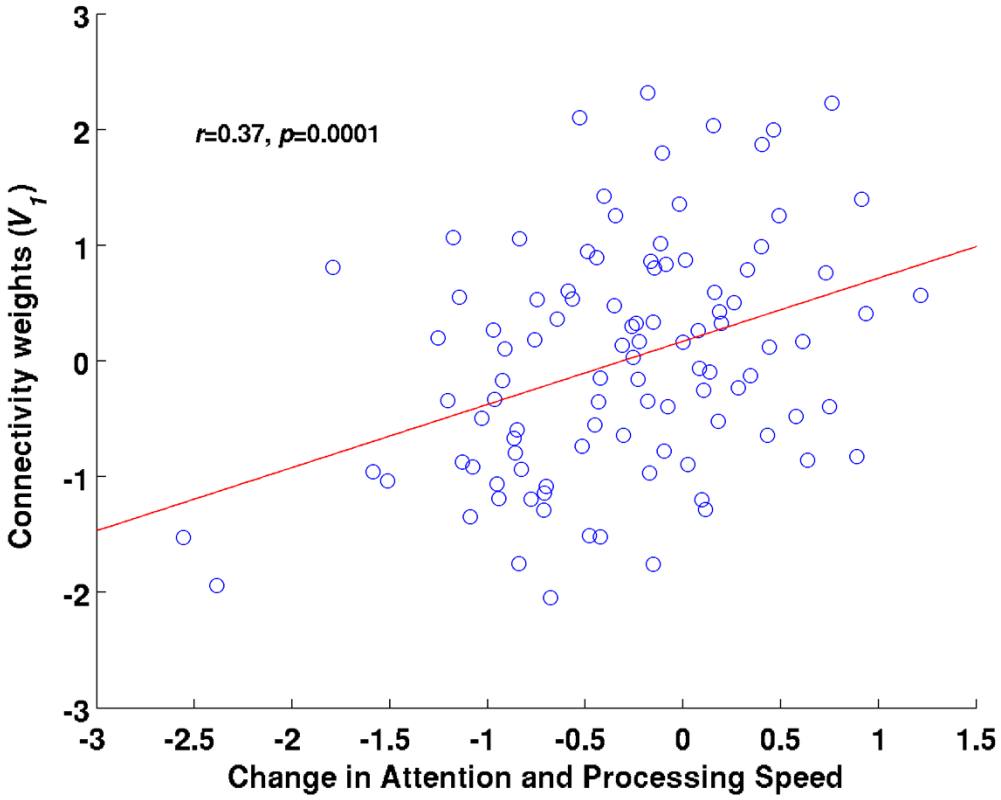

***Figure 5-2**: Scatter plot of functional connectivity variation (V_1) captured by the first CCA mode, as a function of longitudinal change in attention and processing speed. The red line shows the linear regression fit. The moderate correlation visualised here indicates a significant association (r=0.37, p=0.0001) between longitudinal decline and functional connectivity patterns captured in the present wave.*

5.7.5 Improving the biological accuracy of diffusion tractography

The patterns of structural connectomic findings revealed for the young and elderly populations (Chapters 2 and 4) are dependent on the biological accuracy of the reconstructed fibres. The strong, rapid switching of gradients during dMRI acquisition leads to spatial distortions along the phase-encoding direction (Tournier et al., 2011).

Future prospective studies should ideally acquire additional b0 images with opposing phase-encoding directions in order to estimate the spatial inhomogeneity patterns (Andersson and Sotiropoulos, 2016; Holland et al., 2010b). In doing so, accurate co-registration can be achieved between the diffusion and T1-weighted images. Anatomical priors of tissue and fluid types can allow more reliable estimations of fibre orientations (Jeurissen et al., 2014) - as estimates can be noisy in non-pure WM areas (i.e. partial volume effects) (Roine et al., 2014). Furthermore, through a procedure known as Anatomically Constrained Tractography (ACT) (Smith et al., 2012a), information of the GM/WM boundaries allows fibre propagations to only project/terminate at the tissue-interface. Lastly, a recently proposed "spherical-informed filtering tractogram" (SIFT) algorithm can also perform a correction on the streamline counts that more closely reflects the underlying fibre density (Smith et al., 2013a, 2015b). These sophisticated developments prevent reconstruction biases, improve the biological plausibility of streamlines, and thus increase the reliability of resultant connectomes (Jeurissen et al., 2014; Smith et al., 2012a, 2013a; Smith et al., 2015a; Smith et al., 2015b). However, studies of both the young and elderly populations in this thesis were commenced prior to knowledge of the benefits of reverse phase-encoding acquisitions. Future studies would benefit in acquiring optimised acquisitions to demonstrate the replicability of the spatial and topological features in our connectomes.

5.7.6 Confounding issues of tractography in older participants

Whole-brain tractography approaches typically generate an arbitrary pre-defined number of streamlines (five million fibres within the present studies). This parameter setting is chosen to avoid inter-individual network differences being potentially driven by fibre

reconstruction biases. Within the context of ageing research, assuming a constant streamline density over participants of varying ages is inconsistent with the characteristic regional grey and white changes that co-occur. Because of this confounding issue, age-related macroscopic changes were not directly investigated in Chapter 2. Within our elderly data, linear increases in weighted connectivity (Figure 5-3) were uncovered at a liberal significance threshold ($p < 0.10$, FDR-corrected): Increases in connectivity with age were found for the left putamen (left panel), right middle frontal gyrus (middle), and also the right thalamus (right). These findings oppose lifespan studies which reveal decreases in streamline density across a very large age-span (Betzel et al., 2014; Otte et al., 2015). Fibre-seeding within these studies was, however, based upon the number of representative brain voxels in each participant. The contradictory findings in the present study may be attributable to streamlines being continuously generated along relatively-preserved tracts.

A recent computational study showed that the virtual simulation of a pathological lesion in a healthy participant (by removal of grey matter voxels), lead to apparent increases in streamline density within the surrounding tissues (Calamante et al., 2015). This confounding increase in structural connectivity supports the potential biases of current tractography approaches in ageing and neurodegenerative populations. A quadratic (Figure 5-3B; dashed lines) function illustrates the oldest participants (top-right corner) - who presumably experience greater structural changes - appearing to drive linear connectivity increases (solid lines). Whilst severe pathological disturbances may not be present within these relatively-older participants (each scan is checked by a radiologist), future investigations would benefit from addressing these concerns. It would be advantageous to provide biologically-relevant indexes (i.e. SIFT) of streamline counts

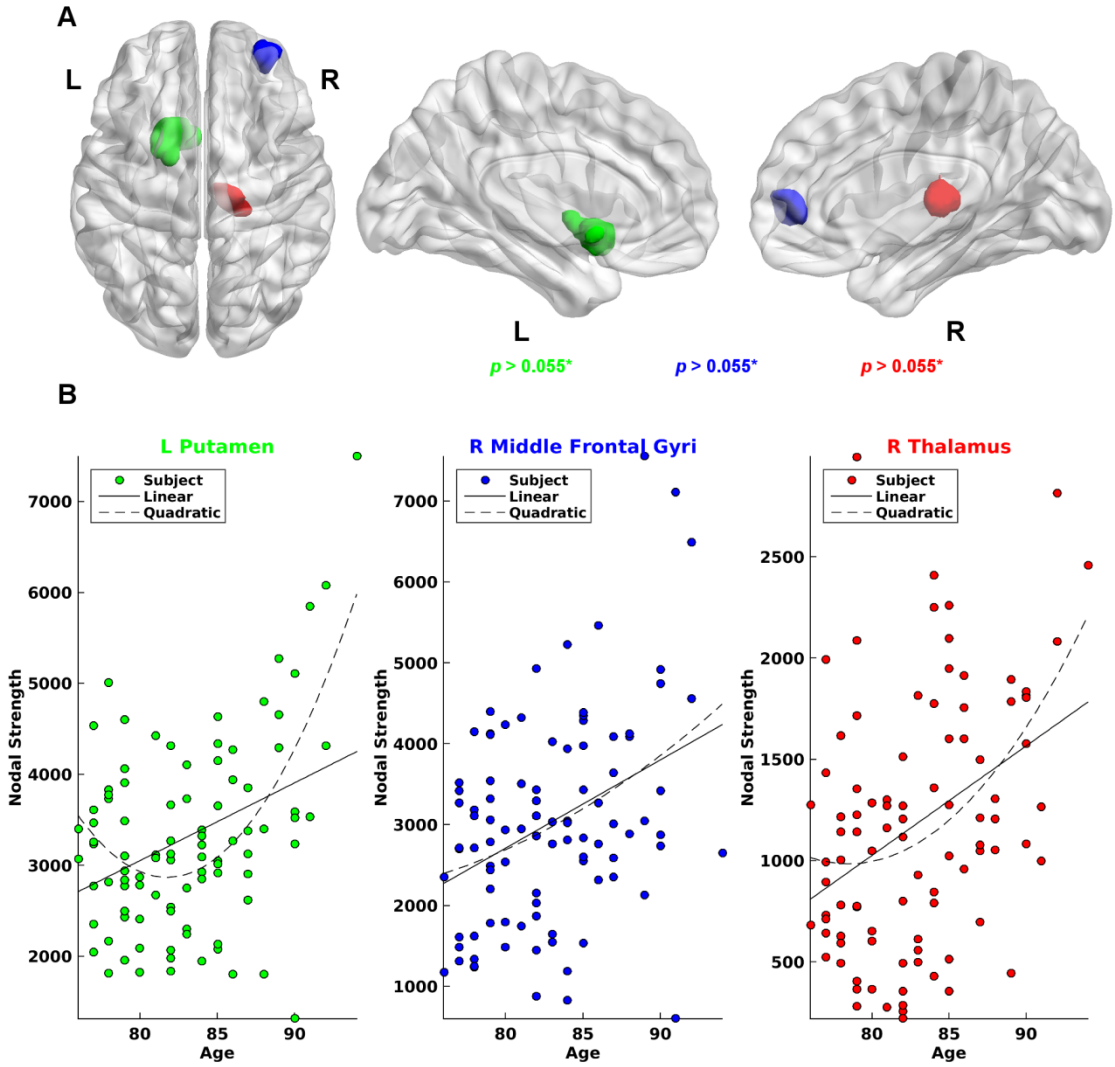

Figure 5-3: *Brain regions that reveal increases in weighted connectivity with age at liberal significance thresholds. A, Volumetric structures of significant regions (p < 0.10, FDR-corrected), presented from axial and medial perspectives. Colour denotes the different regions, including the left putamen (green), right middle frontal gyrus (blue), and right thalamus (red). Linear (solid lines) and quadratic fits (dashed) as a function of age for the regions.*

* FDR-corrected

that matches the underlying axonal density. Approaches such as Apparent Fibre Density (AFD) (Raffelt et al., 2012b) and neurite morphology (Zhang et al., 2012) do not rely on fibre tracking, and can potentially provide localised measures of microstructural white matter changes with age (Raffelt et al., 2016). It is also recommended in future studies to perform a modelled penalisation of reconstructed streamline counts, potentially based upon the volumetric size of the white-matter, age, or indexes of white-matter health.

Appendix 1 | Network Measures

A1.1 Nodal-level

Strength. For weighted networks G_w, nodal strength w_i was calculated as the sum of all connections node *i* shared between other *j* nodes in the network.

Degree. For binary networks G_b, nodal degree k_i was calculated as the number of *j* nodes connected to node *i*.

Betweenness Centrality. For G_b, nodal betweenness centrality b_i was calculated as the fraction of all shortest paths that pass through *i*, and defined formally as:

$$b_i = \sum_{\substack{h,j \in N \\ h \neq j, h \neq i, j \neq i}} \frac{\rho_{hj}(i)}{\rho_{hj}}, \tag{A1.1}$$

where $\mathrm{p}_{jh}$is the number of shortest paths between *j* and *h*, and $\mathrm{p}_{jh}(i)$ is the number of shortest paths between *j* and *h* that pass through *i*.

Subgraph Centrality. For G_b, to characterise the participation of each node in all subgraphs in a network, nodal subgraph centrality SC_i was calculated and defined formally (Estrada and Rodríguez-Velázquez, 2005) as:

$$SC_i = \sum_{k=0}^{\infty} \frac{\mu_k i}{k!}, \tag{A1.2}$$

with *k* the length of walks from *i*, and $\mu_k i$ the local spectral moments of the number of closed walks of length *k* starting and ending at *i*.

Participation Index. For G_b, to identify the level of connectedness of node *i* to other modules within each subject matrix, the participation index (PI) of node *i* was calculated and formally defined as:

$$PI_i = 1 - \sum_{m=1}^{N_m} \left(\frac{k_{im}}{k_i}\right)^2, \tag{A1.3}$$

with N_m, the number of modules; and k_{im}, the number of binary connections from node *i* to module *m*.

Within-module degree Z score. For G_b, to identify the level of connectedness of node *i* to other nodes in the same module *m*, the within-module degree Z-score of node *i* was calculated and formally defined as:

$$Z_i = \frac{k_i\,(m_i) - \overline{k}(m_i)}{\sigma^{k(m_i)}}, \tag{A1.4}$$

with m_i the module containing node *i*, $k_i(m_i)$ is the within-module degree of i (the number of links between *i* and all other nodes in m_i), and $\overline{k}(m_i)$ and $\sigma^{k(m_i)}$ are the respective mean and standard deviation of the within-module m_i degree distribution.

A1.2 Rich-club coefficients and significance

A1.2.1 Weighted rich-club coefficients

To calculate the weighted richness of hub connections, all connections of the individual network *N* were first rank ordered by weight, resulting in a vector $\boldsymbol{W^{ranked}}$. Next, the

sum of the weights of the connections between the predefined hub-regions *h* was calculated and defined as $\boldsymbol{W_h}$. The weighted rich-club parameter $\Phi(h)$ was then computed as the ratio between $\boldsymbol{W_h}$, and their maximum possible weight sum $\boldsymbol{W^{max}}_{\boldsymbol{h}}$. Formally, $\Phi(h)$ is given by the following equation (Samu et al., 2014):

$$\Phi(h) = \frac{W_h}{W_h^{max}} = \frac{W_h}{E_h^{max}}, \qquad \text{(A1.5)}$$
$$\sum_{l=1} w_l^{ranked}$$

where E_h^{max} is the maximum possible number of edges among hub-regions *h*, and W_l^{ranked} is the weight of the *i*th strongest edges in the network.

A1.2.2 Binary rich-club coefficients

Rich-club coefficients can also be measured for binary-relations to connectivity. For each *k*-level within *N*, all nodes (and their connections) with a degree less than *k* were removed from the network. Next, the renaming number of connections of between nodes with degree >*k* were defined as $E_{>k}$. The rich-club parameter ϕ was then computed as the ratio between $E_{>k}$ and the total number of possible of the network if it was fully connected. Formally, ϕ as given by the following equation (Colizza et al., 2006; McAuley et al., 2007):

$$\phi\,(k) = \frac{2E_{>k}}{N_{>k}(N_{>k} - 1)}. \qquad (1.6)$$

A1.2.2 Rich-club organisation and significance

To estimate the specific enrichment of hub connections for both weighted and binary variants of the rich-club coefficients, the normalized rich-club coefficient $\Phi(norm)$ was calculated by dividing the rich-club coefficient against the average rich-club coefficient $\Phi(rand)$ generated from a set of 1000 random networks (Maslov and Sneppen, 2002). For the binary-variant, randomised networks preserve the degree-distribution of regions, whilst weighted random networks were degree-and-strength matched. Rich-club architecture was said to be present if $\Phi(norm) > 1$ (van den Heuvel and Sporns, 2011).

For the weighted variant, a nonparametric test was also used to test whether each subject's hub connections contained rich-club architecture. First, a null distribution of rich-club coefficients $\Phi(rand)$ was obtained from the population of 1000 networks randomised from each subjects empirical network (as above). Next, a subject-specific p value was assigned to $\Phi(norm)$ as the percentage of $\Phi(h)$ which exceeded $\Phi(rand)$.

A1.3 Global-metrics

We characterised the global topology of the connectome using two metrics: (1) The shortest characteristic path length (CPL), a global measure which captures the average binary distance (the number of steps) between each node and all other regions; (2) The normalised clustering coefficient (CC) is a local measure that captures the tendency of nodes to form local cliques. Mathematical definitions of these selected graph metrics are provided below:

***Table A1-1**: Global graph-theoretical measures implemented in Chapter 4*

Measure	Definition
Characteristic path length	Characteristic path length of the network: $L = \frac{1}{n}\sum_{i \in N} L_i = \frac{1}{n}\frac{\sum_{j \in N, j \neq i} d_{ij}}{n-1}$ L_i is the average distance between node i and all other nodes.
Clustering coefficient	Clustering coefficient of the network: $C = \frac{1}{n}\sum_{i \in N} C_i = \frac{1}{n}\sum_{i \in N}\frac{2t_i}{k_i\,(k_i - 1)}$ C_i is the clustering coefficient of node i ($C_i = 0$ for $k_i < 2$).

N is the set of all nodes in the network, and n is the number of nodes. L is the set of all links in the network, and l is number of links: Formulas are adapted from elsewhere (Rubinov and Sporns, 2010).

Appendix 2 | Supplementary figures for study 1

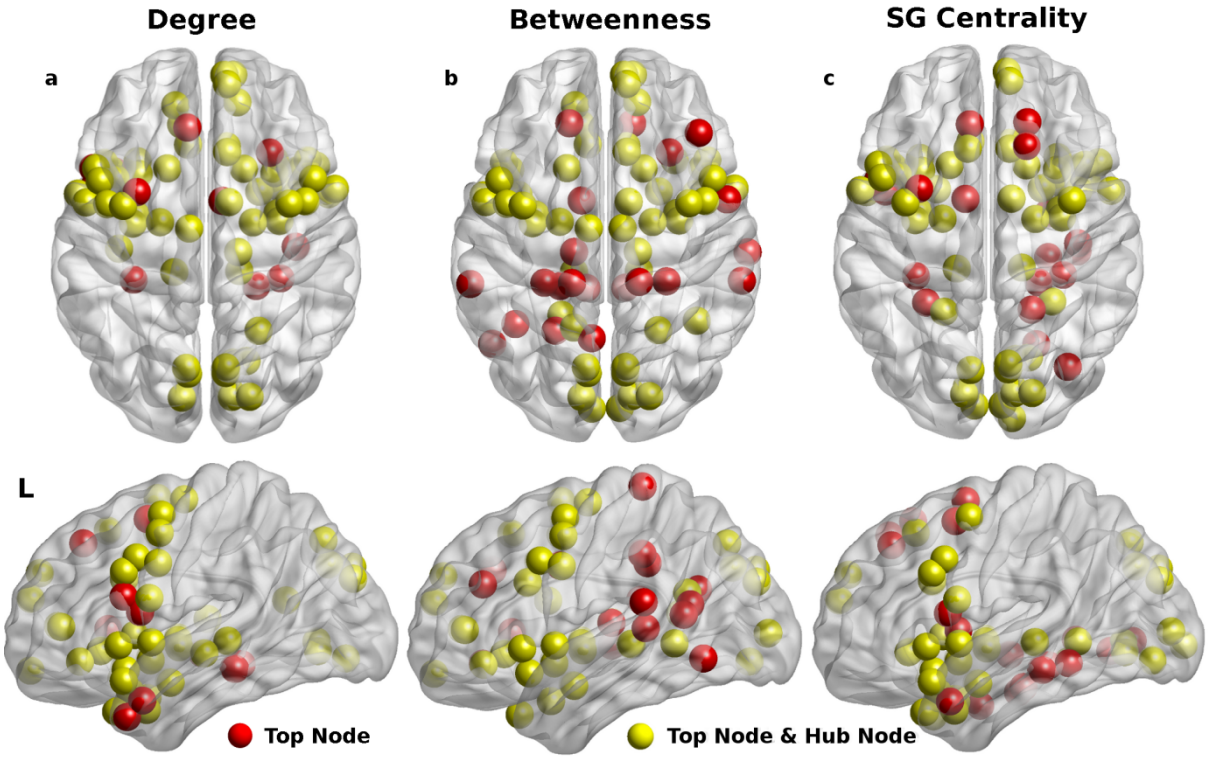

Figure A2-1: *Superior and lateral perspectives of nodal regions most consistently ranked (top 15%) as top nodes across subjects by values of degree (**A**), betweenness centrality (**B**), and subgraph centrality (**C**). For a given metric, yellow dots indicate top ranked regions which are also hub-regions in the elderly connectome at 7.5% sparsity, while red dots index indicate top ranked nodes which are not*

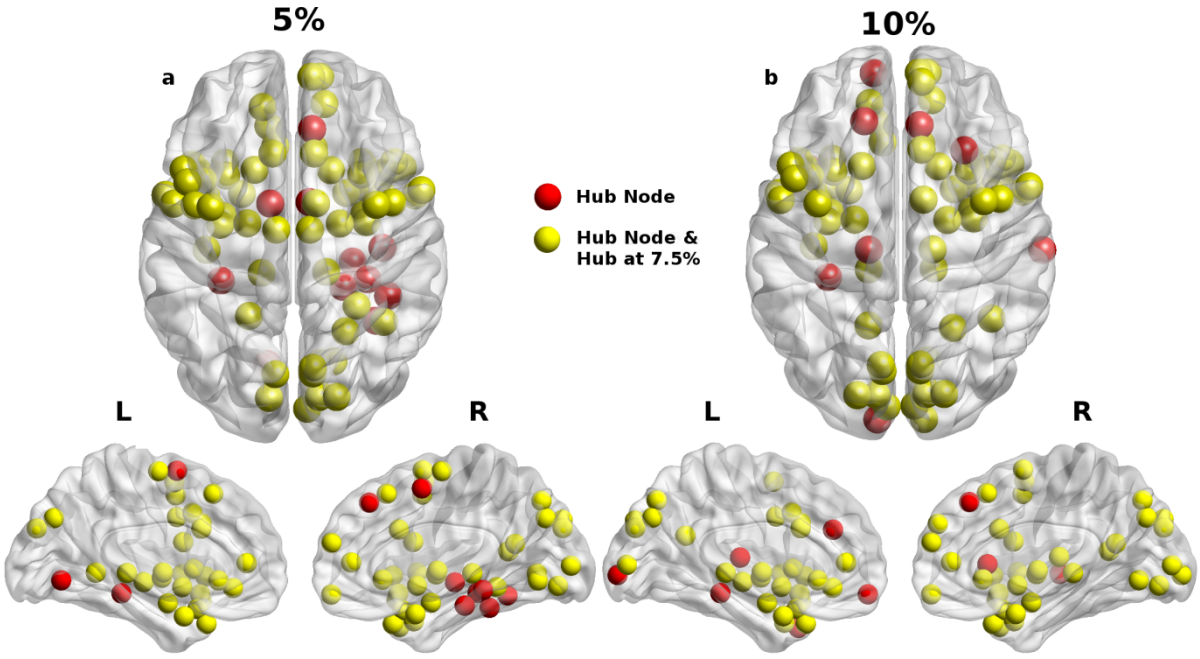

Figure A2-2: *Superior and medial perspectives of nodal regions identified to be hub-regions for subjects connectomes at 5% (**A**) and 10% (**B**) sparsity levels. For a given sparsity level, yellow dots indicate hub-regions which are also hubs in the elderly connectome at 7.5% sparsity, while red dots index indicate hub-regions which are not*

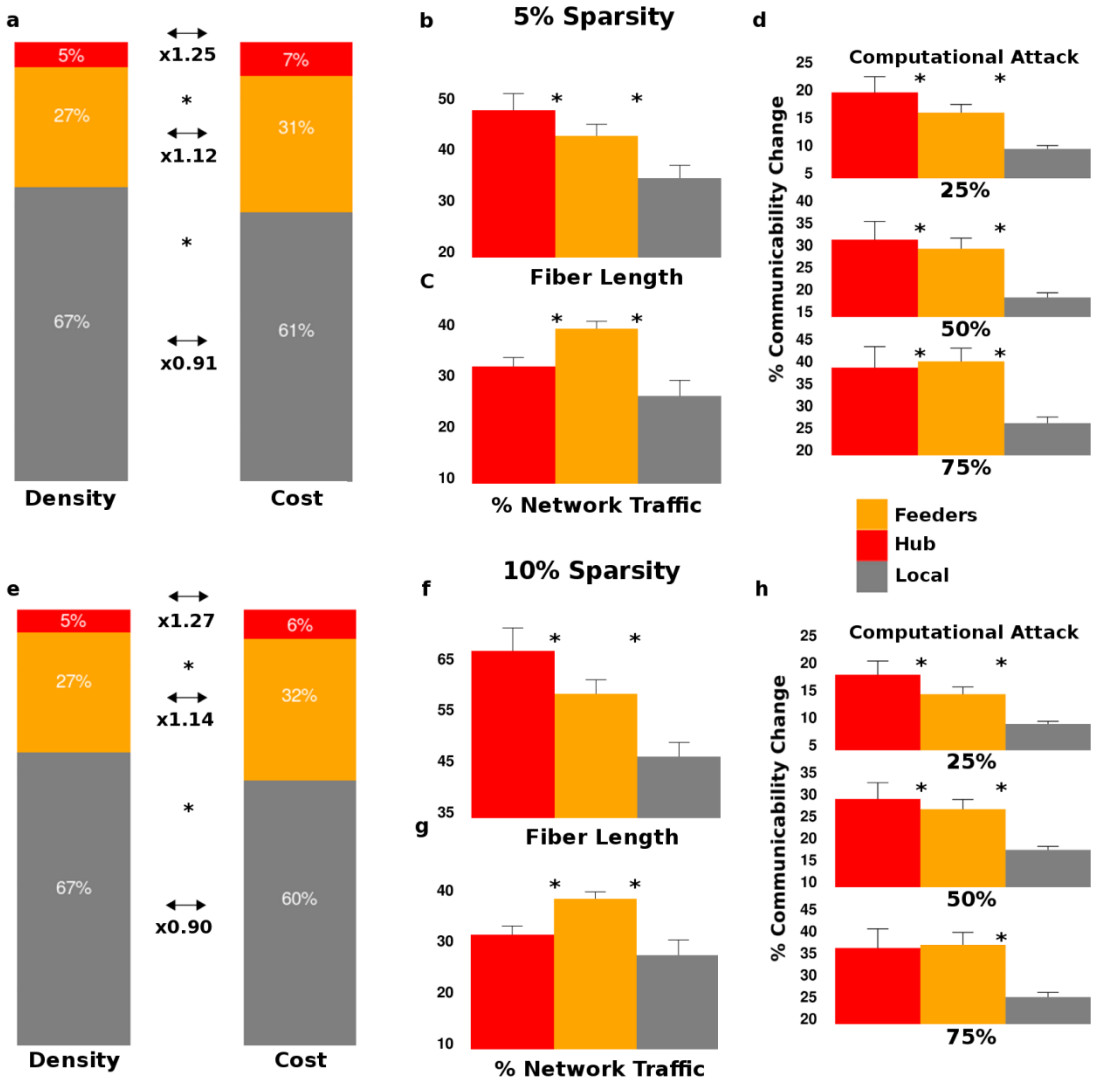

Figure A2-3*: Architectural features of hub (red), feeder (orange), and local (grey) connection classes in the elderly connectome, at 5 (top panel) and 10% (bottom) sparsity levels.* ***A*** *and* ***E****, Mean contributions of each connection class to density (number of streamlines) (left column) and cost to the network (right). The middle text column represents the mean cost/density ratios for each connection class.* ***B*** *and* ***F****, Mean fibre length (mm) for each connection class.* ***C*** *and* ***G****, The mean percentage of network traffic each connection class routes for the shortest path (minimum number of paths) between any region i and j.* ***E*** *and* ***H****, Mean percentage change in network communicability after removing specified number of edges from connection class, at 25% (i.e. 25% of rich-club connections) (top), 50% (middle), and 75% (bottom) increments.*

** $p < .01$, permutation testing ($N = 5000$)*

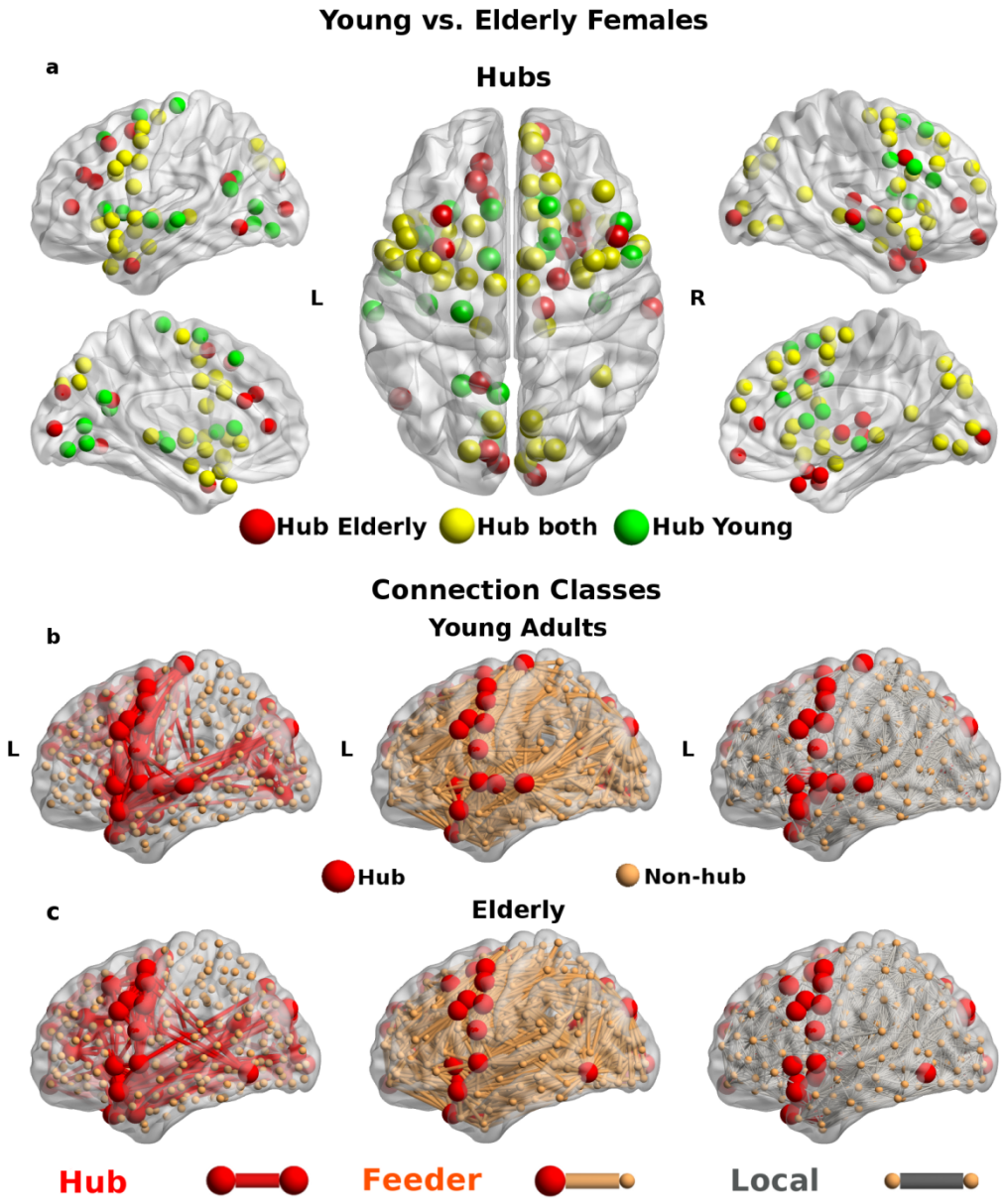

Figure A2-4: *Comparison of hub-regions, and connection classes, across young adult and elderly females. A, Hub regions identified to be either unique to either young (green circles) or elderly (red) female subjects, or those consistent as hubs across both (yellow) populations. This figure shows a high consistency for regions to be identified as hubs in both cohorts.* ***B*** *and* ***C****, Sagittal perspective of connections of either hub (left panel), feeder (middle), or local (right) connection classes in young and elderly females, respectively.*

Appendix 3 | Steps involved in functional network construction

A3.1 Acquisition and pre-processing of MRI data

Structural and functional MRI data were acquired with a Philips 3T Achieva Quasar Dual MRI scanner (Philips Medical System, Best, The Netherlands), utilising an 8 channel head coil. Resting-state fMRI data were acquired while participants lay quietly in the scanner with their eyes closed using a T2* weighted echo-planar imaging sequence (TE = 30 ms, TR = 2000 ms, flip angle = 90º, FOV 250 mm, 136 x 136 mm matrix size in Fourier space). Each volume consisted of twenty-nine contiguous 4.5 mm axial slices (no gap) to achieve whole-brain coverage. A total of 208 volumes were collected for approximately seven minutes and two seconds. Structural T1-weighted MRI were also acquired, using the following parameters: TR = 6.39 ms, TE = 2.9 ms, flip angle = 8°, matrix size = 256 × 256, FOV = 256 × 256 × 190, and slice thickness = 1 mm with no gap between; yielding 1 mm × 1 mm × 1 mm isotropic voxels. The structural and functional MRI scans of all subjects were visualised within FSLView (Smith et al., 2004b) for artifact inspection. All MRI data were visually inspected and excluded if severe signal dropout (particularly around orbitofrontal areas) or spatial distortions were present. Data from 111 participants thus entered the study.

A3.2 rs-fMRI pre-processing

Pre-processing of rs-fMRI data was conducted using the Data Processing Assistant for Resting-State fMRI (DPARSF, v3.2 advanced edition) (Yan and Zang, 2010), which calls

functions from SPM8 (http://www.fil.ion.ucl.ac.uk/spm/) in MatLab. Data were slice-time corrected and volumes were realigned to the mean functional image. Individual structural images were linearly co-registered to the mean functional image (6 degrees-of-freedom), and the resultant spatial alignments were visualised within MRview (MRtrix) (Tournier et al., 2012). Linear detrending was next performed, followed by nuisance covariate regression of 24 head-motion parameters (Friston et al., 1996b), and signals derived from the individually segmented WM/CSF masks (Ashburner and Friston, 2005). The T1 images (in functional space) were processed by the Diffeomorphic Anatomical Registration Through Exponentiated Lie algebra (DARTEL) (Ashburner, 2007) tool to generate an average population-based brain template. This allowed native functional images to be transformed into Montreal Neurological Institute (MNI) space (via the average template) and resampled to 3-mm isotropic voxels. rs-fMRI images were then smoothed with a full-width half-maximum Gaussian kernel (6 mm) performed upon the native image intensities. Finally, temporal band-pass filtering (0.01–0.08 Hz) was applied. Global signal regression was not performed.

A3.3 Construction of functional brain networks

The standard AAL template (Tzourio-Mazoyer et al., 2002b) within MNI space was subdivided into 512 cortical and sub-cortical parcellation regions of approximately uniform size (Zalesky et al., 2010b). A functional connectivity matrix *M* was derived in each participant by calculating the Pearson's correlation coefficient between the mean BOLD signals between all pairs of regions. The entries of *M* were transformed into *Z*-score matrices using Fisher's transformation. The upper triangle of *M* for each subject

was concatenated across all subjects, resulting in a 101 (subjects) x 130816 (unique edges) matrix N_1.

A3.4 Normalization and demeaning of connectivity matrices

The connectivity matrices N_1 were normalized and deconfounded according to the procedure of (Smith et al., 2015b) (available online at http://fsl.fmrib.ox.ac.uk/analysis/HCP-CCA/hcp_cca.m). Each column within N_1 was normalized according to its mean value, resulting in an additional matrix N_2. Badly conditioned columns (mean value < 0.1) within N_2 were removed. Each remaining column within N_2 was further demeaned, and global variance normalization was applied. We note that (Smith et al., 2015b) found almost identical correlations of the subject weightings, and uncorrected data (N_1) to orthogonalized components of either the non-normalized (N_1) or normalized (N_2) matrices. Consequently, the present analysis solely employed N_2 for subsequent analyses.

The potential confounding effect of head motion was additionally addressed. Head motion for each subject was calculated by their mean frame-wise displacement (FD) (Power et al., 2012) across the fMRI acquisition. Subject motion calculations were demeaned and squared, to help account for potentially nonlinear effects of this confound. Subject motion was then regressed out of N_2, resulting in N_3. Regardless, no significant influence of age on subject motion (FD) is identified ($p > 0.39$, $r = -0.09$).

Appendix 4 | Supplementary tables and figures for study 2

Table A4-1: *Cognitive domain scores of subjects*

Cohort	**All subjects (*n*= 101)**	**With baseline IQ (*n*= 91)**
	Mean (+- *SD*)	Mean (+- *SD*)
Attention/Processing Speed	0.07 (0.91)	0.11 (0.93)
Executive Function	0.37 (0.77)	0.43 (0.71)
Visuospatial Ability	0.19 (0.92)	0.23 (0.90)
Language	0.34 (0.93)	0.35 (0.91)
Memory	0.57 (0.90)	0.61 (0.90)
Verbal Memory	0.50 (0.93)	0.55 (0.93)

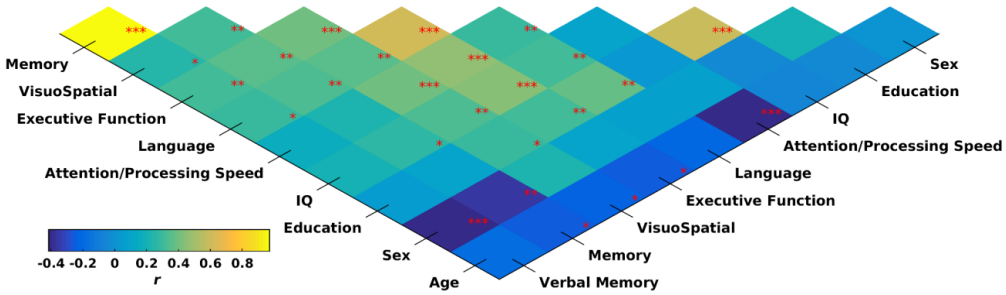

Figure A4-1*: Strength and direction of relations between demographic and cognitive measures for those receiving (n= 91) NART IQ assessment.*

* $p < 0.05$, ** $p < 0.01$, *** $p < 0.001$; FDR-corrected

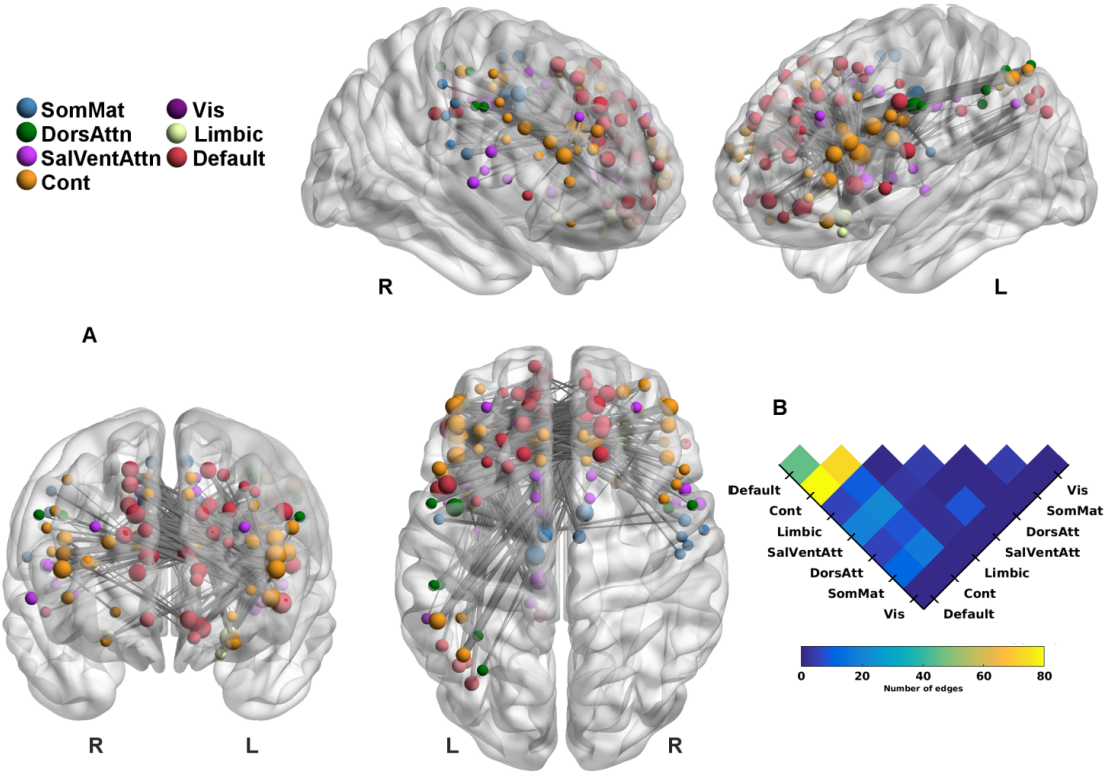

Figure A4-2: *Connectivity edges most positively expressed by the third CCA mode. A, Connectivity edges exhibiting strongest positive associations with functional connectivity patterns (V_3). Line width indexes strength of correlation. Circle size is scaled to the number of connections each region shares within the network, whilst coloured to their functional network specialisation. The brain meshes are presented from axial (middle panel), posterior (top right), and sagittal perspectives of the left and right-hemisphere. B, Coarse perspective of connectivity distributions across the functional networks, with warmer colours indicating greater number of connections.*

Table A4-2: *CCA modes significant with the inclusion of sex*

CCA Mode	One	Two
df_1	81	64
df_2	545.36	490.99
F	1.64	1.38
λ	0.24	0.38
R^2	0.36	0.25
RI	0.067	0.038
p	0.00075	0.033

RI, redundancy index

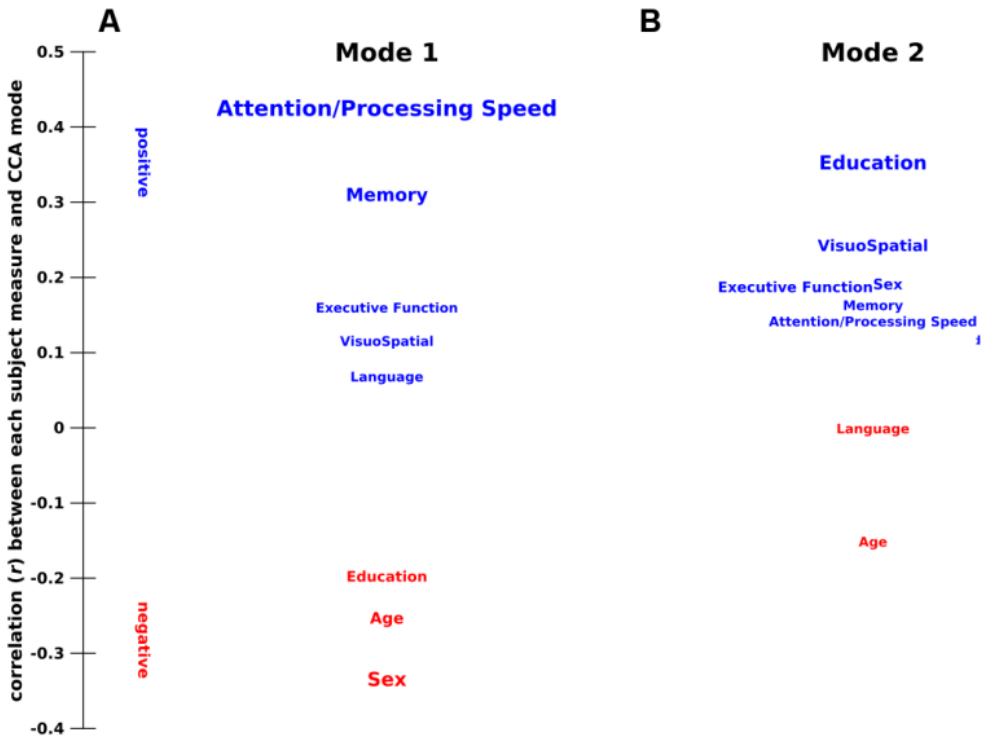

Figure A4-3: Associations between cognitive and demographic measures captured significant CCA modes with including sex. A-B, Correlation between subject measures and functional connectivity variation (V_m)

Table A4-3: CCA modes significant with the removal of verbal-memory scores

CCA Mode	**One**	**Two**
df_1	49	36
df_2	446.11	389.20
F	1.99	1.68
λ	0.37	0.53
R^2	0.31	0.21
RI	0.044	0.030
p	0.00017	0.0097

RI, redundancy index

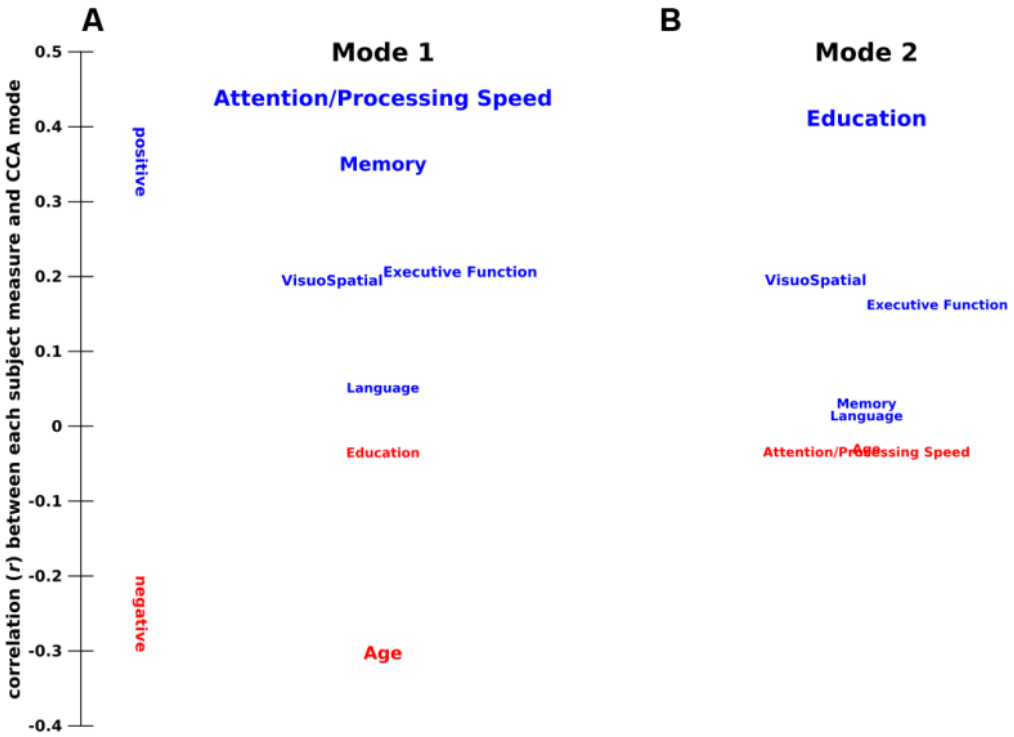

Figure A4-4: *Associations between cognitive and demographic measures captured by the CCA modes with the removal of verbal-memory scores. A-B, Correlation between subject measures and functional connectivity variation (V_m)*

***Table A4-5**: CCA modes significant with a coarser parcellation scheme*

CCA Mode	**One**
df_1	64
df_2	496.76
F	1.59
λ	0.34
R^2	0.30
RI	0.064
p	0.0035

RI, redundancy index

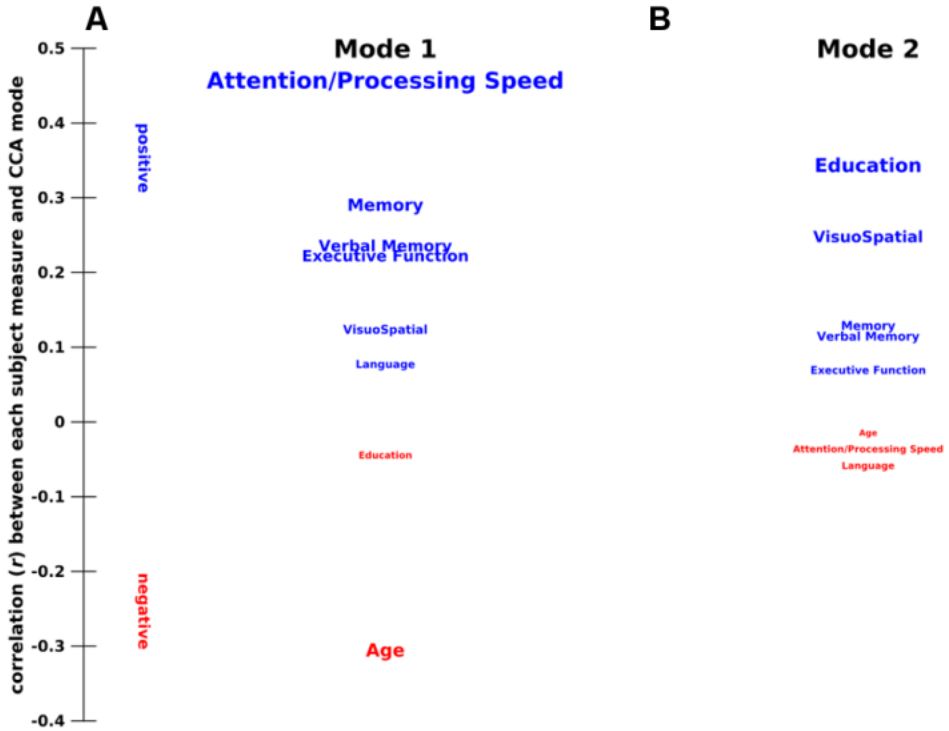

Figure A4-5: *Associations between cognitive and demographic measures captured by the first (p=0.003) and second CCA modes (p=0.057) utilizing a coarser parcellation scheme. A-B, Correlation between subject measures and functional connectivity variation (V_m)*

Table A4-5: CCA modes significant with including intelligence scores

CCA Mode	**One**	**Two**
df_1	81	64
df_2	480.73	433.31
F	1.65	1.38
λ	0.21	0.34
R^2	0.40	0.28
RI	0.077	0.038
p	0.0008	0.037

RI , redundancy index

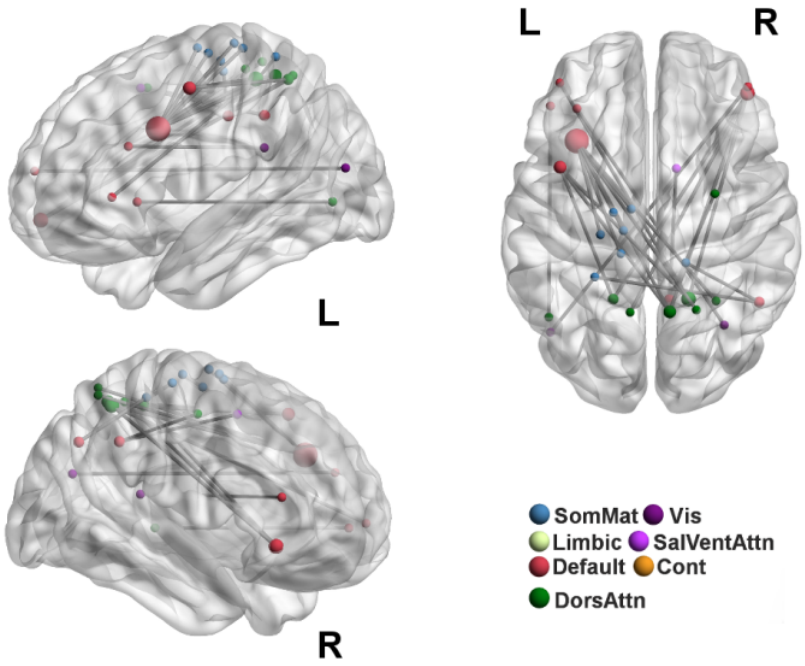

***Figure A4-7**: Functional connections strongly expressed for both with and without including intelligence in the second CCA mode. Circle size is scaled to the number of connections each region shares within the network, whilst coloured to their functional network specialisation. The brain meshes are presented from axial (top right panel), and customised perspectives of the left (top left; elevation= 0, azimuth = -120) and right-hemisphere (bottom left; azimuth = -240)*

Appendix 5 | Supplementary information and results for study 3

A5.1 Sample selection and characterization

A5.1.1 Participants

A total of 326 individuals were scanned, of whom 45 (11 CN, 26 HR, and 8 BD) were removed due to excessive head movement or poor image quality (see below). In order to minimize possible confounding effects of gender and age, we selected three age- and gender-matched sub-groups. The age- and gender-matched sample comprised three groups: i) 96 controls (CN) defined as subjects with no parent or sibling with bipolar I or II disorder, recurrent major depression, schizoaffective disorder, schizophrenia, recurrent substance abuse or any past psychiatric hospitalisation; and no parent with a first degree relative who had a past mood disorder hospitalisation or history of psychosis; ii) 84 subjects genetically at high risk for BD who had not yet developed this condition (HR), defined as children or siblings of a proband with a confirmed DSM-IV diagnosis of bipolar I or II disorder; and iii) 38 BD subjects, meeting DSM-IV criteria for either bipolar I or bipolar II disorder. All participants were aged between 12 and 30 years and with an IQ above 80. Clinical details of the three groups are described (Perich et al., 2015). Of the 84 HR participants, 65 had a parent with BD and 19 a sibling with BD. Of the 38 BD patients, 18 had DSM-IV Bipolar I Disorder and 20 DSM-IV Bipolar II Disorder. The lifetime or current presence of psychiatric disorders besides BD was not an exclusion factor for either HR or CN subjects. This ecological approach has been

used by similar studies of individuals at high genetic risk for BD (Nurnberger et al., 2011).

All participants are involved in an ongoing longitudinal study of individuals at-risk for BD aged 12-30 years. HR and BD participants were recruited from families who had previously participated in a BD pedigree molecular genetics study or a specialized BD research clinic, or were otherwise recruited from clinicians, mental health consumer organisations and other forms of publicity. CN subjects were recruited via print and electronic media, as well as noticeboards in universities and local communities.

The subjects aged between 12-21 years are involved in a collaborative high-risk study with a U.S. consortium headed by Dr John Nurnberger which is based at Indiana University, Johns Hopkins University, Washington University in St. Louis, and Michigan University.(Nurnberger et al., 2011) As this US-Australian collaboration involves common assessments for participants aged 15-21 years, we report separately on instruments used for the younger (15-21years) and older (22-30 years) age groups in this sample. Both groups shared consensus Best-Estimate DSM-IV current and lifetime diagnoses derived from semi-structured diagnostic interviews. Brain imaging studies were only undertaken in the Australian sample. A number of studies on this BD HR sample have been recently reported (Breakspear et al., 2015b; McCormack et al., 2015; Perich et al., 2015; Roberts et al., 2013; Roberts et al., 2016a).

A5.1.2 Clinical and phenotypic characterization

Proband consensus DSM-IV diagnosis was determined by two independent raters following Best Estimate methodology (Leckman JF et al., 1982), using information from the Diagnostic Interview for Genetic Studies (DIGS) Version 4, the Family Interview for Genetic Studies (FIGS) and medical records (where available).

Confidence rating ranges using the Best Estimate Methodology vary from 1-4, where 1 represents criteria not met for a diagnosis and 4 represents a definite diagnosis. All diagnoses reported have a confidence rating of 3 or 4. Structured diagnostic interviews were also performed on all HR, CN and BD participants. For those aged between 15 and 21 (CN, *n*=40; HR group, *n*=36; BD group, *n*=9), an adapted version of the Schedule for Affective Disorders and Schizophrenia for School-Age Children – Present and Lifetime Version (K-SADS-BP) was developed specifically for use in the US-Australia collaborative study of young people at genetic risk for bipolar disorder (Nurnberger et al., 2011). The K-SADS-BP combines items from the K-SADS Present and Lifetime Version (Kaufman J et al., 1997), and uses extended sections on depression, mania and ADHD derived from the Washington University in St Louis K-SADS (WASH-U K-SADS) to elicit detailed information on pre-pubertal mania, rapid-cycling, attentional and sub-threshold bipolar symptoms (Geller B et al., 2001). The KSADS-BP was administered to both the child and one parent. For participants aged under 21, clinicians completed the Children's Global Assessment Scale (CGAS).

For participants aged between 22 and 30 (CN, *n*=56; HR group, *n*=48; BD group, *n*=29), the DIGS (Version 4) was used to measure the current and lifetime presence of axis I DSM-IV disorders. Consensus DSM-IV diagnoses of the HR, BD, and CON subjects were determined by two independent raters with Best Estimate methodology (Leckman JF et al., 1982), using the DIGS, the FIGS and medical records (where available). For participants aged between 22 and 30, clinicians completed the Global Assessment Scale (GAS). To assess current mood state, for those aged between 15 and 21, the Children's Depression Inventory (CDI) was used, and for participants aged 22-30 years, the Montgomery-Asberg Depression Rating Scale (MADRS) was administered. Intellectual ability was assessed with the Wechsler Abbreviated Scale of

Intelligence (WASI). Participants aged 15-30 years completed clinical and neuropsychological assessments on the same day as the scan. The majority of parental reports using the K-SADS were also completed on the same day as the scan.

Among the 26 BD patients taking a mood stabiliser (Table A5-1), 3 were taking lithium, 15 were taking another mood stabiliser, and 8 were taking lithium in addition to another mood stabiliser. Of the 11 BD participants taking an antipsychotic, 10 were also taking a mood stabiliser.

Table A5-1**:** *Clinical information for control, high-risk, and Bipolar patient population groups.*

	CN (*n*=96)	**HR (*n*=84)**	**BD (*n*=38)**	**Difference Statistic**	***p*-value**	**Post-hoc Effects**
Lifetime DSM-IV diagnosis						
Any diagnosis, *n (%)*	24 (25.0)	39 (46.4)	38 (100.0)	$\chi^2 = 61.59$	<.001	HR>CN** BD>CN***
At least one MDE, *n (%)*	9 (9.4)	22 (26.2)	36 (94.7)	$\chi^2 = 94.51$	<.001	HR>CN** BD>CN*** BD>HR***
Recurrent MDD, *n (%)*	1 (1.0)	7 (8.3)	-	$\chi^2 = 5.61$	.01	HR>CN*
Any anxiety disorder, *n (%)*	9 (9.5)	15 (18.3)	15 (39.5)	$\chi^2 = 16.45$	<.001	BD>CN*** BD>HR*
Any behavioural disorder, *n (%)*	1 (1.1)	6 (7.4)	7 (18.9)	$\chi^2 = 13.86$	<.001	HR>CN* BD>CN***
Any substance disorder, *n (%)*	6 (6.3)	9 (10.7)	6 (15.8)	$\chi^2 = 3.03$	.220	-
Symptom severity scales						
22 to 30 years	*n*=51	*n*=41	*n*=25			
MADRS, *mean (SD)*	1.9 (3.2)	2.5 (3.7)	10.1 (9.5)	*F*= 22.10	<.001	BD>CN*** BD>HR***
12 to 21 Years	*n*=34	*n*=33	*n*=9			
CDI, *mean (SD)*	6.8 (3.7)	9.0 (6.6)	21.7 (8.7)	*F*=23.78	<.001	BD>CN*** BD>HR***
Clinical Characteristics						
Global Functioning						
GAF, *mean (SD)*	91.7 (4.7)	87.4 (8.5)	78.6 (12.0)	*F*= 38.49	<.001	CN> HR*** CN> BD*** HR>BD***
Age at First						
MDE, *mean (SD)*	19.1 (3.2)	18.5 (4.5)	15.4 (3.7)	*F*= 6.63	.002	BD<CN**

						BD<HR**
Hypomanic episode, *mean (SD)*	-	-	17.0 (4.3)	-	-	-
Manic episode, *mean (SD)*	-	-	17.5 (3.2)	-	-	-
Elevated mood episode, *mean (SD)*	-	-	17.0 (4.0)	-	-	-
Mood episode, *mean (SD)*	19.1 (3.2)	18.5 (4.5)	14.9 (3.8)	*F*=8.68	<.001	BD<CN** BD<HR**
Any anxiety disorder	10.3 (6.7)	13.5 (6.4)	13.3 (7.0)	*F*=1.31	.277	
Number of Episodes						
Major depressive episode, *mean (SD)*	1.4 (1.3)	2.0 (2.1)	12.0 (12.5)	*F*=12.89	<.001	BD>CN*** BD>HR***
Hypomanic episodes, *mean (SD)*	-	-	10.2 (10.3)	-	-	-
Manic episode, *mean (SD)*	-	-	2.8 (2.5)	-	-	-
Any elevated mood episode, *mean (SD)*	-	-	9.9 (10.9)	-		-
Any mood episode, *mean (SD)*	1.4 (1.3)	2.0 (2.1)	21.7 (21.5)	*F*=16.93	<.001	BD>CN*** BD>HR***
Psychotropic Medication						
Anti-depressants, *n (%)*	0 (0.0)	0 (0.0)	15 (39.5)	-	-	-
Mood stabilisers, *n (%)*	0 (0.0)	0 (0.0)	26 (68.4)	-	-	-
Anti-psychotics, *n (%)*	0 (0.0)	0 (0.0)	11 (28.9)	-	-	-
Benzodiazepines, *n (%)*	0 (0.0)	0 (0.0)	0 (0.0)	-	-	-
Stimulants, *n (%)*	0 (0.0)	0 (0.0)	0 (0.0)	-	-	-

Anti-convulsants, *n (%)*	0 (0.0)	0 (0.0)	21 (65.6)	-	-	-

*** $p < 0.001$, ** $p < 0.01$, * $p < 0.05$

A5.2 Data acquisition, pre-processing and structural network construction

A5.2.1 dMRI acquisition & pre-processing

DWI data were acquired with a 3-T Philips Achieva scanner at Neuroscience Research Australia (NeuRA) in Sydney with an 8-channel head coil (Figure A5-1A). One acquisition of 32 directional DWI (b =1000 s/mm^2, with one non-diffusion-weighed image) was acquired using a single-shot echo planar imaging (EPI) sequence. The imaging parameters were as follows: TR = 7767 ms, TE = 68 ms, 55 slices, slice thickness = 2.5 mm, gap = 0 mm, acquisition matrix size = 96 × 96 (field of view = 240×240×137.5 mm), flip angle = 90°, reconstructed to yield
1 mm × 1 mm × 2.5 mm voxels (where the longer dimension is along the dorsoventral axis). A custom in-house package was employed to correct for head-motion (Raffelt et al., 2012a) followed by rotation of the gradient direction matrix (Leemans and Jones, 2009). To decrease spatial intensity inhomogeneities, bias field correction was performed on the b0 image and subsequently applied to all DW images (Sled et al., 1998b). Data were then visualised using FSL view for quality-control purposes (Smith et al., 2004a). Participants were excluded if there was evidence of substantial signal dropout, most likely caused by subject motion. Excessive signal drop out was defined as characteristic zebra-like blurring, or the complete drop out of diffusion signal across volume slice(s) (Pannek et al., 2012a).

A5.2.2 Whole-brain fibre tractography

The fibre orientation distribution (FOD) within each voxel was estimated using MRtrix software (www.mrtrix.org; version 0.3.12-515), by performing CSD (*lmax* = 6) of the diffusion signal in white matter voxels with singularly-oriented (FA > 0.7) fibre bundles. The iFOD2 (Tournier et al., 2010) probabilistic streamline algorithm was subsequently employed to generate plausible fibre propagations by random sampling of the orientation uncertainty inherent in each FOD at points along each candidate path. Tracking parameters were as follows: step size = 0.2 mm, minimum length = 10 mm, max length = 250 mm, FOD termination threshold = 0.1, curvature constraint = 1 mm radius, with 5 million streamlines per subject initialized from random seeds throughout the brain volume.

A5.2.3 Whole-brain structural network construction

Subject-specific parcellations were achieved by employing affine linear registrations all within the FSL software package (Smith et al., 2004a). First, AAL regions were subdivided into 512 subregions of approximately equivalent volume using a random parcellation (Zalesky et al., 2010b). This parcellation template of 512 regions was co-registered into a standard-space template representing an average FA image (FMRIB58; available within FSL) derived from 58 healthy subjects. For each individual, the FMRIB58 1 mm template was co-registered to the subject's FA image. The parcellation template was transformed into subject space by applying the transformation matrix generated from co-registering the FA template to the individual's FA image. We note this randomized template was employed due to the strong, rapid switching of diffusion gradients in single-shot EPI sequences (Andersson and Sotiropoulos, 2016; Holland et

al., 2010a). Thus, the grey-and-white-matter boundaries of parcellaton regions derived from T1-weighted images will not be perfectly aligned with the anatomical boundaries inherent within the DWI.

The anatomical information of subject-specific parcellations and fibre streamline trajectories are combined to yield whole-brain structural connectivity graphs, termed here as W. A weighted connection between i and j, W_{ij}, represents the total number of fibre streamlines which start/terminate within a radial 2 mm distance of voxels located in the pair of parcels i and j. Due to the greater number of random seeds along longer WM tracts, fibre densities are known to be over-estimated in longer fibre bundles (Smith et al., 2013c). Hence, distance-correction is performed by adjusting each streamline within W_{ij} by the physical fibre length between its start and termination point d_{ij} (Hagmann et al., 2008a). All single subject networks were thresholded to retain the strongest 10% of edges. Binary networks were constructed from these thresholded weighted networks by setting all these remaining 10% of connections to one.

A5.3 Statistical Analyses

A5.3.1 Generalised estimating equations (GEE) analyses

To investigate if the association between total connectivity of our structural subnetworks identified with one-tailed two-sample t-tests, nodal strengths that survived correction for multiple comparisons, graph metrics, and diagnostic category were influenced by depressive mood state, Generalised Estimating Equations (GEE) (Liang and Zeger, 1986) were performed with current mood state included as a mean-centred

covariate. GEEs accommodate within-family correlations arising from the inclusion of siblings from within the same family in either the CN, HR or BD groups (families were not split between diagnostic groups). Because current mood state was assessed by different instruments in younger and older age ranges, each model was run separately for the younger and older age groups.

In the whole-sample (across both younger and older age ranges), GEE models were also used to compare whole-brain nodal strengths, proportion of hub, feeder, and local edges and streamlines, mean rich-club coefficient, and graph metrics across diagnostic groups. To address whether the relationship between age and these dependent variables differed between groups, a second set of GEE models were fitted where the age x group interaction was also included as an interaction term in the base model that only identified group differences. In order to select the most parsimonious model, the base model was selected for dependent variables with no significant age x group interaction (p>0.05 uncorrected). In the whole sample NBS networks were identified as they revealed group-wise differences that survived FWE correction. Therefore, these sub-networks only underwent GEE analyses that included the age x group interaction. All GEE analyses (for total sample, younger only, and older only) included age and gender as covariates. All reported p-values are Wald chi-square statistics and all *post hoc* tests are Šidák tests from the GEE analysis. Correction for multiple testing of the main effects of group was carried out using false-discovery rate (FDR) q values using the Benjamini & Hochberg method (Benjamini and Hochberg, 1995).

A5.3.2 Auxiliary GEE analyses

As rates of non-bipolar psychopathology were significantly higher in the HR compared to the CN group (Table A5-1), a secondary analysis was performed in order to determine whether non-bipolar psychopathology influenced our results. Within the HR group diagnosis of at least one depressive episode (n=22) and anxiety (n=15) were included as predictors. Within the BD group, current use of lithium, mood stabilisers, antipsychotics, and antidepressants were included as predictors. To determine effects of BD sub-type Bipolar I vs Bipolar II diagnosis were included as predictors. Finally, measures of illness severity and course (as assessed by age of onset of any mood episode, and total number of mood episodes) were included as predictors. GEE analyses that included age and gender as covariates were also used for all *post hoc* analyses. Separate models predicted each dependent variable.

A5.4 Group differences in demographic and clinical features

The three groups did not significantly differ on age, IQ, or gender distribution (see Table A5-1). BD subjects had higher depression symptom severity scores (MADRS, CDI) than both the HR and CN participants, with no significant differences between the latter two groups. At the time of testing, no participants in any of the three groups met DSM-IV criteria for a current episode of major depression or mania/hypomania. Consistent with prior reports of at-risk populations (Birmaher B et al., 2009; Nurnberger et al., 2011), the occurrence of any lifetime affective disorder (including at least one major depressive episode) was significantly greater in the HR group (p<0.001) compared to the CN group. Rates of any lifetime anxiety disorder (p<0.001) were also significantly higher in the BD group, compared to both the HR and the CN participants.

There was also a significant difference between the latter two groups ($p<0.001$). Furthermore, rates of any lifetime behavioral disorder ($p<0.05$) and any lifetime substance disorder ($p<0.01$) were significantly higher in the BD group, compared to both the HR and the CN participants.

A5.5 Supplementary results

Table A5-2: *AAL Labels of brain regions identified as hubs in control subjects*

AAL Label	Frequency	AAL Label	Frequency
L. Superior Temporal Pole	4	R. Caudate Nucleus	1
L. Insula	4	L. Caudate Nucleus	1
L. Precentral Gyrus	4	L. Paracentral Lobule	1
R. Middle Temporal Pole	3	L. Precuneus	1
L. Middle Cingulate Gyrus	3	R. Superior Parietal Lobule	1
R. Superior Temporal Pole	2	R. Postcentral Gyrus	1
L. Thalamus	2	L. Postcentral Gyrus	1
R. Precuneus	2	L. Fusiform Gyrus	1
R. Fusiform	2	L. Superior Occipital Gyrus	1
R. Superior Occipital Gyrus	2	L. Lingual	1
R. Lingual	2	L. Cuneus	1
R. Cuneus	2	R. ParaHippocampal Gyrus	1
R. Calcarine Sulcus	2	R. Hippocampus	1
R. Anterior Cingulum	2	R. Middle Cingulate Gyrus	1
L. Anterior Cingulum	2	R. Medial Orbitofrontal Cortex	1
R. Insula	2	L. Olfactory Cortex	1
L. Inferior Frontal Gyrus/Pars Orbitalis	2	R. Supplementary Motor Area	1
L. Inferior Frontal Gyrus/Pars Triangularis	2	R. Rolandic Operculum	1
R. Precentral Gyrus	2	L. Rolandic Operculum	1
L. Middle Temporal Pole	1	R. Inferior Frontal Gyrus/Pars Orbitalis	1
R. Middle Temporal Gyrus	1	L. Inferior Frontal Operculum	1
L. Middle Temporal Gyrus	1	L. Middle Frontal Gyrus	1
R. Thalamus	1	R. Superior Frontal Gyrus	1
R. Putamen	1	L. Superior Frontal Gyrus	1
L. Putamen	1		

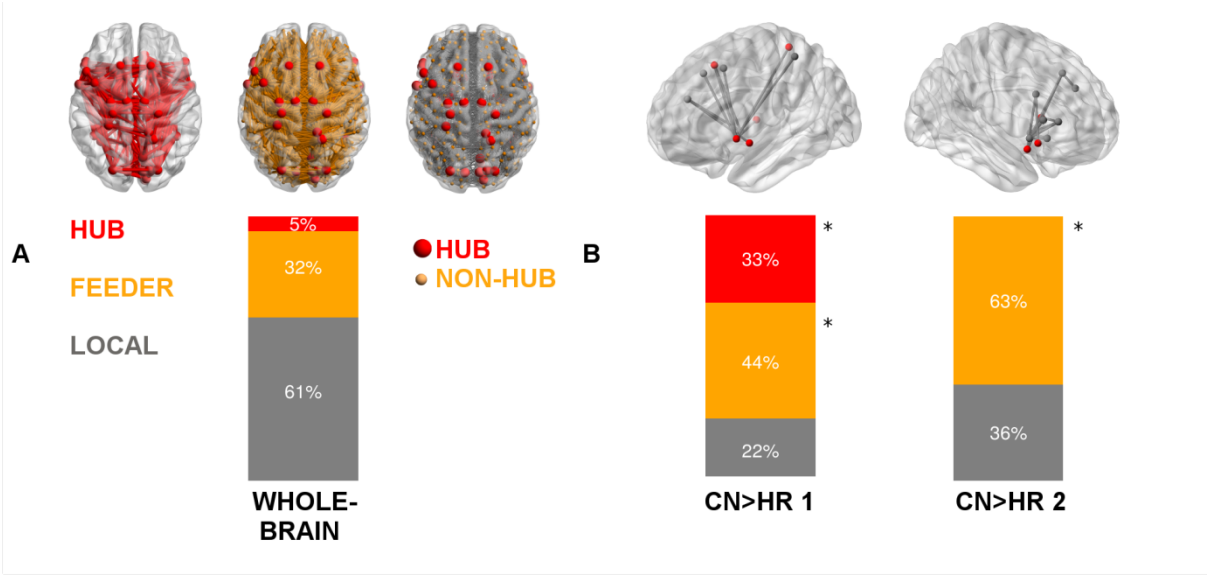

Figure A5-1: *Distribution of connection classes across the whole-brain and CN>HR NBS networks. (A) Proportion of hub (red, hub-to-hub), feeder (orange, hub-to-local), and local (gray, local-to-local) connections across the average CN connectome. Edges involving hub nodes (hub and feeder connections) comprise 5% and 32% of all edges across the network. (B) Proportion of corresponding classes within the first (left panel) and second (right) CN>HR networks. The panels show the significantly disproportionate amount of hub and feeder connections within the NBS networks, relative to the whole brain.*

* $p<0.05$, N=5000 permutations.

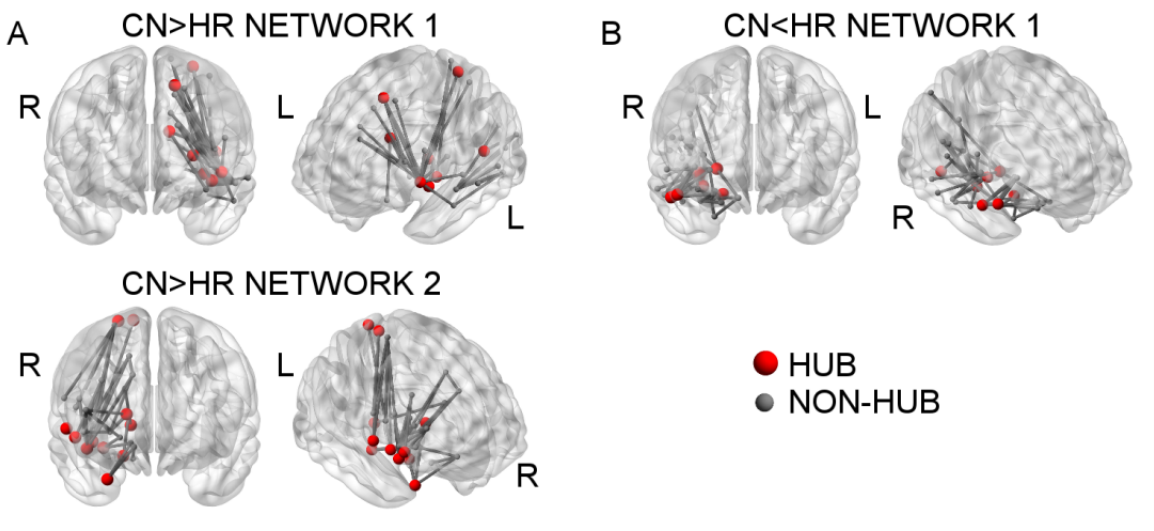

***Figure A5-2**: Significant NBS subnetworks (p<0.05, FWE-corrected) at a relatively liberal test threshold (t = 3.0), for contrasts reported within the main text. The first (A) and second (B) subnetworks to have stronger connectivity in the control group (CN) relative to high-risk subjects (HR). (C) HR>CON network. Brain views are presented from coronal (anterior) and customized angle views (azimuth = 135°, elevation = 10 for left-hemisphere views; azimuth = 225° for right-hemisphere).*

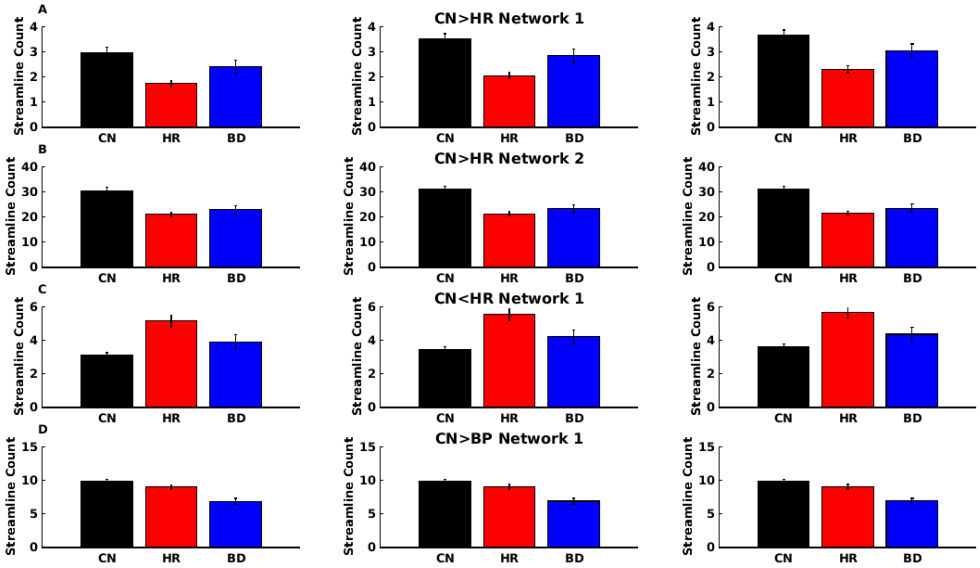

Figure A5-3*: Streamline count of NBS-derived subnetworks (t=3.3) across different sparsity levels of 7.5%, 10%, and 12.5%. Mean streamline counts calculated at network density levels of 7.5% (left panel), 10% (middle), and 12.5% (right). (A) and (B), The first and second CN>HR networks respectively. (C) HR>CN and (D) CN>BD networks. Error bars indicate standard error of mean.*

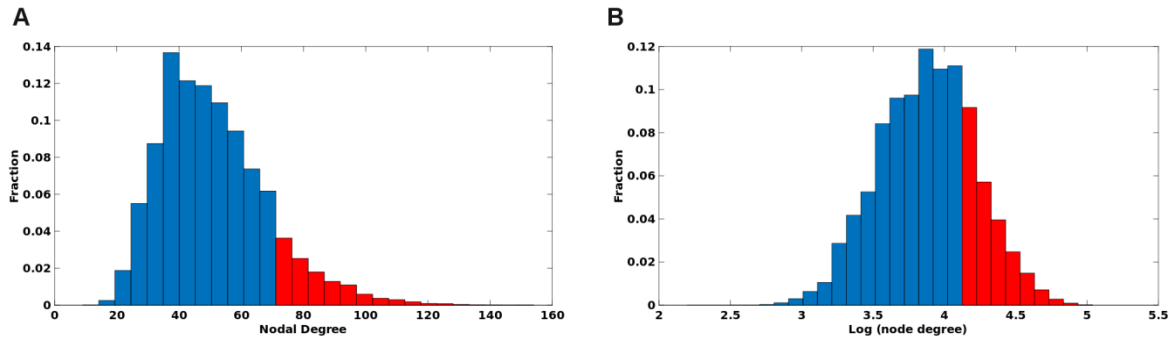

Figure A5-4: *Degree-distribution across brain regions. (A) Distribution of nodal-degree across all structural networks. Nodes classified as hubs based upon their top 15% degree-values correspond to degree of greater or equal to 64 (red bars), with their location on the curves heavy-tail. (B) Histogram of log (node degree) shows that degree is approximately log-normal distributed.*

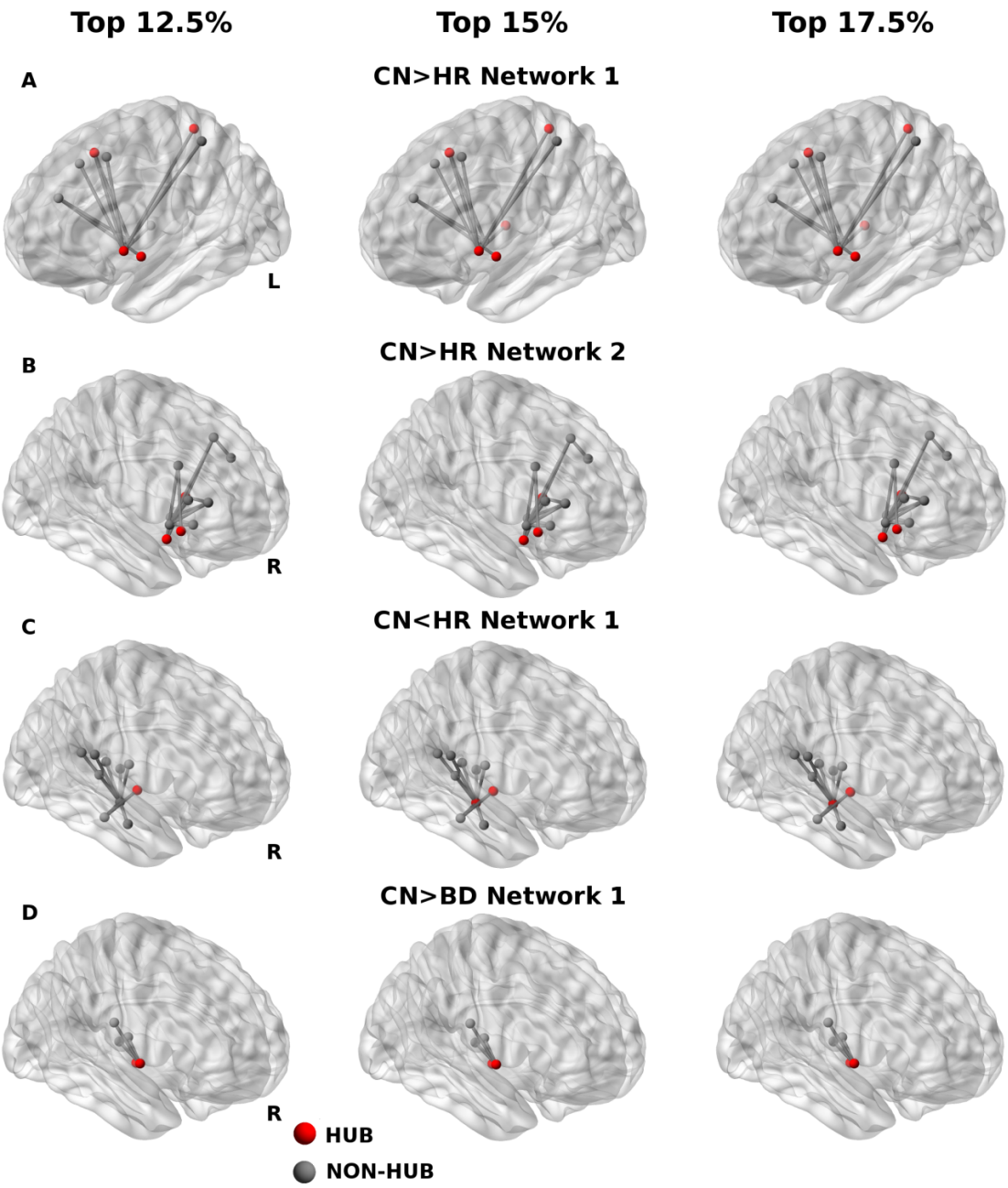

Figure A5-5*: Proportion of hub-regions within each of the four NBS-identified networks as a function of the hub-threshold. Left column, 12.5%; Middle column 15% (as presented in the main text); Right column, 17.5%. (A and B) The first and second subnetwork (bottom) of connections (lines) between nodes (circles) identified in the CN's to exhibit increased connectivity relative to HR subjects. (C) HR>CN and (D)*

CN>BD networks. Brain meshes are presented from customized angle views (azimuth = 135°, elevation = 10 for left-hemisphere views; azimuth = 225° for right-hemisphere)

References

Achard, S., Bullmore, E., 2007. Efficiency and Cost of Economical Brain Functional Networks. PLoS Comput Biol 3, e17.

Achard, S., Salvador, R., Whitcher, B., Suckling, J., Bullmore, E., 2006. A resilient, low-frequency, small-world human brain functional network with highly connected association cortical hubs. J Neurosci 26, 63-72.

Adler, C.M., Adams, J., DelBello, M.P., Holland, S.K., Schmithorst, V., Levine, A., Jarvis, K., Strakowski, S.M., 2006. Evidence of white matter pathology in bipolar disorder adolescents experiencing their first episode of mania: a diffusion tensor imaging study. The American journal of psychiatry 163, 322-324.

Aganj, I., Lenglet, C., Jahanshad, N., Yacoub, E., Harel, N., Thompson, P.M., Sapiro, G., 2011. A Hough transform global probabilistic approach to multiple-subject diffusion MRI tractography. Med Image Anal 15, 414-425.

Aiello, W., Chung, F., Lu, L., 2000. A random graph model for massive graphs. Proceedings of the thirty-second annual ACM symposium on Theory of computing. Acm, pp. 171-180.

Akiskal, H.S., Bourgeois, M.L., Angst, J., Post, R., Möller, H.-J., Hirschfeld, R., 2000. Re-evaluating the prevalence of and diagnostic composition within the broad clinical spectrum of bipolar disorders. Journal of Affective Disorders 59, Supplement 1, S5-S30.

Akiskal, H.S., Pinto, O., 1999. THE EVOLVING BIPOLAR SPECTRUM: Prototypes I, II, III, and IV. Psychiatric Clinics of North America 22, 517-534.

Albert, R., Albert, I., Nakarado, G.L., 2004. Structural vulnerability of the North American power grid. Physical Review E 69, 025103.

Alexander, G.E., Crutcher, M.D., 1990. Functional architecture of basal ganglia circuits: neural substrates of parallel processing. Trends in Neurosciences 13, 266-271.

Alstott, J., Breakspear, M., Hagmann, P., Cammoun, L., Sporns, O., 2009. Modeling the Impact of Lesions in the Human Brain. PLoS Comput Biol 5, e1000408.

Alvarez, J.A., Emory, E., 2006. Executive function and the frontal lobes: a meta-analytic review. Neuropsychology Review 16, 17-42.

American Psychiatric Association, 2013. Diagnostic and statistical manual of mental disorders (DSM-5®). American Psychiatric Pub.

Anderson, T.M., Sachdev, P.S., Brodaty, H., Trollor, J.N., Andrews, G., 2007. Effects of Sociodemographic and Health Variables on Mini-Mental State Exam Scores in Older Australians. The American Journal of Geriatric Psychiatry 15, 467-476.

Andersson, J.L., Sotiropoulos, S.N., 2016. An integrated approach to correction for off-resonance effects and subject movement in diffusion MR imaging. Neuroimage 125, 1063-1078.

Andrews-Hanna, J.R., Snyder, A.Z., Vincent, J.L., Lustig, C., Head, D., Raichle, M.E., Buckner, R.L., 2007. Disruption of Large-Scale Brain Systems in Advanced Aging. Neuron 56, 924-935.

Angst, J., Azorin, J., Bowden, C.L., et al., 2011. Prevalence and characteristics of undiagnosed bipolar disorders in patients with a major depressive episode: The bridge study. Archives of General Psychiatry 68, 791-799.

Antonenko, D., Brauer, J., Meinzer, M., Fengler, A., Kerti, L., Friederici, A.D., Floel, A., 2013. Functional and structural syntax networks in aging. Neuroimage 83, 513-523.
Arat, H.E., Chouinard, V.-A., Cohen, B.M., Lewandowski, K.E., Öngür, D., 2015. Diffusion Tensor Imaging in First Degree Relatives of Schizophrenia and Bipolar Disorder Patients. Schizophrenia research 161, 329-339.
Archer, J.A., Lee, A., Qiu, A., Chen, S.-H.A., 2015. A Comprehensive Analysis of Connectivity and Aging Over the Adult Life Span. Brain Connectivity.
Ashburner, J., 2007. A fast diffeomorphic image registration algorithm. Neuroimage 38, 95-113.
Ashburner, J., Friston, K.J., 2005. Unified segmentation. Neuroimage 26, 839-851.
Assaf, Y., Pasternak, O., 2008. Diffusion Tensor Imaging (DTI)-based White Matter Mapping in Brain Research: A Review. Journal of Molecular Neuroscience 34, 51-61.
Attwell, D., Laughlin, S.B., 2001. An Energy Budget for Signaling in the Grey Matter of the Brain. Journal of Cerebral Blood Flow & Metabolism 21, 1133-1145.
Baggio, H.C., Segura, B., Junque, C., de Reus, M.A., Sala-Llonch, R., Van den Heuvel, M.P., 2015. Rich Club Organization and Cognitive Performance in Healthy Older Participants. Journal of Cognitive Neuroscience, 1-10.
Bai, F., Shu, N., Yuan, Y., Shi, Y., Yu, H., Wu, D., Wang, J., Xia, M., He, Y., Zhang, Z., 2012. Topologically convergent and divergent structural connectivity patterns between patients with remitted geriatric depression and amnestic mild cognitive impairment. Journal of Neuroscience 32, 4307-4318.
Baker, J.T., Holmes, A.J., Masters, G.A., et al., 2014. DIsruption of cortical association networks in schizophrenia and psychotic bipolar disorder. JAMA Psychiatry 71, 109-118.
Baker, S.T.E., Lubman, D.I., Yücel, M., Allen, N.B., Whittle, S., Fulcher, B.D., Zalesky, A., Fornito, A., 2015. Developmental Changes in Brain Network Hub Connectivity in Late Adolescence. The Journal of Neuroscience 35, 9078-9087.
Balázs, J., Benazzi, F., Rihmer, Z., Rihmer, A., Akiskal, K.K., Akiskal, H.S., 2006. The close link between suicide attempts and mixed (bipolar) depression: Implications for suicide prevention. Journal of Affective Disorders 91, 133-138.
Ballard, C., Gauthier, S., Corbett, A., Brayne, C., Aarsland, D., Jones, E., 2011. Alzheimer's disease. The Lancet 377, 1019-1031.
Baltes, P.B., Lindenberger, U., 1997. Emergence of a powerful connection between sensory and cognitive functions across the adult life span: A new window to the study of cognitive aging? Psychology and Aging 12, 12-21.
Barabási, A.-L., Albert, R., 1999. Emergence of Scaling in Random Networks. Science 286, 509-512.
Barrett, L.F., Quigley, K.S., Hamilton, P., 2016. An active inference theory of allostasis and interoception in depression. Philosophical Transactions of the Royal Society B: Biological Sciences 371.
Bartrés-Faz, D., Arenaza-Urquijo, E.M., 2011. Structural and Functional Imaging Correlates of Cognitive and Brain Reserve Hypotheses in Healthy and Pathological Aging. Brain Topography 24, 340-357.
Bartzokis, G., 2004. Age-related myelin breakdown: a developmental model of cognitive decline and Alzheimer's disease. Neurobiol Aging 25, 5-18; author reply 49-62.

Basser, P.J., 1995. Inferring microstructural features and the physiological state of tissues from diffusion-weighted images. NMR in Biomedicine 8, 333-344.
Basser, P.J., Mattiello, J., LeBihan, D., 1994. MR diffusion tensor spectroscopy and imaging. Biophysical Journal 66, 259-267.
Bassett, D.S., Bullmore, E., 2006. Small-world brain networks. The Neuroscientist 12, 512-523.
Bassett, D.S., Bullmore, E., Verchinski, B.A., Mattay, V.S., Weinberger, D.R., Meyer-Lindenberg, A., 2008. Hierarchical organization of human cortical networks in health and schizophrenia. Journal of Neuroscience 28, 9239-9248.
Bassett, D.S., Wymbs, N.F., Porter, M.A., Mucha, P.J., Carlson, J.M., Grafton, S.T., 2011. Dynamic reconfiguration of human brain networks during learning. Proceedings of the National Academy of Sciences 108, 7641-7646.
Bassi, L., Ricci, D., Volzone, A., Allsop, J.M., Srinivasan, L., Pai, A., Ribes, C., Ramenghi, L.A., Mercuri, E., Mosca, F., Edwards, A.D., Cowan, F.M., Rutherford, M.A., Counsell, S.J., 2008. Probabilistic diffusion tractography of the optic radiations and visual function in preterm infants at term equivalent age. Brain 131, 573-582.
Basten, U., Biele, G., Heekeren, H.R., Fiebach, C.J., 2010. How the brain integrates costs and benefits during decision making. Proceedings of the National Academy of Sciences 107, 21767-21772.
Bastiani, M., Roebroeck, A., 2015. Unraveling the multiscale structural organization and connectivity of the human brain: the role of diffusion MRI. Frontiers in Neuroanatomy 9.
Bechara, A., Damasio, H., Damasio, A.R., 2000. Emotion, Decision Making and the Orbitofrontal Cortex. Cerebral Cortex 10, 295-307.
Beckmann, C.F., DeLuca, M., Devlin, J.T., Smith, S.M., 2005. Investigations into resting-state connectivity using independent component analysis. Philosophical Transactions of the Royal Society B: Biological Sciences 360, 1001-1013.
Behrens, T., Berg, H.J., Jbabdi, S., Rushworth, M., Woolrich, M., 2007. Probabilistic diffusion tractography with multiple fibre orientations: What can we gain? Neuroimage 34, 144-155.
Behrens, T.E.J., Woolrich, M.W., Jenkinson, M., Johansen-Berg, H., Nunes, R.G., Clare, S., Matthews, P.M., Brady, J.M., Smith, S.M., 2003. Characterization and propagation of uncertainty in diffusion-weighted MR imaging. Magnetic Resonance in Medicine 50, 1077-1088.
Belleville, S., Fouquet, C., Duchesne, S., Collins, D.L., Hudon, C., 2014. Detecting Early Preclinical Alzheimer's Disease via Cognition, Neuropsychiatry, and Neuroimaging: Qualitative Review and Recommendations for Testing. Journal of Alzheimer's Disease 42, S375-S382.
Belliveau, J.W., Kennedy, D.N., Jr., McKinstry, R.C., Buchbinder, B.R., Weisskoff, R.M., Cohen, M.S., Vevea, J.M., Brady, T.J., Rosen, B.R., 1991. Functional mapping of the human visual cortex by magnetic resonance imaging. Science 254, 716-719.
Benjamini, Y., Hochberg, Y., 1995. Controlling the false discovery rate: a practical and powerful approach to multiple testing. Journal of the Royal Statistical Society. Series B (Methodological), 289-300.
Bennett, I.J., Madden, D.J., 2014. Disconnected aging: Cerebral white matter integrity and age-related differences in cognition. Neuroscience 276, 187-205.

Benton, A.L., Sivan, A.B., Spreen, O., 1996. Der Benton Test, 7th ed. Huber, Bern.
Bergerbest, D., Gabrieli, J.D., Whitfield-Gabrieli, S., Kim, H., Stebbins, G.T., Bennett, D.A., Fleischman, D.A., 2009. Age-associated reduction of asymmetry in prefrontal function and preservation of conceptual repetition priming. Neuroimage 45, 237-246.
Betzel, R.F., Byrge, L., He, Y., Goñi, J., Zuo, X.-N., Sporns, O., 2014. Changes in structural and functional connectivity among resting-state networks across the human lifespan. Neuroimage 102, Part 2, 345-357.
Betzel, R.F., Griffa, A., Avena-Koenigsberger, A., GoÑI, J., Thiran, J.-P., Hagmann, P., Sporns, O., 2013. Multi-scale community organization of the human structural connectome and its relationship with resting-state functional connectivity. Network Science 1, 353-373.
Beyer, J.L., Taylor, W.D., MacFall, J.R., Kuchibhatla, M., Payne, M.E., Provenzale, J.M., Cassidy, F., Krishnan, K.R., 2005. Cortical white matter microstructural abnormalities in bipolar disorder. Neuropsychopharmacology 30, 2225-2229.
Bianciardi, M., Fukunaga, M., van Gelderen, P., Horovitz, S.G., de Zwart, J.A., Shmueli, K., Duyn, J.H., 2009. Sources of functional magnetic resonance imaging signal fluctuations in the human brain at rest: a 7 T study. Magnetic resonance imaging 27, 1019-1029.
Birmaher B, Axelson D, Monk K, Kalas C, Goldstein B, Hickey M B, Obreja, M., Ehmann, M., Iyengar, S., Shamseddeen, W., Kupfer, D., Brent, D., 2009. Lifetime psychiatric disorders in school-aged offspring of parents with bipolar disorder: the Pittsburgh Bipolar Offspring study. Archives of General Psychiatry 66, 287-296.
Birn, R.M., Smith, M.A., Jones, T.B., Bandettini, P.A., 2008. The Respiration Response Function: The temporal dynamics of fMRI signal fluctuations related to changes in respiration. Neuroimage 40, 644-654.
Biswal, B., Zerrin Yetkin, F., Haughton, V.M., Hyde, J.S., 1995. Functional connectivity in the motor cortex of resting human brain using echo-planar mri. Magnetic Resonance in Medicine 34, 537-541.
Biswal, B.B., Van Kylen, J., Hyde, J.S., 1997. Simultaneous assessment of flow and BOLD signals in resting-state functional connectivity maps. NMR in Biomedicine 10, 165-170.
Blennow, K., de Leon, M.J., Zetterberg, H., 2006. Alzheimer's disease. Lancet 368, 387-403.
Blondel, V.D., Guillaume, J.L., Lambiotte, R., Lefebvre, E., 2008. Fast unfolding of communities in large networks. Journal of Statistical Mechanics-Theory and Experiment 2008, P10008.
Bondi, M.W., Edmonds, E.C., Jak, A.J., Clark, L.R., Delano-Wood, L., McDonald, C.R., Nation, D.A., Libon, D.J., Au, R., Galasko, D., Salmon, D.P., 2014. Neuropsychological Criteria for Mild Cognitive Impairment Improves Diagnostic Precision, Biomarker Associations, and Progression Rates. Journal of Alzheimer's disease : JAD 42, 275-289.
Borghesani, P.R., Madhyastha, T.M., Aylward, E.H., Reiter, M.A., Swarny, B.R., Warner Schaie, K., Willis, S.L., 2013. The association between higher order abilities, processing speed, and age are variably mediated by white matter integrity during typical aging. Neuropsychologia 51, 1435-1444.

Bosch, B., Bartrés-Faz, D., Rami, L., Arenaza-Urquijo, E.M., Fernández-Espejo, D., Junqué, C., Solé-Padullés, C., Sánchez-Valle, R., Bargalló, N., Falcón, C., Molinuevo, J.L., 2010. Cognitive reserve modulates task-induced activations and deactivations in healthy elders, amnestic mild cognitive impairment and mild Alzheimer's disease. Cortex 46, 451-461.
Bouchard, K.E., Mesgarani, N., Johnson, K., Chang, E.F., 2013. Functional organization of human sensorimotor cortex for speech articulation. Nature 495, 327-332.
Bozzali, M., Dowling, C., Serra, L., Spano, B., Torso, M., Marra, C., Castelli, D., Dowell, N.G., Koch, G., Caltagirone, C., Cercignani, M., 2015. The impact of cognitive reserve on brain functional connectivity in Alzheimer's disease. J Alzheimers Dis 44, 243-250.
Braga, R.M., Sharp, D.J., Leeson, C., Wise, R.J.S., Leech, R., 2013. Echoes of the Brain within Default Mode, Association, and Heteromodal Cortices. The Journal of Neuroscience 33, 14031-14039.
Braun, U., Schäfer, A., Walter, H., Erk, S., Romanczuk-Seiferth, N., Haddad, L., Schweiger, J.I., Grimm, O., Heinz, A., Tost, H., Meyer-Lindenberg, A., Bassett, D.S., 2015. Dynamic reconfiguration of frontal brain networks during executive cognition in humans. Proceedings of the National Academy of Sciences 112, 11678-11683.
Breakspear, M., Roberts, G., Green, M.J., Nguyen, V.T., Frankland, A., Levy, F., Lenroot, R., Mitchell, P.B., 2015a. Network dysfunction of emotional and cognitive processes in those at genetic risk of bipolar disorder. Brain.
Breakspear, M., Roberts, G., Green, M.J., Nguyen, V.T., Frankland, A., Levy, F., Lenroot, R., Mitchell, P.B., 2015b. Network dysfunction of emotional and cognitive processes in those at genetic risk of bipolar disorder. Brain, awv261.
Brickman, A.M., Meier, I.B., Korgaonkar, M.S., Provenzano, F.A., Grieve, S.M., Siedlecki, K.L., Wasserman, B.T., Williams, L.M., Zimmerman, M.E., 2012. Testing the white matter retrogenesis hypothesis of cognitive aging. Neurobiol Aging 33, 1699-1715.
Bright, P., Jaldow, E., Kopelman, M.D., 2002. The National Adult Reading Test as a measure of premorbid intelligence: A comparison with estimates derived from demographic variables. Journal of the International Neuropsychological Society 8, 847-854.
Brotman, M.A., Deveney, C.M., Thomas, L.A., Hinton, K.E., Yi, J.Y., Pine, D.S., Leibenluft, E., 2014. Parametric modulation of neural activity during face emotion processing in unaffected youth at familial risk for bipolar disorder. Bipolar Disorders 16, 756-763.
Brown, S., Laird, A.R., Pfordresher, P.Q., Thelen, S.M., Turkeltaub, P., Liotti, M., 2009. The somatotopy of speech: Phonation and articulation in the human motor cortex. Brain and Cognition 70, 31-41.
Bruno, S., Cercignani, M., Ron, M.A., 2008. White matter abnormalities in bipolar disorder: a voxel-based diffusion tensor imaging study. Bipolar Disorders 10, 460-468.
Buckner, R.L., Andrews-Hanna, J.R., Schacter, D.L., 2008. The Brain's Default Network. Annals of the New York Academy of Sciences 1124, 1-38.
Buckner, R.L., Sepulcre, J., Talukdar, T., Krienen, F.M., Liu, H., Hedden, T., Andrews-Hanna, J.R., Sperling, R.A., Johnson, K.A., 2009. Cortical Hubs Revealed by Intrinsic

Functional Connectivity: Mapping, Assessment of Stability, and Relation to Alzheimer's Disease. The Journal of Neuroscience 29, 1860-1873.
Bullmore, E., Sporns, O., 2009. Complex brain networks: graph theoretical analysis of structural and functional systems. Nat Rev Neurosci 10, 186-198.
Bullmore, E., Sporns, O., 2012. The economy of brain network organization. Nat Rev Neurosci 13, 336-349.
Bürgel, U., Schormann, T., Schleicher, A., Zilles, K., 1999. Mapping of Histologically Identified Long Fiber Tracts in Human Cerebral Hemispheres to the MRI Volume of a Reference Brain: Position and Spatial Variability of the Optic Radiation. Neuroimage 10, 489-499.
Burns, G.A.P.C., Young, M.P., 2000. Analysis of the connectional organization of neural systems associated with the hippocampus in rats. Philosophical Transactions of the Royal Society of London B: Biological Sciences 355, 55-70.
Cabeza, R., Anderson, N.D., Locantore, J.K., McIntosh, A.R., 2002. Aging gracefully: compensatory brain activity in high-performing older adults. Neuroimage 17, 1394-1402.
Cabeza, R., Dennis, N.A., 2012. Frontal lobes and aging. Principles of frontal lobes function, 628-652.
Caeyenberghs, K., Leemans, A., 2014. Hemispheric lateralization of topological organization in structural brain networks. Hum Brain Mapp 35, 4944-4957.
Cai, W., Ryali, S., Chen, T., Li, C.-S.R., Menon, V., 2014. Dissociable Roles of Right Inferior Frontal Cortex and Anterior Insula in Inhibitory Control: Evidence from Intrinsic and Task-Related Functional Parcellation, Connectivity, and Response Profile Analyses across Multiple Datasets. The Journal of Neuroscience 34, 14652-14667.
Calamante, F., Smith, R.E., Tournier, J.-D., Raffelt, D., Connelly, A., 2015. Quantification of voxel-wise total fibre density: Investigating the problems associated with track-count mapping. Neuroimage 117, 284-293.
Calhoun, Vince D., Miller, R., Pearlson, G., Adalı, T., 2014. The Chronnectome: Time-Varying Connectivity Networks as the Next Frontier in fMRI Data Discovery. Neuron 84, 262-274.
Campbell, K.L., Grady, C.L., Ng, C., Hasher, L., 2012. Age differences in the frontoparietal cognitive control network: Implications for distractibility. Neuropsychologia 50, 2212-2223.
Cao, M., Wang, J.H., Dai, Z.J., Cao, X.Y., Jiang, L.L., Fan, F.M., Song, X.W., Xia, M.R., Shu, N., Dong, Q., Milham, M.P., Castellanos, F.X., Zuo, X.N., He, Y., 2014. Topological organization of the human brain functional connectome across the lifespan. Dev Cogn Neurosci 7, 76-93.
Cao, Q., Shu, N., An, L., Wang, P., Sun, L., Xia, M.-R., Wang, J.-H., Gong, G.-L., Zang, Y.-F., Wang, Y.-F., 2013. Probabilistic diffusion tractography and graph theory analysis reveal abnormal white matter structural connectivity networks in drug-naive boys with attention deficit/hyperactivity disorder. Journal of Neuroscience 33, 10676-10687.
Cardno, A.G., Owen, M.J., 2014. Genetic Relationships Between Schizophrenia, Bipolar Disorder, and Schizoaffective Disorder. Schizophrenia Bulletin 40, 504-515.

Caseras, X., Tansey, K.E., Foley, S., Linden, D., 2015. Association between genetic risk scoring for schizophrenia and bipolar disorder with regional subcortical volumes. Transl Psychiatry 5, e692.
Casey, B.J., Jones, R.M., Levita, L., Libby, V., Pattwell, S., Ruberry, E., Soliman, F., Somerville, L.H., 2010. The Storm and Stress of Adolescence: Insights from Human Imaging and Mouse Genetics. Developmental psychobiology 52, 225-235.
Catani, M., 2005. The rises and falls of disconnection syndromes. Brain 128, 2224-2239.
Catani, M., Dell'Acqua, F., Vergani, F., Malik, F., Hodge, H., Roy, P., Valabregue, R., Thiebaut de Schotten, M., 2012. Short frontal lobe connections of the human brain. Cortex 48, 273-291.
Catani, M., Jones, D.K., ffytche, D.H., 2005. Perisylvian language networks of the human brain. Annals of Neurology 57, 8-16.
Cauda, F., Costa, T., Torta, D.M.E., Sacco, K., D'Agata, F., Duca, S., Geminiani, G., Fox, P.T., Vercelli, A., 2012. Meta-analytic clustering of the insular cortex: Characterizing the meta-analytic connectivity of the insula when involved in active tasks. Neuroimage 62, 343-355.
Chaddock, C.A., Barker, G.J., Marshall, N., Schulze, K., Hall, M.H., Fern, A., Walshe, M., Bramon, E., Chitnis, X.A., Murray, R., 2009. White matter microstructural impairments and genetic liability to familial bipolar I disorder. British Journal of Psychiatry 194, 527-534.
Chan, M.Y., Park, D.C., Savalia, N.K., Petersen, S.E., Wig, G.S., 2014. Decreased segregation of brain systems across the healthy adult lifespan. Proceedings of the National Academy of Sciences 111, E4997-E5006.
Chang, C., Cunningham, J.P., Glover, G.H., 2009. Influence of heart rate on the BOLD signal: the cardiac response function. Neuroimage 44, 857-869.
Chang, C., Glover, G.H., 2010. Time–frequency dynamics of resting-state brain connectivity measured with fMRI. Neuroimage 50, 81-98.
Chang, L.J., Yarkoni, T., Khaw, M.W., Sanfey, A.G., 2012. Decoding the Role of the Insula in Human Cognition: Functional Parcellation and Large-Scale Reverse Inference. Cerebral Cortex.
Chase, H.W., Phillips, M.L., 2016. Elucidating neural network functional connectivity abnormalities in bipolar disorder: toward a harmonized methodological approach. Biological Psychiatry: Cognitive Neuroscience and Neuroimaging 1, 288-298.
Chen, C.H., Suckling, J., Lennox, B.R., Ooi, C., Bullmore, E.T., 2011. A quantitative meta-analysis of fMRI studies in bipolar disorder. Bipolar Disorders 13, 1-15.
Chen, Y.-W., Dilsaver, S.C., Lifetime rates of suicide attempts among subjects with bipolar and unipolar disorders relative to subjects with other axis I disorders. Biological Psychiatry 39, 896-899.
Chenevert, T.L., Brunberg, J.A., Pipe, J.G., 1990. Anisotropic diffusion in human white matter: demonstration with MR techniques in vivo. Radiology 177, 401-405.
Chengappa, K.N.R., Kupfer, D.J., Frank, E., Houck, P.R., Grochocinski, V.J., Cluss, P.A., Stapf, D.A., 2003. Relationship of Birth Cohort and Early Age at Onset of Illness in a Bipolar Disorder Case Registry. American Journal of Psychiatry 160, 1636-1642.
Chiang, M.-C., Barysheva, M., McMahon, K.L., de Zubicaray, G.I., Johnson, K., Montgomery, G.W., Martin, N.G., Toga, A.W., Wright, M.J., Shapshak, P., 2012. Gene

network effects on brain microstructure and intellectual performance identified in 472 twins. Journal of Neuroscience 32, 8732-8745.
Clay, H., Sillivan, S., Konradi, C., 2011. Mitochondrial Dysfunction and Pathology in Bipolar Disorder and Schizophrenia. International journal of developmental neuroscience : the official journal of the International Society for Developmental Neuroscience 29, 311-324.
Cocchi, L., Harding, I.H., Lord, A., Pantelis, C., Yucel, M., Zalesky, A., 2014. Disruption of structure–function coupling in the schizophrenia connectome. NeuroImage: Clinical 4, 779-787.
Cocchi, L., Zalesky, A., Fornito, A., Mattingley, J.B., 2013. Dynamic cooperation and competition between brain systems during cognitive control. Trends Cogn Sci 17, 493-501.
Coffman, J.A., Bornstein, R.A., Olson, S.C., Schwarzkopf, S.B., Nasrallah, H.A., 1990. Cognitive impairment and cerebral structure by MRI in bipolar disorder. Biological Psychiatry 27, 1188-1196.
Cole, M.W., Schneider, W., 2007. The cognitive control network: Integrated cortical regions with dissociable functions. Neuroimage 37, 343-360.
Colizza, V., Flammini, A., Serrano, M.A., Vespignani, A., 2006. Detecting rich-club ordering in complex networks. Nature physics 2, 110-115.
Collin, G., Kahn, R.S., de Reus, M.A., Cahn, W., van den Heuvel, M.P., 2014a. Impaired Rich Club Connectivity in Unaffected Siblings of Schizophrenia Patients. Schizophrenia Bulletin 40, 438-448.
Collin, G., Sporns, O., Mandl, R.C., van den Heuvel, M.P., 2014b. Structural and functional aspects relating to cost and benefit of rich club organization in the human cerebral cortex. Cereb Cortex 24, 2258-2267.
Collin, G., van den Heuvel, M.P., Abramovic, L., Vreeker, A., de Reus, M.A., van Haren, N.E., Boks, M.P., Ophoff, R.A., Kahn, R.S., 2015. Brain network analysis reveals affected connectome structure in bipolar disorder. Human Brain Mapping 37, 122-134.
Cordes, D., Haughton, V.M., Arfanakis, K., Carew, J.D., Turski, P.A., Moritz, C.H., Quigley, M.A., Meyerand, M.E., 2001. Frequencies contributing to functional connectivity in the cerebral cortex in "resting-state" data. AJNR Am J Neuroradiol 22, 1326-1333.
Cordes, D., Haughton, V.M., Arfanakis, K., Wendt, G.J., Turski, P.A., Moritz, C.H., Quigley, M.A., Meyerand, M.E., 2000. Mapping functionally related regions of brain with functional connectivity MR imaging. AJNR Am J Neuroradiol 21, 1636-1644.
Cox, R.W., 1996. AFNI: software for analysis and visualization of functional magnetic resonance neuroimages. Computers and Biomedical research 29, 162-173.
Craig, A.D., 2003. Interoception: the sense of the physiological condition of the body. Current Opinion in Neurobiology 13, 500-505.
Craig, A.D., 2009. How do you feel--now? The anterior insula and human awareness. Nat Rev Neurosci 10, 59-70.
Critchley, H.D., Wiens, S., Rotshtein, P., Ohman, A., Dolan, R.J., 2004. Neural systems supporting interoceptive awareness. Nat Neurosci 7, 189-195.

Crossley, N.A., Mechelli, A., Scott, J., Carletti, F., Fox, P.T., McGuire, P., Bullmore, E.T., 2014. The hubs of the human connectome are generally implicated in the anatomy of brain disorders. Brain 137, 2382-2395.
Crossley, N.A., Mechelli, A., Vértes, P.E., Winton-Brown, T.T., Patel, A.X., Ginestet, C.E., McGuire, P., Bullmore, E.T., 2013. Cognitive relevance of the community structure of the human brain functional coactivation network. Proceedings of the National Academy of Sciences 110, 11583-11588.
Dai, Z., Yan, C., Li, K., Wang, Z., Wang, J., Cao, M., Lin, Q., Shu, N., Xia, M., Bi, Y., He, Y., 2014. Identifying and Mapping Connectivity Patterns of Brain Network Hubs in Alzheimer's Disease. Cerebral Cortex.
Daianu, M., Jahanshad, N., Nir, T.M., Jack, C.R., Weiner, M.W., Bernstein, M.A., Thompson, P.M., the Alzheimer's Disease Neuroimaging, I., 2015. Rich club analysis in the Alzheimer's disease connectome reveals a relatively undisturbed structural core network. Human Brain Mapping, n/a-n/a.
Damoiseaux, J.S., 2012. Resting-state fMRI as a biomarker for Alzheimer's disease? Alzheimer's Research & Therapy 4, 8-8.
Damoiseaux, J.S., Beckmann, C.F., Arigita, E.J.S., Barkhof, F., Scheltens, P., Stam, C.J., Smith, S.M., Rombouts, S.A.R.B., 2008. Reduced resting-state brain activity in the "default network" in normal aging. Cerebral Cortex 18, 1856-1864.
Damoiseaux, J.S., Rombouts, S.A.R.B., Barkhof, F., Scheltens, P., Stam, C.J., Smith, S.M., Beckmann, C.F., 2006. Consistent resting-state networks across healthy subjects. Proceedings of the National Academy of Sciences 103, 13848-13853.
Davis, S.W., Kragel, J.E., Madden, D.J., Cabeza, R., 2012. The architecture of cross-hemispheric communication in the aging brain: linking behavior to functional and structural connectivity. Cereb Cortex 22, 232-242.
De Fruyt, J., Deschepper, E., Audenaert, K., Constant, E., Floris, M., Pitchot, W., Sienaert, P., Souery, D., Claes, S., 2012. Second generation antipsychotics in the treatment of bipolar depression: a systematic review and meta-analysis. J Psychopharmacol 26, 603-617.
de Pasquale, F., Penna, S.D., Sporns, O., Romani, G.L., Corbetta, M., 2015. A Dynamic Core Network and Global Efficiency in the Resting Human Brain. Cerebral Cortex.
de Reus, M.A., Saenger, V.M., Kahn, R.S., van den Heuvel, M.P., 2014. An edge-centric perspective on the human connectome: link communities in the brain. Philosophical Transactions of the Royal Society B: Biological Sciences 369.
de Reus, M.A., van den Heuvel, M.P., 2013. Rich club organization and intermodule communication in the cat connectome. The Journal of Neuroscience 33, 12929-12939.
de Reus, M.A., van den Heuvel, M.P., 2014. Simulated rich club lesioning in brain networks: a scaffold for communication and integration? Frontiers in Human Neuroscience 8.
Deary, I.J., Corley, J., Gow, A.J., Harris, S.E., Houlihan, L.M., Marioni, R.E., Penke, L., Rafnsson, S.B., Starr, J.M., 2009. Age-associated cognitive decline. British Medical Bulletin 92, 135-152.
Deco, G., Jirsa, V.K., 2012. Ongoing Cortical Activity at Rest: Criticality, Multistability, and Ghost Attractors. The Journal of Neuroscience 32, 3366-3375.
Deco, G., Jirsa, V.K., McIntosh, A.R., 2013. Resting brains never rest: computational insights into potential cognitive architectures. Trends in Neurosciences 36, 268-274.

Dehaene, S., Kerszberg, M., Changeux, J.-P., 1998. A neuronal model of a global workspace in effortful cognitive tasks. Proceedings of the National Academy of Sciences 95, 14529-14534.
Dehaene, S., Naccache, L., 2001. Towards a cognitive neuroscience of consciousness: basic evidence and a workspace framework. Cognition 79, 1-37.
DelBello, M.P., Geller, B., 2001. Review of studies of child and adolescent offspring of bipolar parents. Bipolar Disorders 3, 325-334.
Delbeuck, X., Van der Linden, M., Collette, F., 2003. Alzheimer' Disease as a Disconnection Syndrome? Neuropsychology Review 13, 79-92.
Dell'acqua, F., Scifo, P., Rizzo, G., Catani, M., Simmons, A., Scotti, G., Fazio, F., 2010. A modified damped Richardson-Lucy algorithm to reduce isotropic background effects in spherical deconvolution. Neuroimage 49, 1446-1458.
Dennis, E.L., Jahanshad, N., McMahon, K.L., de Zubicaray, G.I., Martin, N.G., Hickie, I.B., Toga, A.W., Wright, M.J., Thompson, P.M., 2013. Development of brain structural connectivity between ages 12 and 30: a 4-Tesla diffusion imaging study in 439 adolescents and adults. Neuroimage 64, 671-684.
Dennis, E.L., Thompson, P.M., 2014. Functional Brain Connectivity Using fMRI in Aging and Alzheimer's Disease. Neuropsychology Review 24, 49-62.
Dennis, N., Cabeza, R.C., 2008. Neuroimaging of Healthy Cognitive Aging. In: Craik, F.I.M., Salthouse, T.A. (Eds.), The Handbook of Aging and Cognition. Psychology Press, New York, New York, pp. 1-54.
Descoteaux, M., Angelino, E., Fitzgibbons, S., Deriche, R., 2007. Regularized, fast, and robust analytical Q-ball imaging. Magnetic Resonance in Medicine 58, 497-510.
Descoteaux, M., Deriche, R., Knosche, T.R., Anwander, A., 2009. Deterministic and Probabilistic Tractography Based on Complex Fibre Orientation Distributions. IEEE Transactions on Medical Imaging 28, 269-286.
Douaud, G., Groves, A.R., Tamnes, C.K., Westlye, L.T., Duff, E.P., Engvig, A., Walhovd, K.B., James, A., Gass, A., Monsch, A.U., Matthews, P.M., Fjell, A.M., Smith, S.M., Johansen-Berg, H., 2014. A common brain network links development, aging, and vulnerability to disease. Proceedings of the National Academy of Sciences 111, 17648-17653.
Duara, R., Grady, C., Haxby, J., Sundaram, M., Cutler, N.R., Heston, L., Moore, A., Schlageter, N., Larson, S., Rapoport, S.I., 1986. Positron emission tomography in Alzheimer's disease. Neurology 36, 879-887.
Duarte-Carvajalino, J.M., Jahanshad, N., Lenglet, C., McMahon, K.L., de Zubicaray, G.I., Martin, N.G., Wright, M.J., Thompson, P.M., Sapiro, G., 2012. Hierarchical topological network analysis of anatomical human brain connectivity and differences related to sex and kinship. Neuroimage 59, 3784-3804.
Dwyer, D.B., Harrison, B.J., Yücel, M., Whittle, S., Zalesky, A., Pantelis, C., Allen, N.B., Fornito, A., 2014. Large-Scale Brain Network Dynamics Supporting Adolescent Cognitive Control. The Journal of Neuroscience 34, 14096-14107.
Edison, P., Archer, H.A., Hinz, R., Hammers, A., Pavese, N., Tai, Y.F., Hotton, G., Cutler, D., Fox, N., Kennedy, A., Rossor, M., Brooks, D.J., 2007. Amyloid, hypometabolism, and cognition in Alzheimer disease: An [11C]PIB and [18F]FDG PET study. Neurology 68, 501-508.

Elton, A., Gao, W., 2014. Divergent task-dependent functional connectivity of executive control and salience networks. Cortex 51, 56-66.
Emsell, L., Chaddock, C., Forde, N., Van Hecke, W., Barker, G., Leemans, A., Sunaert, S., Walshe, M., Bramon, E., Cannon, D., 2014. White matter microstructural abnormalities in families multiply affected with bipolar I disorder: a diffusion tensor tractography study. Psychological Medicine 44, 2139-2150.
Estrada, E., Hatano, N., 2008. Communicability in complex networks. Physical Review E 77, 036111.
Estrada, E., Rodríguez-Velázquez, J.A., 2005. Subgraph centrality in complex networks. Physical Review E 71, 056103.
Faloutsos, M., Faloutsos, P., Faloutsos, C., 1999. On power-law relationships of the Internet topology. SIGCOMM Comput. Commun. Rev. 29, 251-262.
Farquharson, S., Tournier, J.-D., Calamante, F., Fabinyi, G., Schneider-Kolsky, M., Jackson, G., Connelly, A., 2013. White matter fiber tractography: why we need to move beyond DTI. Journal of Neurosurgery 118, 1367-1377.
Farrer, L.A., Cupples, L.A., Haines, J.L., Hyman, B., Kukull, W.A., Mayeux, R., Myers, R.H., Pericak-Vance, M.A., Risch, N., van Duijn, C.M., 1997. Effects of age, sex, and ethnicity on the association between apolipoprotein E genotype and Alzheimer disease. A meta-analysis. APOE and Alzheimer Disease Meta Analysis Consortium. Jama 278, 1349-1356.
Feis, D.-L., Brodersen, K.H., von Cramon, D.Y., Luders, E., Tittgemeyer, M., 2013. Decoding gender dimorphism of the human brain using multimodal anatomical and diffusion MRI data. Neuroimage 70, 250-257.
Felleman, D.J., Van Essen, D.C., 1991. Distributed Hierarchical Processing in the Primate Cerebral Cortex. Cerebral Cortex 1, 1-47.
Finkel, D., Reynolds, C.A., McArdle, J.J., Pedersen, N.L., 2007. Age changes in processing speed as a leading indicator of cognitive aging. Psychology and Aging 22, 558-568.
Fischer, P., Jungwirth, S., Zehetmayer, S., Weissgram, S., Hoenigschnabl, S., Gelpi, E., Krampla, W., Tragl, K.H., 2007. Conversion from subtypes of mild cognitive impairment to Alzheimer dementia. Neurology 68, 288-291.
Fisher, G.G., Stachowski, A., Infurna, F.J., Faul, J.D., Grosch, J., Tetrick, L.E., 2014. Mental work demands, retirement, and longitudinal trajectories of cognitive functioning. Journal of occupational health psychology 19, 231.
Fjell, A.M., Sneve, M.H., Grydeland, H., Storsve, A.B., de Lange, A.-M.G., Amlien, I.K., Røgeberg, O.J., Walhovd, K.B., 2015. Functional connectivity change across multiple cortical networks relates to episodic memory changes in aging. Neurobiology of Aging 36, 3255-3268.
Fjell, A.M., Westlye, L.T., Grydeland, H., Amlien, I., Espeseth, T., Reinvang, I., Raz, N., Dale, A.M., Walhovd, K.B., 2012. Accelerating Cortical Thinning: Unique to Dementia or Universal in Aging? Cerebral Cortex.
Foland-Ross, L.C., Bookheimer, S.Y., Lieberman, M.D., Sugar, C.A., Townsend, J.D., Fischer, J., Torrisi, S., Penfold, C., Madsen, S.K., Thompson, P.M., Altshuler, L.L., 2012. Normal amygdala activation but deficient ventrolateral prefrontal activation in adults with bipolar disorder during euthymia. Neuroimage 59, 738-744.

Folstein, M.F., Folstein, S.E., McHugh, P.R., 1975. “Mini-mental state”: A practical method for grading the cognitive state of patients for the clinician. Journal of Psychiatric Research 12, 189-198.
Forde, N.J., O'Donoghue, S., Scanlon, C., Emsell, L., Chaddock, C., Leemans, A., Jeurissen, B., Barker, G.J., Cannon, D.M., Murray, R.M., McDonald, C., 2015. Structural brain network analysis in families multiply affected with bipolar 1 disorder. Psychiatry Research: Neuroimaging 234, 44-51.
Fornito, A., Bullmore, E.T., 2015. Connectomics: A new paradigm for understanding brain disease. European Neuropsychopharmacology 25, 733-748.
Fornito, A., Harrison, B.J., Zalesky, A., Simons, J.S., 2012a. Competitive and cooperative dynamics of large-scale brain functional networks supporting recollection. Proceedings of the National Academy of Sciences 109, 12788-12793.
Fornito, A., Zalesky, A., Breakspear, M., 2013. Graph analysis of the human connectome: promise, progress, and pitfalls. Neuroimage 80, 426-444.
Fornito, A., Zalesky, A., Breakspear, M., 2015. The connectomics of brain disorders. Nat Rev Neurosci 16, 159-172.
Fornito, A., Zalesky, A., Pantelis, C., Bullmore, E.T., 2012b. Schizophrenia, neuroimaging and connectomics. Neuroimage 62, 2296-2314.
Förster, S., Grimmer, T., Miederer, I., Henriksen, G., Yousefi, B.H., Graner, P., Wester, H.-J., Förstl, H., Kurz, A., Dickerson, B.C., Bartenstein, P., Drzezga, A., 2012. Regional Expansion of Hypometabolism in Alzheimer's Disease Follows Amyloid Deposition with Temporal Delay. Biological Psychiatry 71, 792-797.
Fox, M.D., Raichle, M.E., 2007. Spontaneous fluctuations in brain activity observed with functional magnetic resonance imaging. Nat Rev Neurosci 8, 700-711.
Fox, M.D., Snyder, A.Z., Vincent, J.L., Corbetta, M., Van Essen, D.C., Raichle, M.E., 2005. The human brain is intrinsically organized into dynamic, anticorrelated functional networks. Proceedings of the National Academy of Sciences of the United States of America 102, 9673-9678.
Frangou, S., 2014. A Systems Neuroscience Perspective of Schizophrenia and Bipolar Disorder. Schizophrenia Bulletin.
Frazier, J.A., Breeze, J.L., Papadimitriou, G., Kennedy, D.N., Hodge, S.M., Moore, C.M., Howard, J.D., Rohan, M.P., Caviness, V.S., Makris, N., 2007. White matter abnormalities in children with and at risk for bipolar disorder. Bipolar Disorders 9, 799-809.
Friedland, R.P., Budinger, T.F., Ganz, E., Yano, Y., Mathis, C.A., Koss, B., Ober, B.A., Huesman, R.H., Derenzo, S.E., 1983. Regional Cerebral Metabolic Alterations in Dementia of the Alzheimer Type: Positron Emission Tomography with [1818] Fluorodeoxyglucose. Journal of Computer Assisted Tomography 7, 590-598.
Friston, K., 2008. Hierarchical models in the brain. PLoS Comput Biol 4, e1000211.
Friston, K., Kiebel, S., 2009. Predictive coding under the free-energy principle. Philosophical Transactions of the Royal Society B: Biological Sciences 364, 1211-1221.
Friston, K.J., 1994. Functional and effective connectivity in neuroimaging: A synthesis. Human Brain Mapping 2, 56-78.
Friston, K.J., 1998. The disconnection hypothesis. Schizophrenia research 30, 115-125.

Friston, K.J., Frith, C.D., Fletcher, P., Liddle, P.F., Frackowiak, R.S.J., 1996a. Functional Topography: Multidimensional Scaling and Functional Connectivity in the Brain. Cerebral Cortex 6, 156-164.
Friston, K.J., Frith, C.D., Liddle, P.F., Frackowiak, R.S.J., 1993. Functional Connectivity: The Principal-Component Analysis of Large (PET) Data Sets. Journal of Cerebral Blood Flow & Metabolism 13, 5-14.
Friston, K.J., Harrison, L., Penny, W., 2003. Dynamic causal modelling. Neuroimage 19, 1273-1302.
Friston, K.J., Jezzard, P., Turner, R., 1994. Analysis of functional MRI time-series. Human Brain Mapping 1, 153-171.
Friston, K.J., Tononi, G., Sporns, O., Edelman, G.M., 1995. Characterising the complexity of neuronal interactions. Human Brain Mapping 3, 302-314.
Friston, K.J., Williams, S., Howard, R., Frackowiak, R.S.J., Turner, R., 1996b. Movement-Related effects in fMRI time-series. Magnetic Resonance in Medicine 35, 346-355.
Fulcher, B.D., Fornito, A., 2016. A transcriptional signature of hub connectivity in the mouse connectome. Proceedings of the National Academy of Sciences 113, 1435-1440.
Gasquoine, P.G., 2013. Localization of function in anterior cingulate cortex: from psychosurgery to functional neuroimaging. Neurosci Biobehav Rev 37, 340-348.
Geddes, J.R., Burgess, S., Hawton, K., Jamison, K., Goodwin, G.M., 2004. Long-Term Lithium Therapy for Bipolar Disorder: Systematic Review and Meta-Analysis of Randomized Controlled Trials. American Journal of Psychiatry 161, 217-222.
Geddes, J.R., Miklowitz, D.J., 2013. Treatment of bipolar disorder. The Lancet 381, 1672-1682.
Geerligs, L., Renken, R.J., Saliasi, E., Maurits, N.M., Lorist, M.M., 2015. A Brain-Wide Study of Age-Related Changes in Functional Connectivity. Cerebral Cortex 25, 1987-1999.
Geller B, Zimerman B, Williams M, Bolhofner K, Craney JL, Delbello MP, Soutullo C, 2001. Reliability of the Washington University in St. Louis Kiddie Schedule for Affective Disorders and Schizophrenia (WASH-U-KSADS) mania and rapid cycling sections. Journal of the American Academy of Child and Adolescent Psychiatry 40, 450-455.
Genin, E., Hannequin, D., Wallon, D., Sleegers, K., Hiltunen, M., Combarros, O., Bullido, M.J., Engelborghs, S., De Deyn, P., Berr, C., Pasquier, F., Dubois, B., Tognoni, G., Fievet, N., Brouwers, N., Bettens, K., Arosio, B., Coto, E., Del Zompo, M., Mateo, I., Epelbaum, J., Frank-Garcia, A., Helisalmi, S., Porcellini, E., Pilotto, A., Forti, P., Ferri, R., Scarpini, E., Siciliano, G., Solfrizzi, V., Sorbi, S., Spalletta, G., Valdivieso, F., Vepsalainen, S., Alvarez, V., Bosco, P., Mancuso, M., Panza, F., Nacmias, B., Bossu, P., Hanon, O., Piccardi, P., Annoni, G., Seripa, D., Galimberti, D., Licastro, F., Soininen, H., Dartigues, J.F., Kamboh, M.I., Van Broeckhoven, C., Lambert, J.C., Amouyel, P., Campion, D., 2011. APOE and Alzheimer disease: a major gene with semi-dominant inheritance. Mol Psychiatry 16, 903-907.
Geschwind, N., Galaburda, A.M., 1985. Cerebral lateralization: Biological mechanisms, associations, and pathology: I. A hypothesis and a program for research. Archives of Neurology 42, 428.

Ghosh, A., Rho, Y., McIntosh, A.R., Kötter, R., Jirsa, V.K., 2008. Noise during Rest Enables the Exploration of the Brain's Dynamic Repertoire. PLoS Comput Biol 4, e1000196.
Goldin, P.R., McRae, K., Ramel, W., Gross, J.J., 2008. The neural bases of emotion regulation: reappraisal and suppression of negative emotion. Biological Psychiatry 63, 577-586.
Gollo, L.L., Zalesky, A., Hutchison, R.M., van den Heuvel, M., Breakspear, M., 2015. Dwelling quietly in the rich club: brain network determinants of slow cortical fluctuations. Philosophical Transactions of the Royal Society of London B: Biological Sciences 370.
Gomar, J.J., Bobes-Bascaran, M.T., Conejero-Goldberg, C., Davies, P., Goldberg, T.E., Alzheimer's Disease Neuroimaging Initiative, f., 2011. UTility of combinations of biomarkers, cognitive markers, and risk factors to predict conversion from mild cognitive impairment to alzheimer disease in patients in the alzheimer's disease neuroimaging initiative. Archives of General Psychiatry 68, 961-969.
Gong, G., He, Y., Concha, L., Lebel, C., Gross, D.W., Evans, A.C., Beaulieu, C., 2009a. Mapping Anatomical Connectivity Patterns of Human Cerebral Cortex Using In Vivo Diffusion Tensor Imaging Tractography. Cerebral Cortex 19, 524-536.
Gong, G., Rosa-Neto, P., Carbonell, F., Chen, Z.J., He, Y., Evans, A.C., 2009b. Age- and gender-related differences in the cortical anatomical network. J Neurosci 29, 15684-15693.
Goñi, J., van den Heuvel, M.P., Avena-Koenigsberger, A., Velez de Mendizabal, N., Betzel, R.F., Griffa, A., Hagmann, P., Corominas-Murtra, B., Thiran, J.-P., Sporns, O., 2014. Resting-brain functional connectivity predicted by analytic measures of network communication. Proceedings of the National Academy of Sciences 111, 833-838.
Goodwin, F.K., Jamison, K.R., 2007. Manic-depressive illness: bipolar disorders and recurrent depression. Oxford University Press, New York, New York.
Goodwin, G.M., Consensus Group of the British Association for Psychopharmacology, 2009. Evidence-based guidelines for treating bipolar disorder: revised second edition—recommendations from the British Association for Psychopharmacology. Journal of Psychopharmacology 23, 346-388.
Grabenhorst, F., Rolls, E.T., 2011. Value, pleasure and choice in the ventral prefrontal cortex. Trends Cogn Sci 15, 56-67.
Grady, C., 2012. The cognitive neuroscience of ageing. Nat Rev Neurosci 13, 491-505.
Grady, C., Sarraf, S., Saverino, C., Campbell, K., 2016. Age differences in the functional interactions among the default, frontoparietal control, and dorsal attention networks. Neurobiology of Aging 41, 159-172.
Grahn, J.A., Parkinson, J.A., Owen, A.M., 2008. The cognitive functions of the caudate nucleus. Progress in Neurobiology 86, 141-155.
Green, M.J., Cahill, C.M., Malhi, G.S., 2007. The cognitive and neurophysiological basis of emotion dysregulation in bipolar disorder. Journal of Affective Disorders 103, 29-42.
Greicius, M.D., Krasnow, B., Reiss, A.L., Menon, V., 2003. Functional connectivity in the resting brain: a network analysis of the default mode hypothesis. Proceedings of the National Academy of Sciences 100, 253-258.

Greicius, M.D., Srivastava, G., Reiss, A.L., Menon, V., 2004. Default-mode network activity distinguishes Alzheimer's disease from healthy aging: Evidence from functional MRI. Proceedings of the National Academy of Sciences of the United States of America 101, 4637-4642.
Gu, S., Pasqualetti, F., Cieslak, M., Telesford, Q.K., Yu, A.B., Kahn, A.E., Medaglia, J.D., Vettel, J.M., Miller, M.B., Grafton, S.T., Bassett, D.S., 2015. Controllability of structural brain networks. Nat Commun 6.
Gu, X., Hof, P.R., Friston, K.J., Fan, J., 2013. Anterior Insular Cortex and Emotional Awareness. The Journal of comparative neurology 521, 3371-3388.
Gur, R.C., Richard, J., Calkins, M.E., Chiavacci, R., Hansen, J.A., Bilker, W.B., Loughead, J., Connolly, J.J., Qiu, H., Mentch, F.D., Abou-Sleiman, P.M., Hakonarson, H., Gur, R.E., 2012. Age group and sex differences in performance on a computerized neurocognitive battery in children age 8-21. Neuropsychology 26, 251-265.
Gur, R.C., Turetsky, B.I., Matsui, M., Yan, M., Bilker, W., Hughett, P., Gur, R.E., 1999. Sex differences in brain gray and white matter in healthy young adults: correlations with cognitive performance. J Neurosci 19, 4065-4072.
Hafeman, D.M., Bebko, G., Bertocci, M.A., Fournier, J.C., Bonar, L., Perlman, S.B., Travis, M., Gill, M.K., Diwadkar, V.A., Sunshine, J.L., Holland, S.K., Kowatch, R.A., Birmaher, B., Axelson, D., Horwitz, S.M., Arnold, L.E., Fristad, M.A., Frazier, T.W., Youngstrom, E.A., Findling, R.L., Drevets, W., Phillips, M.L., 2014. Abnormal deactivation of the inferior frontal gyrus during implicit emotion processing in youth with bipolar disorder: Attenuated by medication. Journal of Psychiatric Research 58, 129-136.
Hagmann, P., Cammoun, L., Gigandet, X., Meuli, R., Honey, C.J., Wedeen, V.J., Sporns, O., 2008a. Mapping the structural core of human cerebral cortex. PLoS Biology 6, e159.
Hagmann, P., Cammoun, L., Gigandet, X., Meuli, R., Honey, C.J., Wedeen, V.J., Sporns, O., 2008b. Mapping the structural core of human cerebral cortex. PLoS Biol 6, e159.
Hagmann, P., Kurant, M., Gigandet, X., Thiran, P., Wedeen, V.J., Meuli, R., Thiran, J.-P., 2007. Mapping Human Whole-Brain Structural Networks with Diffusion MRI. PLoS ONE 2, e597.
Hagmann, P., Sporns, O., Madan, N., Cammoun, L., Pienaar, R., Wedeen, V.J., Meuli, R., Thiran, J.-P., Grant, P.E., 2010. White matter maturation reshapes structural connectivity in the late developing human brain. Proceedings of the National Academy of Sciences 107, 19067-19072.
Hajek, T., Alda, M., Hajek, E., Ivanoff, J., 2013a. Functional neuroanatomy of response inhibition in bipolar disorders – Combined voxel based and cognitive performance meta-analysis. Journal of Psychiatric Research 47, 1955-1966.
Hajek, T., Cullis, J., Novak, T., Kopecek, M., Blagdon, R., Propper, L., Stopkova, P., Duffy, A., Hoschl, C., Uher, R., 2013b. Brain structural signature of familial predisposition for bipolar disorder: replicable evidence for involvement of the right inferior frontal gyrus. Biological Psychiatry 73, 144-152.
Haller, S., Xekardaki, A., Delaloye, C., Canuto, A., Lövblad, K.O., Gold, G., Giannakopoulos, P., 2011. Combined analysis of grey matter voxel-based morphometry

and white matter tract-based spatial statistics in late-life bipolar disorder. Journal of Psychiatry & Neuroscience : JPN 36, 391-401.
Hardy, J., Selkoe, D.J., 2002. The Amyloid Hypothesis of Alzheimer's Disease: Progress and Problems on the Road to Therapeutics. Science 297, 353-356.
Harriger, L., Van Den Heuvel, M.P., Sporns, O., 2012. Rich club organization of macaque cerebral cortex and its role in network communication. PLoS ONE 7, e46497.
Harrison, P.J., Weinberger, D.R., 2005. Schizophrenia genes, gene expression, and neuropathology: on the matter of their convergence. Molecular Psychiatry 10, 40-68.
Haznedar, M.M., Roversi, F., Pallanti, S., Baldini-Rossi, N., Schnur, D.B., LiCalzi, E.M., Tang, C., Hof, P.R., Hollander, E., Buchsbaum, M.S., 2005. Fronto-thalamo-striatal gray and white matter volumes and anisotropy of their connections in bipolar spectrum illnesses. Biological Psychiatry 57, 733-742.
He, X., Qin, W., Liu, Y., Zhang, X., Duan, Y., Song, J., Li, K., Jiang, T., Yu, C., 2014. Abnormal salience network in normal aging and in amnestic mild cognitive impairment and Alzheimer's disease. Human Brain Mapping 35, 3446-3464.
Hedden, T., Gabrieli, J.D.E., 2004. Insights into the ageing mind: a view from cognitive neuroscience. Nat Rev Neurosci 5, 87-96.
Heilbronner, S.R., Haber, S.N., 2014. Frontal Cortical and Subcortical Projections Provide a Basis for Segmenting the Cingulum Bundle: Implications for Neuroimaging and Psychiatric Disorders. The Journal of Neuroscience 34, 10041-10054.
Heng, S., Song, A.W., Sim, K., 2010. White matter abnormalities in bipolar disorder: insights from diffusion tensor imaging studies. Journal of Neural Transmission 117, 639-654.
Hermundstad, A.M., Bassett, D.S., Brown, K.S., Aminoff, E.M., Clewett, D., Freeman, S., Frithsen, A., Johnson, A., Tipper, C.M., Miller, M.B., Grafton, S.T., Carlson, J.M., 2013. Structural foundations of resting-state and task-based functional connectivity in the human brain. Proceedings of the National Academy of Sciences 110, 6169-6174.
Herve, P.Y., Zago, L., Petit, L., Mazoyer, B., Tzourio-Mazoyer, N., 2013. Revisiting human hemispheric specialization with neuroimaging. Trends Cogn Sci 17, 69-80.
Heuninckx, S., Wenderoth, N., Swinnen, S.P., 2008. Systems Neuroplasticity in the Aging Brain: Recruiting Additional Neural Resources for Successful Motor Performance in Elderly Persons. The Journal of Neuroscience 28, 91-99.
Holland, D., Kuperman, J.M., Dale, A.M., 2010a. Efficient correction of inhomogeneous static magnetic field-induced distortion in Echo Planar Imaging. NeuroImage 50, 175-183.
Holland, D., Kuperman, J.M., Dale, A.M., 2010b. Efficient correction of inhomogeneous static magnetic field-induced distortion in Echo Planar Imaging. Neuroimage 50, 175-183.
Honey, C.J., Kötter, R., Breakspear, M., Sporns, O., 2007. Network structure of cerebral cortex shapes functional connectivity on multiple time scales. Proceedings of the National Academy of Sciences 104, 10240-10245.
Honey, C.J., Sporns, O., Cammoun, L., Gigandet, X., Thiran, J.P., Meuli, R., Hagmann, P., 2009. Predicting human resting-state functional connectivity from structural connectivity. Proceedings of the National Academy of Sciences 106, 2035-2040.
Honey, C.J., Thivierge, J.-P., Sporns, O., 2010. Can structure predict function in the human brain? Neuroimage 52, 766-776.

Hoogendam, Y.Y., Hofman, A., van der Geest, J.N., van der Lugt, A., Ikram, M.A., 2014. Patterns of cognitive function in aging: the Rotterdam Study. Eur J Epidemiol 29, 133-140.
Ingalhalikar, M., Smith, A., Parker, D., Satterthwaite, T.D., Elliott, M.A., Ruparel, K., Hakonarson, H., Gur, R.E., Gur, R.C., Verma, R., 2014. Sex differences in the structural connectome of the human brain. Proceedings of the National Academy of Sciences 111, 823-828.
Irimia, A., Chambers, M.C., Torgerson, C.M., Van Horn, J.D., 2012. Circular representation of human cortical networks for subject and population-level connectomic visualization. Neuroimage 60, 1340-1351.
Jack, C.R., Knopman, D.S., Jagust, W.J., Petersen, R.C., Weiner, M.W., Aisen, P.S., Shaw, L.M., Vemuri, P., Wiste, H.J., Weigand, S.D., Lesnick, T.G., Pankratz, V.S., Donohue, M.C., Trojanowski, J.Q., 2013. Update on hypothetical model of Alzheimer's disease biomarkers. Lancet neurology 12, 207-216.
Jack, C.R., Knopman, D.S., Jagust, W.J., Shaw, L.M., Aisen, P.S., Weiner, M.W., Petersen, R.C., Trojanowski, J.Q., 2010. Hypothetical model of dynamic biomarkers of the Alzheimer's pathological cascade. The Lancet Neurology 9, 119-128.
Jacomy, M., Venturini, T., Heymann, S., Bastian, M., 2014. ForceAtlas2, a Continuous Graph Layout Algorithm for Handy Network Visualization Designed for the Gephi Software. PLoS ONE 9, e98679.
Jbabdi, S., Sotiropoulos, S.N., Haber, S.N., Van Essen, D.C., Behrens, T.E., 2015. Measuring macroscopic brain connections in vivo. Nat Neurosci 18, 1546-1555.
Jbabdi, S., Sotiropoulos, S.N., Savio, A.M., Graña, M., Behrens, T.E., 2012. Model-based analysis of multishell diffusion MR data for tractography: How to get over fitting problems. Magnetic Resonance in Medicine 68, 1846-1855.
Jenkinson, M., Beckmann, C.F., Behrens, T.E., Woolrich, M.W., Smith, S.M., 2012. Fsl. Neuroimage 62, 782-790.
Jeong, H., Tombor, B., Albert, R., Oltvai, Z.N., Barabasi, A.L., 2000. The large-scale organization of metabolic networks. Nature 407, 651-654.
Jeurissen, B., Leemans, A., Jones, D.K., Tournier, J.-D., Sijbers, J., 2011. Probabilistic fiber tracking using the residual bootstrap with constrained spherical deconvolution. Human Brain Mapping 32, 461-479.
Jeurissen, B., Leemans, A., Tournier, J.D., Jones, D.K., Sijbers, J., 2013. Investigating the prevalence of complex fiber configurations in white matter tissue with diffusion magnetic resonance imaging. Human Brain Mapping 34, 2747-2766.
Jeurissen, B., Tournier, J.-D., Dhollander, T., Connelly, A., Sijbers, J., 2014. Multi-tissue constrained spherical deconvolution for improved analysis of multi-shell diffusion MRI data. Neuroimage 103, 411-426.
Jones, D.K., Knösche, T.R., Turner, R., 2013. White matter integrity, fiber count, and other fallacies: The do's and don'ts of diffusion MRI. Neuroimage 73, 239-254.
Jones, D.T., Knopman, D.S., Gunter, J.L., Graff-Radford, J., Vemuri, P., Boeve, B.F., Petersen, R.C., Weiner, M.W., Jack, C.R., 2016. Cascading network failure across the Alzheimer's disease spectrum. Brain 139, 547-562.
Jones, L., Scott, J.A.N., Haque, S., Gordon-Smith, K., Heron, J., Caesar, S., Cooper, C., Forty, L.I.Z., Hyde, S., Lyon, L., Greening, J., Sham, P.A.K., Farmer, A., McGuffin, P.,

Jones, I.A.N., Craddock, N., 2005. Cognitive style in bipolar disorder. The British Journal of Psychiatry 187, 431.
Kafantaris, V., Kingsley, P., Ardekani, B., Saito, E., Lencz, T., Lim, K., Szeszko, P., 2009. Lower orbital frontal white matter integrity in adolescents with bipolar I disorder. Journal of the American Academy of Child and Adolescent Psychiatry 48, 79-86.
Kanaan, R.A., Allin, M., Picchioni, M., Barker, G.J., Daly, E., Shergill, S.S., Woolley, J., McGuire, P.K., 2012. Gender differences in white matter microstructure. PLoS ONE 7, e38272.
Kaplan, E., 2001. The Boston Naming Test. Lippincott Williams Wilkins, Philadelphia.
Karbowski, J., 2007. Global and regional brain metabolic scaling and its functional consequences. BMC Biology 5, 1-11.
Kaufman J, Birmaher B, Brent D, Rao U, Flynn C, Moreci P, et al, 1997. Schedule for Affective Disorders and Schizophrenia for School-Age Children-Present and Lifetime Version (K-SADS-PL): initial reliability and validity data. Journal of the American Academy of Child and Adolescent Psychiatry 36, 980-988.
Kempton, M.J., Haldane, M., Jogia, J., Grasby, P.M., Collier, D., Frangou, S., 2009. Dissociable brain structural changes associated with predisposition, resilience, and disease expression in bipolar disorder. Journal of Neuroscience 29, 10863-10868.
Keshavan, M.S., Morris, D.W., Sweeney, J.A., Pearlson, G., Thaker, G., Seidman, L.J., Eack, S.M., Tamminga, C., 2011. A dimensional approach to the psychosis spectrum between bipolar disorder and schizophrenia: the Schizo-Bipolar Scale. Schizophr Res 133, 250-254.
Ketcham, C.J., Stelmach, G.E., 2001. Age-related declines in motor control. In: Birren, J., Schaie, K.W. (Eds.), Handbook of the psychology of aging. Academic Press, New York, New York, pp. 313-348.
Khadka, S., Meda, S.A., Stevens, M.C., Glahn, D.C., Calhoun, V.D., Sweeney, J.A., Tamminga, C.A., Keshavan, M.S., O'Neil, K., Schretlen, D., Pearlson, G.D., 2013. Is Aberrant Functional Connectivity A Psychosis Endophenotype? A Resting State Functional Magnetic Resonance Imaging Study. Biological Psychiatry 74, 458-466.
Kieseppä, T., van Erp, T.G., Haukka, J., Partonen, T., Cannon, T.D., Poutanen, V.-P., Kaprio, J., Lönnqvist, J., 2003. Reduced left hemispheric white matter volume in twins with bipolar I disorder. Biological Psychiatry 54, 896-905.
Kim, D.-J., Bolbecker, A.R., Howell, J., Rass, O., Sporns, O., Hetrick, W.P., Breier, A., O'Donnell, B.F., 2013. Disturbed resting state EEG synchronization in bipolar disorder: A graph-theoretic analysis. NeuroImage: Clinical 2, 414-423.
Kimura, D., 2004. Human sex differences in cognition, fact, not predicament. Sexualities, Evolution & Gender 6, 45-53.
Klauser, P., Baker, S.T., Cropley, V.L., Bousman, C., Fornito, A., Cocchi, L., Fullerton, J.M., Rasser, P., Schall, U., Henskens, F., Michie, P.T., Loughland, C., Catts, S.V., Mowry, B., Weickert, T.W., Shannon Weickert, C., Carr, V., Lenroot, R., Pantelis, C., Zalesky, A., 2016. White Matter Disruptions in Schizophrenia Are Spatially Widespread and Topologically Converge on Brain Network Hubs. Schizophrenia Bulletin.
Kleerekooper, I., van Rooij, S.J.H., van den Wildenberg, W.P.M., de Leeuw, M., Kahn, R.S., Vink, M., 2016. The effect of aging on fronto-striatal reactive and proactive inhibitory control. Neuroimage 132, 51-58.

Klingler, J., Ludwig, E., 1956. Atlas cerebri humani. NY: Karger, Basel.
Klunk, W.E., Engler, H., Nordberg, A., Wang, Y., Blomqvist, G., Holt, D.P., Bergström, M., Savitcheva, I., Huang, G.-F., Estrada, S., Ausén, B., Debnath, M.L., Barletta, J., Price, J.C., Sandell, J., Lopresti, B.J., Wall, A., Koivisto, P., Antoni, G., Mathis, C.A., Långström, B., 2004. Imaging brain amyloid in Alzheimer's disease with Pittsburgh Compound-B. Annals of Neurology 55, 306-319.
Kochan, N.A., Slavin, M.J., Brodaty, H., Crawford, J.D., Trollor, J.N., Draper, B., Sachdev, P.S., 2010. Effect of different impairment criteria on prevalence of objective mild cognitive impairment in a community sample. American Journal of Geriatric Psychiatry 18, 711-722.
Koechlin, E., Basso, G., Pietrini, P., Panzer, S., Grafman, J., 1999. The role of the anterior prefrontal cortex in human cognition. Nature 399, 148-151.
Koechlin, E., Ody, C., Kouneiher, F., 2003. The architecture of cognitive control in the human prefrontal cortex. Science 302, 1181-1185.
Kohn, K.W., 1999. Molecular Interaction Map of the Mammalian Cell Cycle Control and DNA Repair Systems. Molecular Biology of the Cell 10, 2703-2734.
Krzywinski, M., Schein, J., Birol, I., Connors, J., Gascoyne, R., Horsman, D., Jones, S.J., Marra, M.A., 2009. Circos: an information aesthetic for comparative genomics. Genome Res 19, 1639-1645.
Lawrence, N.S., Ross, T.J., Hoffmann, R., Garavan, H., Stein, E.A., 2003. Multiple Neuronal Networks Mediate Sustained Attention. Journal of Cognitive Neuroscience 15, 1028-1038.
Le Bihan, D., 1991. Molecular diffusion nuclear magnetic resonance imaging. Magn Reson Q 7, 1-30.
Le Bihan, D., Breton, E., 1985. Imagerie de diffusion in-vivo par résonance magnétique nucléaire. Comptes-Rendus de l'Académie des Sciences 93, 27-34.
Leckman JF, Sholomskas D, Thompson WD, Belanger A, Weissman MM, 1982. Best estimate of lifetime psychiatric diagnosis: a methodological study. Archives of General Psychiatry 39, 879-883.
Leemans, A., Jones, D.K., 2009. The B-matrix must be rotated when correcting for subject motion in DTI data. Magnetic Resonance in Medicine 61, 1336-1349.
Leow, A., Ajilore, O., Zhan, L., Arienzo, D., GadElkarim, J., Zhang, A., Moody, T., Van Horn, J., Feusner, J., Kumar, A., Thompson, P., Altshuler, L., 2013. Impaired Inter-Hemispheric Integration in Bipolar Disorder Revealed with Brain Network Analyses. Biological Psychiatry 73, 183-193.
Liakakis, G., Nickel, J., Seitz, R.J., 2011. Diversity of the inferior frontal gyrus—A meta-analysis of neuroimaging studies. Behavioural Brain Research 225, 341-347.
Liang, K.-Y., Zeger, S.L., 1986. Longitudinal data analysis using generalized linear models. Biometrika 73, 13-22.
Liang, X., Zou, Q., He, Y., Yang, Y., 2013. Coupling of functional connectivity and regional cerebral blood flow reveals a physiological basis for network hubs of the human brain. Proceedings of the National Academy of Sciences 110, 1929-1934.
Lichtenstein, P., Yip, B.H., Björk, C., Pawitan, Y., Cannon, T.D., Sullivan, P.F., Hultman, C.M., 2009. Common genetic determinants of schizophrenia and bipolar disorder in Swedish families: a population-based study. Lancet 373, 234-239.

Lighthall, N.R., Sakaki, M., Vasunilashorn, S., Nga, L., Somayajula, S., Chen, E.Y., Samii, N., Mather, M., 2012. Gender differences in reward-related decision processing under stress. Soc Cogn Affect Neurosci 7, 476-484.
Lim, H.K., Nebes, R., Snitz, B., Cohen, A., Mathis, C., Price, J., Weissfeld, L., Klunk, W., Aizenstein, H.J., 2014. Regional amyloid burden and intrinsic connectivity networks in cognitively normal elderly subjects. Brain 137, 3327-3338.
Lindquist, K.A., Wager, T.D., Kober, H., Bliss-Moreau, E., Barrett, L.F., 2012. The brain basis of emotion: A meta-analytic review. The Behavioral and brain sciences 35, 121-143.
Linke, J., King, A.V., Poupon, C., Hennerici, M.G., Gass, A., Wessa, M., 2013. Impaired anatomical connectivity and related executive functions: differentiating vulnerability and disease marker in bipolar disorder. Biological Psychiatry 74, 908-916.
Liu, Y., Yu, C., Zhang, X., Liu, J., Duan, Y., Alexander-Bloch, A.F., Liu, B., Jiang, T., Bullmore, E., 2014. Impaired Long Distance Functional Connectivity and Weighted Network Architecture in Alzheimer's Disease. Cerebral Cortex 24, 1422-1435.
Lo, C.-Y., Wang, P.-N., Chou, K.-H., Wang, J., He, Y., Lin, C.-P., 2010. Diffusion Tensor Tractography Reveals Abnormal Topological Organization in Structural Cortical Networks in Alzheimer's Disease. The Journal of Neuroscience 30, 16876-16885.
Loranger, A.W., Levine, P.M., 1978. Age at onset of bipolar affective illness. Archives of General Psychiatry 35, 1345-1348.
Luders, E., Toga, A.W., 2010. Sex differences in brain anatomy. Progress in brain research 186, 3-12.
Lui, S., Yao, L., Xiao, Y., Keedy, S.K., Reilly, J.L., Keefe, R.S., Tamminga, C.A., Keshavan, M.S., Pearlson, G.D., Gong, Q., Sweeney, J.A., 2015. Resting-state brain function in schizophrenia and psychotic bipolar probands and their first-degree relatives. Psychological Medicine 45, 97-108.
MacDonald, A.W., Cohen, J.D., Stenger, V.A., Carter, C.S., 2000. Dissociating the role of the dorsolateral prefrontal and anterior cingulate cortex in cognitive control. Science 288, 1835-1838.
Mahley, R.W., Weisgraber, K.H., Huang, Y., 2006. Apolipoprotein E4: a causative factor and therapeutic target in neuropathology, including Alzheimer’s disease. Proceedings of the National Academy of Sciences 103, 5644-5651.
Mahon, K., Burdick, K.E., Ikuta, T., Braga, R.J., Gruner, P., Malhotra, A.K., Szeszko, P.R., 2013. Abnormal temporal lobe white matter as a biomarker for genetic risk of bipolar disorder. Biological Psychiatry 73, 177-182.
Marques, P., Moreira, P., Magalhães, R., Costa, P., Santos, N., Zihl, J., Soares, J., Sousa, N., 2016. The functional connectome of cognitive reserve. Human Brain Mapping, n/a-n/a.
Marques, P., Soares, J.M., Magalhães, R., Santos, N.C., Sousa, N., 2015. The Bounds Of Education In The Human Brain Connectome. Scientific Reports 5, 12812.
Maslov, S., Sneppen, K., 2002. Specificity and stability in topology of protein networks. Science 296, 910-913.
Matsuo, K., Kopecek, M., Nicoletti, M., Hatch, J., Watanabe, Y., Nery, F., Zunta-Soares, G., Soares, J., 2012. New structural brain imaging endophenotype in bipolar disorder. Molecular Psychiatry 17, 412-420.

McAuley, J.J., da Fontoura Costa, L., Caetano, T.S., 2007. Rich-club phenomenon across complex network hierarchies. Applied Physics Letters 91, 084103.
McCormack, C., Green, M., Rowland, J., Roberts, G., Frankland, A., Hadzi-Pavlovic, D., Joslyn, C., Lau, P., Wright, A., Levy, F., 2015. Neuropsychological and social cognitive function in young people at genetic risk of bipolar disorder. Psychological Medicine, 1-14.
McGuffin, P., Rijsdijk, F., Andrew, M., Sham, P., Katz, R., Cardno, A., 2003. THe heritability of bipolar affective disorder and the genetic relationship to unipolar depression. Archives of General Psychiatry 60, 497-502.
McIntosh, A.M., Job, D.E., Moorhead, T.W.J., Harrison, L.K., Lawrie, S.M., Johnstone, E.C., 2005. White matter density in patients with schizophrenia, bipolar disorder and their unaffected relatives. Biological Psychiatry 58, 254-257.
McKeown, M.J., Makeig, S., Brown, G.G., Jung, T.P., Kindermann, S.S., Bell, A.J., Sejnowski, T.J., 1998. Analysis of fMRI data by blind separation into independent spatial components. Hum Brain Mapp 6, 160-188.
McKiernan, K.A., Kaufman, J.N., Kucera-Thompson, J., Binder, J.R., 2003. A Parametric Manipulation of Factors Affecting Task-induced Deactivation in Functional Neuroimaging. Journal of Cognitive Neuroscience 15, 394-408.
Meda, S.A., Gill, A., Stevens, M.C., Lorenzoni, R.P., Glahn, D.C., Calhoun, V.D., Sweeney, J.A., Tamminga, C.A., Keshavan, M.S., Thaker, G., Pearlson, G.D., 2012. Differences in Resting-State Functional Magnetic Resonance Imaging Functional Network Connectivity Between Schizophrenia and Psychotic Bipolar Probands and Their Unaffected First-Degree Relatives. Biological Psychiatry 71, 881-889.
Mega, M.S., Cummings, J.L., Fiorello, T., Gornbein, J., 1996. The spectrum of behavioral changes in Alzheimer's disease. Neurology 46, 130-135.
Menon, V., Uddin, L.Q., 2010. Saliency, switching, attention and control: a network model of insula function. Brain structure & function 214, 655-667.
Meunier, D., Lambiotte, R., Bullmore, E.T., 2010. Modular and Hierarchically Modular Organization of Brain Networks. Frontiers in Neuroscience 4, 200.
Meunier, D., Lambiotte, R., Fornito, A., Ersche, K.D., Bullmore, E.T., 2009. Hierarchical modularity in human brain functional networks. Front Neuroinform 3, 37.
Mišić, B., Betzel, R.F., de Reus, M.A., van den Heuvel, M.P., Berman, M.G., McIntosh, A.R., Sporns, O., 2016. Network-Level Structure-Function Relationships in Human Neocortex. Cerebral Cortex.
Moran, R.J., Symmonds, M., Dolan, R.J., Friston, K.J., 2014. The Brain Ages Optimally to Model Its Environment: Evidence from Sensory Learning over the Adult Lifespan. PLoS Comput Biol 10, e1003422.
Mori, S., Crain, B.J., Chacko, V.P., van Zijl, P.C.M., 1999. Three-dimensional tracking of axonal projections in the brain by magnetic resonance imaging. Annals of Neurology 45, 265-269.
Mori, S., van Zijl, P.C.M., 2002. Fiber tracking: principles and strategies – a technical review. NMR in Biomedicine 15, 468-480.
Mortensen, P.B., Pedersen, C., Melbye, M., Mors, O., Ewald, H., 2003. Individual and familial risk factors for bipolar affective disorders in Denmark. Archives of General Psychiatry 60, 1209-1215.

Moskvina, V., Craddock, N., Holmans, P., Nikolov, I., Pahwa, J.S., Green, E., Owen, M.J., O'Donovan, M.C., 2009. Gene-wide analyses of genome-wide association data sets: evidence for multiple common risk alleles for schizophrenia and bipolar disorder and for overlap in genetic risk. Molecular Psychiatry 14, 252-260.
Nachev, P., Kennard, C., Husain, M., 2008. Functional role of the supplementary and pre-supplementary motor areas. Nat Rev Neurosci 9, 856-869.
Nelson, H.E., Willison, J., 1991. National Adult Reading Test (NART): Test Manual (2nd ed.). NFER Nelson, Windsor, UK.
Neves, M.D.C.L., Albuquerque, M.R., Malloy-Diniz, L., Nicolato, R., Neves, F.S., de Souza-Duran, F.L., Busatto, G., Corrêa, H., 2015. A voxel-based morphometry study of gray matter correlates of facial emotion recognition in bipolar disorder. Psychiatry Research: Neuroimaging 233, 158-164.
Newman, M., 2003. The Structure and Function of Complex Networks. SIAM Review 45, 167-256.
Nielsen, J.A., Zielinski, B.A., Ferguson, M.A., Lainhart, J.E., Anderson, J.S., 2013. An evaluation of the left-brain vs. right-brain hypothesis with resting state functional connectivity magnetic resonance imaging. PLoS ONE 8, e71275.
Northoff, G., Heinzel, A., De Greck, M., Bermpohl, F., Dobrowolny, H., Panksepp, J., 2006. Self-referential processing in our brain—a meta-analysis of imaging studies on the self. Neuroimage 31, 440-457.
Nortje, G., Stein, D.J., Radua, J., Mataix-Cols, D., Horn, N., 2013. Systematic review and voxel-based meta-analysis of diffusion tensor imaging studies in bipolar disorder. Journal of Affective Disorders 150, 192-200.
Nugent, A.C., Milham, M.P., Bain, E.E., Mah, L., Cannon, D.M., Marrett, S., Zarate, C.A., Pine, D.S., Price, J.L., Drevets, W.C., 2006. Cortical abnormalities in bipolar disorder investigated with MRI and voxel-based morphometry. Neuroimage 30, 485-497.
Nurnberger, J.I., McInnis, M., Reich, W., Kastelic, E., Wilcox, H.C., Glowinski, A., Mitchell, P., Fisher, C., Erpe, M., Gershon, E.S., Berrettini, W., Laite, G., Schweitzer, R., Rhoadarmer, K., Coleman, V.V., Cai, X.Y., Azzouz, F., Liu, H., Kamali, M., Brucksch, C., Monahan, P.O., 2011. A high-risk study of bipolar disorder: Childhood clinical phenotypes as precursors of major mood disorders. Archives of General Psychiatry 68, 1012-1020.
O'donovan, M.C., Craddock, N., Norton, N., Williams, H., Peirce, T., Moskvina, V., Nikolov, I., Hamshere, M., Carroll, L., Georgieva, L., 2008. Identification of loci associated with schizophrenia by genome-wide association and follow-up. Nature genetics 40, 1053-1055.
O'Donnell, L.A., Deldin, P.J., Pester, B., McInnis, M.G., Langenecker, S.A., Ryan, K.A., 2017. Cognitive flexibility: A trait of bipolar disorder that worsens with length of illness. Journal of Clinical and Experimental Neuropsychology, 1-9.
O'Sullivan, M., Jones, D.K., Summers, P.E., Morris, R.G., Williams, S.C.R., Markus, H.S., 2001. Evidence for cortical "disconnection" as a mechanism of age-related cognitive decline. Neurology 57, 632-638.
Ogawa, S., 2012. Finding the BOLD effect in brain images. Neuroimage 62, 608-609.

Ogawa, S., Lee, T.-M., Kay, A.R., Tank, D.W., 1990. Brain magnetic resonance imaging with contrast dependent on blood oxygenation. Proceedings of the National Academy of Sciences 87, 9868-9872.
Ogawa, S., Tank, D.W., Menon, R., Ellermann, J.M., Kim, S.G., Merkle, H., Ugurbil, K., 1992. Intrinsic signal changes accompanying sensory stimulation: functional brain mapping with magnetic resonance imaging. Proceedings of the National Academy of Sciences 89, 5951-5955.
Oh, H., Madison, C., Baker, S., Rabinovici, G., Jagust, W., 2016. Dynamic relationships between age, amyloid-β deposition, and glucose metabolism link to the regional vulnerability to Alzheimer's disease. Brain.
Onoda, K., Ishihara, M., Yamaguchi, S., 2012. Decreased Functional Connectivity by Aging Is Associated with Cognitive Decline. Journal of Cognitive Neuroscience 24, 2186-2198.
Otte, W.M., van Diessen, E., Paul, S., Ramaswamy, R., Subramanyam Rallabandi, V.P., Stam, C.J., Roy, P.K., 2015. Aging alterations in whole-brain networks during adulthood mapped with the minimum spanning tree indices: The interplay of density, connectivity cost and life-time trajectory. Neuroimage 109, 171-189.
Pannek, K., Guzzetta, A., Colditz, P.B., Rose, S.E., 2012a. Diffusion MRI of the neonate brain: acquisition, processing and analysis techniques. Pediatric radiology 42, 1169-1182.
Pannek, K., Raffelt, D., Bell, C., Mathias, J.L., Rose, S.E., 2012b. HOMOR: higher order model outlier rejection for high b-value MR diffusion data. Neuroimage 63, 835-842.
Papmeyer, M., Giles, S., Sussmann, J.E., Kielty, S., Stewart, T., Lawrie, S.M., Whalley, H.C., McIntosh, A.M., 2015. Cortical thickness in individuals at high familial risk of mood disorders as they develop major depressive disorder. Biological Psychiatry 78, 58-66.
Park, D.C., Reuter-Lorenz, P., 2009. The adaptive brain: aging and neurocognitive scaffolding. Annu Rev Psychol 60, 173-196.
Paus, T., Keshavan, M., Giedd, J.N., 2008. Why do many psychiatric disorders emerge during adolescence? Nat Rev Neurosci 9, 947-957.
Perich, T., Lau, P., Hadzi-Pavlovic, D., Roberts, G., Frankland, A., Wright, A., Green, M., Breakspear, M., Corry, J., Radlinska, B., McCormack, C., Joslyn, C., Levy, F., Lenroot, R., Nurnberger, J.I.J., Mitchell, P.B., 2015. What clinical features precede the onset of bipolar disorder? Journal of Psychiatric Research 62, 71-77.
Perlis, R.H., Miyahara, S., Marangell, L.B., Wisniewski, S.R., Ostacher, M., DelBello, M.P., Bowden, C.L., Sachs, G.S., Nierenberg, A.A., 2004. Long-Term implications of early onset in bipolar disorder: data from the first 1000 participants in the systematic treatment enhancement program for bipolar disorder (STEP-BD). Biological Psychiatry 55, 875-881.
Perry, A., Wen, W., Lord, A., Thalamuthu, A., Roberts, G., Mitchell, P.B., Sachdev, P.S., Breakspear, M., 2015. The organisation of the elderly connectome. Neuroimage 114, 414-426.
Peters, A., 2002. The effects of normal aging on myelin and nerve fibers: a review. J Neurocytol 31, 581-593.

Peters, E., Dieckmann, N.F., Weller, J., 2011. Chapter 9 - Age Differences in Complex Decision Making A2 - Schaie, K. Warner. In: Willis, S.L. (Ed.), Handbook of the Psychology of Aging (Seventh Edition). Academic Press, San Diego, pp. 133-151.
Petersen, R.C., Doody, R., Kurz, A., et al., 2001. CUrrent concepts in mild cognitive impairment. Archives of Neurology 58, 1985-1992.
Petersen, R.C., Roberts, R.O., Knopman, D.S., et al., 2009. Mild cognitive impairment: Ten years later. Archives of Neurology 66, 1447-1455.
Phillips, M.L., Ladouceur, C.D., Drevets, W.C., 2008. A neural model of voluntary and automatic emotion regulation: implications for understanding the pathophysiology and neurodevelopment of bipolar disorder. Molecular Psychiatry 13, 829-857.
Phillips, M.L., Swartz, H.A., 2014. A critical appraisal of neuroimaging studies of bipolar disorder: toward a new conceptualization of underlying neural circuitry and roadmap for future research. The American journal of psychiatry 171, 829-843.
Phillips, O.R., Clark, K.A., Luders, E., Azhir, R., Joshi, S.H., Woods, R.P., Mazziotta, J.C., Toga, A.W., Narr, K.L., 2013. Superficial white matter: effects of age, sex, and hemisphere. Brain Connect 3, 146-159.
Pierpaoli, C., Jezzard, P., Basser, P.J., Barnett, A., Di Chiro, G., 1996. Diffusion tensor MR imaging of the human brain. Radiology 201, 637-648.
Piver, A., Yatham, L.N., Lam, R.W., 2002. Bipolar spectrum disorders. New perspectives. Canadian family physician 48, 896-904.
Plassman, B.L., Langa, K.M., Fisher, G.G., Heeringa, S.G., Weir, D.R., Ofstedal, M.B., Burke, J.R., Hurd, M.D., Potter, G.G., Rodgers, W.L., Steffens, D.C., Willis, R.J., Wallace, R.B., 2007. Prevalence of dementia in the United States: the aging, demographics, and memory study. Neuroepidemiology 29, 125-132.
Porsteinsson, A.P., Antonsdottir, I.M., 2015. Neuropsychiatric Symptoms in Dementia: A Cause or Consequence? American Journal of Psychiatry 172, 410-411.
Potash, J.B., Bienvenu, O.J., 2009. Neuropsychiatric disorders: Shared genetics of bipolar disorder and schizophrenia. Nat Rev Neurol 5, 299-300.
Power, J.D., Barnes, K.A., Snyder, A.Z., Schlaggar, B.L., Petersen, S.E., 2012. Spurious but systematic correlations in functional connectivity MRI networks arise from subject motion. Neuroimage 59, 2142-2154.
Power, Jonathan D., Schlaggar, Bradley L., Lessov-Schlaggar, Christina N., Petersen, Steven E., 2013. Evidence for Hubs in Human Functional Brain Networks. Neuron 79, 798-813.
Price, C.J., 2012. A review and synthesis of the first 20years of PET and fMRI studies of heard speech, spoken language and reading. Neuroimage 62, 816-847.
Purcell, S.M., Wray, N.R., Stone, J.L., Visscher, P.M., O'Donovan, M.C., Sullivan, P.F., Sklar, P., Ruderfer, D.M., McQuillin, A., Morris, D.W., 2009. Common polygenic variation contributes to risk of schizophrenia and bipolar disorder. Nature 460, 748-752.
Raffelt, D., Tournier, J.-D., Rose, S., Ridgway, G.R., Henderson, R., Crozier, S., Salvado, O., Connelly, A., 2012a. Apparent fibre density: a novel measure for the analysis of diffusion-weighted magnetic resonance images. Neuroimage 59, 3976-3994.
Raffelt, D., Tournier, J.D., Rose, S., Ridgway, G.R., Henderson, R., Crozier, S., Salvado, O., Connelly, A., 2012b. Apparent Fibre Density: A novel measure for the analysis of diffusion-weighted magnetic resonance images. Neuroimage 59, 3976-3994.

Raffelt, D.A., Tournier, J.-D., Smith, R.E., Vaughan, D.N., Jackson, G., Ridgway, G.R., Connelly, A., 2016. Investigating white matter fibre density and morphology using fixel-based analysis. Neuroimage.
Raichle, M.E., 2015. The Brain's Default Mode Network. Annual Review of Neuroscience 38, 433-447.
Raj, A., Kuceyeski, A., Weiner, M., 2012. A Network Diffusion Model of Disease Progression in Dementia. Neuron 73, 1204-1215.
Rao, C.R., 1952. Advanced statistical methods in biometric research. Wiley, Oxford, England.
Raz, N., Lindenberger, U., Rodrigue, K.M., Kennedy, K.M., Head, D., Williamson, A., Dahle, C., Gerstorf, D., Acker, J.D., 2005. Regional Brain Changes in Aging Healthy Adults: General Trends, Individual Differences and Modifiers. Cerebral Cortex 15, 1676-1689.
Richardson, M.P., Strange, B.A., Dolan, R.J., 2004. Encoding of emotional memories depends on amygdala and hippocampus and their interactions. Nature neuroscience 7, 278-285.
Ritchie, K., Artero, S., Touchon, J., 2001. Classification criteria for mild cognitive impairment: a population-based validation study. Neurology 56, 37-42.
Roberts, G., Green, M.J., Breakspear, M., McCormack, C., Frankland, A., Wright, A., Levy, F., Lenroot, R., Chan, H.N., Mitchell, P.B., 2013. Reduced inferior frontal gyrus activation during response inhibition to emotional stimuli in youth at high risk of bipolar disorder. Biological Psychiatry 74, 55-61.
Roberts, G., Lenroot, R., Frankland, A., Yeung, P., Gale, N., Wright, A., Lau, P., Levy, F., Wen, W., Mitchell, P., 2016a. Abnormalities in left inferior frontal gyral thickness and parahippocampal gyral volume in young people at high genetic risk for bipolar disorder. Psychological Medicine, 1.
Roberts, G., Wen, W., Frankland, A., Perich, T., Holmes-Preston, E., Levy, F., Lenroot, R.K., Hadzi-Pavlovic, D., Nurnberger, J.I., Breakspear, M., Mitchell, P.B., 2016b. Interhemispheric white matter integrity in young people with bipolar disorder and at high genetic risk. Psychological Medicine FirstView, 1-12.
Roberts, J.A., Perry, A., Lord, A.R., Roberts, G., Mitchell, P.B., Smith, R.E., Calamante, F., Breakspear, M., 2016c. The contribution of geometry to the human connectome. Neuroimage 124, Part A, 379-393.
Rodrigue, K.M., Kennedy, K.M., 2011. Chapter 5 - The Cognitive Consequences of Structural Changes to the Aging Brain In: Willis, S.L. (Ed.), Handbook of the Psychology of Aging (Seventh Edition). Academic Press, San Diego, pp. 73-91.
Roine, T., Jeurissen, B., Perrone, D., Aelterman, J., Leemans, A., Philips, W., Sijbers, J., 2014. Isotropic non-white matter partial volume effects in constrained spherical deconvolution. Front Neuroinform 8.
Roski, C., Caspers, S., Lux, S., Hoffstaedter, F., Bergs, R., Amunts, K., Eickhoff, S.B., 2013. Activation shift in elderly subjects across functional systems: an fMRI study. Brain Structure and Function 219, 707-718.
Ross, E.D., Monnot, M., 2011. Affective prosody: what do comprehension errors tell us about hemispheric lateralization of emotions, sex and aging effects, and the role of cognitive appraisal. Neuropsychologia 49, 866-877.

Roybal, D.J., Barnea-Goraly, N., Kelley, R., Bararpour, L., Howe, M.E., Reiss, A.L., Chang, K.D., 2015. Widespread white matter tract aberrations in youth with familial risk for bipolar disorder. Psychiatry Research 232, 184-192.
Rubinov, M., Bullmore, E., 2013. Schizophrenia and abnormal brain network hubs. Dialogues in clinical neuroscience 15, 339-349.
Rubinov, M., Sporns, O., 2010. Complex network measures of brain connectivity: uses and interpretations. Neuroimage 52, 1059-1069.
Ryman, S.G., van den Heuvel, M.P., Yeo, R.A., Caprihan, A., Carrasco, J., Vakhtin, A.A., Flores, R.A., Wertz, C., Jung, R.E., 2014. Sex differences in the relationship between white matter connectivity and creativity. Neuroimage 101, 380-389.
Sachdev, P.S., Brodaty, H., Reppermund, S., Kochan, N.A., Trollor, J.N., Draper, B., Slavin, M.J., Crawford, J., Kang, K., Broe, G.A., Mather, K.A., Lux, O., 2010. The Sydney Memory and Ageing Study (MAS): methodology and baseline medical and neuropsychiatric characteristics of an elderly epidemiological non-demented cohort of Australians aged 70–90 years. International Psychogeriatrics 22, 1248-1264.
Sala-Llonch, R., Junqué, C., Arenaza-Urquijo, E.M., Vidal-Piñeiro, D., Valls-Pedret, C., Palacios, E.M., Domènech, S., Salvà, A., Bargalló, N., Bartrés-Faz, D., 2014. Changes in whole-brain functional networks and memory performance in aging. Neurobiology of Aging 35, 2193-2202.
Salami, A., Eriksson, J., Nilsson, L.G., Nyberg, L., 2012. Age-related white matter microstructural differences partly mediate age-related decline in processing speed but not cognition. Biochimica et Biophysica Acta - Molecular Basis of Disease 1822, 408-415.
Salami, A., Pudas, S., Nyberg, L., 2014. Elevated hippocampal resting-state connectivity underlies deficient neurocognitive function in aging. Proceedings of the National Academy of Sciences 111, 17654-17659.
Salmon, D.P., Bondi, M.W., 2009. Neuropsychological assessment of dementia. Annual Review of Psychology 60, 257.
Salthouse, T., 2012. Consequences of age-related cognitive declines. Annual Review of Psychology 63, 201.
Salthouse, T.A., 1996. The processing-speed theory of adult age differences in cognition. Psychological Review 103, 403-428.
Salthouse, T.A., 2000. Aging and measures of processing speed. Biol Psychol 54, 35-54.
Samanez-Larkin, G.R., Levens, S.M., Perry, L.M., Dougherty, R.F., Knutson, B., 2012. Frontostriatal White Matter Integrity Mediates Adult Age Differences in Probabilistic Reward Learning. The Journal of Neuroscience 32, 5333-5337.
Samu, D., Seth, A.K., Nowotny, T., 2014. Influence of Wiring Cost on the Large-Scale Architecture of Human Cortical Connectivity. PLoS Comput Biol 10, e1003557.
Saunders, K.E.A., Goodwin, G.M., 2010. The course of bipolar disorder. Advances in Psychiatric Treatment 16, 318-328.
Scannell, J.W., Burns, G.A.P.C., Hilgetag, C.C., O'Neil, M.A., Young, M.P., 1999. The Connectional Organization of the Cortico-thalamic System of the Cat. Cerebral Cortex 9, 277-299.
Scannell, J.W., Young, M.P., 1993. The connectional organization of neural systems in the cat cerebral cortex. Current Biology 3, 191-200.

Schaie, K.W., 1996. Intellectual development in adulthood: The Seattle longitudinal study. Cambridge University Press.
Scheltens, P., Leys, D., Barkhof, F., Huglo, D., Weinstein, H.C., Vermersch, P., Kuiper, M., Steinling, M., Wolters, E.C., Valk, J., 1992. Atrophy of medial temporal lobes on MRI in "probable" Alzheimer's disease and normal ageing: diagnostic value and neuropsychological correlates. Journal of Neurology, Neurosurgery & Psychiatry 55, 967-972.
Schmidt, A., Crossley, N.A., Harrisberger, F., Smieskova, R., Lenz, C., Riecher-Rössler, A., Lang, U.E., McGuire, P., Fusar-Poli, P., Borgwardt, S., 2016. Structural Network Disorganization in Subjects at Clinical High Risk for Psychosis. Schizophrenia Bulletin.
Schmithorst, V.J., Holland, S.K., Dardzinski, B.J., 2008. Developmental differences in white matter architecture between boys and girls. Hum Brain Mapp 29, 696-710.
Schoenbaum, G., Roesch, M.R., Stalnaker, T.A., Takahashi, Y.K., 2009. A new perspective on the role of the orbitofrontal cortex in adaptive behaviour. Nat Rev Neurosci 10, 885-892.
Seeley, W.W., Crawford, R.K., Zhou, J., Miller, B.L., Greicius, M.D., 2009. Neurodegenerative diseases target large-scale human brain networks. Neuron 62, 42-52.
Seghier, M.L., 2013. The Angular Gyrus: Multiple Functions and Multiple Subdivisions. The Neuroscientist 19, 43-61.
Seidler, R.D., Bernard, J.A., Burutolu, T.B., Fling, B.W., Gordon, M.T., Gwin, J.T., Kwak, Y., Lipps, D.B., 2010. Motor control and aging: Links to age-related brain structural, functional, and biochemical effects. Neuroscience & Biobehavioral Reviews 34, 721-733.
Senden, M., Deco, G., de Reus, M.A., Goebel, R., van den Heuvel, M.P., 2014. Rich club organization supports a diverse set of functional network configurations. Neuroimage 96, 174-182.
Senden, M., Goebel, R., Deco, G., 2012. Structural connectivity allows for multi-threading during rest: The structure of the cortex leads to efficient alternation between resting state exploratory behavior and default mode processing. Neuroimage 60, 2274-2284.
Senden, M., Reuter, N., van den Heuvel, M.P., Goebel, R., Deco, G., 2016. Cortical rich club regions can organize state-dependent functional network formation by engaging in oscillatory behavior. Neuroimage.
Sepede, G., De Berardis, D., Campanella, D., Perrucci, M.G., Ferretti, A., Serroni, N., Moschetta, F.S., Del Gratta, C., Salerno, R.M., Ferro, F.M., 2012. Impaired sustained attention in euthymic bipolar disorder patients and non-affected relatives: an fMRI study. Bipolar Disorders 14, 764-779.
Sepulcre, J., 2014. Integration of visual and motor functional streams in the human brain. Neuroscience Letters 567, 68-73.
Sepulcre, J., Sabuncu, M.R., Yeo, T.B., Liu, H., Johnson, K.A., 2012. Stepwise Connectivity of the Modal Cortex Reveals the Multimodal Organization of the Human Brain. The Journal of neuroscience : the official journal of the Society for Neuroscience 32, 10649-10661.
Seth, A.K., Friston, K.J., 2016. Active interoceptive inference and the emotional brain. Philosophical Transactions of the Royal Society B: Biological Sciences 371.

Shackman, A.J., Salomons, T.V., Slagter, H.A., Fox, A.S., Winter, J.J., Davidson, R.J., 2011. The integration of negative affect, pain and cognitive control in the cingulate cortex. Nat Rev Neurosci 12, 154-167.
Shaffer, J.L., Petrella, J.R., Sheldon, F.C., Choudhury, K.R., Calhoun, V.D., Coleman, R.E., Doraiswamy, P.M., 2013. Predicting Cognitive Decline in Subjects at Risk for Alzheimer Disease by Using Combined Cerebrospinal Fluid, MR Imaging, and PET Biomarkers. Radiology 266, 583-591.
Shmuel, A., Leopold, D.A., 2008. Neuronal correlates of spontaneous fluctuations in fMRI signals in monkey visual cortex: Implications for functional connectivity at rest. Hum Brain Mapp 29, 751-761.
Shmuel, A., Yacoub, E., Pfeuffer, J., Van de Moortele, P.F., Adriany, G., Hu, X., Ugurbil, K., 2002. Sustained negative BOLD, blood flow and oxygen consumption response and its coupling to the positive response in the human brain. Neuron 36, 1195-1210.
Shu, N., Liang, Y., Li, H., Zhang, J., Li, X., Wang, L., He, Y., Wang, Y., Zhang, Z., 2012. Disrupted Topological Organization in White Matter Structural Networks in Amnestic Mild Cognitive Impairment: Relationship to Subtype. Radiology 265, 518-527.
Shu, N., Liu, Y., Li, K., Duan, Y., Wang, J., Yu, C., Dong, H., Ye, J., He, Y., 2011. Diffusion Tensor Tractography Reveals Disrupted Topological Efficiency in White Matter Structural Networks in Multiple Sclerosis. Cerebral Cortex 21, 2565-2577.
Sidor, M.M., MacQueen, G.M., 2012. An update on antidepressant use in bipolar depression. Curr Psychiatry Rep 14, 696-704.
Skudlarski, P., Jagannathan, K., Calhoun, V.D., Hampson, M., Skudlarska, B.A., Pearlson, G., 2008. Measuring brain connectivity: Diffusion tensor imaging validates resting state temporal correlations. Neuroimage 43, 554-561.
Sled, J.G., Zijdenbos, A.P., Evans, A.C., 1998a. A nonparametric method for automatic correction of intensity nonuniformity in MRI data. IEEE Trans Med Imaging 17, 87-97.
Sled, J.G., Zijdenbos, A.P., Evans, A.C., 1998b. A nonparametric method for automatic correction of intensity nonuniformity in MRI data. IEEE Transactions on Medical Imaging 17, 87-97.
Smith, R.E., Tournier, J.-D., Calamante, F., Connelly, A., 2012a. Anatomically-constrained tractography: Improved diffusion MRI streamlines tractography through effective use of anatomical information. Neuroimage 62, 1924-1938.
Smith, R.E., Tournier, J.-D., Calamante, F., Connelly, A., 2013a. SIFT: Spherical-deconvolution informed filtering of tractograms. Neuroimage 67, 298-312.
Smith, R.E., Tournier, J.-D., Calamante, F., Connelly, A., 2015a. The effects of SIFT on the reproducibility and biological accuracy of the structural connectome. Neuroimage 104, 253-265.
Smith, R.E., Tournier, J.-D., Calamante, F., Connelly, A., 2015b. SIFT2: Enabling dense quantitative assessment of brain white matter connectivity using streamlines tractography. Neuroimage 119, 338-351.
Smith, R.E., Tournier, J.D., Calamante, F., Connelly, A., 2013b. SIFT: Spherical-deconvolution informed filtering of tractograms. Neuroimage 67, 298-312.
Smith, R.E., Tournier, J.D., Calamante, F., Connelly, A., 2013c. SIFT: Spherical-deconvolution informed filtering of tractograms. NeuroImage 67, 298-312.

Smith, S.M., Fox, P.T., Miller, K.L., Glahn, D.C., Fox, P.M., Mackay, C.E., Filippini, N., Watkins, K.E., Toro, R., Laird, A.R., Beckmann, C.F., 2009. Correspondence of the brain's functional architecture during activation and rest. Proceedings of the National Academy of Sciences 106, 13040-13045.
Smith, S.M., Hyvärinen, A., Varoquaux, G., Miller, K.L., Beckmann, C.F., 2014. Group-PCA for very large fMRI datasets. Neuroimage 101, 738-749.
Smith, S.M., Jenkinson, M., Woolrich, M.W., Beckmann, C.F., Behrens, T.E., Johansen-Berg, H., Bannister, P.R., De Luca, M., Drobnjak, I., Flitney, D.E., 2004a. Advances in functional and structural MR image analysis and implementation as FSL. Neuroimage 23, S208-S219.
Smith, S.M., Jenkinson, M., Woolrich, M.W., Beckmann, C.F., Behrens, T.E.J., Johansen-Berg, H., Bannister, P.R., De Luca, M., Drobnjak, I., Flitney, D.E., Niazy, R.K., Saunders, J., Vickers, J., Zhang, Y., De Stefano, N., Brady, J.M., Matthews, P.M., 2004b. Advances in functional and structural MR image analysis and implementation as FSL. Neuroimage 23, Supplement 1, S208-S219.
Smith, S.M., Miller, K.L., Moeller, S., Xu, J., Auerbach, E.J., Woolrich, M.W., Beckmann, C.F., Jenkinson, M., Andersson, J., Glasser, M.F., Van Essen, D.C., Feinberg, D.A., Yacoub, E.S., Ugurbil, K., 2012b. Temporally-independent functional modes of spontaneous brain activity. Proceedings of the National Academy of Sciences 109, 3131-3136.
Solé-Padullés, C., Bartrés-Faz, D., Junqué, C., Vendrell, P., Rami, L., Clemente, I.C., Bosch, B., Villar, A., Bargalló, N., Jurado, M.A., Barrios, M., Molinuevo, J.L., 2009. Brain structure and function related to cognitive reserve variables in normal aging, mild cognitive impairment and Alzheimer's disease. Neurobiology of Aging 30, 1114-1124.
Sotiropoulos, S.N., Jbabdi, S., Xu, J., Andersson, J.L., Moeller, S., Auerbach, E.J., Glasser, M.F., Hernandez, M., Sapiro, G., Jenkinson, M., Feinberg, D.A., Yacoub, E., Lenglet, C., Van Essen, D.C., Ugurbil, K., Behrens, T.E.J., 2013. Advances in diffusion MRI acquisition and processing in the Human Connectome Project. Neuroimage 80, 125-143.
Sporns, O., 2013a. Network attributes for segregation and integration in the human brain. Current Opinion in Neurobiology 23, 162-171.
Sporns, O., 2013b. Structure and function of complex brain networks. Dialogues in clinical neuroscience 15, 247-262.
Sporns, O., Betzel, R.F., 2016. Modular Brain Networks. Annual Review of Psychology 67, 613-640.
Sporns, O., Tononi, G., Edelman, G.M., 2000. Connectivity and complexity: the relationship between neuroanatomy and brain dynamics. Neural Networks 13, 909-922.
Sporns, O., Tononi, G., Kotter, R., 2005. The human connectome: A structural description of the human brain. PLoS Comput Biol 1, e42.
Sporns, O., Zwi, J.D., 2004. The small world of the cerebral cortex. Neuroinformatics 2, 145-162.
Spreng, R.N., Sepulcre, J., Turner, G.R., Stevens, W.D., Schacter, D.L., 2013. Intrinsic architecture underlying the relations among the default, dorsal attention, and frontoparietal control networks of the human brain. Journal of Cognitive Neuroscience 25, 10.1162/jocn_a_00281.

Spreng, R.N., Stevens, W.D., Chamberlain, J.P., Gilmore, A.W., Schacter, D.L., 2010. Default network activity, coupled with the frontoparietal control network, supports goal-directed cognition. Neuroimage 53, 303-317.
Sprengelmeyer, R., Rausch, M., Eysel, U., Przuntek, H., 1998. Neural structures associated with recognition of facial expressions of basic emotions. Proceedings of the Royal Society of London. Series B: Biological Sciences 265, 1927-1931.
Sprooten, E., Brumbaugh, M.S., Knowles, E.E., McKay, D.R., Lewis, J., Barrett, J., Landau, S., Cyr, L., Kochunov, P., Winkler, A.M., Pearlson, G.D., Glahn, D.C., 2013. Reduced white matter integrity in sibling pairs discordant for bipolar disorder. The American journal of psychiatry 170, 1317-1325.
Sprooten, E., Sussmann, J.E., Clugston, A., Peel, A., McKirdy, J., Moorhead, T.W.J., Anderson, S., Shand, A.J., Giles, S., Bastin, M.E., 2011. White matter integrity in individuals at high genetic risk of bipolar disorder. Biological Psychiatry 70, 350-356.
Sripada, C., Angstadt, M., Kessler, D., Phan, K.L., Liberzon, I., Evans, G.W., Welsh, R.C., Kim, P., Swain, J.E., 2014. Volitional regulation of emotions produces distributed alterations in connectivity between visual, attention control, and default networks. Neuroimage 89, 110-121.
Stam, C.J., 2004. Functional connectivity patterns of human magnetoencephalographic recordings: a 'small-world' network? Neuroscience Letters 355, 25-28.
Stephan, K.E., Baldeweg, T., Friston, K.J., 2006. Synaptic plasticity and dysconnection in schizophrenia. Biological Psychiatry 59, 929-939.
Stephan, K.E., Friston, K.J., Frith, C.D., 2009. Dysconnection in Schizophrenia: From Abnormal Synaptic Plasticity to Failures of Self-monitoring. Schizophrenia Bulletin 35, 509-527.
Stephan, K.E., Hilgetag, C.C., Burns, G.A.P.C., O'Neill, M.A., Young, M.P., Kotter, R., 2000. Computational analysis of functional connectivity between areas of primate cerebral cortex. Philosophical Transactions of the Royal Society of London B: Biological Sciences 355, 111-126.
Stephan, K.E., Manjaly, Z.M., Mathys, C.D., Weber, L.A.E., Paliwal, S., Gard, T., Tittgemeyer, M., Fleming, S.M., Haker, H., Seth, A.K., Petzschner, F.H., 2016. Allostatic Self-efficacy: A Metacognitive Theory of Dyshomeostasis-Induced Fatigue and Depression. Frontiers in Human Neuroscience 10.
Stern, Y., 2002. What is cognitive reserve? Theory and research application of the reserve concept. Journal of the International Neuropsychological Society 8, 448-460.
Stern, Y., 2009. Cognitive reserve. Neuropsychologia 47, 2015-2028.
Stern, Y., 2012. Cognitive reserve in ageing and Alzheimer's disease. Lancet neurology 11, 1006-1012.
Stern, Y., Zarahn, E., Habeck, C., Holtzer, R., Rakitin, B.C., Kumar, A., Flynn, J., Steffener, J., Brown, T., 2008. A Common Neural Network for Cognitive Reserve in Verbal and Object Working Memory in Young but not Old. Cerebral Cortex 18, 959-967.
Stork, C., Renshaw, P.F., 2005. Mitochondrial dysfunction in bipolar disorder: evidence from magnetic resonance spectroscopy research. Mol Psychiatry 10, 900-919.
Strakowski, S.M., Adler, C.M., Almeida, J., Altshuler, L.L., Blumberg, H.P., Chang, K.D., DelBello, M.P., Frangou, S., McIntosh, A., Phillips, M.L., 2012. The functional neuroanatomy of bipolar disorder: a consensus model. Bipolar Disorders 14, 313-325.

Strauss, E., Sherman, E.M.S., Spreen, O., 2006. A Compendium of Neuropsychological Tests: Administration, Norms, and Commentary, 3rd ed. Oxford University Press, New York.
Stuck, A.E., Walthert, J.M., Nikolaus, T., Büla, C.J., Hohmann, C., Beck, J.C., 1999. Risk factors for functional status decline in community-living elderly people: a systematic literature review. Social Science & Medicine 48, 445-469.
Sullivan, E.V., Pfefferbaum, A., 2003. Diffusion tensor imaging in normal aging and neuropsychiatric disorders. Eur J Radiol 45, 244-255.
Sun, Y., Danila, B., Josić, K., Bassler, K.E., 2009. Improved community structure detection using a modified fine-tuning strategy. EPL (Europhysics Letters) 86, 28004.
Sunderland, T., Linker, G., Mirza, N., Putnam, K.T., Friedman, D.L., Kimmel, L.H., Bergeson, J., Manetti, G.J., Zimmermann, M., Tang, B., Bartko, J.J., Cohen, R.M., 2003. Decreased beta-amyloid1-42 and increased tau levels in cerebrospinal fluid of patients with Alzheimer disease. Jama 289, 2094-2103.
Takao, H., Hayashi, N., Ohtomo, K., 2013. White matter microstructure asymmetry: effects of volume asymmetry on fractional anisotropy asymmetry. Neuroscience 231, 1-12.
Tang, Y., Nyengaard, J.R., Pakkenberg, B., Gundersen, H.J., 1997. Age-induced white matter changes in the human brain: a stereological investigation. Neurobiol Aging 18, 609-615.
Thermenos, H.W., Goldstein, J.M., Milanovic, S.M., Whitfield-Gabrieli, S., Makris, N., LaViolette, P., Koch, J.K., Faraone, S.V., Tsuang, M.T., Buka, S.L., Seidman, L.J., 2010. An fMRI study of working memory in persons with bipolar disorder or at genetic risk for bipolar disorder. American Journal of Medical Genetics Part B: Neuropsychiatric Genetics 153, 120-131.
Thiebaut de Schotten, M., Dell'Acqua, F., Forkel, S.J., Simmons, A., Vergani, F., Murphy, D.G., Catani, M., 2011a. A lateralized brain network for visuospatial attention. Nat Neurosci 14, 1245-1246.
Thiebaut de Schotten, M., ffytche, D.H., Bizzi, A., Dell'Acqua, F., Allin, M., Walshe, M., Murray, R., Williams, S.C., Murphy, D.G.M., Catani, M., 2011b. Atlasing location, asymmetry and inter-subject variability of white matter tracts in the human brain with MR diffusion tractography. Neuroimage 54, 49-59.
Thomas, C., Ye, F.Q., Irfanoglu, M.O., Modi, P., Saleem, K.S., Leopold, D.A., Pierpaoli, C., 2014. Anatomical accuracy of brain connections derived from diffusion MRI tractography is inherently limited. Proceedings of the National Academy of Sciences of the United States of America 111, 16574-16579.
Toga, A.W., Thompson, P.M., 2003. Mapping brain asymmetry. Nat Rev Neurosci 4, 37-48.
Toga, A.W., Thompson, P.M., 2014. Connectopathy in ageing and dementia. Brain 137, 3104-3106.
Tomasi, D., Volkow, N.D., 2011. Association between functional connectivity hubs and brain networks. Cereb Cortex 21, 2003-2013.
Tomasi, D., Volkow, N.D., 2012a. Aging and Functional Brain Networks. Molecular Psychiatry 17, 549-558.
Tomasi, D., Volkow, N.D., 2012b. Laterality patterns of brain functional connectivity: gender effects. Cereb Cortex 22, 1455-1462.

Tomasi, D., Wang, G.-J., Volkow, N.D., 2013. Energetic cost of brain functional connectivity. Proceedings of the National Academy of Sciences 110, 13642-13647.
Tononi, G., 2004. An information integration theory of consciousness. BMC neuroscience 5, 1.
Tononi, G., Sporns, O., Edelman, G.M., 1994. A measure for brain complexity: relating functional segregation and integration in the nervous system. Proceedings of the National Academy of Sciences of the United States of America 91, 5033-5037.
Tournier, J., Calamante, F., Connelly, A., 2010. Improved probabilistic streamlines tractography by 2nd order integration over fibre orientation distributions. Proc. 18th Annual Meeting of the Intl. Soc. Mag. Reson. Med.(ISMRM), p. 1670.
Tournier, J.-D., Mori, S., Leemans, A., 2011. Diffusion tensor imaging and beyond. Magnetic Resonance in Medicine 65, 1532-1556.
Tournier, J.D., Calamante, F., Connelly, A., 2007. Robust determination of the fibre orientation distribution in diffusion MRI: Non-negativity constrained super-resolved spherical deconvolution. Neuroimage 35, 1459-1472.
Tournier, J.D., Calamante, F., Connelly, A., 2012. MRtrix: Diffusion tractography in crossing fiber regions. International Journal of Imaging Systems and Technology 22, 53-66.
Tournier, J.D., Calamante, F., Connelly, A., 2013. Determination of the appropriate b value and number of gradient directions for high-angular-resolution diffusion-weighted imaging. NMR Biomed 26, 1775-1786.
Tournier, J.D., Yeh, C.H., Calamante, F., Cho, K.H., Connelly, A., Lin, C.P., 2008. Resolving crossing fibres using constrained spherical deconvolution: validation using diffusion-weighted imaging phantom data. Neuroimage 42, 617-625.
Towlson, E.K., Vertes, P.E., Ahnert, S.E., Schafer, W.R., Bullmore, E.T., 2013. The rich club of the C. elegans neuronal connectome. J Neurosci 33, 6380-6387.
Tremblay, P., Gracco, V.L., 2010. On the selection of words and oral motor responses: Evidence of a response-independent fronto-parietal network. Cortex 46, 15-28.
Trzepacz, P.T., Yu, P., Sun, J., Schuh, K., Case, M., Witte, M.M., Hochstetler, H., Hake, A., 2014. Comparison of neuroimaging modalities for the prediction of conversion from mild cognitive impairment to Alzheimer's dementia. Neurobiology of Aging 35, 143-151.
Tsang, R.S., Sachdev, P.S., Reppermund, S., Kochan, N.A., Kang, K., Crawford, J., Wen, W., Draper, B., Trollor, J.N., Slavin, M.J., Mather, K.A., Assareh, A., Seeher, K.M., Brodaty, H., 2013. Sydney Memory and Ageing Study: an epidemiological cohort study of brain ageing and dementia. Int Rev Psychiatry 25, 711-725.
Tsvetanov, K.A., Henson, R.N.A., Tyler, L.K., Razi, A., Geerligs, L., Ham, T.E., Rowe, J.B., Cambridge Centre for, A., Neuroscience, 2016. Extrinsic and Intrinsic Brain Network Connectivity Maintains Cognition across the Lifespan Despite Accelerated Decay of Regional Brain Activation. The Journal of Neuroscience 36, 3115-3126.
Tuch, D.S., 2004. Q-ball imaging. Magnetic Resonance in Medicine 52, 1358-1372.
Tuch, D.S., Reese, T.G., Wiegell, M.R., Makris, N., Belliveau, J.W., Wedeen, V.J., 2002. High angular resolution diffusion imaging reveals intravoxel white matter fiber heterogeneity. Magnetic Resonance in Medicine 48, 577-582.
Tzourio-Mazoyer, N., Landeau, B., Papathanassiou, D., Crivello, F., Etard, O., Delcroix, N., Mazoyer, B., Joliot, M., 2002a. Automated anatomical labeling of

activations in SPM using a macroscopic anatomical parcellation of the MNI MRI single-subject brain. Neuroimage 15, 273-289.
Tzourio-Mazoyer, N., Landeau, B., Papathanassiou, D., Crivello, F., Etard, O., Delcroix, N., Mazoyer, B., Joliot, M., 2002b. Automated anatomical labeling of activations in SPM using a macroscopic anatomical parcellation of the MNI MRI single-subject brain. NeuroImage 15, 273-289.
Uddin, L.Q., Supekar, K.S., Ryali, S., Menon, V., 2011. Dynamic Reconfiguration of Structural and Functional Connectivity Across Core Neurocognitive Brain Networks with Development. The Journal of Neuroscience 31, 18578-18589.
Utevsky, A.V., Smith, D.V., Huettel, S.A., 2014. Precuneus Is a Functional Core of the Default-Mode Network. The Journal of Neuroscience 34, 932-940.
Vaessen, M.J., Hofman, P.A.M., Tijssen, H.N., Aldenkamp, A.P., Jansen, J.F.A., Backes, W.H., 2010. The effect and reproducibility of different clinical DTI gradient sets on small world brain connectivity measures. Neuroimage 51, 1106-1116.
Valenzuela, M.J., Sachdev, P., 2006. Brain reserve and dementia: a systematic review. Psychological Medicine 36, 441-454.
van den Bos, R., Homberg, J., de Visser, L., 2013. A critical review of sex differences in decision-making tasks: focus on the Iowa Gambling Task. Behav Brain Res 238, 95-108.
van den Brink, R.L., Cohen, M.X., van der Burg, E., Talsma, D., Vissers, M.E., Slagter, H.A., 2014. Subcortical, Modality-Specific Pathways Contribute to Multisensory Processing in Humans. Cerebral Cortex 24, 2169-2177.
van den Heuvel, M.P., de Reus, M.A., Feldman Barrett, L., Scholtens, L.H., Coopmans, F.M.T., Schmidt, R., Preuss, T.M., Rilling, J.K., Li, L., 2015. Comparison of diffusion tractography and tract-tracing measures of connectivity strength in rhesus macaque connectome. Human Brain Mapping 36, 3064-3075.
van den Heuvel, M.P., Hulshoff Pol, H.E., 2010. Exploring the brain network: A review on resting-state fMRI functional connectivity. European Neuropsychopharmacology 20, 519-534.
van den Heuvel, M.P., Kahn, R.S., Goñi, J., Sporns, O., 2012. High-cost, high-capacity backbone for global brain communication. Proceedings of the National Academy of Sciences 109, 11372-11377.
van den Heuvel, M.P., Mandl, R.C.W., Stam, C.J., Kahn, R.S., Hulshoff Pol, H.E., 2010. Aberrant Frontal and Temporal Complex Network Structure in Schizophrenia: A Graph Theoretical Analysis. The Journal of Neuroscience 30, 15915-15926.
van den Heuvel, M.P., Sporns, O., 2011. Rich-club organization of the human connectome. J Neurosci 31, 15775-15786.
van den Heuvel, M.P., Sporns, O., 2013a. An Anatomical Substrate for Integration among Functional Networks in Human Cortex. The Journal of Neuroscience 33, 14489-14500.
van den Heuvel, M.P., Sporns, O., 2013b. Network hubs in the human brain. Trends Cogn Sci 17, 683-696.
van den Heuvel, M.P., Sporns, O., Collin, G., et al., 2013. ABnormal rich club organization and functional brain dynamics in schizophrenia. JAMA Psychiatry 70, 783-792.

Van Essen, D.C., Drury, H.A., Dickson, J., Harwell, J., Hanlon, D., Anderson, C.H., 2001. An Integrated Software Suite for Surface-based Analyses of Cerebral Cortex. Journal of the American Medical Informatics Association 8, 443-459.
Van Essen, D.C., Smith, S.M., Barch, D.M., Behrens, T.E.J., Yacoub, E., Ugurbil, K., for the, W.U.M.H.C.P.C., 2013. The WU-Minn Human Connectome Project: An Overview. Neuroimage 80, 62-79.
van Wijk, B.C.M., Stam, C.J., Daffertshofer, A., 2010. Comparing Brain Networks of Different Size and Connectivity Density Using Graph Theory. PLoS ONE 5, e13701.
Váša, F., Shanahan, M., Hellyer, P.J., Scott, G., Cabral, J., Leech, R., 2015. Effects of lesions on synchrony and metastability in cortical networks. Neuroimage 118, 456-467.
Vederine, F.-E., Wessa, M., Leboyer, M., Houenou, J., 2011. A meta-analysis of whole-brain diffusion tensor imaging studies in bipolar disorder. Progress in Neuro-Psychopharmacology and Biological Psychiatry 35, 1820-1826.
Vergani, F., Lacerda, L., Martino, J., Attems, J., Morris, C., Mitchell, P., Thiebaut de Schotten, M., Dell'Acqua, F., 2014. White matter connections of the supplementary motor area in humans. J Neurol Neurosurg Psychiatry 85, 1377-1385.
Versace, A., Ladouceur, C.D., Romero, S., Birmaher, B., Axelson, D.A., Kupfer, D.J., Phillips, M.L., 2010. Altered development of white matter in youth at high familial risk for bipolar disorder: a diffusion tensor imaging study. Journal of the American Academy of Child and Adolescent Psychiatry 49, 1249-1259. e1241.
Vöhringer, P.A., Barroilhet, S.A., Amerio, A., Reale, M.L., Alvear, K., Vergne, D., Ghaemi, S.N., 2013. Cognitive Impairment in Bipolar Disorder and Schizophrenia: A Systematic Review. Frontiers in Psychiatry 4, 87.
W. H. O. World Mental Health Survey Consortium, 2004. Prevalence, severity, and unmet need for treatment of mental disorders in the world health organization world mental health surveys. Jama 291, 2581-2590.
Wang, F., Kalmar, J.H., Edmiston, E., Chepenik, L.G., Bhagwagar, Z., Spencer, L., Pittman, B., Jackowski, M., Papademetris, X., Constable, R.T., Blumberg, H.P., 2008. Abnormal corpus callosum integrity in bipolar disorder: a diffusion tensor imaging study. Biological Psychiatry 64, 730-733.
Wang, L., Li, Y., Metzak, P., He, Y., Woodward, T.S., 2010. Age-related changes in topological patterns of large-scale brain functional networks during memory encoding and recognition. Neuroimage 50, 862-872.
Wang, L., Su, L., Shen, H., Hu, D., 2012. Decoding Lifespan Changes of the Human Brain Using Resting-State Functional Connectivity MRI. PLoS ONE 7, e44530.
Wang, Z., Dai, Z., Gong, G., Zhou, C., He, Y., 2015. Understanding Structural-Functional Relationships in the Human Brain. The Neuroscientist 21, 290-305.
Ward, A., Arrighi, H.M., Michels, S., Cedarbaum, J.M., 2012. Mild cognitive impairment: disparity of incidence and prevalence estimates. Alzheimers Dement 8, 14-21.
Watts, D.J., Strogatz, S.H., 1998. Collective dynamics of 'small-world' networks. Nature 393, 440-442.
Wechsler, D., 1981. WAIS-R manual. The Psychological Corporation, New York.
Wechsler, D., 1997a. Wechsler Adult Intelligence Scale-III. The Psychological Corporation, San Antonio.

Wechsler, D., 1997b. Wechsler Memory Scale. Third edition manual. The Psychological Corporation, San Antonio.
Weintraub, S., Wicklund, A.H., Salmon, D.P., 2012. The neuropsychological profile of Alzheimer disease. Cold Spring Harbor perspectives in medicine 2, a006171.
Weissman, M.M., Leaf, P.J., Tischler, G.L., Blazer, D.G., Karno, M., Bruce, M.L., Florio, L.P., 1988. Affective disorders in five United States communities. Psychological Medicine 18, 141-153.
Weissman, M.M., Merikangas, K.R., John, K., Wickramaratne, P., Prusoff, B.A., Kidd, K.K., 1986. Family-genetic studies of psychiatric disorders: Developing technologies. Archives of General Psychiatry 43, 1104-1116.
Wen, W., Zhu, W., He, Y., Kochan, N.A., Reppermund, S., Slavin, M.J., Brodaty, H., Crawford, J., Xia, A., Sachdev, P., 2011. Discrete Neuroanatomical Networks Are Associated with Specific Cognitive Abilities in Old Age. The Journal of Neuroscience 31, 1204-1212.
Whalley, H.C., Sussmann, J.E., Chakirova, G., Mukerjee, P., Peel, A., McKirdy, J., Hall, J., Johnstone, E.C., Lawrie, S.M., McIntosh, A.M., 2011. The Neural Basis of Familial Risk and Temperamental Variation in Individuals at High Risk of Bipolar Disorder. Biological Psychiatry 70, 343-349.
White, J.G., Southgate, E., Thomson, J.N., Brenner, S., 1986. The Structure of the Nervous System of the Nematode Caenorhabditis elegans. Philosophical Transactions of the Royal Society of London B: Biological Sciences 314, 1-340.
Whittle, S., Yucel, M., Yap, M.B., Allen, N.B., 2011. Sex differences in the neural correlates of emotion: evidence from neuroimaging. Biol Psychol 87, 319-333.
Widjaja, E., Zamyadi, M., Raybaud, C., Snead, O., Doesburg, S., Smith, M., 2015. Disrupted global and regional structural networks and subnetworks in children with localization-related epilepsy. American Journal of Neuroradiology 36, 1362-1368.
Williams, R.J., Martinez, N.D., 2000. Simple rules yield complex food webs. Nature 404, 180-183.
Willis, S.L., Tennstedt, S.L., Marsiske, M., et al., 2006. Long-term effects of cognitive training on everyday functional outcomes in older adults. Jama 296, 2805-2814.
Winblad, B., Palmer, K., Kivipelto, M., Jelic, V., Fratiglioni, L., Wahlund, L.O., Nordberg, A., Bäckman, L., Albert, M., Almkvist, O., Arai, H., Basun, H., Blennow, K., De Leon, M., DeCarli, C., Erkinjuntti, T., Giacobini, E., Graff, C., Hardy, J., Jack, C., Jorm, A., Ritchie, K., Van Duijn, C., Visser, P., Petersen, R.C., 2004. Mild cognitive impairment – beyond controversies, towards a consensus: report of the International Working Group on Mild Cognitive Impairment. Journal of Internal Medicine 256, 240-246.
Winecoff, A., Clithero, J.A., Carter, R.M., Bergman, S.R., Wang, L., Huettel, S.A., 2013. Ventromedial Prefrontal Cortex Encodes Emotional Value. The Journal of Neuroscience 33, 11032-11039.
Wittchen, H.-U., Jacobi, F., 2004. Size and burden of mental disorders in Europe: A critical review and appraisal of 27 studies. European Neuropsychopharmacology 15, 357-376.
World Health Organization, 2003. The world health report 2003: shaping the future. World Health Organization.

Xekardaki, A., Giannakopoulos, P., Haller, S., 2011. White matter changes in bipolar disorder, Alzheimer disease, and mild cognitive impairment: new insights from DTI. Journal of Aging Research September 2011.
Xia, M., Wang, J., He, Y., 2013. BrainNet Viewer: a network visualization tool for human brain connectomics. PLoS ONE 8, e68910.
Yan, C., Zang, Y., 2010. DPARSF: a MATLAB toolbox for "pipeline" data analysis of resting-state fMRI. Frontiers in Systems Neuroscience 4.
Yeo, B.T., Krienen, F.M., Sepulcre, J., Sabuncu, M.R., Lashkari, D., Hollinshead, M., Roffman, J.L., Smoller, J.W., Zöllei, L., Polimeni, J.R., 2011. The organization of the human cerebral cortex estimated by intrinsic functional connectivity. Journal of neurophysiology 106, 1125-1165.
Yeo, B.T.T., Krienen, F.M., Chee, M.W.L., Buckner, R.L., 2014. Estimates of segregation and overlap of functional connectivity networks in the human cerebral cortex. Neuroimage 88, 212-227.
Ystad, M., Hodneland, E., Adolfsdottir, S., Haasz, J., Lundervold, A.J., Eichele, T., Lundervold, A., 2011. Cortico-striatal connectivity and cognition in normal aging: a combined DTI and resting state fMRI study. Neuroimage 55, 24-31.
Zald, D.H., Andreotti, C., 2010. Neuropsychological assessment of the orbital and ventromedial prefrontal cortex. Neuropsychologia 48, 3377-3391.
Zalesky, A., Cocchi, L., Fornito, A., Murray, M.M., Bullmore, E., 2012. Connectivity differences in brain networks. Neuroimage 60, 1055-1062.
Zalesky, A., Fornito, A., Bullmore, E.T., 2010a. Network-based statistic: identifying differences in brain networks. Neuroimage 53, 1197-1207.
Zalesky, A., Fornito, A., Cocchi, L., Gollo, L.L., Breakspear, M., 2014. Time-resolved resting-state brain networks. Proceedings of the National Academy of Sciences 111, 10341-10346.
Zalesky, A., Fornito, A., Cocchi, L., Gollo, L.L., van den Heuvel, M.P., Breakspear, M., 2016. Connectome sensitivity or specificity: which is more important? Neuroimage.
Zalesky, A., Fornito, A., Harding, I.H., Cocchi, L., Yücel, M., Pantelis, C., Bullmore, E.T., 2010b. Whole-brain anatomical networks: Does the choice of nodes matter? Neuroimage 50, 970-983.
Zalesky, A., Fornito, A., Seal, M.L., Cocchi, L., Westin, C.-F., Bullmore, E.T., Egan, G.F., Pantelis, C., 2011. Disrupted axonal fiber connectivity in schizophrenia. Biological Psychiatry 69, 80-89.
Zhang, H., Schneider, T., Wheeler-Kingshott, C.A., Alexander, D.C., 2012. NODDI: Practical in vivo neurite orientation dispersion and density imaging of the human brain. Neuroimage 61, 1000-1016.
Zhao, T., Cao, M., Niu, H., Zuo, X.-N., Evans, A., He, Y., Dong, Q., Shu, N., 2015. Age-related changes in the topological organization of the white matter structural connectome across the human lifespan. Human Brain Mapping 36, 3777-3792.
Zhou, J., Gennatas, Efstathios D., Kramer, Joel H., Miller, Bruce L., Seeley, William W., 2012. Predicting Regional Neurodegeneration from the Healthy Brain Functional Connectome. Neuron 73, 1216-1227.